THE UNIVERSITY
of EDINBURGH

Process-based modelling of ammonia emission from grazing

Andrea Móring

Submitted for the degree of Doctor of Philosophy

School of GeoScineces

The University of Edinburgh

2016

Declaration

I declare that this thesis has been composed by myself, and this work is my own, except where otherwise indicated. This work has not been submitted for any other degree or professional qualification.

Chapter 2, Chapter 3 and Section 5.2 represent an extended version of the study published by Móring et. al (2016) that includes also parts of Chapter 1. In this work, the observations used in the model evaluation were carried out and provided by Johannes Laubach and Arezoo Taghizadeh-Toosi. A re-print of this paper is included in the appendix.

Based on Sections 4.1-4.5, a conference paper was submitted (Móring et al., in review) to the 7th International Nitrogen Initiative Conference. In this work (Chapter 4), the measurements used for the presented modelling study were taken and provided by Eiko Nemitz, Marsailidh Twigg and Celia Milford.

_____ _____

Andrea Móring Date

Abstract

Excessive ammonia (NH_3) emission, originating largely from agriculture, can affect water, air and soil quality, and through these, endanger ecosystem and human health. Since NH_3 emission is strongly dependent on temperature and also influenced by other meteorological variables, the question arises: how will NH_3 emission alter in a changing climate? A way to address this question and predict the subsequent environmental consequences is to construct meteorology-driven models of NH_3 emission from every agricultural source. Furthermore, NH_3 emission is a highly localised and dynamic process. The focus of this thesis is NH_3 emission from grazing. In the first stage a new process-based model for NH_3 emission from a urine patch was developed. The GAG model (Generation of Ammonia from Grazing) is capable of simulating the TAN (total ammoniacal nitrogen) and the water content of the soil under a urine patch and also soil pH dynamics. In the second stage, GAG was applied to the scale of a grazed field, combining multiple simulations of the patch-scale model including both urine-affected and unaffected ("clean") areas. The modelled NH_3 fluxes were found to be in good agreement with the observations for both model types. The sensitivity of NH_3 flux was assessed to various soil physical and chemical parameters for both the patch and the field scale models. It was found that ammonia volatilization from a urine patch could be influenced by the possible restart of urea hydrolysis after a rain event as well as carbon-dioxide emissions from the soil. Over the field scale, it was shown that the temporal evolution of the NH_3 exchange flux was dominated by the NH_3 emission from the patches within the field. The results also suggested that NH_3 fluxes over the field in a given day could be considerably affected by the NH_3 emission from urine patches deposited several days earlier. In the last stage of the work, a comprehensive sensitivity analysis was carried out with a special focus on temperature, for both versions of the GAG model. It was shown that due to the different governing dynamics over the patch and the field scale, the temperature-dependence of NH_3 exchange is stronger over the field scale. It was also concluded that the temperature-dependence of NH_3 exchange is stronger if the sinks of NH_3 are stronger within the system. Finally, it was found, that Q_{10}, a widely-used metric to express the relative increase of trace gas emissions over a range of 10 °C, is influenced by the length of the period of investigation and the initial value of the temperature range.

Lay Summary

Ammonia gas (NH_3) is released mainly during the breakdown of animal excreta and fertilizers containing ammonium. As such, the main global source of NH_3 is agriculture. Excessive emission of NH_3 can affect water, air and a soil quality, and through these, endanger ecosystems and human health. NH_3 emission is controlled by meteorology, especially temperature. This meteorological dependence raises the question: how will NH_3 emissions alter in a changing climate? The approach to address this question depends on the given agricultural source investigated. The focus of this thesis is NH_3 emission from grazed fields. Over a grazed field not only NH_3 emission to the atmosphere, but its opposite, also deposition can occur, transferring NH_3 from the atmosphere to the surface. This NH_3 exchange consists of two components: NH_3 emission from the urine patches and NH_3 exchange with the area on the field that is not affected by urine ("clean area"). Therefore, in the first stage, a model called GAG (Generation of Ammonia from Grazing) was constructed that simulates NH_3 emission from a single urine patch. This model takes into account the relevant soil chemical processes and the influence of meteorology. In the second stage, the GAG model was applied to a grazed field, by using the patch-scale model for every urine patch deposited on the field and a modified version of it for the clean area. The modelled NH_3 exchange was in a good agreement with the observations in the case of both the single urine patch and the field. In both cases, a series of sensitivity model simulations were carried out to examine the model response to the change of various environmental and soil physical parameters. In the third stage of the work the effect of meteorology was investigated with a special focus on temperature in the case of the urine patch as well as the grazed field. It was shown that due to the different governing dynamics over the patch and the field scale, the temperature-dependence of NH_3 exchange is stronger over the field scale. It was also concluded that the temperature-dependence of NH_3 exchange is stronger if the sinks of NH_3 are stronger within the system. Finally, it was found, that Q_{10}, a widely-used metric to express the relative increase of trace gas emissions over a range of 10 °C, is influenced by the length of the period of investigation and the initial value of the temperature range.

To Mama and Zoli

“If you can't explain it simply, you don't understand it well enough.”

- Albert Einstein

Acknowledgement

First and foremost, my deepest gratitude goes to my supervisors, Mark Sutton, Massimo Vieno and Ruth Doherty for their expertise and excellent guidance throughout my research. I am grateful to Mark for his amazing enthusiasm for this research area, and his novel and insightful ideas that deeply inspired me. I thank Massimo for organizing the PhD group meetings that greatly helped my progress in the first two years. Also, I thank him for the long hours of brainstorming that always showed me the way forward when I was stuck. Finally, I thank Ruth for tirelessly stimulating me to reach my maximum potential.

I wish to thank my former master's supervisor, my good friend László Horváth, for bringing to my attention this PhD project and encouraging me to apply for it. I am also grateful to my former manager, the president of the Hungarian Meteorological Service, Zoltán Dunkel for supporting me to take this opportunity.

I would like to acknowledge the financial and professional support from the ÉCLAIRE project (Effects of Climate Change on Air Pollution and Response Strategies for European Ecosystems) funded by the EU's Seventh Framework Programme for Research and Technological Development (FP7). In addition, I would like to thank Johannes Laubach, Arezoo Taghizadeh-Toosi, Eiko Nemitz, Marsailidh Twigg, and Celia Milford for providing their measurement datasets and for their valuable advice.

I thank my friends I met during my PhD, Emma, Chun, Pietro and Robyn, for making my days happier and for their support in the tough periods. When I moved to Edinburgh I did not expect that one day, one of my best friends in the city would be a Hungarian girl. Special thanks go to her, Eszter, for always being available for a tea, or just a comforting Hungarian chat during the writing-up period. I am also grateful to my two "Honorary Moms" in Hungary, Ági and Márti. Without their love and endless support I would have not been able to achieve what I did so far.

I thank my parents for bringing me up to be who I am today. I also would like to express my gratitude to my grandmother, my dearest Mama, for her support and love during the first two years of my PhD. I wish she could have stayed longer, and I could share with her the moment of euphoria at my thesis submission and graduation.

Finally, I wish to thank my beloved husband, Zoli. His patience, understanding and unconditional love have given me the greatest strength, not just to my PhD, but everything else in my life.

Contents

List of Symbols

[X] (mol dm^{-3})	Concentration of compound *X*, (*X*= H_2CO_3, HCO_3^-, CO_3^{2-}, $CO_{2(g)}$, NH_4^+, $NH_{3(aq)}$, $NH_{3(g)}$, H^+, TAN)
a	Parameter for calculating R_w
A_{clean} (m^2)	Area of the field unaffected by urine
AD (ha^{-1})	Animal density
A_{field} (m^2)	Field area
A_h	Parameter for urea hydrolysis simulation
A_{patch} (m^2)	Area of a urine patch
B_C (mol)	Carbon content of the source layer (originating from urea)
B_{H2O} (dm^3)	Water budget in the source layer
B_{H2O}(max) (dm^3)	Maximal water amount in the source layer
B_{H2O}(min) (dm^3)	Minimal water amount in the source layer
B_{H2O}^j (dm^3)	Water budget in the source layer under the urine patches deposited in the j^{th} time step
B_N (mol)	TAN + gaseous ammonia content in the source layer
B_{TAN} (g N)	TAN budget in the source layer
B_{urea} (g N)	Urea budget under a urine patch
B_X (mol)	Budget of a chemical compound *X* under the urine patch (*X*= H_2CO_3, HCO_3^-, CO_3^{2-}, $CO_{2(g)}$, NH_4^+, $NH_{3(aq)}$, $NH_{3(g)}$, H^+)
C_d	Effect of day and night on evapotranspiration
c_N (g N dm^{-3})	N content of the urine
c_N^{Ave}	Average urinary N concentration in urine patches deposited in the same time step
c_N^{Dil} (g N dm^{-3})	Urine N content after dilution in the soil
c_N^k (g N dm^{-3})	Urinary N concentration in the k^{th} urine patch
$Cond_A$, $Cond_B$	Conditions in Eq. 2.53
c_p (J kg^{-1} K^{-1})	Heat capacity of air
d (m)	Displacement height
$D(c_N)$	Distribution function of urinary nitrogen content
D_g (m^2 s^{-1})	Diffusivity of NH_3 in air

$\frac{D_{O_3}}{D_{NH_3}}$	Ratio of diffusivity of O_3 and NH_3
D_t	Proportion of the urine-covered area over a *t* time period on field if there is no overlap between the urine patches
e	Euler's constant
E (mm h^{-1})	Soil evaporation rate
e_a (kPa)	Actual water vapour pressure
e_s (kPa)	Saturated water vapour pressure
ET (mm h^{-1})	Actual evapotranspiration rate
ET_0 (mm h^{-1})	Reference evapotranspiration rate
F_1, F_2 (μg N m^{-2} s^{-1})	Theoretical NH_3 fluxes in Eqs. 5.3 and 5.4
F_1^{ind}, F_2^{ind} (μg N m^{-2} s^{-1})	Theoretical non-temperature-dependent component fluxes of NH_3 in Eqs. 5.3, 5.4 and 5.6-5.10
f_c (m^2 m^{-2})	Percentage of vegetation coverage
F_{clean} (μg N m^{-2} s^{-1})	Net NH_3 exchange flux over the clean area
F_f (μg N m^{-2} s^{-1})	NH_3 exchange flux with the foliage
F_g (μg N m^{-2} s^{-1})	NH_3 exchange flux over the ground
F_{net} (μg N m^{-2} s^{-1})	Net NH_3 exchange flux for the whole field
F_{patch}^{j} (μg N m^{-2} s^{-1})	NH_3 emission flux from the urine patches deposited in the j^{th} time step
F_{sto} (μg N m^{-2} s^{-1})	NH_3 exchange flux with stomata
F_t (μg N m^{-2} s^{-1})	Total NH_3 exchange flux over the canopy
F^{temp} (μg N m^{-2} s^{-1})	Theoretical temperature-dependent component flux of NH_3 in Eqs. 5.3-5.9
F_w (μg N m^{-2} s^{-1})	NH_3 deposition flux to water and waxes on the leaf surface
f_w (m^2 m^{-2})	Wetted uncovered soil fraction
F_χ (μg N m^{-2} s^{-1})	NH_3 exchange flux derived based on measurements with AMANDA
g (m s^{-2})	Acceleration of gravity
G (MJ m^2 h^{-1})	Soil heat flux
g_{light}	Relative conductance for the effect of light on g_s
g_{max} (mmol O_3 m^{-2})	Maximal stomatal conductance

g_{min}	Minimal relative stomatal conductance
g_{pot}	Relative stomatal conductance for the effect of plant phenological state on g_s
g_s (mmol O_3 m^{-2})	Stomatal conductance for O_3
g_{SWP}	Relative conductance for the effect of soil water on g_s
g_{temp}	Relative conductance for the effect of temperature on g_s
g_{VPD}	Relative conductance for the effect of vapour pressure deficit on g_s
H (J m^{-2} s^{-1})	Sensible heat flux
h (m)	Canopy height
H(X) (mol dm^{-3} (mol dm^{-3})$^{-1}$)	Henry coefficient for the given gas *X*
i_C (mol)	Carbon input to the urine patch
i_N (mol)	TAN input to the urine patch (TAN production in moles)
k	Karman constant
K	Parameter representing the uniformity of the excretal distribution on a field
K(X) (mol dm^{-3})	Dissociation constant for the given compound *X*
K_c	Crop coefficient
K_{cb}	Transpiration coefficient
K_{cb}(Tab)	Coefficient to calculate *ET*
K_e	Soil evaporation coefficient
k_h	Urea hydrolysis constant
L (m)	Monin-Obukhov length
LAI (m^2 m^{-2})	Leaf area index
$n(t_j)$	Number of urine patches deposited in the j^{th} time step
N_{app} (kg N ha^{-1})	Nitrogen applied over a urine patch
N_{prod} (g N)	TAN production
N_t	Total number of urine patches deposited over a *t* time period on a field
p (kPa)	Surface atmospheric pressure
P (mm)	Precipitation
PAR (µmol m^2 s^{-1})	Photosynthetically active radiation

P_t	Proportion of the field covered by urine patches after a *t* time period
q	Parameter in the calculation of P_t
Q_{10}	Relative increase of the emission of a trace gas over a range of 10 °C
Q_{10}^{Em}	Q_{10} calculated for the positive NH_3 exchange (emission) fluxes
Q_{10}^{Ex}	Q_{10} calculated for NH_3 exchange fluxes
R (kg^{-1} K^{-1})	Specific gas constant of dry air
R_a (s m^{-1})	Aerodynamic resistance over the canopy
R_{ac} (s m^{-1})	Aerodynamic resistance in the canopy
R_b (s m^{-1})	Resistance of the quasi-laminar layer over the canopy
R_{bg} (s m^{-1})	Resistance of the quasi-laminar layer in the canopy
Re	Reynolds number
REW (mm)	Readily evaporable water in the soil
R_{glob} (MJ m^2h^{-1})	Global radiation / solar radiation
RH (%)	Relative humidity
R_n (MJ m^2 h^{-1})	Net radiation
r_{RX} (mol)	Consumption or production of a given compound in reaction *X*
R_{soil} (s m^{-1})	Soil resistance
R_{sto} (s m^{-1})	Stomatal resistance
$R_{sto}(O_3)$(s m^{-1})	Stomatal resistance for O_3
R_w (s m^{-1})	Cuticular resistance
R_w(min) (s m-1)	Minimal cuticular resistance
Sc	Schmidt number
$Sens_{net}$ (%)	Sensitivity of the total NH_3 exchange over the whole field
$Sens_{patch}$ (%)	Sensitivity of the total NH_3 exchange over the urine patches on the field
SH	Specific humidity
S_{MI}	Soil moisture index
T (ºC)	Air temperature at 2 m
t_i	i^{th} time step
T_{min} (°C)	Temperature for minimal stomatal conductance

T_{opt} (°C)	Temperature for optimal stomatal conducatnce
T_{soil} (ºC)	Soil temperature
T_v (K)	Virtual temperature
u (m s^{-1})	Wind speed
u_{dir} (°)	Wind direction
u_* (m s^{-1})	Friction velocity
u_{*g} (m s^{-1})	Friction velocity at ground level in the canopy
U_{add} (g N)	Urea added to the source layer
UF (animal^{-1} day^{-1})	Urination frequency
V_{air} (dm^3)	Volume of the air in the source layer
VPD (kPa)	Vapour pressure deficit
VPD_{max} (kPa)	VPD for maximal stomatal conductance
VPD_{min} (kPa)	VPD for minimal stomatal conductance
W_{evap} (dm^3)	Water loss as soil evaporation from the urine patch
W_{rain} (dm^3)	Water input as rain water over the urine patch
W_{urine} (dm^3)	Volume of urine
x	Parameter for calculating the stability functions
z_0 (m)	Surface roughness
z_l (m)	Height of the top of logarithmic wind profile
z_w (m)	Height of wind measurement
α	Parameter for calculating R_{ac}
α_{PAR} (µmol m^2 s^{-1})$^{-1}$	Parameter for calculating g_{PAR}
β (mol H^+ (pH unit)$^{-1}$ dm^{-3})	Soil buffering capacity
β_{patch} (mol H^+ (pH unit)$^{-1}$)	Buffering capacity of the source layer
γ (kPa ºC^{-1})	Psychometric constant
Γ_p	NH_3 emission potential in the soil pore
$\Gamma_{p,rel}$	Γ_p when the temperature is changed by a given ΔT, expressed relative to its value when ΔT = 0 °C
Γ_{sto}	NH_3 emission potential from the stomata
Γ_{sto}(max)	Maximal NH_3 emission potential from the stomata
Δ (kPa ºC^{-1})	Slope of saturation vapour pressure curve
δ_0 (m)	Height where eddy and molecular diffusivity are the same in magnitude
Δz (mm)	Thickness of the source layer
Δz_E (m)	Thickness of the evaporation layer

θ ($m^3\ m^{-3}$)	Volumetric water content
θ_{fc} ($m^3\ m^{-3}$)	Field capacity
θ_{por} ($m^3\ m^{-3}$)	Porosity
θ_{pwp} ($m^3\ m^{-3}$)	Permanent wilting point
θ_{urine} ($m^3\ m^{-3}$)	Proportion of the source layer that can be filled up by urine
ν ($m^2\ s^{-1}$)	Kinematic viscosity
ξ	Soil tortuosity
ρ ($kg\ m^{-3}$)	Air density
σ, μ	Scale parameters of the log-normal distribution
ΣEm	Sum of the positive NH_3 exchange (emission) fluxes over a period
ΣEx	Sum of the NH_3 exchange fluxes over a period
ΣX_{rel}	Sum of a given X NH_3 exchange flux ($X = F_f$, F_g, F_{sto}, F_w, Ex, Em) when the temperature is changed by a given ΔT, expressed relative to its value when $\Delta T = 0$ °C
τ (days)	Decay parameter
χ_a ($\mu g\ N\ m^{-3}$)	Air concentration of NH_3
χ_c ($\mu g\ N\ m^{-3}$)	Compensation point above the vegetation
χ_g ($\mu g\ N\ m^{-3}$)	Compensation point on the ground
χ_p ($\mu g\ N\ m^{-3}$)	Compensation point in the soil pores
$\chi_{p,\ rel}$	χ_p when the temperature is changed by a given ΔT, expressed relative to its value when $\Delta T = 0$ °C
χ_{sto} ($\mu g\ N\ m^{-3}$)	Stomatal compensation point
χ_{z0} ($\mu g\ N\ m^{-3}$)	Canopy compensation point
Ψ_H	Stability function for heat
Ψ_M	Stability function for momentum

Chapter 1

Introduction

1. 1. Motivation

Excessive ammonia (NH_3) emission can affect water, air and a soil quality, and through these, endanger ecosystems and human health. The main global NH_3 emitting sector is agriculture. Since NH_3 emission is strongly dependent on temperature and also influenced by other meteorological variables, the question arises: how will these environmental threats be influenced by the climate change in the future? To provide an answer, first of all, it is necessary to gain a clear understanding of the weather-related dynamics of NH_3 emission.

A way to deepen our knowledge on this field is to learn lessons from model simulations. This requires the development and application of models that account for the weather dependencies of NH_3 emission. The mechanism of NH_3 release varies among sources, while there are also atmospheric drivers of NH_3 emission, deposition, atmospheric dispersion and mixing. These dependencies apply through various scales (regional, field and even smaller). As the whole picture is rather complex, the challenge of weather-dependent NH_3 modelling can be addressed step-by-step, focusing on selected processes and context. This study represents one of these steps, developing, describing and assessing an NH_3 emission model for grazed fields that incorporates the effect of meteorology and accounts for the particular characteristics of this source of NH_3.

The present chapter firstly, provides a summary of the environmental effects of NH_3 emission, as well as an overview of the main sources of ammonia globally and in the UK (Section 1.2). Secondly, the theoretical background of NH_3 exchange between the surface and the atmosphere is introduced (Section 1.3). This is followed by a review of the existing NH_3 exchange models based on this theory, as well as other NH_3 emission models for urine and urea-affected soils (Section 1.4). Finally, the chapter concludes with the research questions and the outline of the way they were addressed in this thesis (Section 1.5).

1. 2. Ammonia emission, as an environmental threat

Human perturbation of the nitrogen cycle is becoming an increasing environmental issue in our rapidly developing world. The natural cycle of nitrogen is driven by the conversion between inert nitrogen gas (N_2) and reactive nitrogen compounds (N_r). N_r includes any chemical form of nitrogen other than N_2, such as nitrates (NO_3^-), nitrogen oxides (NO_x), nitrous oxide (N_2O), organic nitrogen compounds, ammonium (NH_4^+) and NH_3. Under natural conditions these reactive substances are sparse; however, they are necessary for all life forms on the Earth, including humans.

With a growing world population also the food demand of humans increased during the 19th century, which required larger amounts of fertilizer to increase crop yields. This was satisfied by the invention of the Haber-Bosch process that enabled the transformation of atmospheric N_2 to the usable form of NH_3, utilizing a high pressure reaction with hydrogen gas ($N_2 + 3\ H_2 \rightarrow 2\ NH_3$) (Erisman et al., 2008). Since this invention, the global production of reactive nitrogen compounds has doubled (Galloway et al., 2003).

Although the enhanced N_r production increases the risk to the natural nitrogen cycle, a more serious danger is caused by the inefficient and excessive usage of these products, with especially high N losses from agriculture. According to EDGAR (2011), 51% of the total N_r is emitted as NH_3 (43% is released in the form of NO_x mainly during fossil fuel combustion, and 6% as N_2O predominantly from agriculture). Specifically, the main source of NH_3 is the breakdown of urea in livestock excreta, and

a similar process takes place in the case of urea-based fertilisers. Livestock houses and manure storage facilities represent strong NH_3 hotspots, while fields treated by manure represent the largest intermittent area sources.

In the last 40 years, following the growth of N_r production, the global emission of NH_3 has been increasing substantially (Fig 1.1). In this emission time series, an overall linear growing can be observed with a dominant contribution from agriculture (ca. 70%). However, some high emission years have also occurred since 1970, triggered predominantly by non-agricultural sources, such as biomass burning, energy industry, transportation and waste handling. The highest among these emission peaks, in 1997, was caused by a severe peat fire in Indonesia.

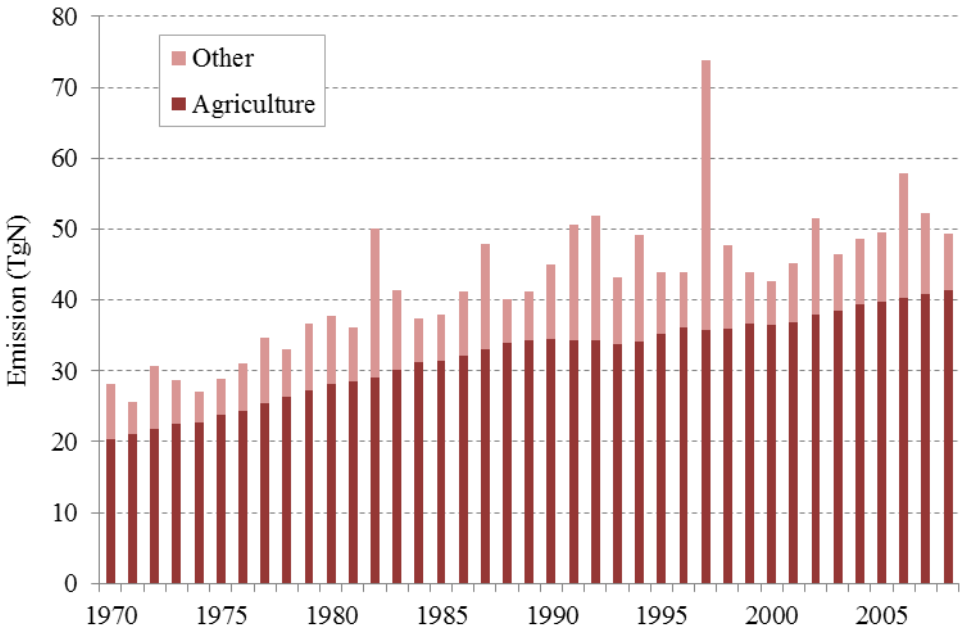

Figure 1.1. Global NH_3 emission between 1970 and 2008, including the agricultural emissions (based on data from EDGAR, 2011).

The excessive emission of N_r, including NH_3, cause a series of environmental impacts, called the "nitrogen cascade" (Galloway et al., 2003, and see a schematic in Fig. 1.2 from Sutton et al., 2011). This means that an emitted N_r molecule is transferred among the environmental systems (atmosphere, terrestrial and aquatic ecosystems), and chemically transformed within them to other forms of N_r, until it is eventually

converted into nonreactive N_2 gas. Since the conversion of reactive nitrogen species to each other is rather rapid (e.g. NH_4^+ in the soil is oxidized to nitrite (NO_2^-) and NO_3^-, etc.), the environmental effects of NH_3 emission are inseparable from the N cascade.

Since N_r creation is stronger than its removal through denitrification to N_2, N_r accumulates in the environment (Galloway et al., 2003). This accumulation leads to various environmental problems. Absorption of atmospheric acidic components (NH_4^+, HNO_3) at the ground can result in soil acidification (van Breemen et al., 1982), whilst nitrates may have a fertilising effect on nature, causing severe eutrophication of terrestrial and aquatic ecosystems (Bobbink et al., 2010, Rabalais, 2002). By altering pH and nitrogen balance, both processes can potentially harm biodiversity (Cape et al., 2009).

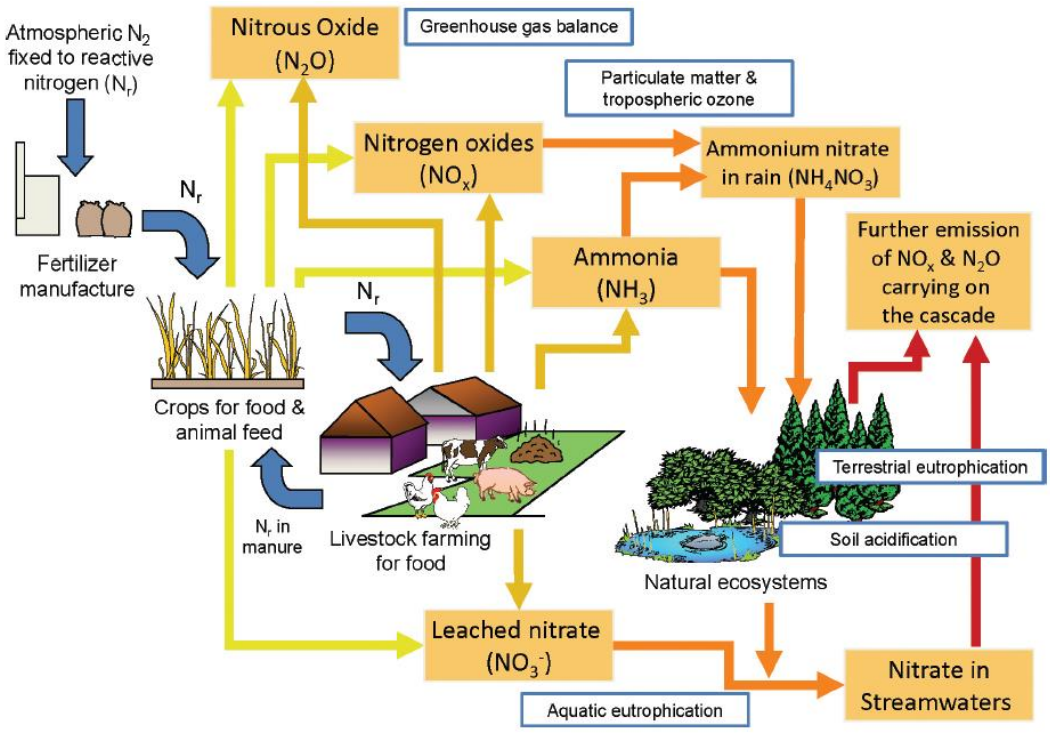

Figure 1.2. A simplified schematic of the nitrogen cascade, indicating the losses, transformation and the environmental effects of N_r originating from fertilizers. A similar picture can be drawn to illustrate the environmental processes related to the N_r forms released during fossil fuel combustion. (Taken from Sutton et al., 2011.)

Furthermore, growing atmospheric concentrations of reactive nitrogen compounds can lead to worsened air-quality. On one hand, NO_x has a vital role in the formation of tropospheric ozone. On the other hand, NH_4^+ and NO_3^- can serve as a base for particulate matter production, both affecting human health (Wolfe and Patz, 2002). In addition to air pollution, effects on the global climate change can also be detected: whilst NH_4^+ and NO_3^- form aerosols which, through cloud formation, can affect the radiation balance, N_2O emitted from the soil enhances the greenhouse warming potential. Moreover, N_2O also plays a role in the stratospheric ozone depletion (Cowling et al., 1998, Butterbach-Bahl et al., 2011).

Although in the UK ammonia emission has been decreased by 13.4% since 1980, it is still considered as an environmental risk (DEFRA, 2015). According to Misselbrook et al. (2013) UK agricultural NH_3 emission was 237.7 Gg in 2012 (Table 1.1). The strongest management category was animal housing (75.8 Gg), whilst among the source sectors, the strongest emission originated from cattle farming (127.7 Gg). In addition to the sources of livestock management, fertilizers accounted for a significant amount of the total NH_3 released (37.9 Gg, ca. 16% of the total).

Table 1.1. Ammonia emission by source sectors (rows) and management categories (columns) for the year 2012 in the UK (Gg NH_3) (based on emission data from Misselbrook et al., 2013).

	Grazing	**Manure spreading**	**Housing**	**Manure storage**	**Total**
Cattle	15.4	35.8	52.7	23.8	127.7
Sheep + other	7.2	0.2	1.5	0.8	9.7
Pigs	1.1	3.7	9.1	3.7	17.7
Poultry	0.9	13.9	12.5	2.5	29.8
Horses	15	-	-	-	15
Fertilizer	-	-	-	-	37.9
Total	39.6	53.6	75.8	30.8	**237.7**

Figure 1.3 (from Hellsten et al., 2008) gives an approximate picture about the spatial distribution of NH_3 source sectors over the UK (where the background indicates the region with emission lower than 1 kg N ha^{-1} $year^{-1}$, originating mainly from vegetation and grazing). Although a relatively low level of NH_3 is released during grazing (according to Table 1.1, ca. 10% of the total emission), about two thirds of grasslands are grazed, affecting a significant percentage of the UK (Hellsten et al., 2008).

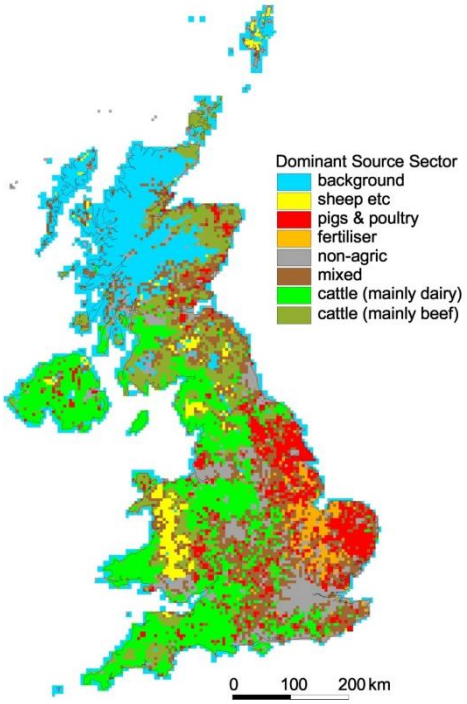

Figure 1.3. Dominant NH_3 sources in the UK in 2000. (Taken from Hellsten et al., 2008.)

1. 3. Bi-directional exchange of ammonia, the compensation point theory

After emission, there are two ways for NH_3 to return to the surface from the atmosphere: by wet or dry deposition. Wet deposition occurs when NH_3 is washed out from the atmosphere by being dissolved in precipitation, whilst during dry deposition NH_3 is transported to the surface by turbulent flux. In addition, the conversion of NH_3 to NH_4^+ in the atmosphere also contributes to wet and dry deposition. As the scavenging of NH_4^+ aerosol is relatively inefficient, most of the NH_4^+ is removed from

the atmosphere through wet deposition or by conversion back to NH_3 (Asman et al., 1998).

The atmospheric transfer of NH_3 between the atmosphere and the different types of surfaces can be considered as bi-directional (e.g. Farquhar et al., 1980, Sutton et al., 1995), resulting in net emission (considered as positive flux) or net deposition (considered as negative flux) at different moments in time.

The effective exchange of NH_3 typically occurs with an aquatic solution on the surface (as illustrated on Fig. 1.4). Within the ecosystem of a vegetated surface, the following can act as such a solution, i.e. an ammonia sink or source: soil moisture, the liquid content of manure or dead leaves on the soil, animal urine or even just a thin water layer, which covers leaf surfaces most of the time (Burkhardt et al., 1999). In the case of plant leaves, NH_3 exchange occurs also through the stomata. Here, the source solution is the fluid of the apoplast (the intercellular space that surrounds plant cells, which includes plant cell walls) in the sub-stomatal cavity.

This bi-directional exchange of NH_3 is well described by the so-called "compensation point" theory (Farquhar et al., 1980) (Fig. 1.4). According to this theory, there is a compensation point (χ_{cp}), which is a theoretical, equilibrium, atmospheric NH_3 concentration, right above the surface of the given source/sink solution of NH_3.

As explained above, various sources and sinks are present in an ecosystem, and above all of them a different compensation point can be distinguished. The value of χ_{cp} determines the direction of NH_3 transfer: if χ_{cp} is greater than the ambient ammonia concentration (χ_a) emission occurs, otherwise deposition takes place. If $\chi_{cp} = \chi_a$ there is no net NH_3 exchange.

The value of χ_{cp} is controlled by two chemical equilibrium processes: 1) the dissolution of NH_3 (Eq. 1.1), and 2) the dissociation of NH_4^+ in the solution (Eq. 1.2).

$$NH_{3(g)} \leftrightarrow NH_{3(aq)} \quad (1.1)$$

$$NH_{3(aq)} + H^+ \leftrightarrow NH_4^+ \quad (1.2)$$

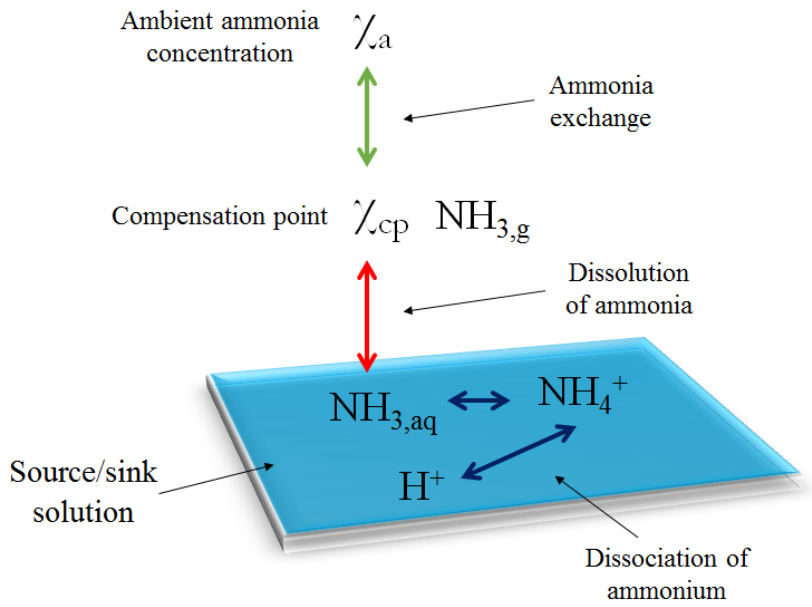

Figure 1.4. Schematic of the compensation point theory as interpreted in this thesis.

In the discussion of the study by Sutton et al. (1995), the authors explained that the definition of compensation point assumes that it is controlled not only by these chemical equilibrium processes, but also by plant physiological or microbial processes. Therefore, above a wet sheet of glass only a concentration potential can be defined. Nevertheless, to avoid confusion between the different terms, in this thesis also this concentration potential is referred to as a compensation point.

Both processes (Eq. 1.1 and 1.2) are characterized by a temperature dependent coefficient: the Henry-coefficient for dissolution (*H*, mol dm^{-3} atm^{-1}, Eq. (1.3) based on Dasgupta and Dong, 1986), and the dissociation coefficient (*K*, mol dm^{-3}, Eq. (1.4) based on Bates and Pinching, 1949).

$$\mathrm{H(T)} = \frac{[\mathrm{NH_{3(aq)}}]}{[\mathrm{NH_{3(g)}}]} = 56.0 \times \exp\left(4092\left(\frac{1}{\mathrm{T}} - \frac{1}{298.15}\right)\right) \tag{1.3}$$

$$\mathrm{K(T)} = \frac{[\mathrm{NH_{3(aq)}}][\mathrm{H^+}]}{[\mathrm{NH_4^+}]} = 5.67 \times 10^{-10} \times \exp\left(-6286\left(\frac{1}{\mathrm{T}} - \frac{1}{298.15}\right)\right) \tag{1.4}$$

In Eqs. (1.3) and (1.4) [$NH_{3(g)}$] represents the partial pressure (atm) of gaseous NH_3 above the solution, [$NH_{3(aq)}$] indicates the concentration (mol dm^{-3}) of dissolved NH_3 in the solution, [NH_4^+] and [H^+] represent the ammonium and hydrogen ion concentration (mol dm^{-3}) in the solution, respectively, and T stands for temperature (K). From these equations an expression can be compiled for χ_{cp} (µg m^{-3}) (in the form suggested by Nemitz et al., 2001):

$$\chi_{cp} = [NH_{3(g)}] = \frac{2.75 \times 10^{15}}{T} exp\left(\frac{-1.04 \times 10^{4}}{T}\right)\frac{[NH_4^+]}{[H^+]} \qquad (1.5)$$

The strong relationship of χ_{cp} with temperature can be clearly seen in Fig. 1.5. For instance, as also shown by Flechard and Fowler (2008), a 4-5 degrees warming can double χ_{cp} for a given [NH_4^+]/[H^+] ratio, referred to as Γ (gamma). Although temperature has its strongest effect on NH_3 exchange through χ_{cp}, on the level of an ecosystem, there are further ways through which temperature can act as an influencing factor. For example, temperature affects plant physiology as well as microbial and soil processes (Riedo et al., 2002). Moreover, temperature also determines how much water vapour can be held by the air (Tetens, 1930). This means that the formation of the water film on the leaf surface, which is regulated by relative humidity (Sutton and Fowler, 1993), is indirectly influenced also by temperature.

It has to be noted, that beside temperature, also other meteorological variables can play a governing role in NH_3 exchange. Wind speed, by enhancing turbulence, has a positive impact on exchange. The effect of rainfall can either increase or decrease NH_3 fluxes. Precipitation helps the infiltration to the soil, supressing NH_3 volatilization. On the other hand, after a dry period rainwater can dissolve NH_4^+ particles on the surface, as well as activate NH_3 producing enzymes, facilitating NH_3 release. A further influencing factor is incoming solar radiation, which, beside its heating effect, controls the openness of stomata during day-time.

In addition to meteorological factors, through χ_{cp}, NH_3 exchange is strongly influenced by Γ (as reflected in Eq. (1.5) and illustrated in Fig. 1.5). The value of Γ characterises the NH_3 emission potential and (according to its definition) is determined by [NH_4^+] and [H^+] (or expressed as $pH=-\log_{10}([H^+])$).

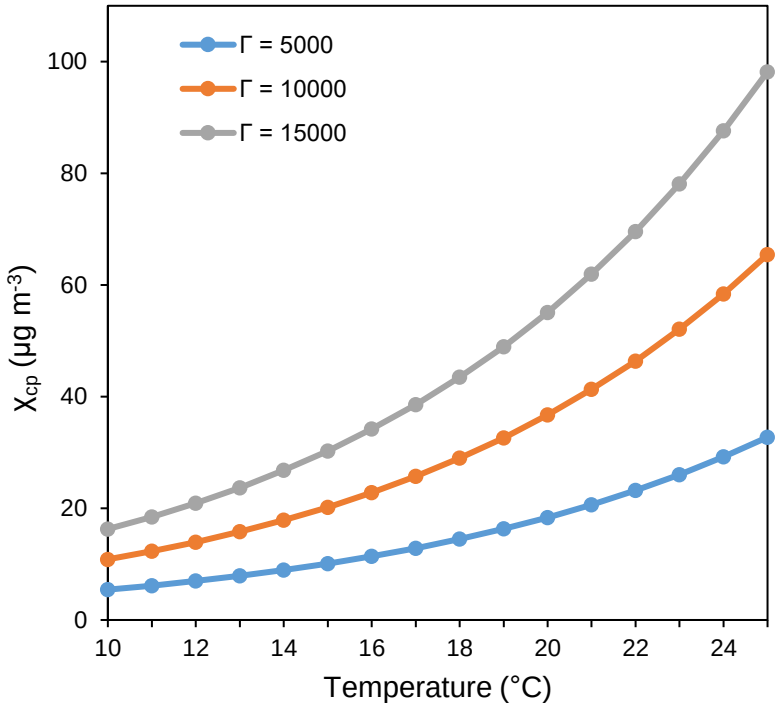

Figure 1.5. Compensation point (χ_{cp}) as a function of temperature based on Eq. 1.5 with various emission potentials (Γ).

The concentration of NH_4^+ and H^+ are changing continuously in the different source/sink solutions within an ecosystem (Mattsson et al., 2009), with the changes driven by different processes. For example, in the case of non-managed soils pH has a natural variability and [NH_4^+] is determined by the mineralization of organic matter with the constant production and immobilization through microbial turnover, the consumption by root uptake and nitrification. The driving process are different in the apoplastic fluid. Here, [NH_4^+] is influenced by the nitrogen uptake status and the development stage of the plant (Massad et al., 2010a), whilst apoplastic pH is influenced by the plant metabolic processes (Massad et al., 2008). Agricultural management, including fertilisation, cutting and grazing, can cause further massive alterations in [NH_4^+] and [H^+], resulting in highly variable emission potentials for the apoplast as well the soil. In the GRAMINAE measurement campaign (Sutton et al., 2009) conducted over an intensively managed grassland, the measured Γ values for soil and apoplast varied between 11,000–30,000 and 30-1000, respectively.

During grazing, the dominant NH_3 source is urine, rather than dung (Petersen et al., 1998, Laubach et al., 2013). Therefore, in the case of this NH_3 source, the emission potential of the urine affected-soil has a vital importance. In a urine patch NH_4^+ is produced by the hydrolysis of the urea present in urine. The process is catalysed in the presence of water by the enzyme urease, which is the product of several bacteria species. To maintain the chemical equilibria between NH_4^+ and NH_3, production of NH_4^+ by ureolysis is accompanied by NH_3 release from the urine solution to the gas phase. This leads to a high compensation point (usually higher than the ambient air concentration) above the urine patch, generally resulting in NH_3 emission.

Four stages of soil pH evolution after urine or urea application were described by Sherlock and Goh (1985), which suggest considerable changes of Γ in the soil under a urine patch (Fig. 1.6). In the first stage, after a rapid increase from the initial level (pH 6-8) governed by the intensive urea hydrolysis, soil pH usually peaks at 8-9.5 around 6-48 hours after urine deposition. Subsequently, the pH tends to drop to about 8 due to NH_3 emission over a period of about 2-8 days (second stage). This is followed by a 1-3 week long constant phase (third stage) when soil pH does not change considerably and, finally, a phase (fourth stage) with a moderate decline in soil pH, regulated by the nitrification of TAN.

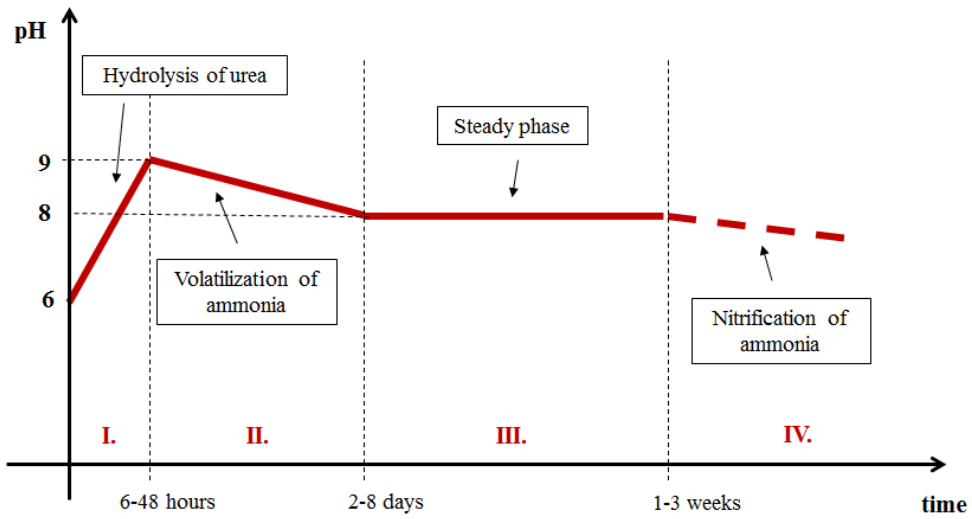

Figure 1.6. Schematic of the four stage process of pH evolution in urine or urea affected soils as described by Sherlock and Goh (1985).

1. 4. Modelling of ammonia exchange and ammonia emission

Depending on the scale of examination (ecosystem or regional scale), different NH_3 exchange/emission regulating processes can be distinguished. On ecosystem scale (in the present context, also referred to as canopy or field scale) a model has to account for the sources and sinks within an ecosystem and usually a single, measured χ_a is used to represent the ambient NH_3 concentration at the given location. In contrast, on regional (or global) scale, χ_a has to be ascertained in series of grid points, covering the modelled region (or the globe).

1. 4. 1. Ecosystem-scale models

State-of-the-art NH_3 exchange models for vegetated surfaces, called 'canopy compensation point models', use the (electrical) resistance analogy to capture the influence of meteorological factors and the canopy on NH_3 exchange. In these models emission potentials are mostly handled as constant, parametrised or simulated by a sub-model since their measurement is very difficult (David et al., 2009, Mattsson et al., 2009). For example, such sub-models are able to simulate plant metabolism processes inside a leaf (e.g. Massad et al., 2010a) or the dynamic chemistry of a water droplet on the leaf surace (Flechard et al., 1999).

Among the ecosystem-scale models applied to excretal and fertilizer sources (e.g. guano, liquid manure, urine, urea and mineralized fertilizers), examples are reviewed in the following sections that assume only unidirectional ammonia emission. Although many of the reviewed emission models fail to capture the effect of weather on NH_3 volatilization, they usually operate with a more complex approach for soil processes.

1. 4. 1. 1. The resistance analogy

Canopy compensation point models are widely used for simulating field-scale NH_3 emission. These calculate the compensation point over a vegetated surface ("canopy compensation point") based on the interaction of component sources and sinks within the canopy (as explained in Section 1.3). The models work with resistances (R_a, R_b… etc.) on the analogy of an electrical circuit where electrical current and potential

difference represent NH_3 fluxes and the difference between the NH_3 concentrations at the different levels of the canopy, respectively (Fig. 1.7 B-F). The influence of meteorological factors on the total flux (F_t), except that of the temperature on compensation point, is mostly taken into account in these resistances. F_t (µg m^{-2} s^{-1}) for a given z height above the canopy can be expressed as:

$$F_t(z) = \frac{\chi(z_0\prime) - \chi_a(z)}{R_a(z) + R_b}, \quad (1.6)$$

where $R_a(z)$ is the aerodynamic resistance (s m^{-1}) for the given z height, R_b is the resistance (s m^{-1}) of the quasi-laminar layer, $\chi(z_0\prime)$ is the canopy compensation point (µg m^{-3}) over the canopy referenced to the notional height of exchange, $z_0\prime$, and $\chi_a(z)$ is the ambient NH_3 concentration in the atmosphere at z height.

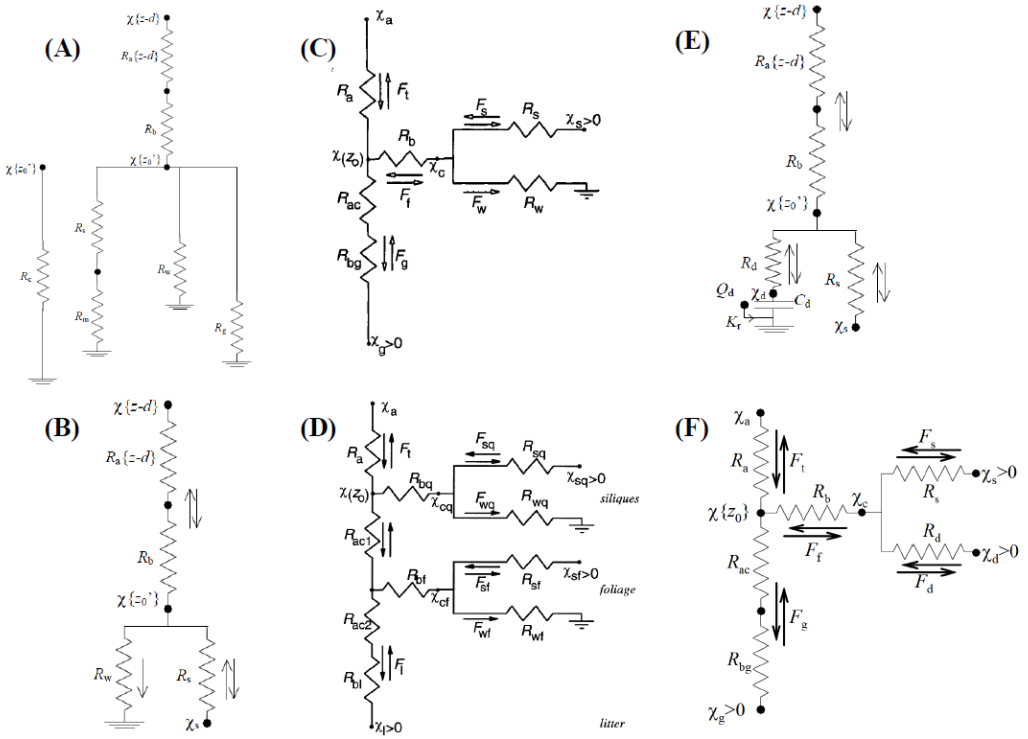

Figure 1.7. Modelling structures simulating NH_3 fluxes over a canopy: resistance model without assuming any compensation point (A), one-layer canopy compensation point model (B, Sutton et al., 1995), two-layer canopy compensation point model (C, Nemitz et al., 2001), three-layer canopy compensation point model (D, Nemitz et al., 2000), one-layer capacitance canopy compensation point model (E, Sutton et al., 1998), two-layer dynamic chemistry canopy compensation point model (F, Burkhardt et al., 2009). Taken from Flechard et al. (2013).

The value of $\chi(z_{0'})$ regulates NH_3 exchange over the canopy based on the rules of the compensation point theory (discussed in Section 1.3). Canopy compensation point models can be considered as process-based models, since the flux calculation accounts for the effects of turbulent exchange (through R_a) and the quasi-laminar boundary layer (R_b), as well as $\chi(z_{0'})$ and $\chi_a(z)$ can be described in relation to controlling processes with their values changing over time.

Whilst $\chi_a(z)$ is measurable and the parametrization of $R_a(z)$ and R_b is well-established (Massad et al., 2010b), $\chi(z_{0'})$ is not easily measurable and its value is rather uncertain. It can be calculated from fluxes from different sources and sinks within the canopy, such as the plant itself, the soil, the dead leaves or any kind of fertilizer on the soil surface. In the typical resistance approach, these sources and sinks are assigned to different levels. Depending on how many levels within the canopy are taken into account in the calculation of $\chi(z_{0'})$, one-layer (exchange just with the plant through stomata and cuticle, (Fig. 1.7 B and E) and two (Fig. 1.7 C and F) or more layer models (Fig. 1.7 D) can be distinguished.

To derive NH_3 fluxes from the different sources, the compensation point over every level has to be ascertained, which requires an estimation of every corresponding Γ. In field-scale models, empirically estimated constants are often used for Γ. However, as mentioned in Section 1.3, in reality the value of Γ is not invariant over time. Therefore, by coupling the field-scale models to sub-models, which account for mechanisms regulating the dynamics of Γ, a much sophisticated approach can be derived for simulating bi-directional exchange.

1. 4. 1. 2. Simulation of the emission potential

Several models has been developed to simulate changing Γ on different levels within the canopy. The PaSim model (Riedo et al., 2002) is a dynamic grassland ecosystem model. It calculates stomatal and soil compensation points based on the equilibrium NH_3 concentration in the stomatal cavity above the apoplastic fluid, and at the soil surface, respectively. For both sources the corresponding Γ values are derived from changing NH_4^+ concentrations, but constant pH values (which are set empirically),

using a multilayer approach for soil processes and accounting for plant physiological processes.

The MLBC model (Wu et al., 2009) is a stomatal compensation point model, which accounts for dynamically changing NH_4^+ as well as pH. However, it is a purely chemical model and lacks any biochemical and physiological aspects. The STAMP model (Massad et al., 2010a) provides another approach to estimate the stomatal compensation point. In this model, pH is assumed to be constant, hence the change of stomatal Γ depends only on the variation in NH_4^+ concentration. Nevertheless, $[NH_4^+]$ is derived by taking into account plant physiological and biochemical processes with more details than in PaSim.

In addition to plant physiological and soil interactions, the interaction of chemical processes on leaf surfaces can also be important in controlling net NH_3 fluxes. While models in Fig. 1.7 (A)-(D) and (F) all treat uptake of NH_3 on to leaf surfaces as a simple resistance (R_w), in fact, both adsorption and desorption processes can occur. In the simplest approach to treat this effect (Sutton et al., 1998), a leaf-surface water pool is assumed with fixed pH (parametrized as a capacitance), allowing subsequent diffusion in to the plant apoplast.

This approach was further developed in the model by Flechard et al. (1999), which was termed DEWS in Flechard et al. (2013). This model describes the chemistry of water droplets on the leaf surface. It calculates a compensation point over the droplets as a function of a comprehensive ion balance, calculating a dynamically changing pH. The model uses the equilibrium processes within the water droplets for - besides NH_3 - SO_2, CO_2, HNO_2, HNO_3 and HCl.

1. 4. 1. 3. Applied models for excretal sources

The GUANO model (Riddick, 2012) can be considered as a special application of a compensation point model, because it is not related to canopy processes. The model simulates NH_3 emission from sea bird excreta. It is driven by meteorological variables, such as temperature, wind speed, solar radiation, relative humidity and precipitation. This model is process-based, which besides the calculation of a compensation point

for the ground surface, accounts for continuous guano input over the simulation period. A water balance model is also included, using the Penman equation for evaporation. Although the model keeps the pH of guano on a constant level, it captures the changes of NH_4^+ concentration, simulating the conversion of uric acid content of guano to ammoniacal nitrogen (NH_4^+ and dissolved NH_3).

Another recent example of process-based emission modelling of excretal sources is the VOLT'AIR model (Génermont and Cellier, 1997, Hamaoui-Laguel et al., 2012). This model simulates the NH_3 emission from liquid manure and mineral fertilizers applied to the land, containing a complex approach for the transfer of heat, water and ammoniacal nitrogen between different soil layers. VOLT'AIR does not operate with a compensation point model for deriving NH_3 fluxes, but uses a local advection model (Itier and Perrier, 1976). In VOLT'AIR a constant pH is used over the modelling period, which is determined by a pre-calibration run. During this calibration process the model finds the pH value that gives the best representation of the NH_3 fluxes that were measured at the field investigated in the given modelling study. In addition to the handling of pH, another disadvantage of the model is the difficult applicability due to the large amount of specific input data required by the model.

The SURFATM-NH3 model (Personne et al., 2009) can be also used for manure or fertilizer application. In SURFATM-NH3, two models are coupled to calculate ammonia flux over terrestrial ecosystems: one for energy budget and one for NH_3 exchange. For the latter, a two-layer canopy compensation point model is applied (Fig. 1.7 C) extended with a soil resistance, assuming a compensation point in the soil with a corresponding soil Γ. The limitation of the model is that for a simulation both the soil and the stomatal Γ has to be prescribed (measured or assumed).

Several modelling studies were carried out to simulate NH_3 emission also from urine patches. For example, the model of Sherlock and Goh (1985) accounted for the NH_3 volatilization from urine patches and aqueous urea. Their model simulated the process of urea hydrolysis, describing the transfer of NH_3 between surface and atmosphere with a constant "volatilization exchange coefficient", rather than a system of dynamically changing resistances.

Rachhpal and Nye (1986) also published an NH_3 emission model from applied urea. Their model also employed a constant "transfer coefficient" for NH_3 volatilization while a constant rate of urea hydrolysis was applied. In addition, they reported an alternative to simulate the chemistry of a urine patch, as well as the vertical distribution of the different nitrogen compounds under it.

Recently, Laubach et al. (2012) published an NH_3 volatilization model from urine patches, applying also a simple compensation point model, which was run in 'reverse mode' to calculate soil resistance based on NH_3 flux measurements. The equilibrium gaseous NH_3 concentration in the soil pores was considered as a compensation point, and three resistances (a soil, an aerodynamic, and a quasi-laminar resistance) were assumed between the soil and air concentration, excluding any interaction with the overlaying vegetation. The simulation of NH_3 exchange with the model required soil sampling and measurement of pH and NH_4^+ concentration of soil water.

1. 4. 2. Regional scale modelling

To examine the process of NH_3 exchange on a larger scale, such as regional or global scale, χ_a has to be ascertained in numerous grid points covering the simulated region. This can be obtained by using an atmospheric chemistry transport model (ACTM). An ACTM is driven by a meteorological model, therefore, it is capable of simulating the horizontal transfer of NH_3 via atmospheric advection. During the atmospheric transport, ACTMs also simulate the mixing of NH_3 and its possible chemical reactions with numerous other atmospheric pollutants.

Generally, ACTMs calculate NH_3 deposition and emission separately; at every time step over every grid point each primary pollutant (including ammonia) is emitted and removed from the model atmosphere. Such a separation of emission and deposition of NH_3 is not consistent with the bi-directional behaviour of NH_3 exchange, which is clearly either emission (positive flux) or deposition (negative flux) in every moment, depending on the difference between the surface and the atmospheric concentration of NH_3 (according to Eq. (1.6)). Even though the sum of the separately calculated

emission and deposition can be considered as a net flux, they are derived neglecting the strong effect of temperature.

Dry deposition of NH_3 is usually calculated from the atmospheric NH_3 concentration (Eq. 1.7) using dry deposition velocities (v_d, m s^{-1}) (Seinfeld and Pandis, 2006). Values of v_d are derived from resistances, such as illustrated in Fig. 1.7 (A), where R_c is a bulk canopy resistance, representing the overall surface sink:

$$F(z) = -\chi_a(z)v_d = -\chi_a(z)\frac{1}{R_a + R_b + R_c} \quad (1.7)$$

This approach is climate-dependent to some extent since R_a and R_b are affected by turbulence, while R_c can be influenced by temperature (through the stomata) and moisture availability. However, it does not account for bi-directional NH_3 exchange as no compensation point is included.

An example of an ACTM is the EMEP model (Simpson et al., 2012). In this model emissions are derived in every hour based on annual emissions reported by the European countries, using pre-determined, constant time factors. These factors represent monthly, daily and hourly weights, used to distribute the amount of reported yearly total emitted NH_3. Firstly, this is divided into monthly emissions, then these are further distributed to daily emissions and finally, they are divided into hourly emissions.

Annual NH_3 emissions (like the ones reported to EMEP) are usually estimated on the basis of characteristics that describe agricultural management practices (e.g. number of different animals, duration of grazing and housing, amount of spread manure, duration of manure storage...etc.), using constant emission factors (e.g. in Misselbrook et al. (2000) 16.9 g NH_3-N dairy cow^{-1} day^{-1} for grazing or 4.8 g NH_3-N m^{-2} day^{-1} for storage of solid pig and poultry waste as manure heaps, where NH_3-N stands for nitrogen in the form of NH_3).

Hellsten et al. (2007) presented an illustrative result for the weakness of emission factors. In their study average monthly NH_3 emissions were calculated for different source sectors for the year 2000, by taking into account the temporal variability of agricultural practice and using emission factors. Due to the short atmospheric lifetime

(a few days), NH_3 concentration is primarily driven by NH_3 emissions. Thus, the seasonal cycles of the calculated emissions were compared to those of atmospheric concentrations, which were measured at sites dominated by the given source sector (Fig. 1.8).

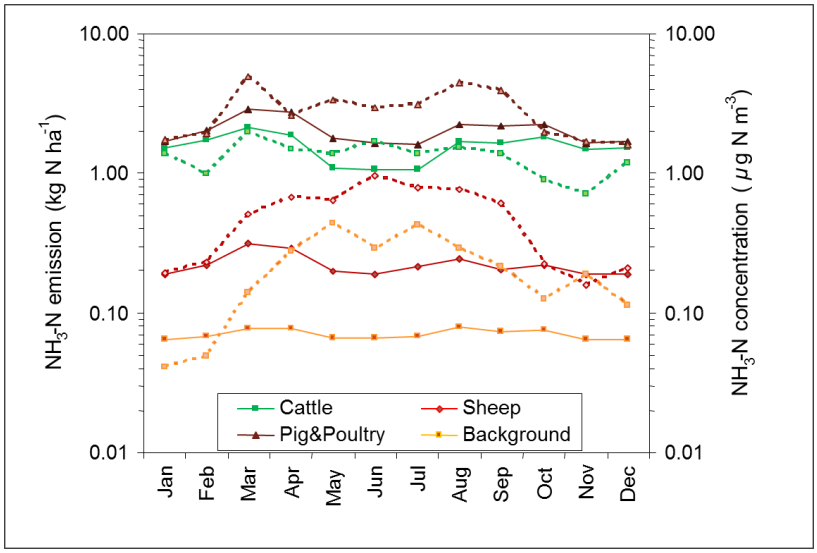

Figure 1.8. Measured NH_3–N concentration (dotted line) and average modelled NH_3–N emissions (solid line) for 2002 at 83 UK sites in areas dominated by four source sectors: cattle, sheep, pig and poultry, and background. The values of NH_3–N concentration were obtained from the UK National Ammonia Monitoring Network (Sutton et al., 2001). The figure is taken from Hellsten et al. (2007).

While the differences in agricultural practice were partly able to explain the seasonal pattern of NH_3 from pig and poultry (including a spring peak), the seasonal cycles of emissions and concentrations were inconsistent, especially in the case of background sites and in the case of sheep emissions. Sheep emissions mainly originate from grazing since animals spend most of their time outdoors (Table 1.1). Therefore, in both the background and sheep sectors (apart from the urine input in the sheep sector) NH_3 volatilization is mostly driven by meteorology, which can explain the large difference in the summer between the emissions and concentrations. Consequently, this example shows a possible contribution of the meteorological variables to emissions, highlighting the importance of considering meteorological effects in the emission approach.

Skjøth et al. (2011) downscaled the annual emissions in a climate-dependent way, incorporating the effect of the seasonal variations of temperature and wind speed. The approach was tested in the DEHM ACTM for a North-European region. It was found that modelled NH_3 concentrations were in better agreement with measurements than they were when using the ACTM with the traditional emission approach.

Although the concentrations were represented better by the approach by Skjøth et al. (2011), a serious limiting factor for applying it to a more extended area over Europe is the detailed agricultural management dataset required to the calculations, which is not easily available for every region in Europe. A further important fundamental limitation is that, in this approach, the total estimated annual emissions are left unchanged. They are only disaggregated, and therefore, the method does not truly treat the climatic dependence of emissions, which could lead to warm years having larger emissions than cold years.

Several model experiments have been conducted where a compensation point model was coupled to an ACTM. Among these, the first modelling study was carried out by Dentener and Crutzen (1994), assuming a compensation point for the unfertilized soils and vegetation. However, the resistances to NH_3 exchange with the stomata and deposition to the leaf surface were apparently handled in a single constant canopy resistance (R_c) for the different surface types.

Also the classical one and two-layer canopy compensation point models were applied to ACTMs. Sorteberg and Hov (1996) coupled the one-layer model of Sutton et al. (1995) to an early version of the EMEP model. Recently two other model experiments were published by Wichink Kruit et al. (2012) and by Bash et al. (2012). Wichink Kruit et al. incorporated a one-layer compensation point model into the 3-D chemistry-transport model LOTOS-EUROS (Schaap et al., 2008), which also assumed bidirectional exchange with the external leaf surface. Bash et al. coupled an agro-ecosystem model (CONUS EPIC, Cooter et al., 2012) to a photochemical air-quality model (CMAQ, Foley et al., 2010). In this modelling framework NH_3 exchange was simulated by the two-layer model of Nemitz et al. (2001).

All of the three coupled model systems mentioned above operated with a simplified estimation for compensation point, neglecting the temporal variation of Γ. In addition, in the case of Sorteberg and Hov (1996) as well as Wichink Kruit et al. (2012) anthropogenic NH_3 emission inputs to the ACTM were based on annual emissions, distributed to hourly emissions by using time factors as mentioned earlier. Bash et al. (2012) simulated the emissions from fertilizers dynamically with CONUS EPIC, however, hourly emissions from the other sources were downscaled from annual emissions using an inverse modelling technique based on wet deposition (Gilliland et al., 2006). In spite of the weaknesses of these models, their results were in a better agreement with NH_3 measurements (e.g. concentration, wet deposition… etc.) than it was by using the traditional approach that assumes constant emission and separate NH_3 deposition.

1. 5. Initial conclusions and research questions

Based on the above review of the knowledge in the field of NH_3 relevant to the topic of this thesis, the following can be concluded:

- The exchange of NH_3 between the surface and atmosphere is strongly dependent on temperature and it is also affected by other meteorological variables (Section 1.3). This implies that climate change is very likely to affect NH_3 emission from agricultural sources.
- The magnitude of the NH_3 exchange flux depends on the emission potential of the different sources and sinks of NH_3 within an ecosystem, which is highly variable especially as a result agricultural management practices (Section 1.3).
- In ACTMs these effects are generally not handled. However, experimental results suggest that with a process-based approach for NH_3 emission a better representation of NH_3 concentration can be achieved (Section 1.4.2).
- Compared with other agricultural NH_3 sources, the governing role of meteorology in ammonia emission is the strongest over a grazed field (Section 1.4.2). In addition, in the case of a urine patch (emitting the majority of ammonia over a

grazed field) the soil pH changes considerably, suggesting a similarly substantial change in the soil emission potential (Section 1.3).

- The existing NH_3 exchange and NH_3 emission models applied to excretal sources
    1. either do not account for the dynamic and parallel change of NH_4^+ concentration and pH in the soil (Section 1.4.1.2),
    2. or do not account for the effect of meteorology (Section 1.4.1.3),
    3. and / or require input data that are difficult to obtain for a regional scale application (Section 1.4.1.3).

By identifying the above challenges and gaps concerning NH_3 exchange with grazed fields, the following three research questions are formulated to be addressed further in this thesis:

1. **How can an NH_3 exchange model be constructed for a urine patch that accounts for the regulating effect of temperature (and other meteorological variables) and changing emission potential of the soil, while being applicable at field scale?**
2. **How can such a urine patch model be applied to the scale of a grazed field, so that it still accounts for the main emission drivers, while being applicable for the regional scale (i.e. in ACTMs)?**
3. **How do the different meteorological variables (e.g. temperature, wind, relative humidity, precipitation… etc.) affect NH_3 exchange over a grazed field?**

To address the first question, a process-based ammonia emission model was created for a single urine patch (GAG, Generation of Ammonia from Grazing). The description of the GAG model is provided in Chapter 2, which is followed by the results from model evaluation and a comprehensive sensitivity analysis to non-meteorological factors (Chapter 3). The second question is investigated in Chapter 4. Firstly, the application of the GAG model to field scale is described, where urine patches are deposited by animals continuously. Secondly, in Chapter 4 a model evaluation based on field measurements is presented.

The third question is the focus of Chapter 5. A comprehensive sensitivity analysis was carried out in relation to the meteorological variables on both patch and field scales, with a strong emphasis on temperature-dependency. A detailed comparison of temperature sensitivity between the patch and field scale is presented, examining also the applicability of the widely-used metric for the strength of temperature-dependency, Q_{10}. In Chapter 6, a synthesis of the main findings and conclusions is provided.

Chapter 2

Development of a new ammonia exchange model for a urine patch: model formulation

2. 1. Introduction

As it was pointed out in Chapter 1, over a grazed field the great majority of emitted NH_3 originates from urine patches, rather than dung (Petersen et al., 1998, Laubach et al., 2013). Therefore, to simulate NH_3 exchange over a field, first of all, an approach is needed to simulate NH_3 emission from a single urine patch. The focus of this chapter is to outline the equations of such a modelling approach.

The soil chemical processes driving NH_3 exchange from a urine patch are controlled by: 1) the hydrolysis of the urea content of urine and 2) the subsequent emission of NH_3. Both processes strongly influence soil pH and NH_4^+, and consequently, the soil emission potential. Whilst the first process is a H^+ consuming and NH_4^+ producing process, the second does the opposite, producing H^+ and consuming NH_4^+ in the soil solution. To represent all these chemical transformations, an ideal model has to be capable of simulating soil pH, the total ammoniacal nitrogen (TAN) content of the soil and, since these are in an aqueous solution, also the water content of the soil.

In addition to soil chemistry, NH_3 emission is also affected directly by meteorology, especially temperature. This requires the application of a model framework that accounts for this dependence. For this purpose, based on the review in Chapter 1, a suitable choice is the application of a canopy compensation point model.

In this chapter, the description of a process-based NH_3 emission model for a single urine patch (GAG, Generation of Ammonia from Grazing) is presented that incorporates the soil chemical and meteorological effects mentioned above. After providing the theoretical background of GAG, the model equations are identified for the NH_3 exchange flux (Section 2.3-2.5), the TAN budget (Section 2.6), the water budget (Section 2.7) and soil pH (Section 2.8).

2. 2. Theoretical background of the GAG model

To simulate NH_3 emission over a urine patch, the GAG model calculates the TAN budget and the water budget, as well as the soil pH (H^+ - hydrogen ion - budget) under the patch. For this purpose, firstly, it was assumed that, during urination and rain events, the incoming liquid infiltrates the soil so that it fills soil pores until the wetted soil layer reaches its field capacity. On Fig. 2.1 this soil layer is referred to as "urine affected layer". After all the liquid penetrates to the soil any further downward or upward motion (capillary rise) is neglected.

It was also assumed that soil NH_3 emission occurs only from the 'source layer', the very top layer of the wetted soil column (similarly to Riedo et al., 2002, who also assumed a source layer on the top of their multilayer system), while reduced nitrogen (here the sum of NH_x and urea) that infiltrates beneath this layer is assumed to be nitrified and no longer available for NH_3 emission. This assumption allows the handling of the numerous soil pores in the source layer as a single big pore – referred hereafter as 'model soil pore' -, the liquid content of which represents the soil pores filled by liquid, while its gaseous section represents the air-filled soil pores in the source layer (Fig. 2.1). All the liquid content was assumed to be at the bottom of this model soil pore / source layer (see in more detail in Section 2.5).

The input to the TAN budget is generated by hydrolysis of the urea contained within the incoming urine, while NH_3 emission acts as a loss from the TAN budget. Soil pH is also regulated by urea hydrolysis, which is a proton (H^+) consuming process, and by NH_3 emission which is a proton producing process. The water budget is increased by rain water and the liquid content of urine, whilst it is decreased by soil evaporation.

Water is assumed to evaporate from the "evaporation layer" (as defined by Allen et al., 1998, see in more details in Section 2.7), and the soil dries from the top, that is, during evaporation a dry front moves downwards in the soil.

The model was coded in R (version 3.1.2, 2014-10-31) (R Core Team, 2012). The steps of the calculation are shown in Fig. 2.2. This figure indicates the main modules within GAG (described each in the following sections), and the variables that are carried from one module to another.

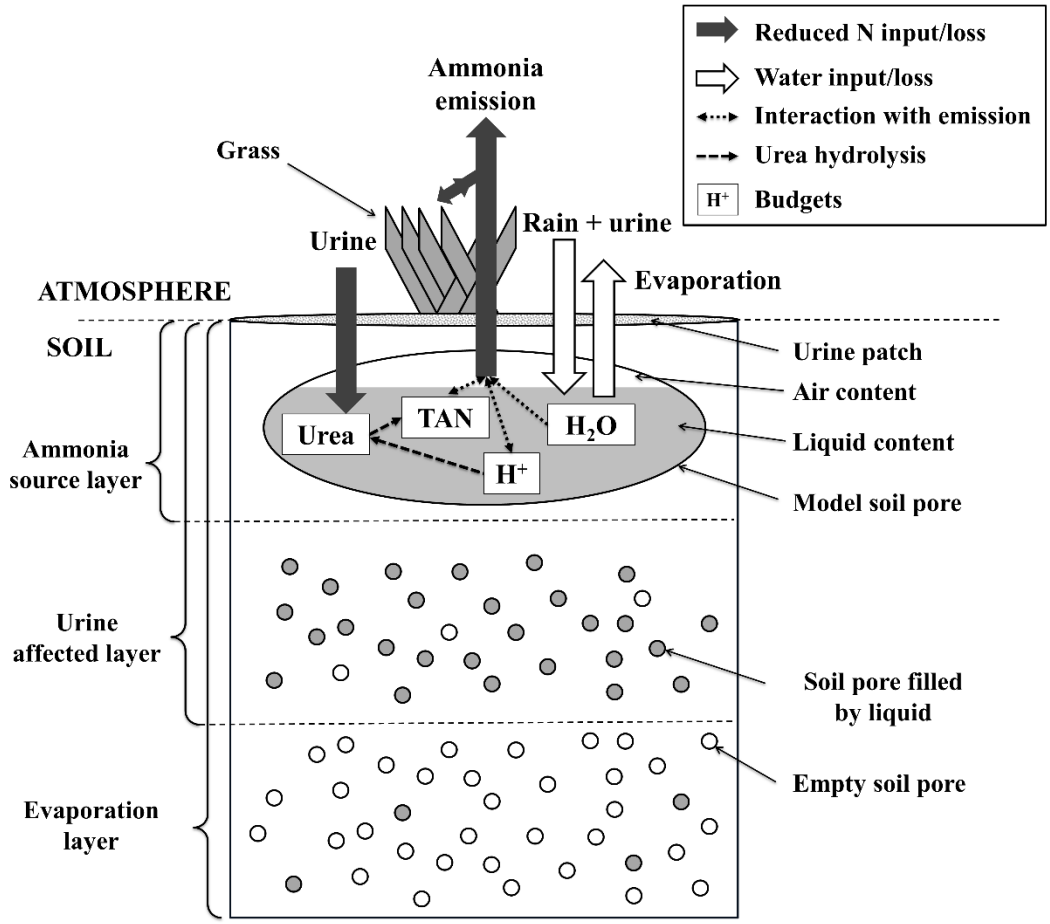

Figure 2.1. Schematic of major relationships in the GAG model. Empty soil pores in the middle layer represents that the maximum water content in the model is field capacity instead of being saturated. Whilst in the bottom layer the soil pores filled by liquid represents that the lowest water content is at the permanent wilting point instead of being completely dry. For more details on schematic see the text of Section 2.2.

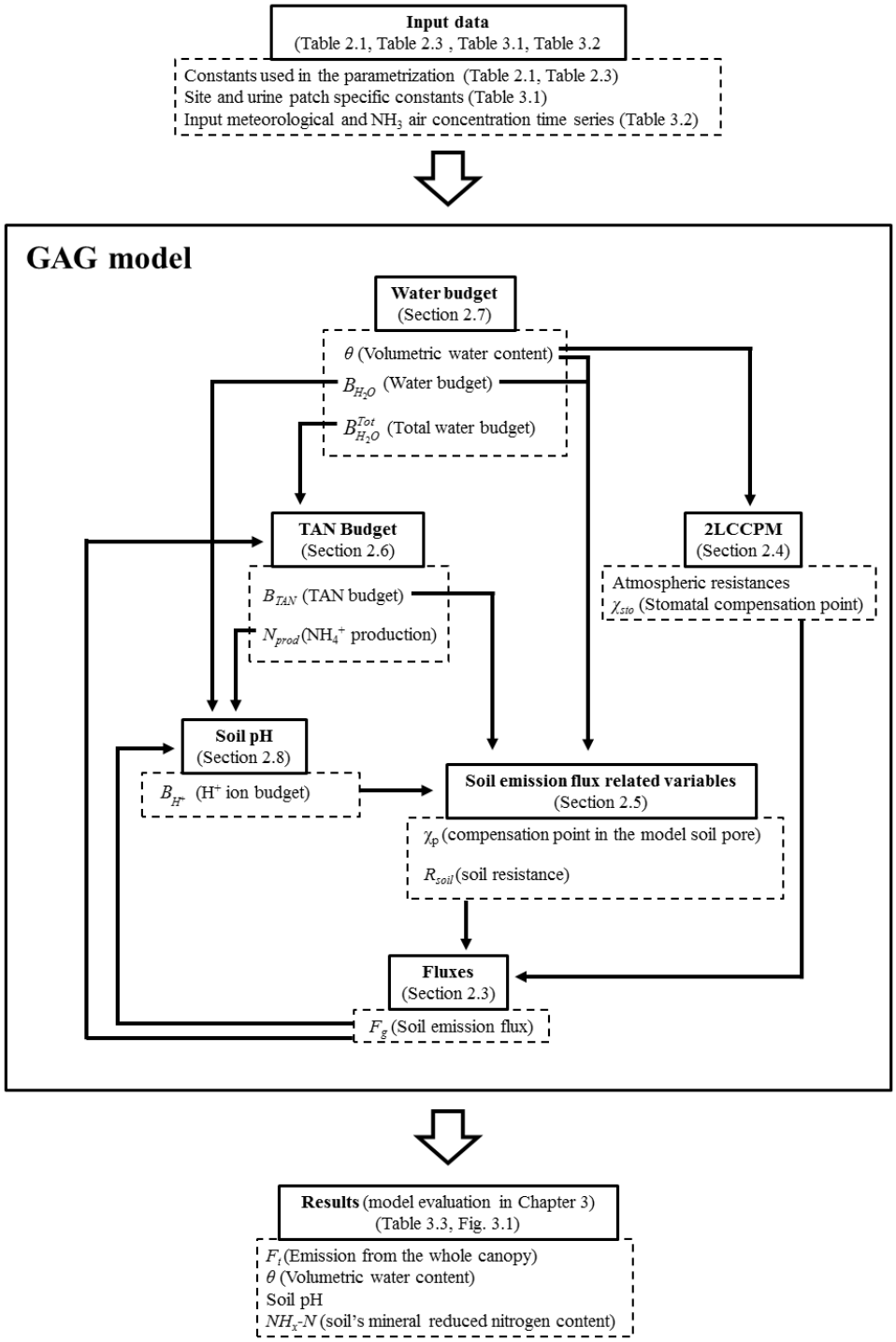

Figure 2.2. A flowchart depicting the steps of the calculation in the GAG model (middle panel), processing the input data (top panel) to the results that were evaluated in this thesis (bottom panel). The figure indicates the key variables that are carried from one module (bold heading in the middle panel) to another module(s). The figure, table and section numbers referred in the figure show where further description of the different model parts can be found in this thesis. (2LCCPM stands for Two-Layer Canopy Compensation Point Model.)

2. 3. Simulation of ammonia exchange flux

As urine deposition by grazing animals typically happens on vegetated surfaces of grassland, the effect of vegetation on the total net NH_3 flux (F_t) over a urine patch needs to be taken into account. Therefore, an ideal model should capture not just the ground flux at the soil surface (F_g) (referred hereafter as 'soil emission'), but also the exchange with foliage (F_f), including NH_3 deposition to water and waxes on the leaf surface (F_w) and the NH_3 exchange with stomata (F_{sto}).

To achieve this, the framework of the two-layer canopy compensation point model (abbreviated in this thesis to 2LCCPM) of Nemitz et al. (2001) (Fig. 2.3) was extended. The original exchange model calculates F_g assuming a bulk soil compensation point on the soil surface. Instead of calculating this compensation point, the compensation point for the model soil pore (χ_p) was derived. To capture the constraint due to soil particles on NH_3 exchange with the soil, a soil resistance (R_{soil}) was added to the original framework.

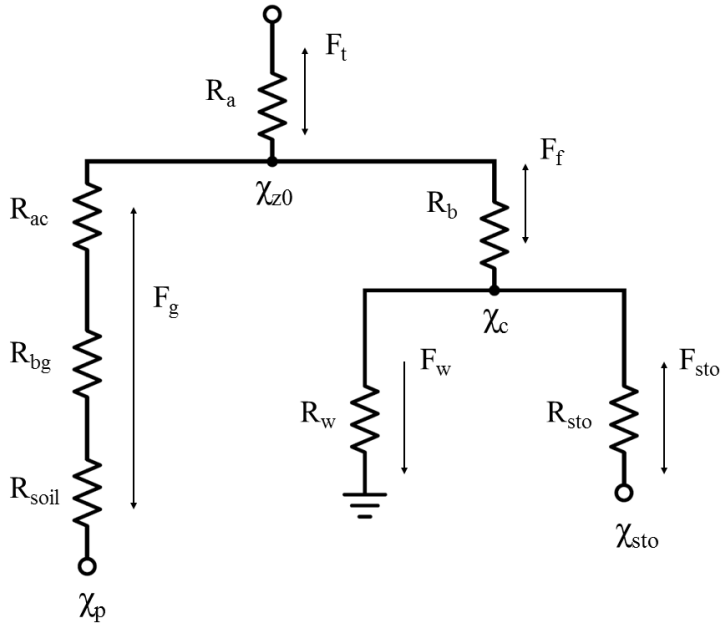

Figure 2.3. The network of gaseous resistances (R), NH_3 concentrations (χ) and NH_3 fluxes (F) used in the GAG model, which is based on the two-layer canopy compensation point model of Nemitz et al. (2001), incorporating concentration of the soil pore (χ_p) and soil resistance (R_{soil}). For the description of the other parameters in the framework see the text of this section.

Based on the analogy of electrical circuits, seven equations (Eq. (2.1)-(2.7)) can be derived to determine the five unknown fluxes (F_t, F_g, F_f, F_w, F_{sto}) and the two unknown compensation points (over the vegetation, χ_c, and over the whole canopy, χ_{z0}). Parametrising the resistances - aerodynamic (R_a) and quasi-laminar resistance (R_b) over the canopy, aerodynamic resistance within the canopy (R_{ac}), quasi-laminar resistance at the ground (R_{bg}), R_{soil}, resistance to water and wax on the leaf surface (R_w) and stomatal resistance (R_{sto}) - as well as calculating the compensation point in the soil pore and in the stomata (χ_{sto}), a solvable linear system of equations can be obtained.

$$F_t = F_g + F_f \tag{2.1}$$

$$F_f = F_w + F_{sto} \tag{2.2}$$

$$F_t = \frac{\chi_{z_0} - \chi_a}{R_a} \tag{2.3}$$

$$F_g = \frac{\chi_p - \chi_{z_0}}{R_{ac} + R_{bg} + R_{soil}} \tag{2.4}$$

$$F_f = \frac{\chi_c - \chi_{z_0}}{R_b} \tag{2.5}$$

$$F_w = \frac{-\chi_c}{R_w} \tag{2.6}$$

$$F_{sto} = \frac{\chi_{sto} - \chi_c}{R_{sto}} \tag{2.7}$$

Assuming that the changes are close to linear within a time step (1 h), and taking the air concentration of NH_3 high above the canopy (χ_a) from measurements, the system of equations was solved for every time step by using the solve function of R programming language. In this way all of the component fluxes were determined in every time step.

2. 4. Parametrisation of the resistances and stomatal compensation point (R_a, R_b, R_{ac}, R_{bg}, R_w, R_{sto}, χ_{sto})

Atmospheric resistances (R_a, R_b, R_{ac}, R_{bg}) are usually derived for homogenous (virtually infinite) surfaces, whereas the current model application is for a single, finite urine patch. The GAG model will be applied to field scale (Chapter 4), where the meteorological measurements and the canopy specific parameters, required to calculate these resistances, can be obtained for overall canopy types. Therefore, to apply atmospheric resistances to urine patches, it was assumed that all the required variables and parameters to calculate them are representative for the whole experimental site including every single urine patch on the field (also, GAG was evaluated using measurements from a field experiment, as detailed in Section 3.2).

The value of R_a (s m^{-1}) is dependent on the stability of atmosphere. An unstable stratification – when perturbing an air parcel it ascends from its initial position – favours smaller R_a, whilst a stable one – when the perturbed air parcel returns to its initial position – favours larger R_a. Atmospheric stability can be determined based on the measurements of the sensible heat flux (H, J m^2 s^{-1}); for H>0, the stratification is unstable, while for H<0, it is stable. The following parametrization of R_a was used (following Garland, 1977):

$$R_a(z_w) = \frac{u}{u_*^2} \qquad \text{if } H<0, \tag{2.8}$$

$$R_a(z_w) = \frac{u}{u_*^2} - \frac{\Psi_H\left(\frac{z_w - d}{L}\right) - \Psi_M\left(\frac{z_w - d}{L}\right)}{k u_*} \quad \text{if } H>0, \tag{2.9}$$

where u is the wind speed measured at z_w (m) height above ground, u_* (m s^{-1}) is the friction velocity, Ψ_H and Ψ_M are the stability functions for heat and momentum flux, respectively, L (m) is the Monin-Obukhov length, d is the displacement height of the vegetation, and k is the von Karman constant (see its value together with all the model constants used in the parametrization of the compensation point model in Table 2.1).

Table 2.1. Constants used in the parametrization of the 2LCCPM. References are listed in the footnotes.

Model constants	Value	Reference
For R_a and R_b		
k (von Karman constant)	0.41	
d (displacement height)	0.189 m	M
z_0 (surface roughness)	0.039 m	M
ν (kinematic viscosity)	1.56×10^{-5} m^2 s^{-1}	
D_g (diffusivity of NH_3 in air)	2.28×10^{-5} m^2 s^{-1}	S1
R (specific gas constant of dry air)	287 J kg^{-1} K^{-1}	
g (acceleration of gravity)	9.81 m s^{-2}	
c_p (heat capacity of air)	1005 J kg^{-1} K^{-1}	
For R_{ac} and R_{bg}		
α (parameter for calculating R_{ac})	65.24	M
z_l (height of the top of logarithmic wind profile)	0.1 m	N
For R_w and R_{sto}		
$R_{w(min)}$ (minimal cuticular resistance)	1 s m^{-1}	H
a (parameter for calculating R_w)	0.074	H
$\frac{D_{O_3}}{D_{NH_3}}$ (ratio of diffusivity of O_3 and NH_3)	$\frac{1}{1.6}$	S2
LAI (leaf area index)	3.5 m^2 m^{-2}	M
g_{max} (maximal stomatal conductance)	270 mmol O_3 m^{-2}	S2
g_{pot} (effect of phenological change on stomatal conductance)	1	S
g_{min} (minimal stomatal conductance)	0.1	E
α_{PAR} (parameter for calculating g_{PAR})	0.009 (μmol m^2 s^{-1})$^{-1}$	E
T_{opt} (temperature for optimal stomatal conducatnce)	26 ºC	E
T_{min} (temperature for minimal stomatal conductance)	12 ºC	E
VPD_{min} (VPD for minimal stomatal conductance)	3 kPa	E
VPD_{max} (VPD for maximal stomatal conductance)	1.3 kPa	E
For Γ_{sto}		
τ^M (decay parameter)	2.88 days	

M: Massad et al., 2010b, for summer grassland (values are available also for the other seasons)
N: Nemitz et al., 2001, for oilseed rape
H: Horváth et al., 2005, for summer, semi-natural grassland (values are available also for the other seasons)
S1: Spiller, 1989
S2: Simpson et al., 2012, for grassland
E: Emberson et al., 2000, for grassland

In the case of stable conditions, Ψ_H and Ψ_M were parametrized following Webb (1970):

$$\Psi_H = \Psi_M = \frac{-5(z_w - d)}{L}, \tag{2.10}$$

and for unstable conditions the approach of Paulson (1970) was applied:

$$\Psi_M = \ln\left(\frac{1+x}{2}\right)^2 + \ln\left(\frac{1+x^2}{2}\right) - 2\arctan x + \frac{\pi}{2}, \tag{2.11}$$

$$\Psi_H = 2\ln\left(\frac{1+x^2}{2}\right), \tag{2.12}$$

where:

$$x = \left(1 - 16\frac{z_w - d}{L}\right)^{\frac{1}{4}}. \tag{2.13}$$

In the original study on the 2LCCPM u_* and L were measured. In the absence of the measurements of these, a parametrisation should be used. As these two parameters depend on each other, an iteration was applied to calculate both. Eq. (2.14) expresses u_*, with z_0 (m) roughness length. L was derived following Eq. (2.15), where T (K) is the temperature at 2 m above ground, ρ (kg m^{-3}) is air density, c_p is the specific heat capacity of dry air, and g is the acceleration of gravity.

$$u_* = \frac{ku}{\ln\left(\frac{z_w - d}{z_0}\right) - \Psi_M\left(\frac{z_w - d}{L}\right)} \tag{2.14}$$

$$L = -\frac{Tu_*^3 \rho c_p}{kgH} \tag{2.15}$$

The values of ρ can be calculated as a function of atmospheric pressure (p, Pa) and virtual temperature (T_v, K), which is the temperature that the dry air would have if its pressure and density was the same as that of the moist air (via the ideal gas law):

$$\rho = \frac{p}{RT_v}, \tag{2.16}$$

where R is the gas constant and T_v as a function of specific humidity (SH) (for actual vapour pressure (e_a, Pa) see Eq. (2.32)) :

$$T_v = \frac{T}{1 + 0.608SH}, \tag{2.17}$$

where

$$SH = \frac{0.622e_a}{p - 0.378e_a}. \tag{2.18}$$

Based on Nemitz et al. (2001) for R_b, the formula of Owen and Thomson (1963) was used, where Re is the Reynolds number ($R_e = u_* z_0 \nu^{-1}$, with ν as kinematic viscosity) and Sc is the Schmidt number ($Sc = \nu D_g^{-1}$, with D_g as the diffusivity of NH_3 in air):

$$R_b = 1.45 \times Re^{0.24} Sc^{0.8} u_*^{-1}. \tag{2.19}$$

Following also Nemitz et al., R_{ac} was assumed to be inversely proportional to u_* ($R_{ac} = \alpha\, u_*^{-1}$). Massad et al. (2010b) recommended values for parameter α for many surface types - including grass - as well as for all of the four seasons (Table 2.1). Nemitz et al. (2001) applied a parametrisation for R_{bg} (s m^{-1}) for oilseed rape (Eq. 2.20). As the approach for calculation of this resistance for grasslands is not widely discussed in the literature, the parametrization for oilseed rape was adapted for grassland. In the GAG model, soil emission is dependent also on R_{soil}, which is larger at least by one order of magnitude than any of the atmospheric resistances. Thus, GAG is not highly sensitive to this approximation for R_{bg} (for detailed analysis of the model sensitivity see Section 3.4.1).

$$R_{bg} = \frac{\frac{\nu}{D_g} - \ln\left(\frac{\delta_0}{z_l}\right)}{k u_{*g}}, \tag{2.20}$$

where δ_0 (m) is the height where eddy and molecular diffusivity are the same in magnitude and z_l (m) is the height of the top of logarithmic wind profile (assumed to be 0.1 m as for oilseed rape). According to Schuepp (1977), δ_0 (Eq. (2.21)) is a function of friction velocity at ground level in the canopy (u_{*g}, s m^{-1}), which can be derived

from the wind speed (Eq. (2.22), as an approximation for oilseed rape by Nemitz et al., 2001).

$$\delta_0 = \frac{\nu}{k u_{*_g}} \tag{2.21}$$

$$u_{*_g} = \frac{1.68 \times u}{20} \tag{2.22}$$

The cuticular exchange of NH_3 is strongly linked to the presence of a water film on the waxy leaf surface (Flechard et al., 1999). This can form even below the saturation point for pure water vapour, as a result of condensation facilitated by hygroscopic particles on the plant surface (Burkhardt et al., 1999). Therefore, the cuticular resistance (R_w) describes the effect of this water film on NH_3 absorption. The extent to which such a thin water layer is present affects the value of R_w; however, NH_3 absorption is also dependent on the air concentration of the acidic components (especially SO_2). These compounds, decreasing the pH of the water film, favour NH_3 deposition (Flechard et al., 1999). The process is referred to as co-deposition of the different components. The modelling of this phenomenon requires the knowledge of the chemical composition of the atmosphere and substantially increases model complexity.

For a simpler approach, R_w (s m^{-1}, Eq. (2.23)) can be estimated as a function of relative humidity (*RH*, %). For this purpose – similarly also to Nemitz et al. (2001) - the formula from Massad et al. (2010b) was used (based on Sutton and Fowler, 1993). For the current model application, parameters for summer grassland were used as recommended by Massad et al. (2010b) ($R_{w(min),}$ minimal cuticular resistance and *a* for grassland as reported by Horváth et al., 2005):

$$R_w = R_{w(\min)} \times \exp\left(a\left(100 - RH\right)\right) \tag{2.23}$$

In the original description of the 2LCCPM by Nemitz et al. (2001) R_{sto} is parametrised based on Hicks et al. (1987). Instead of this, a more state-of-the-art approach was used. As in Massad et al. (2010b), the value of R_{sto} (s m^{-1}, Eq. (2.24)) was derived from the stomatal resistance to ozone ($R_{sto(O_3)}$, s m^{-1}), taking into account

the difference between the diffusivity of the two gases (D_{O3} / D_{NH3} = 1 / 1.6). On the other hand, R_{sto} (O_3) (Eq. (2.25), where 41000 is the conversion from mmol O_3 m^{-2} to m s^{-1}) was parametrised based on LAI applying the stomatal conductance (g_s, mmol O_3 m^{-2}) model of Emberson et al. (2000). For LAI, values were used based on the recommendation of Massad et al. (2010b) for grasslands.

$$R_{sto} = R_{sto}(\mathrm{O_3}) \times \frac{D_{O_3}}{D_{NH_3}} \tag{2.24}$$

$$R_{sto}(\mathrm{O_3}) = \left(\frac{g_s \times LAI}{41000} \right)^{-1} \tag{2.25}$$

Stomatal conductance Eq. (2.26) is defined based on the relative conductances that express how the openness of the stomata changes in the function of the phenological state of the plant (g_{pot}) (assuming that grass could grow equally over the year, g_{pot} = 1), light (g_{light}), temperature (g_{temp}), vapour pressure deficit (g_{VPD}) and soil water potential (g_{SWP}). The combined effect of these, through the openness of stomata, controls g_s between its maximal value (g_{max}) and its minimal value ($g_{max} \times g_{min}$):

$$g_s = g_{\max} g_{pot} \max\left\{ g_{\min}, \left(g_{light} g_{temp} g_{VPD} g_{SWP} \right) \right\}. \tag{2.26}$$

The components g_{light}, g_{temp} and g_{VPD} were derived following Emberson et al. (2000). Whilst g_{light} (Eq. (2.27)) is expressed as a function of photosynthetically active radiation (PAR, µmol m^2 s^{-1}), g_{temp} (Eq. (2.28)) and g_{VPD} (Eq. (2.29)) takes into account air temperature (^{0}C) and vapour pressure deficit (VPD, kPa), respectively. The latter is defined (Eq. (2.30)) as the difference between saturated (e_s (kPa), Eq. (2.31)) and actual vapour pressure (e_a (kPa), Eq. (2.32)).

$$g_{light} = 1 - \exp\left(-\alpha_{PAR} \times PAR\right) \tag{2.27}$$

$$g_{temp} = \min\left\{ g_{\min}, \left(1 - \left(\frac{T - T_{opt}}{T_{opt} - T_{\min}} \right)^2 \right) \right\} \tag{2.28}$$

$$g_{VPD} = \begin{cases} g_{\min} & if \quad VPD > VPD_{\min} \\ 1 & if \quad VPD < VPD_{\max} \\ \left(\frac{(1-g_{\min})(VPD_{\min} - VPD)}{VPD_{\min} - VPD_{\max}} + g_{\min} \right) & otherwise \end{cases} \quad (2.29)$$

$$VPD = e_s - e_a \quad (2.30)$$

$$e_s = 0.6108 \times \exp\left(\frac{17.27 \times T}{T + 237.3} \right) \quad (2.31)$$

$$e_a = e_s \frac{RH}{100} \quad (2.32)$$

Since the GAG model simulates the volumetric water content of the soil (θ, $m^3\ m^{-3}$; see the formulation in Section 2.6) and the approach by Emberson et al. (2000) for g_{SWP} (Eq. (2.33)) is based on the soil water potential, a different approach was applied. The formulation by Simpson et al. (2012) was adapted, who defined a soil moisture index ($S_{MI,}$ Eq. (2.34)), based on θ, influenced also by the soil's permanent wilting point (θ_{pwp}) and field capacity (θ_{fc}).

$$g_{SWP} = \begin{cases} 1 & if\ S_{MI} \geq 0.5 \\ 2 \times S_{MI} & if\ S_{MI} < 0.5 \end{cases} \quad (2.33)$$

$$S_{MI} = \frac{\theta - \theta_{pwp}}{\theta_{fc} - \theta_{pwp}} \quad (2.34)$$

Finally, the stomatal compensation point, as the equilibrium gaseous NH_3 concentration in the stomata, can be derived from the temperature dependent form of Henry's law for dissolution of NH_3 (R1 in Table 2.2) and the dissociation coefficient of NH_4^+ (R4 in Table 2.2). Based on these, Nemitz et al. (2000) derived χ_{sto} (Eq. (2.35)) as a function of temperature (K) and the emission potential of the stomata (Γ_{sto}), which equals to the ratio of the NH_4^+ and H^+ concentrations (mol dm^{-3}) in the apoplastic fluid in the stomatal cavity.

Table 2.2. Chemical equations – indicated by R0-5 - simulated within the model, (where applicable) their equilibrium coefficient according to definition (K for dissociation and H for dissolution) and the coefficients expressed as the function of soil temperature (T_{soil} (K)) as well as their references (squared brackets denotes that the concentration of every compound is in mol dm^{-3}).

Chemical equation	Equilibrium coefficient	Equilibrium coefficient as a function of temperature	Reference
R0: $CO(NH_2)_2 + 2H_2O + H^+ \rightarrow 2NH_4^+ + HCO_3^-$	-	- -	
R1: $NH_4^+ \Leftrightarrow NH_{3(aq)} + H^+$	$K(NH_4^+) = \frac{[NH_{3(aq)}][H^+]}{[NH_4^+]}$	$K(NH_4^+) = 5.67 \times 10^{-10} \exp\left(-6286\left(\frac{1}{T_{soil}} - \frac{1}{298.15}\right)\right)$	Bates and Pinching, 1949
R2: $HCO_3^- \Leftrightarrow CO_3^{2-} + H^+$	$K(HCO_3^-) = \frac{[H^+][CO_3^{2-}]}{[HCO_3^-]}$	$\lg(K(X)) = -\left(\left(\frac{a}{T_{soil}}\right) + (b \times T_{soil}) - c\right)$ a= 2902.39 b=0.02379 c=6.4980	Harned and Scholes, 1941
R3: $H_2CO_3 \Leftrightarrow HCO_3^- + H^+$	$K(H_2CO_3) = \frac{[HCO_3^-][H^+]}{[H_2CO_3]}$	a=3404.71 b=0.032786 c=14.8435	Harned and Davis, 1943
R4: $NH_{3(aq)} \Leftrightarrow NH_{3(g)}$	$H(NH_{3(g)}) = \frac{[NH_{3(aq)}]}{[NH_{3(g)}]}$	$H(NH_{3(g)}) = 56 \times \exp\left(4092 \times \left(\frac{1}{T_{soil}} - \frac{1}{298.15}\right)\right) \times c_{con}$	Dasgupta and Dong, 1986
R5: $H_2CO_3 \Leftrightarrow CO_{2(g)}$	$H(CO_{2(g)}) = \frac{[H_2CO_3]}{[CO_{2(g)}]}$	$H(CO_{2(g)}) = 0.034 \times \exp\left(2400 \times \left(\frac{1}{T_{soil}} - \frac{1}{298.15}\right)\right) \times c_{con}$	Wilhelm et al., 1977
		(where $c_{con} = \left(\frac{0.001 \frac{m^3}{dm^3}}{8.314 \frac{J}{Kmol}} \times \frac{1.013 \times 10^5 \frac{Pa}{atm}}{T_{soil}}\right)^{-1}$ is the conversion from atm $(mol\ dm^{-3})^{-1}$ to $(mol\ dm^{-3})\ (mol\ dm^{-3})^{-1}$)	

$$\chi_{sto} = \frac{161500}{T} \times \exp\left(\frac{-10380}{T}\right) \times \Gamma_{sto} \quad (2.35)$$

In the original 2LCCPM by Nemitz et al. (2001), Γ_{sto} is an input parameter from measurements. Since the measurement of Γ_{sto} is very difficult (David et al., 2009, Mattsson et al., 2009), in models it is usually handled as a constant, parametrised or simulated by a sub-model (e.g. Massad et al., 2010a, Wu et al., 2009). As there were no Γ measurements in the experiment and over a urine patch NH_3 exchange is dominated by soil emission, the parametrisation of Γ_{sto} recommended by Massad et al. (2010b) was chosen for grazed fields (Eq. (2.36)). This equation assumes that Γ_{sto} reaches its maximum, $\Gamma_{sto}(max)$ right after N application (in this case after urine deposition), and then decays exponentially with time (t_i indicates the time step, the hours spent after urine deposition, with a decay parameter τ set at 2.88×24 hours).

$$\Gamma_{sto}(t_i) = \Gamma_{sto}(\max) \times \exp\left(-\frac{t_i - 1}{\tau}\right) \quad (2.36)$$

Massad et al. (2010b) proposed a parametrization, describing an empirical relationship (Eq. (2.37)) between the total N applied to the ecosystem (N_{app} in kg N ha^{-1}, see Eq. (2.38)) and the observed maximal stomatal NH_3 emission potential ($\Gamma_{sto}(max)$). To apply the formula for a urine patch, N_{app} was calculated as the total N content of the urine - the volume of urine (W_{urine}, dm^3) multiplied by its nitrogen content (c_N, g N dm^{-3}) - divided by the area of the urine patch (A_{patch}, m^2) (with 10 as a conversion factor between the different units).

$$\Gamma_{sto}(\max) = 12.3 \times N_{app} + 20.3 \quad (2.37)$$

$$N_{app} = \frac{W_{urine} \times c_N}{A_{patch}} \times 10 \quad (2.38)$$

2. 5. Simulation of the soil pore (χ_p) compensation point and the soil resistance (R_{soil})

The simulation of χ_p (mol dm^{-3}) is very similar in theory to that of χ_{sto}. Similarly, it is derived from Henry's law for NH_3 dissolution and the dissociation coefficient of NH_4^+. In this way Eq. (2.39) can be obtained (Nemitz et al., 2000), where T_{soil} is the soil temperature (K) and Γ_p is the ratio of the NH_4^+ and H^+ concentration in the model soil pore. In Eq. (2.40) Γ_p is expressed as a function of TAN concentration ([TAN] = $[NH_4^+]$ + $[NH_{3(aq)}]$) based on the definition of dissociation constant ($K(NH_4^+)$, second column of Table 2.2 and its temperature dependent form in the third column). This formulation equals to the basic definition of Γ ($[NH_4^+]/[H^+]$), but it enables an easier handling of the reduced nitrogen species in the solution, considering them together as TAN.

$$\chi_p = \frac{161500}{T_{soil}} \times \exp\left(\frac{-10380}{T_{soil}}\right) \times \Gamma_p \tag{2.39}$$

$$\Gamma_p = \frac{[TAN]}{K(NH_4^+) + [H^+]} \tag{2.40}$$

TAN and H^+ concentration (both in mol dm^{-3}) are derived from the TAN budget (B_{TAN}, g N) and H^+ budget (B_{H+}, mol), respectively, according to their mass ratio with water budget (B_{H2O}, dm^3) (Eqs. (2.41)-(2.42)), where 14 is the molar mass of nitrogen). All budgets are simulated within GAG (B_{TAN}: Section 2.6, B_{H+}: Section 2.8, and B_{H2O}: Section 2.7).

$$[TAN] = \frac{\frac{B_{TAN}}{14}}{B_{H_2O}} \tag{2.41}$$

$$[H^+] = \frac{B_{H^+}}{B_{H_2O}} \tag{2.42}$$

For R_{soil} (s m^{-1}) the approach by Laubach et al. (2012) was applied, as expressed in Eq. (2.43). This captures the effect of soil depth (Δz), that is, from how deep the soil NH_3 emission occurs on average. In the study of Laubach et al. Δz is referred as 'source depth', and in GAG model it was considered as the thickness of the source layer, assuming that all of the liquid is at the bottom of this layer. The model experiments by Laubach et al. suggested that the distribution of Δz has a median of 0.002 m with an

uncertainty factor of 2 and a similar value was used in the study of Riedo et al. (2002) as well.

In reality the thickness of the source layer changes in parallel with the moisture content of the top soil layer. However, its approximation, due to the thinness of the layer, is difficult. Therefore, at the moment GAG operates with a constant Δz of 0.004 m. In Section 3.4.2 the model sensitivity was tested also to Δz.

$$R_{soil} = \frac{\Delta z}{\xi D_g} \tag{2.43}$$

According to this approach, R_{soil} is inversely proportional to soil tortuosity (ξ) and diffusivity of NH_3 (D_g). For ξ, Laubach et al. (2012) suggested the parametrisation by Millington and Quirk (1961), based on the volumetric water content as well as porosity (θ_{por}):

$$\xi = \frac{\left(\theta_{por} - \theta\right)^{\frac{10}{3}}}{\theta_{por}{}^{2}} \tag{2.44}$$

2. 6. Simulation of the TAN budget under the urine patch (B_{TAN})

The amount of TAN in the model soil pore in a given time step t_i ($B_{TAN}(t_i)$, g N), depends on its value in the previous time step ($B_{TAN}(t_{i-1})$, g N) and is controlled by the amount of TAN produced during urea hydrolysis (N_{prod}, g N) and soil NH_3 emission (F_g, g N m^{-2}) calculated in the previous time step (Eq. (2.45)). It was assumed that B_{TAN} before urine deposition is negligibly small compared to that of after urine deposition. Therefore, its initial value is set to 0. The model does not allow to emit more NH_3 than TAN is available in the source layer, as it is described by Eq. (2.46).

$$B_{TAN}(t_i) = N_{prod}(t_i) + B_{TAN}(t_{i-1}) - F_g(t_{i-1}) \times A_{patch} \tag{2.45}$$

$$F_g = \begin{cases} \dfrac{B_{TAN}(t_{i-1})}{A_{patch}} & if\ \left(B_{TAN}(t_{i-1}) - F_g(t_{i-1}) \times A_{patch}\right) < 0 \\ \dfrac{\chi_p - \chi_{z_0}}{R_{ac} + R_{bg} + R_{soil}} & otherwise \end{cases} \tag{2.46}$$

TAN production depends on the current amount of urea nitrogen within the model soil pore (B_{urea}, g N), as well as soil temperature (T_{soil}, ^{0}C). For N_{prod} Sherlock and Goh (1985) suggested an empirical formula (Eq. (2.47)), with a temperature dependent parameter (A_h, Eq. (2.48)) and a hydrolysis constant (k_h).

$$N_{prod}(t_i) = B_{urea}(t_i)(1 - \exp(A_h(t_i) \times k_h)) \tag{2.47}$$

$$A_h(t_i) = 0.25 \times \exp(0.0693 \times T_{soil}(t_i)) \tag{2.48}$$

Urea nitrogen content in a given time step (Eq. (2.49)) is determined by its value in the previous time step, the loss as conversion to TAN ($-N_{prod}$) and, in the first time step, the amount of urea nitrogen added (U_{add}, g N) with the incoming urine. In U_{add} (Eq.(2.50)) the dilution effect of rain on the nitrogen concentration of urine is taken into account, if it occurs in the first time step together with urine application. The amount of nitrogen infiltrating to the source layer with the incoming liquid can be calculated as the product of the diluted concentration (c_N^{Dil}, g N dm^{-3}) and the amount of infiltrating liquid (i.e. the difference in the water budget after infiltration: $B_{H2O}(t_1)$-$B_{H2O}(t_0)$). The concentration after dilution (Eq. (2.51)) can be determined as the total amount of N in the urine applied (nitrogen concentration of urine, c_N - g N dm^{-3} - multiplied by the volume of urine, W_{urine} - dm^3) divided by the volume of the total incoming liquid (the sum of W_{urine} and the amount of the rain water, W_{rain}).

$$B_{urea}(t_i) = B_{urea}(t_{i-1}) - N_{prod}(t_{i-1}) + U_{add}(t_i) \tag{2.49}$$

$$U_{add} = c_N^{Dil}\left(B_{H_2O}(t_1) - B_{H_2O}(t_0)\right) \tag{2.50}$$

$$c_N^{Dil} = \left(\frac{c_N W_{urine}}{W_{urine} + W_{Rain}}\right) \tag{2.51}$$

2. 7. Simulation of the water budget under the urine patch (θ, B_{H2O}, B_{H2O}(max))

After urine deposition, actual volumetric water content (θ, Eq. (2.52)) of the source layer can be expressed as the volume of the water in the layer ($B_{H2O,}$ dm^3) divided by

the volume of the soil column under the urine patch with a surface area of A_{patch} (m^2) and a thickness of Δz (m) (in Eq. (2.52), 1000 is the conversion from m^3 to dm^3).

$$\theta = \frac{B_{H2O}}{1000 \times \Delta z \times A_{patch}} \tag{2.52}$$

The actual water content of the soil at any time step ($B_{H20}(t_i)$, Eq. (2.53)) depends on the water content in the previous time step, soil evaporation ($W_{evap,}$ dm^3), rain events and in the very first time step the volume of urine (e.g. if the volume of the urine is 1.5 dm^3 then $W_{urine}(t_1)$=1.5 dm^3, otherwise 0). Both the volume of evaporation from the source layer and incoming rain to this layer are derived as the product of A_{patch} and soil evaporation (with E ($dm^3\ m^{-2}$): $W_{evap} = E \times A_{patch}$) as well as precipitation (with P ($dm^3\ m^{-2}$): $W_{rain} = P \times A_{patch}$) for a m^2, respectively.

In Eq. (2.53) the first condition ($Cond_A$) expresses that it is not possible for more water to be evaporated from the source layer than the minimal water content (water content of the layer at the permanent wilting point, θ_{pwp}: $B_{H2O}(min)$ (dm^3), Eq. (2.54)). On the other hand, (expressed by $Cond_B$) this layer cannot store more water than the maximal water content (water content of the layer at field capacity, θ_{fc}: $B_{H2O}(max)$ (dm^3), Eq.(2.55)). The excess water is assumed to infiltrate to the deeper soil layers. In Eq. (2.54) and (2.55) 1000 is the conversion from m^3 to dm^3.

$$B_{H_2O}(t_i) = \begin{cases} B_{H_2O}(\min) + W_{rain}(t_i) + W_{urine}(t_i) & if \quad Cond_A \\ B_{H_2O}(\max) & if \quad Cond_B \\ B_{H_2O}(t_{i-1}) - W_{evap}(t_{i-1}) + W_{rain}(t_i) + W_{urine}(t_i) & otherwise \end{cases} \tag{2.53}$$

$$Cond_A: \quad \left(B_{H_2O}(t_{i-1}) - W_{evap}(t_{i-1})\right) < B_{H_2O}(\min)$$
$$Cond_B: \quad B_{H_2O}(t_{i-1}) - W_{evap}(t_{i-1}) + W_{rain}(t_i) + W_{urine}(t_i) > B_{H_2O}(\max)$$

$$B_{H_2O}(\min) = 1000 \times \Delta z \times A_{patch} \times \theta_{pwp} \tag{2.54}$$

$$B_{H_2O}(\max) = 1000 \times \Delta z \times A_{patch} \times \theta_{fc} \tag{2.55}$$

To estimate the soil evaporation the dual crop method of Allen et al. (1998) was adapted. Although this approach might be less accurate than a comprehensive energy

balance model (driving NH_3 and water vapour flux at the same time), numerically it is easier to handle. The approach firstly calculates the reference evapotranspiration (ET_0, evaporation from soil + transpiration by plants) for a reference surface (a surface covered by grass with a height of 0.12 m, a fixed surface resistance to water exchange of 70 s m^{-1} and albedo of 0.23). Then, defining a 'crop coefficient' (K_c) for the actual surface, it gives an estimation for the actual evapotranspiration ($ET = K_c \times ET_0$). In the final step, K_c is split to a coefficient for transpiration and a coefficient for soil evaporation ($K_c = K_{cb} + K_e$).

In GAG for ET_0 a slightly modified form of the Penman-Monteith equation (Eq. (2.56), Walter et al., 2001) was incorporated compared with that of Allen et al. (1998). In this way the model accounts for the effect of change of day and night on evapotranspiration (C_d, Eq. (2.57)). For the formulation of Δ (the slope of the saturation vapour pressure temperature relationship), R_n (net radiation), G (soil heat flux) and γ (psychrometric constant), see Allen et al. (1998) for details.

$$ET_0 = \frac{0.408 \times \Delta(R_n - G) + \gamma \frac{37}{T + 273.15} u(e_s - e_a)}{\Delta + \gamma(1 + C_d u)} \tag{2.56}$$

$$C_d = \begin{cases} 0.24 & if \quad R_n > 0 \quad (daytime) \\ 0.96 & otherwise \quad (nighttime) \end{cases} \tag{2.57}$$

When calculating soil evaporation ($E = K_e \times ET_0$) the following assumptions were made:

1. According to Allen et al. (1998) soil evaporation occurs from the wetted, uncovered soil fraction (f_w). Applying the evapotranspiration model for a urine patch, the whole modelled soil will be wet. In addition, it was assumed that the percentage of the whole field covered by vegetation (f_c) was the same over a urine patch. In this way $f_w = (1 - f_c)$ for a urine patch.
2. Following the recommendations of Allen et al. (1998), it was assumed that there was no runoff, no transpiration from the evaporation layer (including the NH_3 source layer) and no 'deep percolation' (which occurs when θ exceeds θ_{fc}, but in GAG θ_{fc} is assumed to be the maximum of θ). According to Allen et al.

(1998), the top soil layer – to which GAG is applied – even in the case of a strong rain event that could cause runoff, would be probably filled up by the incoming water to $\theta_{fc.}$ Thus, the effect of runoff on the B_{H2O} can be ignored. Based on the same study, in the case of shallow rooted plants, like grass, the influence of transpiration compared to the other water inputs and evaporation in the top soil layer is negligibly small.

3. In the original evaporation approach by Allen et al. (1998) it was assumed that soil evaporation attenuated when more water was evaporated from the soil evaporation layer (characterized by a thickness of Δz_E) than the amount of 'readily evaporable water' (*REW*). The study of Allen et al. (1998) recommends *REW* values for different soil types defined by their θ_{fc} and θ_{pwp}. However, for the site whose observations were used in the model evaluation (see Section 3.2), the recommended θ_{fc} and θ_{pwp} values were not in accordance with the measurements. Therefore *REW* was calculated as the water content of the evaporation layer halfway between θ_{fc} and θ_{pwp} (Eq. (2.58)). The model sensitivity is examined to this choice of *REW* in Section 3.4.4.

$$REW = 1000\left(\theta_{fc} - 0.5\left(\theta_{fc} - \theta_{pwp}\right)\right) \times \Delta z_E \qquad (2.58)$$

The model constants used in the soil evaporation estimation are listed in Table 2.3.

Table 2.3. Constants used in the parametrization of soil evaporation.

Constants	**Value**
H (canopy height)[1]	0.3 m
K_{cb}(Tab) (coefficient)[2]	0.7
Δz_E (thickness of evaporation layer)[2]	0.125 m

[1]recommended by Massad et al., 2010b for grass
[2]recommended by Allen et al., 1998 (for extensively grazed pasture)

2. 8. Simulation of soil pH (B_{H+})

After urine deposition, soil pH is affected by two main reactions: urea hydrolysis and NH_3 emission. When a urea molecule is decomposed (based on R0 in Table 2.2) an H^+

ion is consumed, producing two NH_4^+ ions and a bicarbonate ion (HCO_3^-). In the early stages of urea hydrolysis, when a large amount of urea is hydrolysed, a large amount of H^+ is required, resulting in a peak of soil pH (minimum of soil H^+ concentration). This triggers the dissociation of the produced NH_4^+ and consequently the formation of gaseous NH_3, which also leads to an emission peak shortly after urine deposition. Once the majority of urea has been hydrolysed, NH_3 emission may still continue. To balance the lost gaseous NH_3, more NH_4^+ dissociates, resulting in H^+ production, which tends to compensate the H^+ consumption associated with urea hydrolysis.

According to Sherlock and Goh (1985) – as also outlined in Chapter 1 -, after a rapid increase, soil pH usually peaks around 6-48 hours after urine deposition (referred to as 'first stage' of emission). Subsequently, the pH tends to drop for the reasons explained above over a period of about 2-8 days (second stage). Sherlock and Goh also identified two further stages: a 1-3 week long constant phase (third stage) when soil pH does not change considerably and, finally, a phase (fourth stage) with a moderate decline in soil pH, regulated by the nitrification of TAN.

As Sherlock and Goh (1985) pointed out, the bulk of TAN is volatilized over the first and second periods, and nitrification is a significantly slower process than NH_3 volatilization (see the cited references in the study of Sherlock and Goh), in the GAG model the effect of nitrification is neglected. In addition, the chemical influence of the solid material of the soil was taken into account in the soil buffering capacity (as explained later in this section). Apart from this, the solid material of the soil was assumed to be chemically inert, and consequently, NH_3 emission from soil is only affected by the composition of urine solution.

Whitehead et al. (1989) showed that not only urea but other urinary nitrogen components, such as allantoin, creatine and creatinine can contribute to NH_3 emission through their decomposition. However, Whitehead et al. (1989) found that only allantoin can have a comparable influence on NH_3 volatilization (from the solutions of these compounds with the same N concentration, over 8 days 15% of the applied N was emitted from urea and 11% from the allantoin); that of the other two components, creatine and creatinine, is rather small (over 8 days 4% and less than 1% of the applied

N was emitted as NH_3, respectively). In addition, according to Dijkstra et al. (2013) the proportion of allantoin in urinary nitrogen is considerably lower than that of urea, 2.2-14.2% compared to 57.8-93.5% and the proportions for creatine and creatinine are even lower.

Therefore, to further focus our model onto the key reactions, urine chemistry is simulated considering only the water and urea available in the beginning, and the products of urea breakdown afterwards. In this way, the reactions taken into account in the change of soil pH are listed in Table 2.2: urea hydrolysis (R0), NH_4^+ dissociation (R1), dissociation of HCO_3^- and H_2CO_3 (carbonic acid) (R2 and R3, respectively), formation of gaseous NH_3 and CO_2 (carbon dioxide) (R4 and R5, respectively). However, considering that soil is a buffered system, a soil buffering capacity (β mol H^+ (pH unit)$^{-1}$ dm^{-3}) was also incorporated.

Buffering capacity moderates the change of H^+ ion concentration. When H^+ ions are produced in the system to balance this change H^+ ions are consumed by buffers, and similarly, when H^+ ions are consumed in the system, buffers releases H^+ ions. In the model this buffering effect is expressed by the term of $\beta_{patch}(\mathrm{pH}(t_i)-\mathrm{pH}(t_{i-1}))$ in Eq. (2.66). This term is positive when the H^+ ion concentration decreases (pH increases), and it is negative in the opposite case. The value of β was defined during test simulations with GAG. It was found, that the model represents the measured pH the best with a β of 0.021 mol H^+ (pH unit)$^{-1}$ dm^{-3}. To obtain the buffering effect in the volume of the model soil pore $\beta_{patch} = \beta \times A_{patch} \times \Delta z$ was calculated. For a sensitivity analysis to β see Section 3.4.3.

As urine is a relatively concentrated solution, non-ideal ionic behaviour may have an effect on the chemical equilibria. To explore this influence in the model, a simulation was carried out with the maximum activity coefficients derived for the highest ion concentrations (0.2 mol dm^{-3}) published by Kielland (1937) (the highest ionic concentration in the modelled solution was 0.14 mol dm^{-3}). With this modification, the difference, in the total NH_3 emission was - 4.7% and the average change in pH was - 0.019. Since the ion concentration decreases toward the end of the

modelling period, and consequently, the activity coefficients converge to 1, the effect of non-ideal behaviour in the solution was neglected.

Thirteen equations were defined to calculate soil pH (Eqs. (2.59)-(2.71)). Eight of these (Eqs. (2.59)-(2.66)) are predictive equations, where B_X (mol) is the budget of the component X in the urine solution and r_{Rx} (mol) is the production or consumption of the compound predicted by the given equation in the reaction X (following the numbering of reactions in Table 2.2). Variables i_N and i_C indicate the nitrogen and carbon input generated during urea hydrolysis, respectively. The nitrogen input is the same as N_{prod} but in mol ($i_N = N_{prod} / 14$) and based on the stoichiometry of R0 (Table 2.2), $i_C = i_N / 2$.

The remaining five equations (Eqs. (2.67)-(2.71)) describe the equilibrium in every time step. These were derived by reorganizing the equations in the second column in Table 2.2, where, for a dissolved component X: $[X] = B_x / B_{H2O}$ and for a gaseous component $X_{(g)}$: $[X_{(g)}] = B_{X(g)} / V_{air}$. V_{air} is the volume of the air in the model soil pore, which can be calculated as the volume of the space in the model soil pore that is not taken up by the liquid content ($V_{air} = \theta_{por} A_{patch} \Delta z \times 1000 - B_{H2O}$, where 1000 is the conversion between m^3 and dm^3).

Variables B_C and B_N represent the total inorganic carbon and nitrogen budget in the urine solution, respectively. Both can be derived as a sum of the different components and their input (by urea breakdown) and loss (via emission as gas) (Eqs. (2.72) and (2.73)).

$$B_{H_2CO_3}(t_i) = B_{H_2CO_3}(t_{i-1}) + (-r_{R5} + r_{R3}) \tag{2.59}$$

$$B_{HCO_3^-}(t_i) = B_{HCO_3^-}(t_{i-1}) + (-r_{R2} - r_{R3} + i_C(t_i)) \tag{2.60}$$

$$B_{CO_3^{2-}}(t_i) = B_{CO_3^{2-}}(t_{i-1}) + r_{R2} \tag{2.61}$$

$$B_{CO_{2(g)}}(t_i) = B_{CO_{2(g)}}(t_{i-1}) + r_{R5} \tag{2.62}$$

$$B_{NH_4^+}(t_i) = B_{NH_4^+}(t_{i-1}) + (-r_{R1} + i_N(t_i)) \tag{2.63}$$

$$B_{NH_{3(aq)}}(t_i) = B_{NH_{3(aq)}}(t_{i-1}) + (r_{R1} - r_{R4}) \tag{2.64}$$

$$B_{NH_{3(g)}}(t_i) = B_{NH_{3(g)}}(t_{i-1}) + \left(r_{R4} - \frac{F_g(t_{i-1}) \times A_{patch}}{14} \right) \tag{2.65}$$

$$B_{H^+}(t_i) = B_{H^+}(t_{i-1}) - i_C(t_i) + (-r_{R3} + r_{R2} + r_{R1}) + \beta_{patch}(pH(t_i) - pH(t_{i-1})) \tag{2.66}$$

$$K(NH_4^+)(t_i) B_{H_2O}(t_i) B_{NH_4^+}(t_i) - B_{H^+}(t_i) B_{NH_{3(aq)}}(t_i) = 0 \tag{2.67}$$

$$K(CO_3^-)(t_i) B_{H_2O}(t_i) B_{HCO_3^-}(t_i) - B_{H^+}(t_i) B_{CO_3^{2-}}(t_i) = 0 \tag{2.68}$$

$$K(H_2CO_3)(t_i) B_{H_2O}(t_i) B_{H_2CO_3}(t_i) - B_{H^+}(t_i) B_{HCO_3^-}(t_i) = 0 \tag{2.69}$$

$$\left(H(CO_{2(g)})(t_i) \frac{B_{H_2O}(t_i)}{V_{air}(t_i)} + 1 \right) B_{H_2CO_3}(t_i) + H(CO_{2(g)})(t_i) \frac{B_{H_2O}(t_i)}{V_{air}(t_i)} B_{HCO_3^-}(t_i) +$$

$$+ \mathrm{H}(\mathrm{CO}_{2(g)})(t_i) \frac{\mathrm{B}_{\mathrm{H_2O}}(t_i)}{\mathrm{V}_{\mathrm{air}}(t_i)} \mathrm{B}_{\mathrm{CO_3^{2-}}}(t_i) = \mathrm{H}(\mathrm{CO}_{2(g)})(t_i) \frac{\mathrm{B}_{\mathrm{H_2O}}(t_i)}{\mathrm{V}_{\mathrm{air}}(t_i)} \mathrm{B}_{\mathrm{C}}(t_i) \tag{2.70}$$

$$\left(H(NH_{3(g)})(t_i) \frac{B_{H_2O}(t_i)}{V_{air}(t_i)} + 1 \right) B_{NH_{3(aq)}}(t_i) + H(NH_{3(g)})(t_i) \frac{B_{H_2O}(t_i)}{V_{air}(t_i)} B_{NH_4^+}(t_i) =$$

$$= H(NH_{3(g)})(t_i) \frac{B_{H_2O}(t_i)}{V_{air}(t_i)} B_N(t_i) \tag{2.71}$$

$$B_C(t_i) = B_{H_2CO_3}(t_{i-1}) + B_{HCO_3^-}(t_{i-1}) + B_{CO_3^{2-}}(t_{i-1}) + B_{CO_2}(t_{i-1}) + i_C(t_i) \tag{2.72}$$

$$B_N(t_i) = B_{NH_{3(aq)}}(t_{i-1}) + B_{NH_4^+}(t_{i-1}) + B_{NH_{3(g)}}(t_{i-1}) + i_N(t_i) - \frac{F_g(t_{i-1}) \times A_{patch}}{14} \tag{2.73}$$

Although references can be found in the literature for measurements of CO_2 emission from urine patches (e.g. Wang et al., 2013, Ma et al., 2006 and Lin et al., 2009), it was considered that the driving processes behind them are not well-enough described for an hourly model application. Therefore, in the case of carbon budget (Eq. (2.72)) a term for CO_2 emission is not assumed in the basic GAG model, but the effect of CO_2 emission was tested in Section 3.4.3. The dissociation coefficients ($K(X)(t_i)$)

and Henry constants ($H(X(g))(t_i)$) for the given t_i time step were derived as a function of actual soil temperature (third column of Table 2.2).

For a given $B_{H+}(t_i)$ Eqs. (2.59)-(2.65) and Eqs. (2.67)-(2.71) constitute a linear system of equations (12 equations, and seven $B_X(t_i)$ budgets and five r_{Rx} consumptions/productions as unknowns). As $B_{H+}(t_i)$ is unknown, a solution with a particular value of B_{H+} (indicated as B_{H+}^*) has to be found for this equation system, whose roots also satisfy Eq.(2.66), giving back B_{H+}^*. To find this B_{H+}^*, the uniroot function of programming language R was used. B_{H+}^* provides the H^+ budget in the given time step from which pH can be calculated as $pH = -\log_{10} (B_{H+}^* / B_{H2O})$.

2. 9. Conclusions

In the present chapter a process-based NH_3 exchange model for a single urine patch has been described. The model incorporates the main drivers of the process: the effect of meteorology and soil chemistry. The meteorological dependence was taken into account in a canopy compensation model. For this purpose the two-layer canopy compensation point model by Nemitz et al. (2001) was applied, extended with a soil resistance and a compensation point in the model soil pore. The variability in soil chemistry was represented by the dynamic simulation of soil pH, TAN budget and water budget of the soil under the urine patch.

It can be concluded that the model is ready to be evaluated using measurement data. In addition, it was pointed out that the sensitivity analysis should have a special focus on the parameters assumed in this chapter: Δz and β. Furthermore, it has to be also investigated, how the model results are affected by the exclusion of CO_2 as well as the parametrization of R_{bg} and REW. These simulations were carried out in Chapter 3 accompanied by experiments based on further modelling aspects.

Chapter 3

Model evaluation and uncertainties

3. 1. Introduction

In Chapter 2 the description of the GAG model was presented. To assess the model performance and identify the uncertainties, measurements are required as input data and as a basis for model evaluation. To simulate NH_3 emission, the input data set has to include meteorological time series and soil characteristic parameters. For model evaluation, in addition to NH_3 flux measurements, observational data for soil pH, TAN and water content of the soil are also necessary. Since this study has a focus on modelling, the data needed to carry out a simulation were taken from the literature.

In this chapter firstly, an overview of a measurement campaign used for the baseline simulation is provided (Section 3.2). Since the data used in the model experiment were collected with various time resolution, the same section also describes how these data were adjusted to the hourly resolution of GAG. Secondly, the comparison of the measured and the modelled NH_3 fluxes, soil pH, TAN budget and water budget is presented (Section 3.3). Finally, the results of a sensitivity analysis to the most critical model parameters and processes regulating these modelled variables are reported (Section 3.4).

3. 2. Measurement data used to evaluate GAG

The GAG model described in Chapter 2 was developed to simulate NH_3 emission from a single urine patch. However, for model evaluation in this chapter a field experiment

was utilized where the NH_3 emission flux was measured from several urine patches deposited relatively close in time. The only experiment found with these features was conducted by Laubach et al. (2012), who measured the NH_3 fluxes over a field covered with a regular pattern of urine patches.

In the experiment, 156 artificial urine patches were deposited within 45 minutes (see an overview of the urine patch characteristics in Table 3.1) over a circular plot at an experimental site in Lincoln, New Zealand. In the middle of the plot NH_3 concentrations were measured at five heights with Leuning samplers (Leuning et al., 1985) from which the fluxes were derived by different methods. The fluxes used in this study were calculated by Laubach et al. (2012) according to the mass balance (MB) method.

Table 3.1. Urine patch details from the experiment of Laubach et al., (2012) and site specific model constants.

Model constants	**Value**
Urine patch specific constants	
A_{patch} (area of a urine patch)[1]	0.25 m^2
c_N (N content of the urine)	10 g N dm^{-3}
W_{urine} (volume of urine)	1.5 dm^3
Δz (thickness of the source layer)	4 mm
k_h (urea hydrolysis constant)[2]	0.23
Site specific constants	
Longitude	$172^0$27.34'E
Latitude	$43^0$38.56'S
Height above sea level	11 m
θ_{pwp} (permanent wilting point)[3]	0.1
θ_{fc} (field capacity)[3]	0.4
θ_{por} (porosity)	0.62
f_c (vegetation coverage)	35%
z_w (height of wind measurement)	2.1 m
β (buffering capacity)	0.021 H^+(pH unit)$^{-1}$ dm^{-3}

[1]In the experiment the expansion of the patches was observed up to 0.5 m^2. For model sensitivity to A_{patch} see Section 3.4.
[2]For summer (Sherlock and Goh, 1984)
[3]Assumed based on the measured volumetric water content dataset provided by Laubach et al. (2012).

Soil samples were taken from 24 patches on the edge of the plot to measure soil pH, volumetric water content and mineral N content. Soil temperature was measured at two heights, and meteorological measurements were also carried out (from which wind speed, temperature, photosynthetically active radiation (PAR), sensible heat flux and atmospheric pressure data were used). For more details on measurements and flux calculation, see Laubach et al. (2012).

To carry out a simulation with GAG, in addition to the available measurements, further meteorological data not measured in the experiment were required: global radiation (R_{glob}) and relative humidity (RH). These data were obtained from the National Climate Database for New Zealand (NIWA, 2015).

The model results were compared with measurements of NH_3 exchange flux (F_t), soil pH and volumetric water content (θ) for the measurement period between 24/02/2010 11:30 AM and 01/03/2010 1:30 AM. These variables, however, were measured with various time resolution, whilst GAG operates with hourly time steps. In the case of F_t, the length of the collecting period of each measurement varied mostly between 1-1.5 hour for daytime measurements, and 7-7.5 hours for the night-time measurements. Since emission fluxes were not expected to change considerably over the night due to the weak night time turbulent mixing, it was assumed that the measured average NH_3 flux over the collecting period was representative for the midpoint of the period (see these periods on Fig. 3.1 a), and these were compared to the modelled values in the hour closest to the midpoint of the corresponding measurements. Assuming that the change of the soil's mineral reduced nitrogen content (NH_x-N) is parallel with the B_{TAN} in the model soil pore, these two variables were also compared. All of the input data, as well as the data used to evaluate GAG together with their modification for the hourly simulation, are listed in Table 3.2.

To compare the measured and modelled F_t for a single urine patch, it was assumed that the great majority of NH_3 in the experiment of Laubach et al. (2012) was emitted from the urine patches rather than the field area that was not affected by urine. Therefore, the observed fluxes were multiplied by the effective source area (804.9 m^2

Table 3.2. Measurements used as input data and to evaluate GAG, together with their original time resolution and their conversion to hourly time resolution.

Variable	**Original time resolution**	**Adaptation to hourly time resolution**
Input data		
χ_a (air concentration of NH_3, µg N m^{-3})	Various (2-10 hourly)	Interpolated for the required hours.
u (wind speed, m s^{-1}) - at 2.1 m *PAR* (photosynthetically active radiation, µmol m^{-2} s^{-1}) T_{soil} (soil temperature, ºC) - at 2 cm p (atmospheric pressure, kPa) H (sensible heat flux, MJ m^{-2} h^{-1})	Half hourly	Averaged for the given hour.
P (precipitation, mm)	Half hourly	Summed up for the given hour.
T (air temperature, ºC) - at 3.85 m	Half hourly	Averaged for the given hour then calculated to 2 m height considering the average temperature gradient 6.5 ^{0}C/km: T(2 m)=T(3.85 m)-0.0065×1.85
R_{glob} (global radiation, MJ m^{-2} h^{-1})* *RH* (relative humidity, %)*	Hourly	-
Data used to evaluate GAG		
F_t (total NH_3 exchange flux over the canopy, µg N m^{-2} s^{-1})	Various (2-10 hourly)	Measurements in the midpoints of the collection periods were considered as representative hourly averages.
θ (volumetric water content, m^3 m^{-3}) pH NH_x-N (soil mineral N content, µg N (g soil)$^{-1}$)	Various (2-19 hourly)	Measurements in the given hour were considered as representative hourly averages.

*From the National Climate Database for New Zealand (NIWA, 2015), all the other parameters were measured at the site.

as calculated by Laubach et al., 2012), then divided by the total area of the deposited 156 patches (Eq. (3.1), where F_t^{single} stands for the converted measured flux).

$$F_t^{single} = \frac{F_t \times 804.9}{156 \times A_{patch}} \quad (3.1)$$

Measurements of θ were taken by using a sharp-edged metal ring that was pushed to about 5 mm to the soil, whereas the model simulates θ in a 4 mm thick layer (Δz = 4 mm, Table 3.1). This means that the same water loss via evaporation would result in different values of θ from those measured in the 5 mm depth sample. Since none of the other soil modules affects the water budget, a simulation was carried out also with a Δz of 5 mm to derive results that are comparable with the measurements.

3. 3. Baseline simulation and model evaluation

The results of the model evaluation are depicted in Fig. 3.1 and Table 3.3. The GAG model captures NH_3 emission reasonably well (Fig. 3.1 a). Considering that a relatively simple model was used to simulate a complex phenomenon, the Pearson's correlation coefficient (hereafter referred to as "correlation") for NH_3 flux, can be considered as relatively high (r=0.54, p=0.01, Table 3.3). The model slightly overestimates the fluxes before the rain event on the second day and it rather underestimates the measured values after it. However, the model is still capable of reproducing the daily pattern of emissions with the midday peaks. The only exception is the third day, when the emission flux remained low over the whole day (this was investigated in more detail in Section 3.4.3).

Soil pH is well simulated before the rain event, but similarly to the emission fluxes, it is underestimated afterwards (Fig. 3.1 b). Overall, for soil pH, there was a high and significant correlation (r=0.75) between the model and the measurements. The sudden drop in soil pH at the beginning of the rain event is thought to be caused by the lack of handling of CO_2 emission in the basic version of the model (see Section 3.4.3 for further examination of this effect).

Despite the large error bars on the measured mineral reduced soil N, its tendency is fairly similar to that of the TAN budget simulated by GAG (Fig. 3.1 c). This is

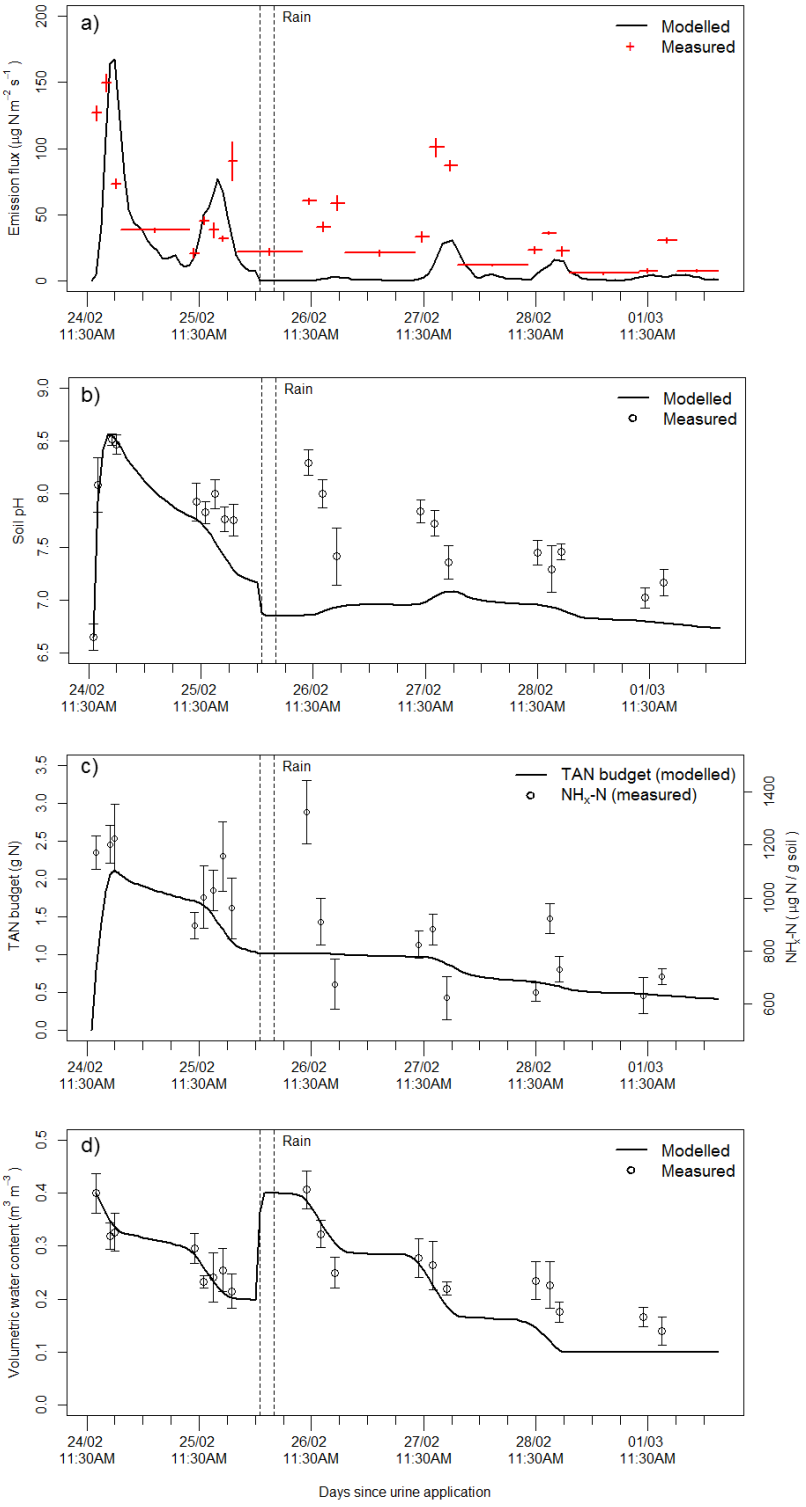

Figure 3.1. Comparison of modelled and measured values for NH_3 emission flux with the corresponding sampling periods of the measurements (a), soil pH (b), TAN budget and NH_x-N (c), and volumetric water content of the top 5 mm layer of the soil (d). The vertical error bars stand for the standard deviation in the measurements. Vertical dashed lines indicate the beginning and the end of a rain event occurred on 25/02.

Table 3.3. Statistics for model evaluation: root mean square error (RMSE), Pearson's correlation coefficient (r), the equation of the fitted least-squares equation (x - observation, y - model) and the level of significance of the correlation.

Variable*	**RMSE**	**Equation**	**r**	**Level of significance**
Ammonia emission flux	43.06 μg N $m^{-2}g^{-1}$	y=34.63+0.50x	0.54	0.01
Soil pH	0.56	y=3.04+0.64x	0.75	0.001
Model TAN budget vs. measured soil NH_x-N	-	-	0.63	0.01
Volumetric water content	0.05 m^3 m^{-3}	y=0.10+0.67x	0.92	0.001

*All the modelled and measured variables are the same as shown in Fig. 3.1 In the case of the emission flux, the measured flux was compared in the given measurement period with the value simulated at the time of the midpoint of the corresponding measurement period as explained in Table 3.2.

supported also by the significant correlation (r=0.63) between the two variables. In terms of θ, the statistical analysis showed a high correlation of 0.92 at a 0.001 significance level.

Analysing the NH_3 emission, pH and TAN budget together (Fig. 3.1 a-c), it can be concluded that the rain event on 25/02 affected all three variables considerably. As it can be seen from the measured pH and NH_x-N dataset (Fig. 3.1 b and c, respectively), their values right after the rain event peaked close to the level (or even higher) of the first peaks, which were generated by urea hydrolysis. This suggests that urea breakdown might have restarted after the rain event, which was not captured by GAG, explaining the difference between the modelled and measured values.

The GAG model does not account for any retention of urine by vegetation; however, it can occur in reality. For example, Doak (1952) found that the urine held on the leaf surfaces was 36% of fresh herbage weight. In addition, the model assumptions do not allow the model soil pore to dry out (the minimum water content is at the permanent wilting point). In reality, however, the moisture content of urine retained on the leaf surfaces can evaporate easily and also some soil pores can completely dry out leaving

behind the urine components undissolved. Under such dry conditions, with no available water urea hydrolysis stops. Then, after a rainfall, urea is dissolved (as well as from the leaf surface it is washed into the soil) and hydrolysis can begin again. This can lead to a high peak in pH, TAN budget and consequently, NH_3 emission (see the further model results presented in Section 3.4.3), after a rain event.

3. 4. Sensitivity analysis to the regulating parameters and processes

In the following, the response of the modelled NH_3 flux to the variation of the most critical regulating parameters and processes of the 2LCCPM (two-layer canopy compensation point model), the TAN budget, the soil pH and the water budget is investigated. Those parameters and processes were considered as the "most critical" ones that were assumed specifically for the GAG model or for the model experiment presented in Section 3.3. These parameters and processes were not observed at the experimental site and were assumed based loosely on references in the literature.

Table 3.4. The percentage of the change in total emitted NH_3 compared to the baseline simulation after modifying the different model constants by -20, -10, +10 and +20%.

Module	**Parameters**	**Total NH_3 emission change in response to change if parameter by**			
		-20%	**-10%**	**+10%**	**+20%**
2LCCPM	z_l (height of the top of logarithmic wind profile)	+0.02%	+0.01%	-0.01%	-0.02%
TAN budget	Δz (thickness of NH_3 emission layer)	-11.7%	-5.57%	+5.07%	+10.5%
	Δz – only in R_{soil} *	+2.39%	+1.15%	-1.06%	-2.06%
	Δz – only in TAN budget *	-12.3%	-5.75%	+5.74%	+11.7%
	A_{patch} (area of a urine patch)	+1.39%	+0.67%	-0.58%	-1.61%
Soil pH	β (soil buffering capacity)	+1.29%	+0.64%	-0.62%	-1.22%
Water budget	REW (readily evaporable water)	-2.98%	-1.69%	+2.06%	+4.32%
	θ_{fc} (field capacity)	-18.4%	-6.63%	+6.34	+9.12%
	θ_{pwp} (permanent wilting point)	+9.48	+4.60%	-4.42%	-8.85%

* It was investigated separately, how the modification of Δz affects the total NH_3 emission when it is modified only in the expression for soil resistance (R_{soil}, Eq. 2.43), and when it was modified only in the equations affecting the TAN budget (i.e. Δz was modified in every equation except in R_{soil}).

In the case of the constant parameters a sensitivity analysis was carried out. During these simulations, the given assumed model constant was increased and decreased by 10% and 20%, and the resulted difference in the total NH_3 flux summed for the whole modelling period was calculated. These differences were expressed as the percentage of the total NH_3 flux in the original model experiment (presented in Section 3.3), hereby referred to as "baseline simulation". In this simulation total emission over the urine patch was 1.78 g N. An overview of the results of this sensitivity analysis can be seen in Table 3.4. These results are discussed in the following subsections (Sections 3.4.1-3.4.4.).

Further model experiments were performed to investigate in detail the effect of Δz, β, and the processes assumed during the development of GAG (Chapter 2) on the simulated variables. All of these simulations are listed in Table 3.5, together with their short descriptions as well as their labels used to refer to them in the following.

Table 3.5. The baseline simulation and the model experiments carried out in Section 3.4.2 and 3.4.3. The labels of the experiments and the modifications in the baseline simulation are also indicated. The rationale and detailed description of the model experiments is provided in the corresponding sections.

Thesis section	**Experiment**	**Modification in the baseline simulation**
Section 3.3	baseline	the original model experiment presented in Section 3.3
Section 3.4.2	GAG_Δz20	Δz = 20 mm
	GAG_Δz2	Δz = 2 mm
	GAG_Δz1	Δz = 1 mm
	GAG_GrPatch	A_{patch} gradually grows from 0.25 m^2 to 0.5 m^2
	GAG_TAN-10	-10% daily change in the TAN budget
	GAG_TAN+10	+10% daily change in the TAN budget
	GAG_TAN+50	+50% daily change in the TAN budget
Section 3.4.3	GAG_TotBuff	the system is totally buffered
	GAG_NoBuff	the system is not buffered
	GAG_CO2Em	CO_2 emission is assumed
	GAG_NoRain	no rain in the model
	GAG_UHRestart	restart of urea hydrolysis with rain

3. 4. 1. Sensitivity to atmospheric resistances

As shown by Fig. 3.2, the net NH_3 flux is dominated by the soil emission flux (F_g). Therefore, here only the influence of the atmospheric resistances was investigated that directly affect the soil emission (Figure 2.3): the soil resistance (R_{soil}), the resistance of the quasi-laminar layer in the canopy (R_{bg}), the aerodynamic resistance in the canopy (R_{ac}) and the aerodynamic resistance over the canopy (R_a). In Fig. 3.3, on the logarithmic scale it can be clearly seen that the dominant resistance is R_{soil}, and R_{ac} is the only atmospheric resistance that reaches the magnitude of the estimated R_{soil}.

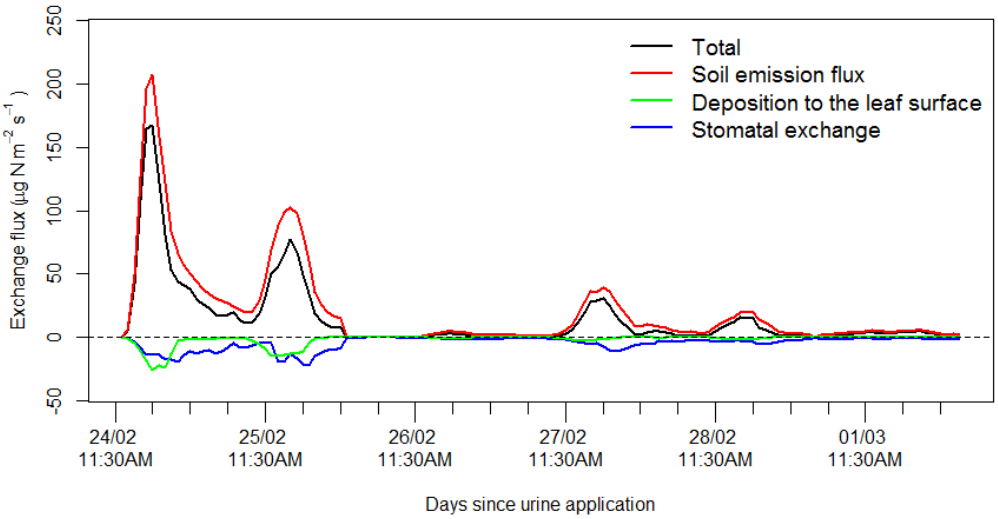

Figure 3.2. NH_3 fluxes simulated by the GAG model: Total net flux of NH_3 over the canopy (F_t), soil emission flux (F_g), deposition to the leaf surface (F_w) and the stomatal exchange (F_{sto})

In the simulation the main driver of the temporal variation of R_{soil} is the actual volumetric water content (Fig. 3.3 and Fig. 3.1 d). In the case of R_a, R_b, and R_{bg} there is at least on order of magnitude difference compared with R_{soil}, illustrating how the model performance is much less sensitive to the exact values of R_a, R_{ac}, and R_{bg}. The close temporal correlation of all these atmospheric resistances illustrates how they are all controlled by variations in wind speed (Figure 5.1 c) for a single canopy type. All the atmospheric resistances are the closest to the soil resistance when weak wind (large atmospheric resistances) is coupled to dry soil conditions (small R_{soil}).

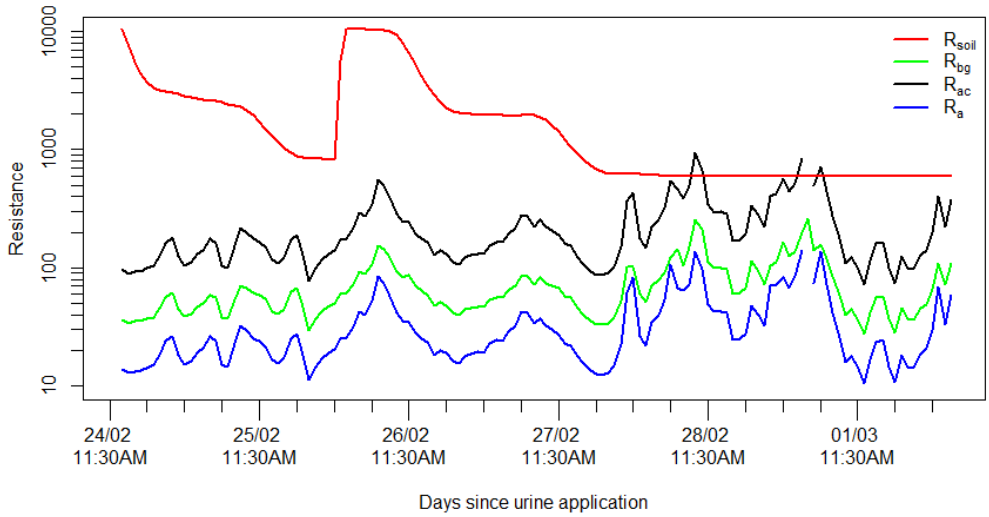

Figure 3.3. The atmospheric and the soil resistances over the modelling period. (At the time of the missing values in R_{bg}, R_{ac} and R_a u_* was 0, for which resistances are infinite. In these cases emission flux was assumed to be 0.)

For the parametrization of R_{bg} the approach recommended by Nemitz et al. (2001) for oilseed rape was implemented to the GAG model (Eq. 2.20), which describes a single urine patch deposited over a surface covered by grass. As Table 3.4 shows, the model is hardly sensitive to the value of z_l. In addition, u_{*g}, as formulated by Nemitz et al. (2001) (see Eq. 2.22), can also change within wide ranges without significantly affecting soil emission: R_{bg} could overcome the effect of R_{soil} on NH_3 emission only with a 10 times higher value of u_{*g}.

3. 4. 2. Sensitivity to the estimation of the TAN budget

The parameters expected to be uncertain in the estimation of the TAN budget are the thickness of the source layer (Δz) and the area of the patch (A_{patch}). When Δz was changed in the entire model, the results showed (Table 3.4, second row) that the change in the total NH_3 emission is approximately half of the change in Δz. Therefore, this source of error must be considered when model results are evaluated.

The value of Δz affects the total NH_3 emission flux in two ways: through R_{soil} (Eq. 2.43) and through determining how much urine can be stored in the source layer, i.e. how much TAN is available for NH_3 emission. A larger Δz is coupled with a larger

R_{soil} and consequently, weaker NH_3 emission. On the other hand, in the case of a larger Δz, more TAN can be stored in the source layer, and as a result, more NH_3 can be emitted over the modelling period. These effects of the variation of Δz on the total NH_3 emission were tested separately in two additional perturbation experiments (Table 3.4, third and fourth row). The results supported the above described mechanisms and also suggested that the influence of Δz on the NH_3 flux is dominated by its effect through the available TAN. Furthermore, because of the relationship between R_{soil} and Δz (Eq. 2.43) the perturbation experiment for the "R_{soil} only" case (Table 3.4, third row), can be regarded as a perturbation experiment for $R_{soil,}$ suggesting a weak response in the total NH_3 emission to the ±10%, ±20% changes in R_{soil}.

The model was also tested with Δz values between the ranges reported by Laubach et al. (2012) in the experiments GAG_Δz1 (Δz = 1 mm) and GAG_Δz2 (Δz = 2 mm). It was found (Fig. 3.4) that the smaller the value of Δz, the higher is the emission peak after urine application and smaller are the emission peaks in the following days. Firstly, this is caused by a smaller value of R_{soil}, due to the thinner source layer. Secondly, since the thinner layer can store less TAN in total, the source layer runs out of TAN more quickly leading to lower peaks in the later part of the modelling period.

In addition, a further simulation was carried out (GAG_Δz20) with the maximum value of Δz. This value is the penetration depth of the incoming urine and can be derived as follows: since the water content of a y dm thick soil layer can be expressed as $A_{patch} \times y \times (\theta_{fc}\text{-}\theta_{pwp})$, the urine deposited in a single patch (W_{urine}) in this experiment will fill up a y = 0.2 dm = 20 mm thick soil layer. With Δz = 20 mm, R_{soil} is at least 5 times higher than in the baseline simulation, that prevents NH_3 from escaping from the soil shortly after urine deposition (Fig. 3.4). However, from the second day due to the higher available TAN budget, the fluxes are closer to the measurements.

In contrast to Δz, the simulated total NH_3 emission does not appear to be very sensitive to A_{patch}, with even a +20% change causing less than 2% change in total emission (Table 3.4). Laubach et al. (2012) estimated that the patches gradually grew by lateral diffusion, so that the area of the patches had doubled over the modelling period at the validation site. Therefore, a simulation was conducted with GAG

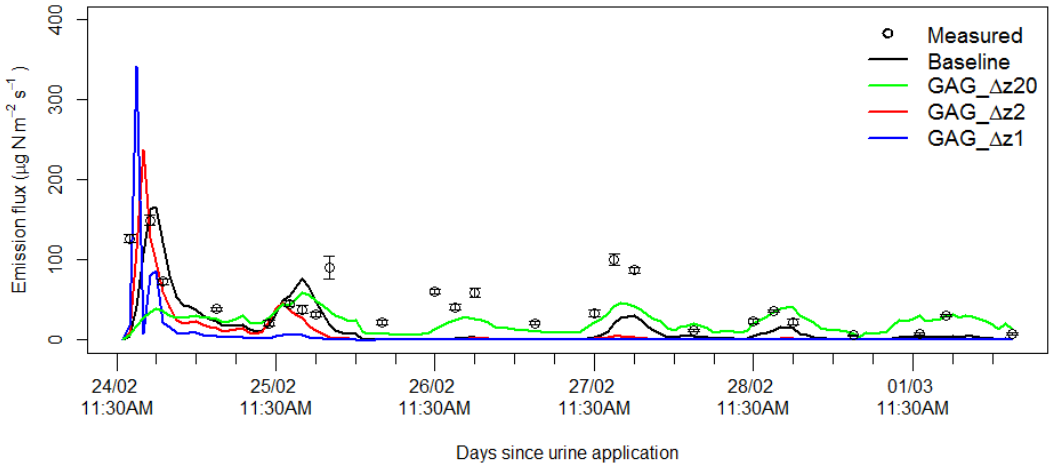

Figure 3.4. Simulated NH_3 fluxes from a urine patch with different Δz values: 4 mm (Baseline), 20 mm (GAG_Δz20), 2 mm (GAG_Δz2) and 1 mm (GAG_Δz1). The measured fluxes are also indicated.

with a gradually growing patch, whose area doubles by the end of the period (GAG_GrPatch). In Fig. 3.5 the measured emission fluxes are shown in relation to constant and gradually increasing values of A_{patch}, with the model results expressed for the whole area (converted based on the reorganized form of Eq. (3.1)).

Comparing the results from the baseline simulation and GAG_GrPatch, the largest difference occurred over the first two days. Later, the emission rates became smaller for the growing patches than with the constant patch area. The difference is a consequence of the combined effect of the growing source area ($156 \times A_{patch}(t_i)$) and the changing emission flux from a single patch.

In the GAG model if a urine patch grows, it means physically that the liquid content diffuses in the soil horizontally, leading to gradually declining volumetric water content. In addition, the area of evaporation grows simultaneously, further intensifying the decrease of water content. Thus, R_{soil} will be smaller which permits stronger NH_3 emissions in the first two days. This also leads to lower TAN budget in the second half of the period, resulting in slightly smaller emissions than in the baseline simulation.

A limitation of the calculation of the TAN budget in GAG is that the vertical movement of the dissolved compounds as well as their mixing with the soil layers under the source layer are excluded from the model. To test the sensitivity of the model

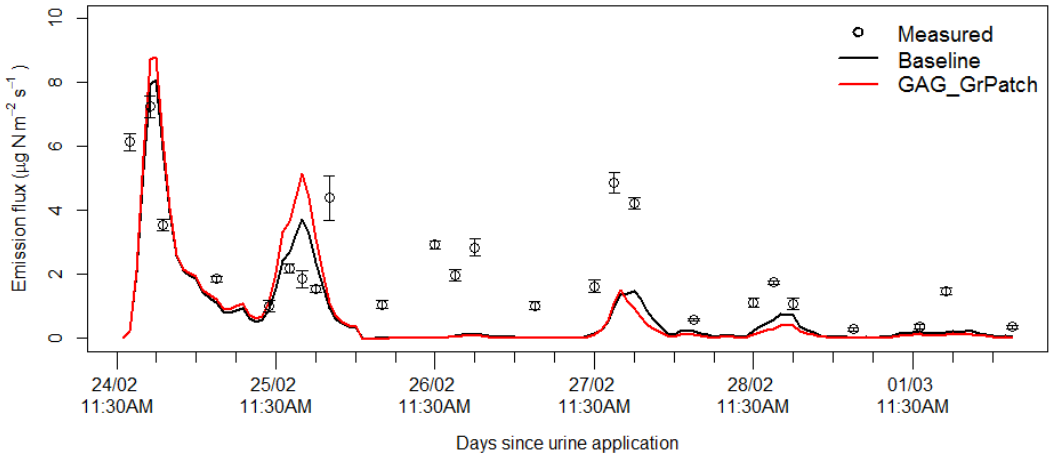

Figure 3.5. Simulated NH_3 fluxes from the whole experimental area with constant (Baseline) and with gradually growing urine patches (GAG_GrPatch). The measured fluxes are also indicated.

to such changes in TAN two model integrations were performed: in one of them (GAG_TAN-10) it was assumed that 10% of the TAN budget migrates to deeper soil layers daily or is taken up by the plants (which equals to 1 – 0.9^(1/24) = 0.4% per hour), whilst in the other run (GAG_TAN+10) the model was tested with an additional +10% to the TAN budget daily, transferred up from the deeper soil layers.

Based on the results (Fig. 3.6), the modelled NH_3 emission appears more sensitive to these changes in the second half of the modelling period than in the first half of it. The reason for this is that the TAN production from urea hydrolysis subsided at this later stage, so that this type of a sink or source of TAN can become more effective. In a third simulation (GAG_TAN+50) the TAN budget was increased by +50% daily (which is +2% per hour). Although the resulting fluxes (Fig. 3.6) are closer to the measurements on the third day, the GAG model still fails to capture the measured NH_3 fluxes right after the second day and the overestimation of the fluxes on the first two days is even stronger. This suggests, that the second peak in the measurement might be a consequence of an external and stronger N source, supporting the feasibility of the idea of the possible restart of urea hydrolysis (this effect was investigated in more detail in Section 3.4.3).

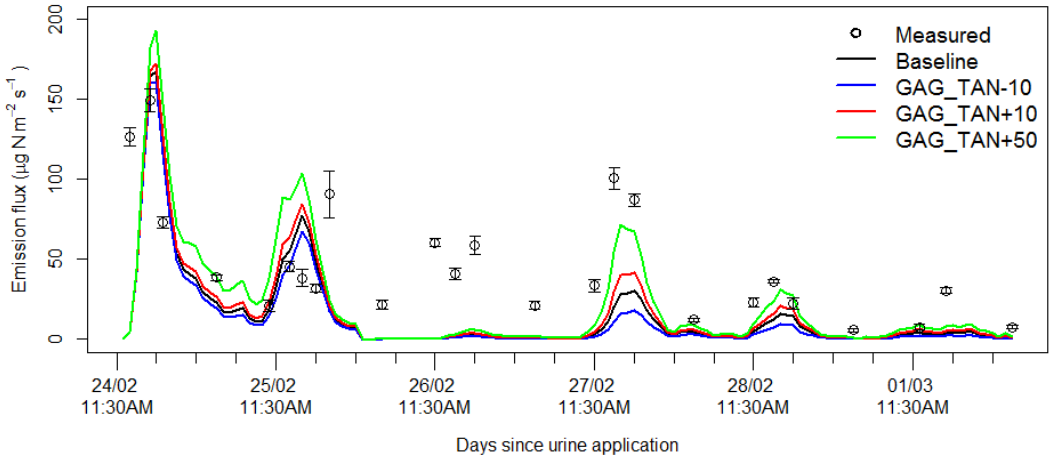

Figure 3.6. Simulated NH_3 fluxes when there was no change in the TAN budget (Baseline), and when a daily -10% (GAG_TAN-10), +10% (GAG_TAN+10), +50% (GAG_TAN+50) change was assumed in it. In the simulations the daily change was scaled down to hourly changes. The measured fluxes are also indicated.

The model integrations GAG_TAN-10, GAG_TAN+10 and GAG_TAN+50 were also carried out with a simultaneously changing urea budget, losing and gaining the same fraction of the urea budget as that of the TAN budget. The difference in the results compared to the simulations illustrated in Fig. 3.6 was negligibly small, because in the model on an hourly basis at least 12% of the urea is converted to TAN, which is a considerably larger loss compared to the loss and inputs terms assumed in these experiments (±0.4% and +2% hourly).

Finally, it has to be pointed out that the effect of the presence of hippuric acid, which is present in real urine, is neglected. Hippuric acid may increase urea hydrolysis and consequently, NH_3 emission (Whitehead et al., 1989). Whitehead et al. (1989) found that ignoring this triggering effect can lead to up to -10% difference in the cumulative NH_3 volatilization (expressed as the proportion of the total nitrogen content of urine) compared to real urine containing the same amount of urinary N.

In the measurement campaign (Laubach et al. 2012), used here as the base of model evaluation, an artificial urine solution was spread on the experimental plot that was enriched with additional urea. Hence, a urea based model was validated against a concentrated urea solution. Therefore, the difference in the modelled and the measured NH_3 fluxes, originating from this simplification, is presumably negligible.

Nevertheless, it could be relevant if the model is applied in real grazing situation. The possible effects of the exclusion of hippuric acid on NH_3 emission at the field scale are discussed in more detail in Chapter 6.

3. 4. 3. Sensitivity to the estimation of soil pH

The main anticipated uncertainty in the model pH calculation is the applied buffering capacity (β). Apparently, the model is not highly sensitive to the tested changes of β (Table 3.4); however, using the same β for every soil type could lead to errors in NH_3 emission estimation. Therefore, GAG was tested with two contrasting assumptions about buffering capacity: a) when the system is totally buffered, i.e. pH is constant (GAG_TotBuff), and b) when there is not any buffering effect ($\beta = 0$, GAG_NoBuff). For the constant pH scenario (GAG_TotBuff), the soil pH measured before the deposition of the urine patches (pH=6.65) was chosen.

The results show that with a constant soil pH (GAG_TotBuff), GAG fails to capture the first, dominant peak in emission (Fig. 3.7). This suggests that the dynamic modelling of pH is necessary for a proper estimation of NH_3 emission from a urine patch. By contrast, with $\beta = 0$ (GAG_NoBuff) the GAG model overestimates the first emission peak, while there is little difference in NH_3 fluxes in the rest of the period. Thus, with $\beta = 0$ the model is still capable of reproducing the daily cycle of NH_3 emission.

Another feature of the GAG model which affects the pH as well as the NH_3 emission flux calculation is the handling of CO_2 emission following urine deposition (as mentioned in Section 2.8). A sudden drop can be seen in the simulated pH at the beginning of the rain event (Fig. 3.1 b), which tends to disappear if there is no rainfall over the modelling period (Fig. 3.8 a, GAG_NoRain).

At the beginning of the period of the rainfall, the volume of the gaseous part of the model soil pore suddenly shrinks as the liquid part grows with the incoming water. As a result (given that the base model does not allow CO_2 emission), gaseous CO_2 accumulates in the model soil pore and is forced to dissolve into the liquid phase. This

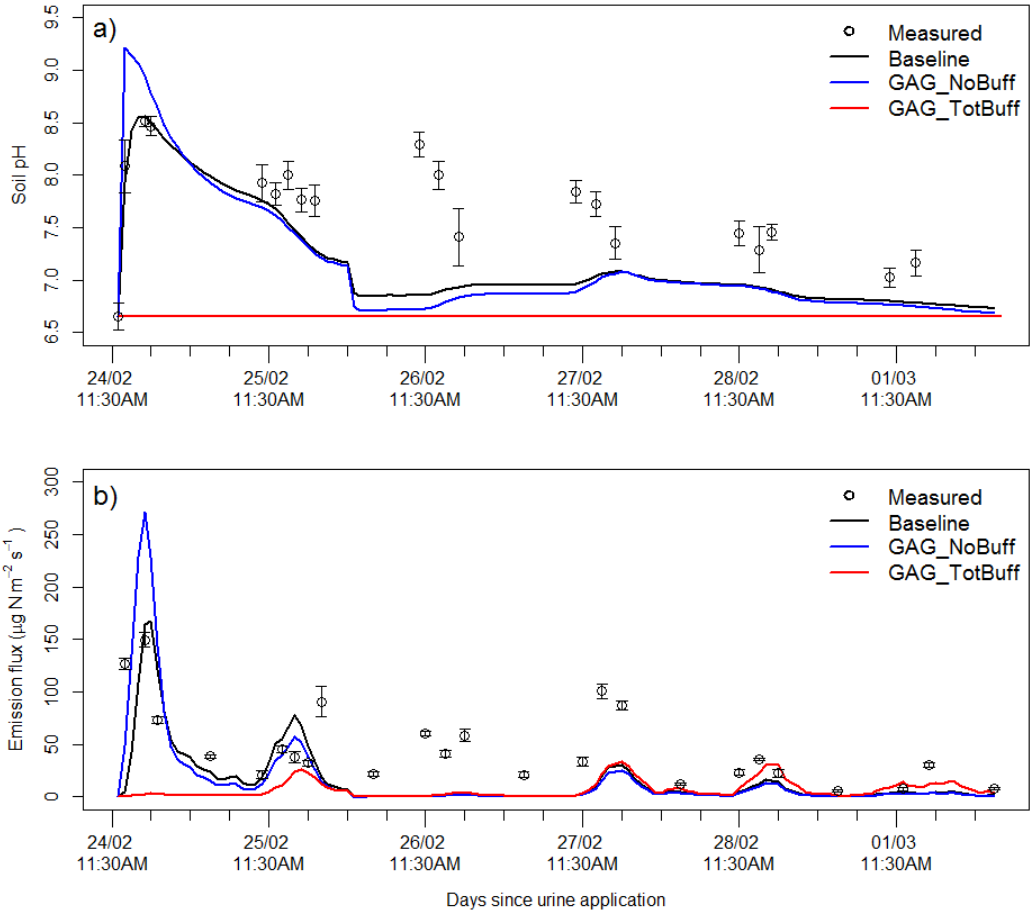

Figure 3.7. Measured and simulated soil pH under a urine patch (a) and NH_3 emission from it (b) assuming: a buffering capacity of 0.021 (β = 0.021, Baseline), zero buffering capacity (β = 0, GAG_NoBuff) and a totally buffered system (constant pH of 6.65, GAG_TotBuff).

intensifies the formation of carbonic acid and its subsequent dissociation, leading to a significant drop in the simulated pH.

In the experiment by Wang et al. (2013) CO_2 emission over urine patches peaked within 8 hours after urine application, while both Ma et al. (2006) and Lin et al. (2009) found that the first peak of CO_2 emission occurred on the first day. In addition, Lin et al. (2009) reported a high correlation (r=0.63) between CO_2 emission and soil temperature, suggesting a strong temperature dependency in CO_2 emission (similarly, a correlation of r=0.58 for NH_3 was found by Móring et al., 2016).

Based on the above similarities between the temporal development of NH_3 and CO_2 emission, to test the effect of CO_2 emission on the GAG simulations, a model

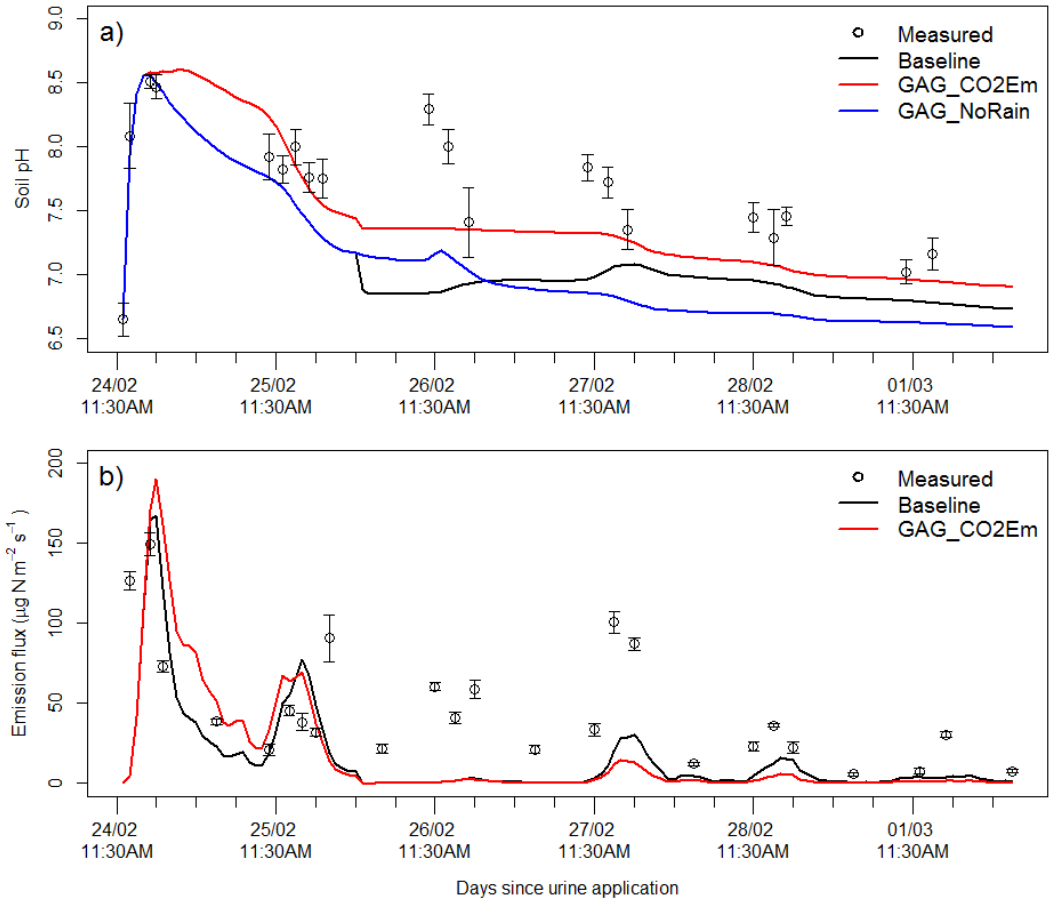

Figure 3.8. Measured and simulated soil pH under a urine patch (a) and NH_3 emission from it (b) without CO_2 emission (Baseline) and with an assumed CO_2 emission (GAG_CO2Em). On panel a) a simulation assuming no rain in the baseline experiment is also plotted (GAG_NoRain).

integration was carried out (GAG_CO2Em), assuming that the amount of emitted CO_2 is half of the emitted NH_3 in moles (similarly to urea hydrolysis where from one urea molecule two NH_4^+ and one HCO_3^- ions are produced). Even if this is a simplification for CO_2 emission, the results (Fig. 3.8) show the potential of a future more comprehensive incorporation of the process into the GAG model. By accounting for CO_2 emission, the modelled pH values were found to be closer to the measured ones, while the sudden drop at the start of the rain event also largely disappeared. As a consequence of these changes, the NH_3 emission fluxes were larger before the second day and were smaller in the latter part of the experiment due to the larger loss in TAN budget.

The apparently contradictory results with the assumed CO_2 emission above - better agreement in pH and poorer agreement in the NH_3 fluxes – may suggest that the TAN in the model soil pore is depleted too early, leading to a significant underestimation of the emission fluxes in the second part of the modelling period. Two hypotheses can be envisaged that could cause this effect: hypothesis 1) the simulated rate of urea hydrolysis is higher than it is in reality, or hypothesis 2) at the experimental site fresh urea that had been intercepted by leaves and dried onto leaf surfaces, was washed to the soil during the rain event, thereby maintaining NH_3 emission afterwards.

As discussed in Section 3.2, the measurement data also suggest the feasibility of scenario 2. Therefore, to test the model for a possible restart of urea hydrolysis after the rain event, it was assumed that 10% of the urine (0.1 litre, containing 1.5 g of urea N) was intercepted on the vegetation. From there, due to the dry and warm weather conditions (according to the meteorological data in Fig. 5.1 in Chapter 5, on the first day of the experiment relative humidity was particularly low and air temperature relatively high compared to the following days) the liquid content might have evaporated quickly leaving behind dry urea, which could be washed into the soil by precipitation.

With this assumption, allowing the hydrolysis to restart in the soil (GAG_UHRestart), the model gives a better representation of the peaks in NH_3 emission (Fig. 3.9 a) on the following three days after the rain event. In addition, a peak in both soil pH and TAN budget (Fig. 3.9 b-c) appears in the model results after the rain event, similarly to the observed time series of soil pH and NH_x-N, respectively. These results clearly support the idea of the possible restart of breakdown of the fresh urea penetrating to the soil dissolved in rain water.

It is interesting to observe in Fig. 3.9 c that the peak in the TAN budget after the rain event in GAG_UHRestart is higher than the peak at the beginning of the modelling period. This can be explained by the amount of urine in the NH_3 source layer. In the beginning of the modelling period, the penetration depth of the urine in the soil was 20 mm (Section 3.4.2), and Δz was assumed to be 4 mm. This means that in the beginning of the simulation 20% of the urine was in the source layer. In the

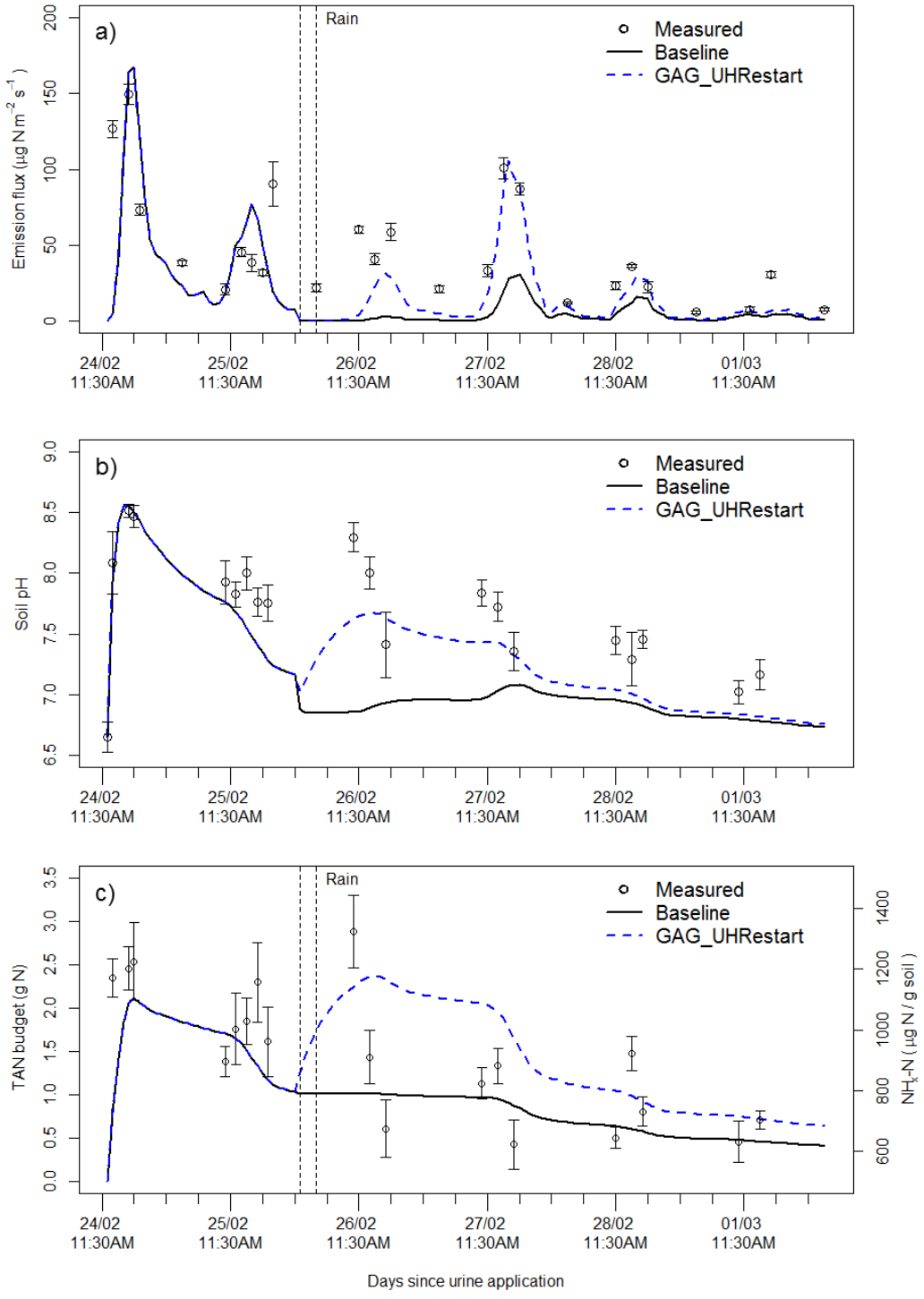

Figure 3.9. Measurements and model results for NH_3 emission flux (a), soil pH (b) and TAN budget (b) when there was no extra urine washed into the soil (Baseline), and when an assumed 1.5 g of urea was washed into the soil in the beginning of the rain event, triggering the restart of the urea hydrolysis (GAG_UHRestart). Vertical dashed lines indicate the beginning and the end of a rain event occurred on 25/02.

GAG_UHRestart model integration 10% of the urine was assumed to be intercepted on the vegetation. Due to the small amount of precipitation in the first hour of the rain event (0.8 mm), all of this urine was washed into the source layer with the rain water. This amount of urine, together with the TAN in the source layer before the start of the rain event, could lead to a higher peak in the TAN budget after the rain event in GAG_UHRestart, than occurred at the beginning of the simulation.

3. 4. 4. Uncertainties in the estimation of the water budget

The total NH_3 flux simulated by the GAG model was found to be sensitive to model constants related to the water budget, especially field capacity (θ_{fc}) (Table 3.4). On one hand, this is because the maximum amount of urine that can be stored in the source layer is determined by θ_{fc} and θ_{pwp} (permanent wilting point). According to the definition of θ_{fc} and θ_{pwp}, these parameters are the maximum and the minimum amount of water in the source layer, respectively, expressed as the percentage of the volume of the source layer. Based on this, the maximum volumetric percentage of the soil that can be filled up with urine (θ_{urine}) is the difference of the two:

$$\theta_{urine} = \theta_{fc} - \theta_{pwp} . \qquad (3.2)$$

Eq. (3.2) suggests that in the case of a higher θ_{fc}, more urine can infiltrate to the source layer, carrying a larger amount of urea available for hydrolysis. This results in higher total NH_3 emission at the end of the modelling period. Whilst in the case of a lower value of θ_{fc}, less urine is allowed to penetrate to the source layer, leading to a lower total NH_3 emission. Based on Eq. (3.2), θ_{pwp} has the opposite effect on the total emission. Since in the GAG model the initial water content of the soil was assumed to be θ_{pwp} and the urine filled up the soil to θ_{fc}, the effects of these two parameters are clearly reflected in the results of the sensitivity analysis (Table 3.4).

Nevertheless, θ_{fc} and θ_{pwp} can affect NH_3 emission also through the water budget. A higher value of θ_{fc}, at the beginning of the simulation when the urine patch is deposited, allows more liquid to infiltrate. This leads to a higher water budget afterwards and as a consequence, higher R_{soil}. The increased R_{soil} in turn, decreases the NH_3 emission flux. In the case of a smaller θ_{fc}, the opposite effect can be expected,

leading to stronger NH_3 emission. The effect of θ_{fc} on NH_3 emission through R_{soil} is the same, when rain water infiltrates to the soil.

This impact of a larger θ_{fc} through the water budget is the contrary of that was described above through θ_{urine}. However, since the sensitivity analysis showed an overall positive response in the total NH_3 flux to the change of θ_{fc} (higher θ_{fc} coupled with higher emission flux), it can be concluded that the influence of θ_{fc} on NH_3 emission through θ_{urine} overcomes its effect through R_{soil}.

An additional influence of θ_{pwp} through R_{soil} can be also distinguished. On one hand, if θ_{pwp} is larger, when the soil dries out in the GAG model, i.e. reaches θ_{pwp}, R_{soil} will be larger, which leads to a weaker NH_3 emission. On the other hand, in the case of a low amount of precipitation that cannot fill the source layer to θ_{fc}, a larger minimal water content in the soil (larger θ_{pwp}) will add up with the incoming liquid to a larger water budget. This, again, leads to a higher R_{soil} and a weaker NH_3 emission flux over the urine patch. In the case of a smaller θ_{pwp}, the opposite mechanism takes place, leading to a stronger emission flux.

The direction of the changes in the NH_3 emission in response to the variation in θ_{pwp} through R_{soil} is the same that was described in the case of its effect through θ_{urine}. To test the magnitude of the effect of θ_{pwp} on the total NH_3 emission through R_{soil}, an additional perturbation experiment (not shown here) was carried out. In this, the influence of θ_{pwp} on the amount of urea in the source layer was excluded. According to the results, the response in the total NH_3 flux (±2%, ±1%) to the changes in θ_{pwp} was considerably weaker than was reported in Table 3.4, when θ_{pwp} was perturbed in the entire model. This suggests that θ_{pwp} affects NH_3 emission dominantly through θ_{urine}.

The third way, through which θ_{fc} and θ_{pwp} can affect the total NH_3 emission in GAG is the readily evaporable water (*REW*, Eq. 2.58). However, the sensitivity of the total NH_3 emission to the changes in *REW* (Table 3.4) is weak, and the ±10%, ±20% perturbations in θ_{fc} and θ_{pwp} result in smaller proportional changes in REW (±2% – ±16%) than the ±10%, ±20% modifications tested in the sensitivity analysis. Therefore, the effect of θ_{fc} and θ_{pwp} on NH_3 emission through REW can be considered negligible.

On regional scale it is not likely to have a database of measured θ_{fc} and θ_{pwp} values over a dense grid. It is more feasible that a soil texture map can be used for this purpose with recommended values of θ_{fc} and θ_{pwp} for different soil types. Both θ_{fc} and θ_{pwp} can have an uncertainty of ±20% (e.g. in Allen et al., 1998, for sandy loam θ_{fc}=0.18-0.28). This means that the uncertainty is similar to the extent of modifications shown in Table 3.4. Therefore, at regional application, this uncertainty has to be considered when interpreting the model results.

In addition, a limitation of the calculation of the water budget is that GAG does not account for the water movement in the soil, including the effect of capillary force, diffusion of water in the soil as well as the concentration of TAN and urea within the moving liquid. However, the simulation of these processes is very complex. Nevertheless, the model code is easily amendable which enables the extension of the GAG model with additional modules in the future, in order to develop a more sophisticated modelling approach for the water budget as well as the TAN budget.

3. 5. Conclusions

In this chapter, based on field measurements, a baseline simulation with the GAG model has been performed and a sensitivity analysis to the regulating parameters and processes has been carried out. The comparison with measurements showed that NH_3 fluxes, soil pH, TAN budget and water budget are well represented by the model (r = 0.54-0.92). The largest difference could be explained by a possible restart of urea hydrolysis with the rain event occurred during the modelling period.

The sensitivity analysis showed that soil resistance had more than an order of magnitude stronger effect on soil NH_3 emission than the atmospheric resistances. An exceptional case is when weak wind speed is coupled with dry soil, in which case atmospheric and soil resistances may become comparable.

The perturbation analysis also implied that if the thickness of the source layer (Δz) is modified by a given percentage, the difference in the resulting total NH_3 emission over the modelling period will be half of this percentage. Also, the simulated NH_3

emission flux turned out to be sensitive to the value of soil water content at field capacity (θ_{fc}) and at permanent wilting point (θ_{pwp}).

The sensitivity of the modelled NH_3 emission flux was also examined to the exclusion of the upward and downward movement of TAN within the soil, assuming a hypothetical TAN gain and loss within the source layer. It was found that the model is more sensitive to these when TAN production from urea hydrolysis subsided, so that this type of TAN sink or source can become more effective over a larger time period.

In the case of pH it was shown that process-based modelling of pH is necessary to reproduce the very first high peak in NH_3 emission. The GAG model operates with an assumed soil buffering capacity (β). While this can affect the timing of emissions, it was found that the total NH_3 emission was not sensitive to the value of β and it is able to represent the main temporal development of NH_3 emission even with $\beta = 0$. Furthermore, it was found that incorporating a simple estimation of CO_2 emission allows the model to reproduce the measured soil pH values more accurately than neglecting CO_2 emissions.

Although the model experiments with the assumed restart of urea hydrolysis and CO_2 emission resulted in a considerably better representation of the measurements than in the baseline simulation, in both experiments the assumptions were hypothetical or specific for the experimental site. For a general model application these processes need to be further investigated. Therefore, the possible restart of urea hydrolysis and CO_2 emission were concluded not to be implemented to the GAG model, and to apply GAG for field scale (Chapter 4) based on the equations defined for the baseline simulation.

Chapter 4

Extension of the GAG model for field-scale application

4. 1. Introduction

Over a grazed field the great majority of NH_3 is emitted from the urine patches (Laubach et al., 2013, Petersen et al., 1998). The GAG model constructed in Chapter 2 is a tool to simulate NH_3 volatilization from a unit of NH_3 source: a single urine patch. However, over a grazed field, multiple patches are deposited in every hour. The present chapter describes how the GAG model can be extended and applied for this situation, simulating NH_3 exchange over a whole field.

Firstly, the theoretical background of the field-scale model application is presented (Section 4.2). Secondly, the equations required for upscaling to a field are provided (Section 4.3). In the third part of this chapter, the data used in the model evaluation are introduced (Section 4.4), which is followed by the presentation of the model simulations for two experimental periods (Section 4.5). Finally, the chapter concludes with the outcomes of a sensitivity analysis concerning the model parameters that regulates NH_3 exchange over the whole field and the TAN budget, as well as the water budget under the urine patches (Section 4.6).

4. 2. Theoretical background of the field-scale approach

Among all the naturally varying factors related to urination events on a grazed field, the following subsections describe those that are likely to be the most relevant from the point of view of NH_3 exchange at this larger scale. Firstly, the possible overlap of

the patches is examined (Section 4.2.1), then further parameters are discussed that can vary among urination events, such as the area of the patches, the frequency of urination events and the nitrogen content of urine (4.2.2). Finally, model assumptions for calculating the total NH_3 net flux for the field are identified (Section 4.2.3).

4. 2. 1. Exclusion of the overlap of the urine patches

According to observations (e.g. Dennis et al., 2013, Moir et al., 2011, Betteridge et al., 2010), urine patches over a grazed paddock may overlap. It was found that the overlap can have a large effect on N leaching (Pleasants et al., 2007, Shorten and Pleasants, 2007); however, no studies are available that investigate the effect of overlap in particular on NH_3 emission from urine patches.

It is reasonable to assume that the emission flux from the area of the overlap will differ from both the previously and the newly deposited patches due to the differences in the soil chemical properties (Fig. 4.1). Since urea hydrolysis is in a different stage in the two urine patches, the soil chemistry under them will be different, and their mixture under the overlap is likely to result in a third, different chemical composition. In addition, if patches partly cover each other, the total source area will be smaller than if they were completely separate, which may influence the total NH_3 emission from the field.

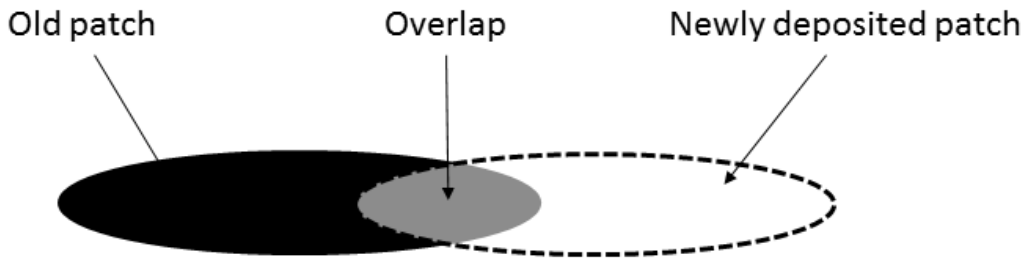

Figure 4.1. The different colours of the old and the newly deposited urine patches (black and white, respectively) as well as the overlap between them (grey) show the different soil chemical properties in the different areas.

It is likely that the possible overlap of the patches affects NH_3 emission. However to predict in every time step of the model which patches will cover each other, and what size the overlap will be is very difficult. Therefore, it would be preferable to neglect the overlap of the patches. To assess the resulting error arising from such a simplification, the difference in the field proportion covered by urine patches was investigated between the two cases: when overlap is assumed and when it is excluded.

A way to estimate the temporal evolution of the urine-covered proportion of the field is to use a negative binomial distribution function as suggested by Petersen et al. (1956), or the Poisson distribution tested by Romera et al. (2012). Based on the distribution suggested by Petersen et al. (1956), Pakrou and Dillon (2004) determined the proportion of the paddock covered by urine patches (P_t) after a t time period as:

$$P_t = 1 - q^{-K}, \tag{4.1}$$

where K is a parameter that represents the uniformity of the excretal distribution. Following Pakrou and Dillon (2004), a representative value of K=7 was used. The value of q is calculated as:

$$q = \frac{D_t + K}{K}, \tag{4.2}$$

in which D_t is the proportion of the urine-covered area over a t time period if there is no overlap (Eq. 4.3), i.e. the total number of the patches (N_t) deposited over t multiplied by the patch area (A_{patch}) and divided by the field area (A_{field}).

$$D_t = \frac{N_t A_{patch}}{A_{field}} \tag{4.3}$$

Using the same abbreviations, Romera et al. (2012) derived P_t assuming a Poisson distribution as follows:

$$P_t = 1 - e^{-D_t}, \tag{4.4}$$

where e is Euler's constant (~2.718).

To investigate the highest possible difference that the exclusion of overlap can cause, in the following calculation a "worst case scenario" was assumed with the highest possible coverage by urine, i.e. the highest realistic animal density over a field,

Table 4.1. Ranges of the parameters used in the calculation of the urine–covered proportion of a field with an area of 1 ha (= 10 000 m^2).

Animal	**Sheep**	**Cattle**	**Reference**
Number of animals on A_{field}	1 – 100	0.1 - 10	EC, 2015
Urination frequency (UF) (urination $animal^{-1}$ day^{-1})	15 – 20	8 - 12	Whitehead, 1995
Patches deposited per day (N_t)	15 - 2 000	0.8 - 120	-
Patch area (A_{patch}) (m^2)	0.043 - 0.055	0.38 - 0.42	Williams and Haynes, 1994

the largest A_{patch} and the highest urination frequency. The ranges of all these parameters are listed in Table 4.1 for sheep and cattle, together with their references.

According to the agricultural statistics of the European Commission for 2010 (EC, 2015), the maximal grazing animal densities on the agricultural holdings Europe-wide were higher than 10 LSU ha^{-1} (where LSU stands for livestock unit, which equals to 1 dairy cow or 10 sheep). Since no higher values than 10 were identified, 10 LSU ha^{-1} was assumed as the maximum. The value of N_t was calculated as the product of animal density over a hectare (A_{field} = 10 000 m^2) and the maximum daily urination frequency (urination events per animal per day, Table 4.1).

Fig. 4.2 shows P_t, using the two different equations, Eq. (4.1) and (4.4). These results are very close to each other, with slightly smaller values from Eq. (4.1). Therefore, for further investigation the P_t values from Pakrou and Dillon (2004) (Eq. 4.1) were taken and compared with the no overlap case ($P_t = D_t$). In the case of sheep (Fig. 4.2 a), the difference between P_t and D_t became higher than 5% after the eighth day (and exceeds 10% after the 16^{th} day – not shown here), whilst in the case of cattle (Fig. 4.2 b) the same occured after the 17^{th} day.

The great majority of NH_3 is emitted in the first 8 days after the deposition of a urine patch (Sherlock and Goh, 1985). This means that after the eighth day the NH_3

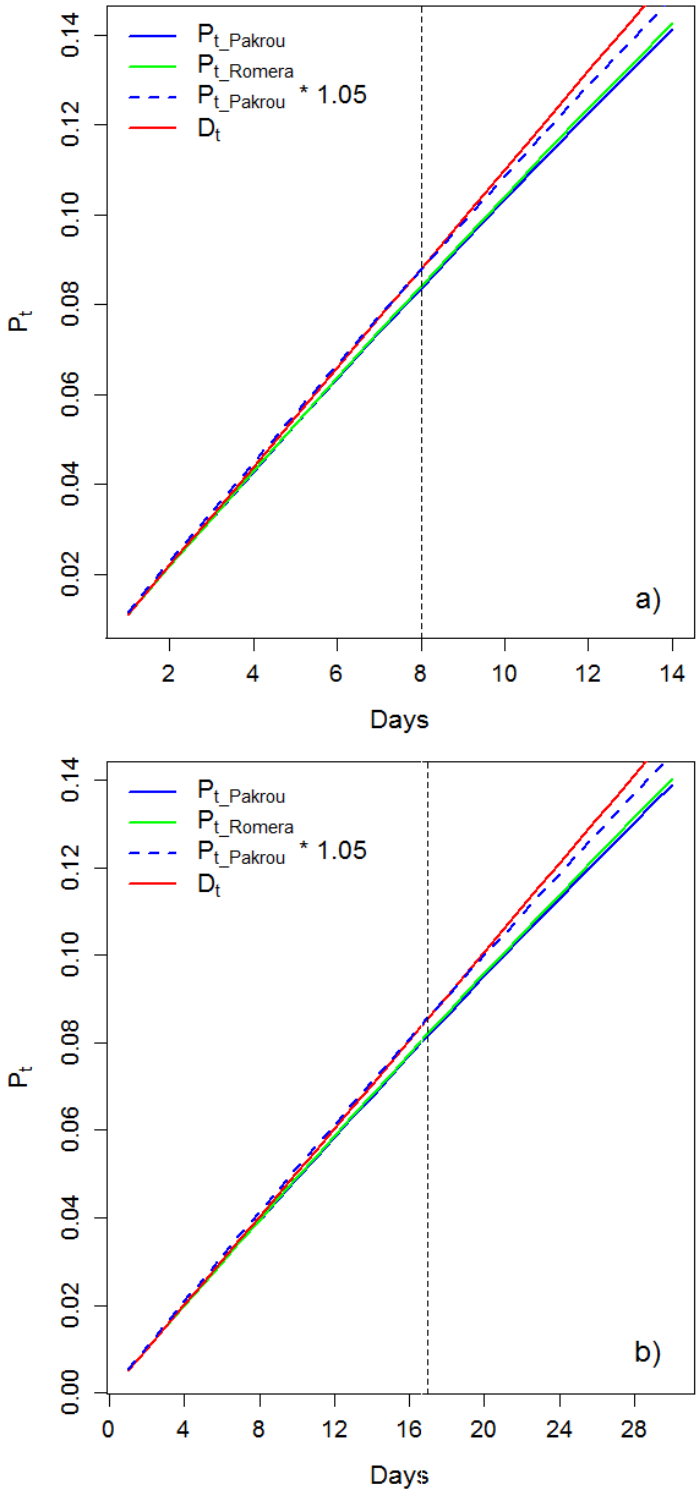

Figure 4.2: Proportion of the field covered by urine patches (P_t) calculated for sheep (a)) and cattle (b)) as suggested by Pakrou and Dillon (2004) (P_{t_Pakrou}), Romera et al. (2012) (P_{t_Romera}) and when there is no overlap between the patches (D_t).

exchange flux over the urine patches will be very close to that of the unaffected area of the field. Presumably, (as suggested also by the GAG model results for patch scale in Fig. 3.1 c and d) at this stage the chemical composition of the soil solution in the source layer under these patches will be also close to that of the initial, unaffected soil. Thus, practically, the patches deposited eight or more days before the given time step can be treated as part of the unaffected area of the field, or in other words, these patches disappear from the field. As a consequence, the total area of the patches grows in the first eight days, then it remains constant while the animals are on the field. Therefore, the probability of overlap after the eighth day will be the same as on the eighth day, since the total area of the patches prone to overlap with the new patches does not change after the eighth day.

Finally, it has to be noted that the results in Fig. 4.2 illustrate an extreme situation (the "worst case scenario"), and in reality P_t are much likely to grow rather more slowly. This allows a longer time before the exceedance of the 5% difference in P_t between the overlap and no-overlap case. Hence, for field-scale application of GAG the effect of overlap between the patches was concluded to be negligible, assuming completely separated urine patches in every time step.

4. 2. 2. Assumptions for other model parameters

As shown in the previous subsection, the parameters that regulate the extent of the paddock covered by urine are (i) the number of the animals on the field, (ii) A_{patch} and (iii) the urination frequency (UF). The first parameter at a field-scale model application is easy to obtain, but the observations of the area of every single urine patch, as well as the number of urinations on an hourly basis, are rather difficult (see the overview of the observation techniques in Dennis et al., 2013).

Therefore, in the field-scale simulations (Section 4.5), a constant A_{patch} for every individual urination event and a constant frequency of urination was assumed. There are values reported for the patch area in the literature (Table 4.1), whose average was used in the baseline simulations and with a sensitivity test an estimation was given for the uncertainty resulting from this simplification (Section 4.6.5).

In the literature observational data can be also found for *UF* (as shown in Table 4.1), but the temporal resolution of these data is usually a day. Based on personal communication with farmers, the hourly number of urine patches deposited over a field varies between the grazing and rumination periods and also between day and night. However, for the current modelling study an even distribution of urination events was assumed over the day, dividing the reported average daily *UF* by 24 hours. As for A_{patch}, a sensitivity analysis was carried out for this parameter as well (Section 4.6.5).

Another feature of the individual urination events that strongly influences the subsequent NH_3 volatilization is the N content of the urine (c_N). This parameter ranges widely (2 – 20 g N l^{-1}, Whitehead, 1995), not just amongst different animals, but also for different urination events by the same animal (Betteridge et al., 1986 and Hoogendoorn et al., 2010). In the baseline simulation a constant average N content was applied. In Section 4.6.5 the model sensitivity was analysed to this choice of N content and also to the uncertainty originating from the temporal variation of this parameter.

4. 2. 3. Assumptions for the calculation of the net ammonia flux

With all the above assumptions, two types of area can be distinguished over a grazed field: (a) area covered by urine, and (b) area that are not affected by urine, referred to hereafter as "clean area" (as shown on Fig. 4.3). Therefore, it was assumed that the total flux over the field is the sum of the emission from the urine affected area (calculated by GAG) and the exchange with the clean area (derived by GAG, assuming constant emission potentials, as explained in Section 4.3). Since a grazed field, due to the urine patches, is not a uniform source of NH_3, an error of the estimation of the total NH_3 flux can originate from the exclusion of the horizontal advection. Although this could be handled by using a dispersion model, since the purpose of this thesis is to construct a model that can be applied for regional scale, the model was kept at this lower level of complexity.

Finally, the field was assumed to have spatially homogenous physical and soil chemical properties before urine application. This assumption in tandem with the

exclusion of the overlap of the urine patches and the horizontal dispersion of NH_3, leads to the consequence that the total flux over the field is independent of the placement of the patches on the surface.

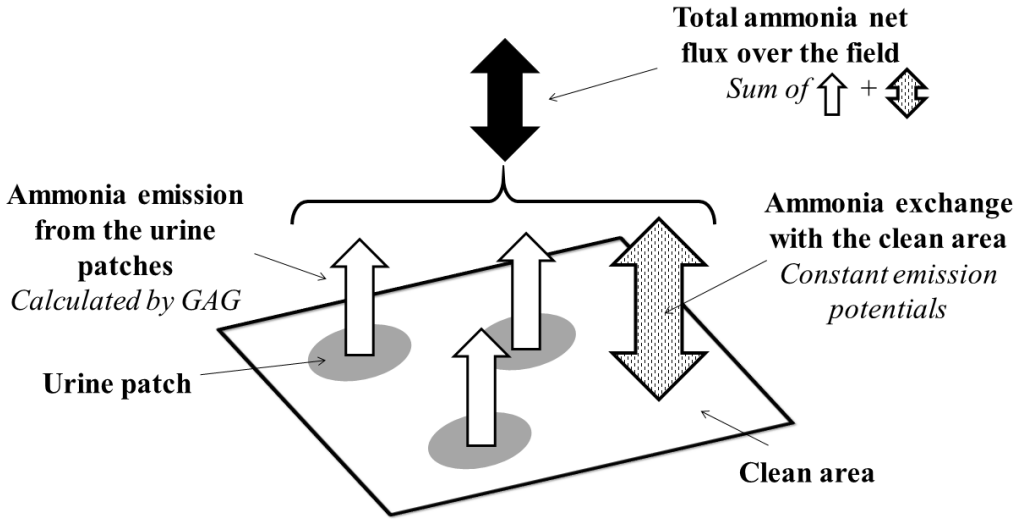

Figure 4.3. The schematic of the field-scale model, depicting the components of the total net NH_3 flux over the field.

4. 3. Model equations for the field-scale application

The field-scale application and the patch-scale version of GAG (Chapter 2) is referred to hereafter as "GAG_field" and "GAG_patch", respectively. Based on the considerations outlined in the previous subsections, for GAG_field it was assumed that physically and chemically identical urine patches are deposited in every time step over the modelling period. To capture the effect of all of the urine patches, in calculating the net NH_3 flux for the whole field (F_{net}), an $n \times n$ matrix can be considered (see Table 4.2, where n is the number of the time steps in the modelling period). In this matrix i index denotes the time step the given flux is derived for and j shows the time step when the patches were deposited. In this way, F_{net} in the i^{th} time step (t_i) can be expressed by Eq. (4.5).

The first term in the numerator of Eq. (4.5) represents the NH_3 emitted by the clean area: the NH_3 exchange flux over the clean area (F_{clean}) multiplied by the size of this area (A_{clean}). While the second term in the numerator equals to the total NH_3 emitted from the urine patches, where F_{patch}^{j} is the emission flux from the urine patches

deposited in the j^{th} time step, and $n(t_j)$ is the number of the patches deposited in the same time step. To calculate F_{net}, the sum of the two has to be divided by A_{field}.

$$F_{net}(t_i) = \frac{F_{clean}(t_i)A_{clean}(t_i) + \sum_{j=1}^{n} F_{patch}^{j}(t_i)n(t_j)A_{patch}}{A_{field}} \quad (4.5)$$

Table 4.2. Schematic for the temporal development of NH_3 flux (in every i^{th} time step, t_i) as derived by GAG_field from the urine patches ($F_{patch}^{j}(t_i)$) deposited in the j^{th} time step (t_j) and the clean area ($F_{clean}(t_i)$). The bottom row shows how many urine patches were deposited in the given j^{th} time step ($n(t_j)$). Fluxes with striped background are calculated by GAG_patch, and the fluxes with clear background are calculated by a modified version of GAG_patch for clean area (explained in the text).

		NH_3 emission from the urine patches					**NH_3 exchange with the clean area**
		Time of the deposition of the urine patches					
		$t_{j=1}$	**$t_{j=2}$**	**$t_{j=3}$**	**…**	**$t_{j=n}$**	
Time since the beginning of the modelling period	**$t_{i=1}$**	**$F_{patch}^{j=1}(t_{i=1})$**	$F_{clean}(t_{i=1})$	$F_{clean}(t_{i=1})$	…	$F_{clean}(t_{i=1})$	$F_{clean}(t_{i=1})$
	$t_{i=2}$	**$F_{patch}^{j=1}(t_{i=2})$**	**$F_{patch}^{j=2}(t_{i=2})$**	$F_{clean}(t_{i=2})$	…	$F_{clean}(t_{i=2})$	$F_{clean}(t_{i=2})$
	$t_{i=3}$	**$F_{patch}^{j=1}(t_{i=3})$**	**$F_{patch}^{j=2}(t_{i=3})$**	**$F_{patch}^{j=3}(t_{i=3})$**	…	$F_{clean}(t_{i=3})$	$F_{clean}(t_{i=3})$
	…	…	…	…	…	…	…
	$t_{i=n}$	**$F_{patch}^{j=1}(t_{i=n})$**	**$F_{patch}^{j=2}(t_{i=n})$**	**$F_{patch}^{j=3}(t_{i=n})$**	…	**$F_{patch}^{j=n}(t_{i=n})$**	$F_{clean}(t_{i=n})$
Number of patches deposited in t_j		$n(t_{j=1})$	$n(t_{j=2})$	$n(t_{j=3})$	…	$n(t_{j=4})$	0

In the clean area, in the absence of any considerable nitrogen input, the soil chemistry is practically undisturbed. Thus, for the clean area a modified version of GAG_patch was applied in which constant soil chemistry was assumed. Based on this, F_{clean} was derived in the same way as the net NH_3 flux (F_t) described by Eqs. (2.1)-(2.7) with the following simplifications:

- Since over the clean area the dynamic simulation of soil chemistry is not needed, the original version of the two-layer canopy compensation point model by Nemitz et al. (2001) was used. This includes only the original compensation point on the ground (χ_g), instead of the soil resistance and

compensation point in the soil assumed for GAG_patch (Fig. 2.3). As a consequence, the form of Eq. (2.4) will change to:

$$F_g = \frac{\chi_g - \chi_{z_0}}{R_{ac} + R_{bg}}. \tag{4.6}$$

- The value of χ_g (Eq. 4.7) was calculated similarly to that of the compensation point in the soil pore (χ_p, Eq. 2.39), except that the emission potential for the ground (Γ_g) was handled as constant instead of being modelled dynamically as in the original version of GAG_patch.

$$\chi_g = \frac{161500}{T_{soil}} \times \exp\left(\frac{-10380}{T_{soil}}\right) \times \Gamma_g \tag{4.7}$$

- Since over the clean area no N input is assumed, instead of applying a decay function, like Eq. (2.36), for the emission potential of the stomata (Γ_{sto}), it was treated as constant.

The size of A_{clean} in the given t_i time step is the area of the field that is not covered by any urine patches:

$$A_{clean}(t_i) = A_{field} - \sum_{j=1}^{i} n(t_j) A_{patch}, \tag{4.8}$$

where $n(t_j)$ (Eq. 4.9) is the number of the urine patches deposited in the j^{th} (hourly) time step. This can be expressed as the product of the animal density on the field in t_j ($AD(t_j)$, animals ha^{-1}), A_{field} (ha) and the daily UF (urinations day^{-1} animal^{-1}), divided by 24 hours.

$$n(t_j) = \frac{(AD(t_j) \times A_{field} \times UF)}{24} \tag{4.9}$$

Finally, $F_{patch}^{j}(t_i)$ was determined as follows:

$$F_{patch}^{j}(t_i) = \begin{cases} F_{clean}(t_i) & \text{if} \quad i < j \\ F_t(t_i) & \text{otherwise} \end{cases}, \tag{4.10}$$

which means that before the deposition of the urine patch, the area is handled as clean (first condition), and afterwards GAG_patch calculates the patch emission ($F_t(t_i)$, second condition).

When calculating $F_t(t_i)$ a slight modification is also required, regarding the urea added with a single urination (U_{add}). At field scale it has to be considered that during the modelling period urine patches may be deposited at the same time as a rain event occurs or right after it. A rain event i) will dilute the incoming urea solution and ii) may lead to the maximal water content ($B_{H2O(max)}$) in the NH_3 source layer, which in the model formulation presented in Chapter 2 prevents infiltration, resulting in no N input to the system and consequently no NH_3 emission.

To address the first point, it has to be noted that although over the clean area GAG_field does not simulate the dynamic, temporal evolution of the TAN budget and the soil pH (a constant Γ_g *is* used), it does account for the changes in water budget (B_{H2O}) in the source layer. Therefore, the water budget calculated by the GAG_patch model modified for the clean area right before the j^{th} patch deposition ($B_{H2O}^{j}(t_i = (j - 1))$) can be updated by GAG_patch in the next time step ($B_{H2O}^{j}(t_i = j)$). Although the effect of dilution is treated in GAG_patch, it is defined only for the first time step (Eq. 2.50), when urine is applied to the surface. Therefore, in the field-scale model U_{add} was calculated for the patch deposited in t_j as:

$$U_{add}(t_j) = c_N^{Dil}(t_j)\left(B_{H_2O}^{j}\left(t_{i=(j)}\right) - B_{H_2O}^{j}\left(t_{i=(j-1)}\right)\right), \tag{4.11}$$

where the diluted N concentration in the mixture of rain water and urine (c_N^{Dil}, Eq. 4.12) equals to the total amount of N in the urine (c_N x W_{urine}) divided by the sum of the volume of the liquid phase ($W_{urine} + W_{Rain}(t_i = j)$).

$$c_N^{Dil}(t_j) = \left(\frac{c_N W_{urine}}{W_{urine} + W_{Rain}(t_{i=j})}\right) \tag{4.12}$$

To avoid the possible error resulting from the second point, it was assumed that the minimum amount of urine that is always allowed to penetrate to the source layer equals to 5% of $B_{H2O(max)}$:

$$\left(B_{H_2O}^{j}\left(t_{i=(j)}\right) - B_{H_2O}^{j}\left(t_{i=(j-1)}\right)\right) \geq 0.05 \times B_{H2O}(\max). \tag{4.13}$$

4. 4. Dataset used in the baseline simulations and model evaluation

4. 4. 1. Measurements

The field-scale application of the GAG model was evaluated using measurements taken at a grassland site near Easter Bush, UK (see the field specific data in Table 4.3.) by CEH (Centre for Ecology and Hydrology). The field is divided into two halves, the North Field and the South Field, and the instruments were placed on the boundary of the two (Fig. 4.4). For the site, NH_3 flux measurements are available for a number of years (2001-2007). These fluxes were derived using the gradient method, which calculates the fluxes (F_χ) based on measurements of the vertical gradient of NH_3 air concentration and micrometeorological variables (Eq. 4.14). In Eq. (4.14) χ denotes NH_3 air concentration and k, u_*, z, d, Ψ_H, L are the same variables as defined in Chapter 2.

$$F_\chi = -ku_* \frac{\partial \chi}{\partial\left[\ln(z-d) - \Psi_H\left(\frac{z-d}{L}\right)\right]}, \tag{4.14}$$

Ammonia concentration measurements were conducted by using a high-resolution NH_3 analyzer, AMANDA (Ammonia Measurement by ANnular Denuder sampling with online Analysis) (Wyers et al., 1993). During the sampling, gaseous NH_3 is captured in a continuous flow annular denuder applying a stripping solution of 3.6 mM sodium hydrogen sulphate ($NaHSO_4$). The technique determines the air concentration of NH_3 online by conductivity (Milford et al., 2001). The concentration gradients were obtained from concentration measurements at three heights: 0.44, 0.96 and 2.06 m.

The meteorological input variables that are required for a simulation with GAG_field are the same as for GAG_patch (Table 3.2). From these, air and soil temperature (T_{air} and T_{soil}), relative humidity (RH), precipitation (P), atmospheric pressure (p), global radiation (R_{glob}), wind speed (u), wind direction (u_{dir}) and sensible heat flux (H) were observed at the measurement site. For further details on instrumentation see Milford et al. (2001). Since photosynthetically active radiation (PAR) was not measured at the site, it was calculated from R_{glob} as shown in Eq. (4.15).

Table 4.3. Urine, soil and site specific constants used in the evaluation of the field-scale model. The source of the values that were not measured at the site are also indicated. P2002 and P2003 stand for the modelling periods in 2002 and 2003, respectively. Constants not mentioned here were kept the same as defined for the baseline simulation with GAG_patch (Table 3.1).

Model constants	**Value**	**Source (if not measured)**
Urine specific constants		
A_{patch} (area of a urine patch)	40 dm^2	Williams and Haynes, 1994 (average value)
c_N (nitrogen content of urine)	11 g N dm^{-3}	Whitehead, 1995 (average values)
W_{urine} (volume of urine)	2.5 dm^3	
Soil specific constants		
θ_{fc} (field capacity)	0.37	
θ_{pwp} (permanent wilting point)	0.192	
θ_{por} (porosity)	0.54	
$pH(t_0)$ (initial soil pH)	4.95	
Γ_g (soil emission potential)	3000	Modelled (Section 4.4.3)
$\theta(t_0)$ (initial volumetric water content)	0.356 (P2002) 0.24 (P2003)	
Site specific constants		
Latitude	55.87°	
Longitude	3.03°	
Height above sea level	190 m	
A_{field} (field area)	5.424 ha	
Γ_{sto} (stomatal emission potential)	500	Massad et al., 2010b (average value)
UF (urination frequency)	10 $animal^{-1}$ day^{-1}	Whitehead, 1995 (average values)
z_w (height of wind measurement)	1 m	
h (canopy height)	0.07 m (P2002) 0.08 m (P2003)	
LAI (leaf area index)	0.9 m^2 m^{-2} (P2002)[a] 1.1 m^2 m^{-2} (P2003)[b]	
Number of cattle on the field	40, 17 (P2002)[c] 50, 52 (P2003)[c]	

[a]There was no measurement in P2002, therefore, the average of the measurements for P2003 was used.
[b]The value was measured on 23/06/2003.
[c]The date when the number of animals changed in P2002 and P2003 were 28/08/2002 and 23/06/2003, respectively.

Figure 4.4. Satellite photo of the Easter Bush site generated by Google Maps, indicating the two halves of the field and the place of the instruments on the border of the two denoted by the small yellow rectangle. (The figure is taken from the metadata file by CEH.)

According to Emberson et al. (2000), *PAR* is 45-50% of R_{glob} (0.475 in Eq. 4.15), and it is expressed in μmol m^{-2} s^{-1} (to the unit of R_{glob}, Wm^{-2}, a conversion factor of 4.57 should be applied).

$$PAR = R_{glob} \times 0.475 \times 4.57 \tag{4.15}$$

4. 4. 2. Processing of the measured data for model application

For the baseline simulation and model evaluation, a subset of the measurement data for 2001-2007 was selected that fulfilled the following criteria:

1. there were animals on the field;
2. grazing started at the beginning of the modelling period;
3. there had been no grazing, fertilizer spreading or grass cutting in the week before the grazing started;
4. there are no significant gaps in the meteorological input data;
5. flux measurements are available for validation.

The second criterion is important because NH_3 fluxes over the field can be affected by emission from urine patches deposited earlier. If the model does not account for these, it may underestimate the fluxes. The management practices listed in the third criteria can also affect the NH_3 exchange in a given time step, as well as, fertilization can considerably affect the chemical balance of the soil. The latter would conflict with the model assumption that urine patches are deposited to a "clean" soil. The fourth criterion is necessary, because a continuous input dataset is needed for a simulation, since within GAG_patch the TAN, the water and the H^+ budgets in a given time step are dependent on the values in the previous time step (Chapter 2).

As a result of the filtering, two suitable time periods were found: 26/08/2002 00:00 - 04/09/2002 09:00 and 20/06/2003 00:00 - 25/06/2003 05:00. These periods are referred hereby to as P2002 and P2003, respectively. In both time intervals cattle were grazing on the South Field. Their number over the two modelling periods is indicated in Table 4.3.

To prepare the measured datasets for the hourly model application, firstly, they were averaged for an hour. The time resolution of the ambient air concentration (χ_a), u, T_{air} and F_χ (all at 1 m height) as well as T_{soil} was 15 minutes, whilst it was 30 minutes for p, R_{glob} and RH. Secondly, in the resulted averaged time series (except in F_χ) gap-filling was carried out. Data were missing from the χ_a dataset for the simulation for P2002:

- over 27/08 13:00 – 28/08 13:00,
- on 02/09 at 23:00,
- and over 03/09 13:00 – 17:00.

The individual gap was interpolated from the values from the previous and next time step, whilst over the longer periods of missing data in χ_a (25 and 5 consecutive hourly time steps), the values were assumed to be zero. In P2003 a single, hourly wind speed was missing at 01:00 on 25/06, which was interpolated based on the data in the neighbouring two time steps.

In the third step of data processing, the measured fluxes were filtered according to the wind direction. As mentioned above, animals were grazing on the South Field and

the fluxes were measured at the border line of the two fields (Fig. 4.4). Therefore, to distinguish the fluxes over the investigated part of the field, only the fluxes were used in the comparison that were associated with wind from the direction of the South Field, between 135° and 315°. The wind blew from this direction in most of the time. In the two modelling periods in P2002 and P2003 the wind direction was the opposite in the 7% and 15% of the hourly time steps, respectively. The fluxes were further filtered according to when AMANDA was working properly as described in Section 4.5.

In addition, although the NH_3 concentrations measured in the time steps with u_{dir} from the North Field represents the concentration in the North Field, in order to keep the continuity in the input data, these values were kept in the dataset. If they were substituted with zeros (similarly as it was handled in the gap-filling of χ_a), another type of error would have been added to the input data. Considering the small number of u_{dir} values from the direction of the North Field, this choice is not anticipated to result in large errors in the NH_3 flux simulations.

4. 4. 3. Model constants

The main urine-patch-specific constants defined in Chapter 3, the soil buffering capacity (β) and the thickness of the NH_3 source layer (Δz), were not changed in the field-scale model experiments (Table 3.1). The other field, urine and site specific constants together with their sources are listed in Table 4.3.

For the constant Γ_{sto} for the clean area of the field, the values from the emission potential inventory by Massad et al. (2010b) for unfertilized grasslands were averaged. Since in the referenced inventory there was no Γ_g data for non-fertilized grasslands, it was defined during preliminary simulations with GAG_field over a time interval when the grassland was not disturbed by any kind of management practice (grazing, fertilizer spreading or grass cutting). The time period of 01/06/2003 00:00 – 09/06/2003 00:00 fulfilled this criteria. These preliminary model experiments indicated a close agreement between the measured and simulated NH_3 fluxes with a Γ_g of 3000. Therefore, this value of Γ_g was applied in the baseline simulations with GAG_field.

4. 5. Field-scale model results

The model results for P2002 and P2003 are illustrated in Fig. 4.5. These simulations are regarded as the baseline simulations and are separately discussed and evaluated in Sections 4.5.1 and 4.5.2. In order to illustrate the uncertainty in the measured NH_3 fluxes, in Fig. 4.5 the simulations were plotted together with three flux estimates derived from: 1) the bottom and middle level NH_3 concentration measurements ("low-mid"), 2) the middle and top level measurements ("mid-top"), and 3) the bottom and top level measurements ("low-top"). In addition to the general evaluation of the baseline simulations, in Section 4.5.3, the contribution of the NH_3 emission from the urine patches to the NH_3 exchange over the whole field is also investigated.

4. 5. 1. Baseline simulation and model evaluation in P2002

In P2002, the three flux estimates were highly different (Fig. 4.5 a), not just in the magnitude of the fluxes but also in their direction. The metadata of the measurements suggested that there might have been a failure in the bottom denuder, implying that the fluxes calculated for the "mid-high" case are closest to the real fluxes. However, the almost completely symmetrical variation of the "mid-high" and "low-high" measurements and the twice as high "low-mid" as "low-high" fluxes indicate that the measurements in the middle level and the top level might have been swapped in the measurement dataset. To test this hypothesis, the fluxes were recalculated, using the medium level NH_3 concentrations as had been measured in the top level and vice versa. The three fluxes calculated in this way (Fig. 4.6) are in a broad agreement, representing consistently emissions from 31/08 to the night of 03/09.

Although the feasibility of such a swap between the denuders is noted also in the metadata of the measurements, it is unclear exactly over which period were the middle and top level concentrations mishandled. On the one hand, the agreement between the three measured NH_3 fluxes was better around 03/09 00:00 (between 02/09 20:00 to 03/09 6:00) in the original dataset (Fig. 4.5 a) than in the modified one (Fig. 4.6). On the other hand, from the beginning of the modelling period to 28/08 6:00, GAG_field gives a better representation of the original observations than the modified ones, suggesting

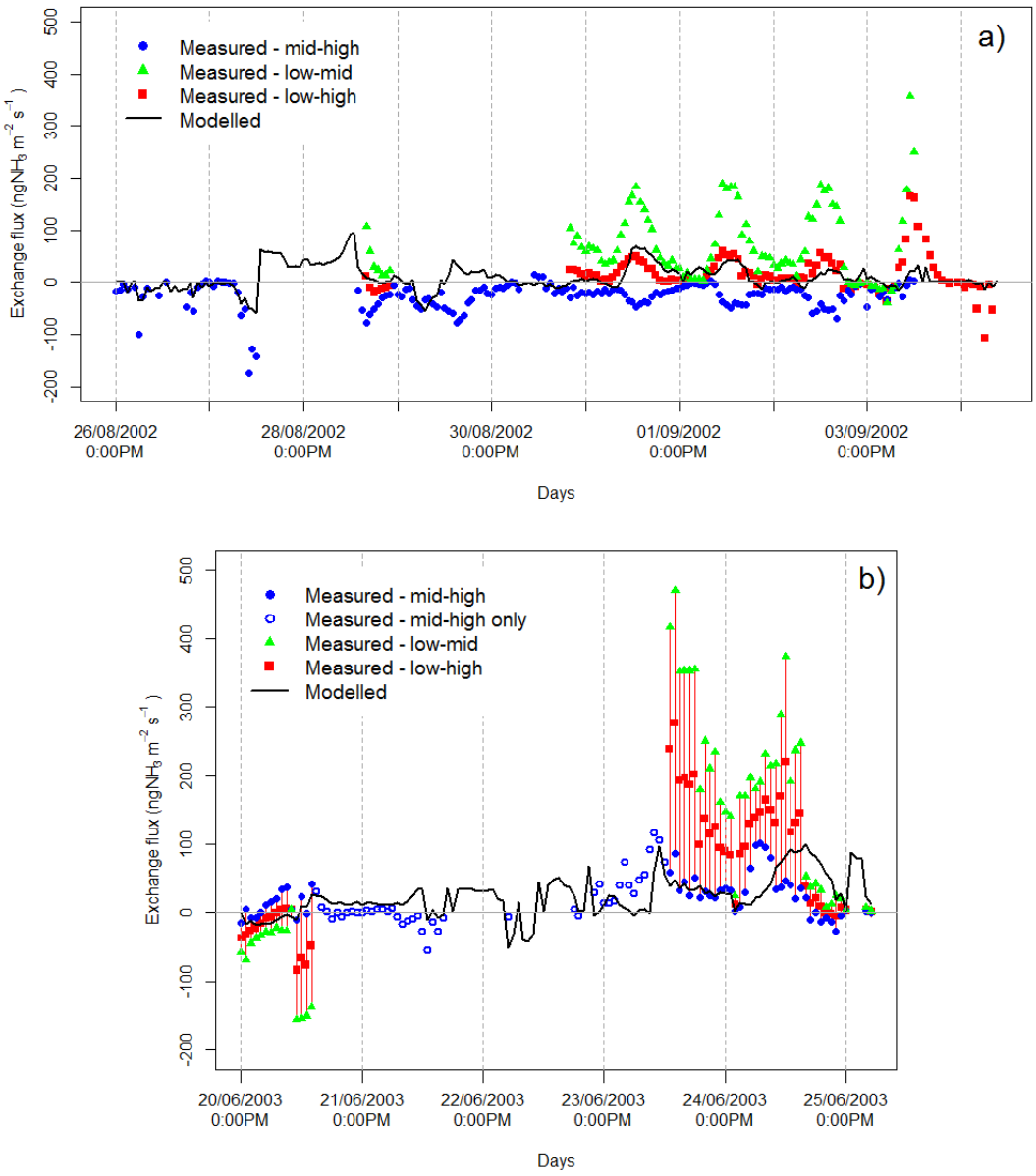

Figure 4.5. The simulated NH_3 fluxes and the measured fluxes derived based on the NH_3 concentration gradients between the three heights of measurement in the modelling periods in P2002 (a) and P2003 (b). In the bottom panel the uncertainty of the flux measurements is depicted as error bars (vertical lines, connecting the measured data points in a given time step).

that the swap between the denuders might have occurred afterwards. It is concluded that the NH_3 concentration measurements were most likely swapped between 28/08 6:00 and 03/09 6:00.

Examining the differences between the measurements (as modified above) and the simulation (Fig. 4.6), it can be concluded that the model is in a broad accordance with the observations. It captures the characteristic daily variation of NH_3 exchange detected over 31/08-02/09, with the magnitudes of the modelled and measured values being quite close to each other.

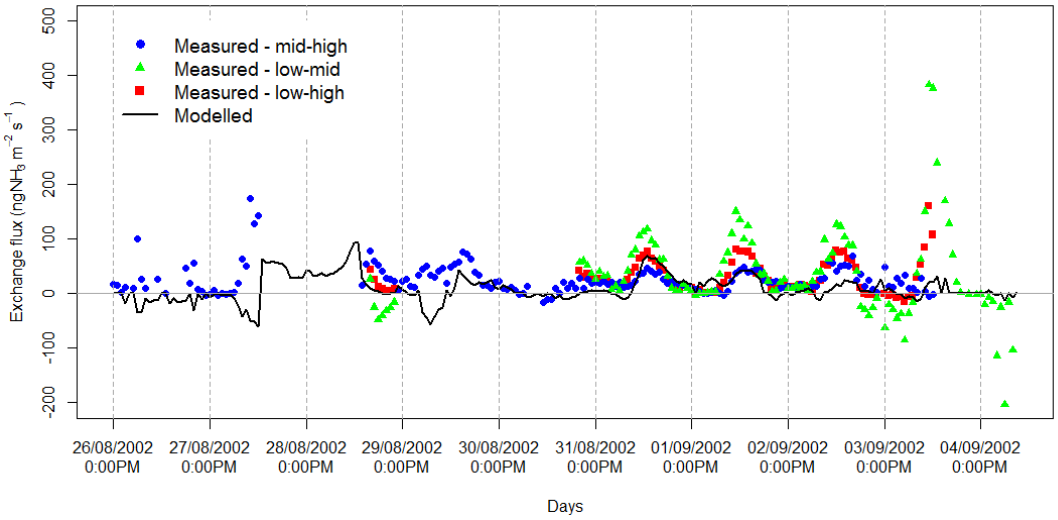

Figure 4.6. The simulated and the measured NH_3 fluxes in the modelling period P2002 when the NH_3 concentrations measured at the top and middle level were swapped.

The largest difference occurs on 02/09 when the model clearly underestimates the observations. Discrepancies between the simulated and measured values can be also seen in the first two days of the modelling period and on the fourth day. Nevertheless, on these days the bottom sensor did not work; therefore, the reliability of the single flux calculated based only on the concentration measurements at the middle and top level is less certain.

Also, according to the metadata, on 27/08, before the gap in the observed fluxes (Fig. 4.6), the stripping solution of the denuder ran out. This could explain the last 2-3 measured values beforehand, which were very high in the modified measured flux dataset (Fig. 4.6) and very low in the original one (Fig. 4.5). Finally, on 03/09 the measurements suggest a higher NH_3 flux than was simulated; however, the large differences in the measured fluxes imply that these observations are also coupled with

uncertainty. This is also suggested by the metadata, indicating a failure at midday in the middle (or if it was swapped, the top) sensor.

4. 5. 2. Baseline simulation and model evaluation in P2003

In the case of the P2003, the three measured fluxes were in a good agreement at the beginning of 20/06 (Fig. 4.5 b), then a large difference occurred between them until the "low-mid" and "low-high" fluxes ceased to be reported at 15:00. The three fluxes were available again on 23/06 from 13:00; however, they showed a large uncertainty, which seemed to disappear on the next day from 16:00 PM, when the fluxes were again close to each other.

According to the metadata, on the first day a failure was detected in the bottom denuder, which could lead to unrealistic "low-high" and "low-mid" fluxes. This also implies that the single flux measurement, after the bottom sensor completely stopped, most probably represents concentrations close to reality. On 23/06 the faulty denuder was fixed, which probably had to settle before correct functioning. This might also explain why the difference between the three fluxes diminished on 24/06. As a consequence of these considerations, among the observed fluxes, most likely the "mid-high" one represents reality the best.

Comparing the model results for P2003 with the measurements (Fig. 4.5 b), it can be concluded that the simulation is in a close agreement with the observations. The match with the "mid-high" fluxes is especially close in the second half of 23/06. The largest difference emerged on the next day, in the morning, when an emission peak was detected in the measurements. Although during the day there was also a midday peak in the simulation, it occurred 6 hours later than the maximum in the observation. When the flux peaked in the observation, a local maximum was also observed in u (see in Chapter 5, in Fig. 5.4), whose effect might have been not captured by GAG_field. Although the effect of u on the NH_3 flux is included in the model, the stronger measured fluxes could imply that the influence of u is proportionally larger through the atmospheric and within canopy resistances than estimated by the model.

4. 5. 3. Contribution of the urine patches to ammonia exchange over the field

Examining the contribution of the urine patches as well as the clean area to the simulated NH_3 exchange flux over the whole field in the two modelling periods (Fig. 4.7), it can be seen that the temporal variation of the NH_3 fluxes over the whole field were dominated by the NH_3 emission from the urine patches, which was substantially reduced by simultaneous NH_3 deposition to the clean area. Without the urine patches in both experiments, deposition would have occurred for most of the time.

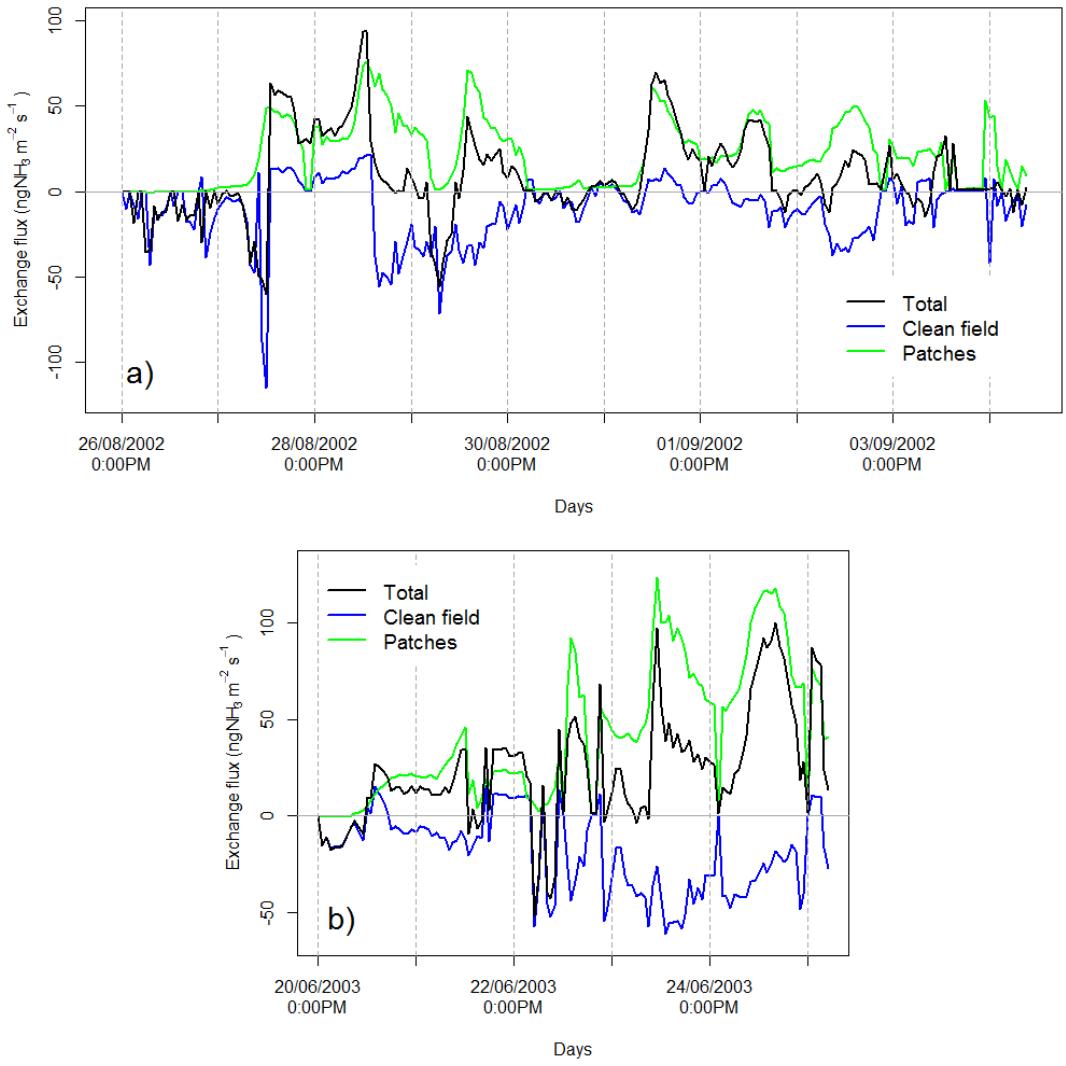

Figure 4.7. Simulated NH_3 exchange fluxes over the urine patches, the clean area and the whole field in the modelling periods P2002 (a) and P2003 (b).

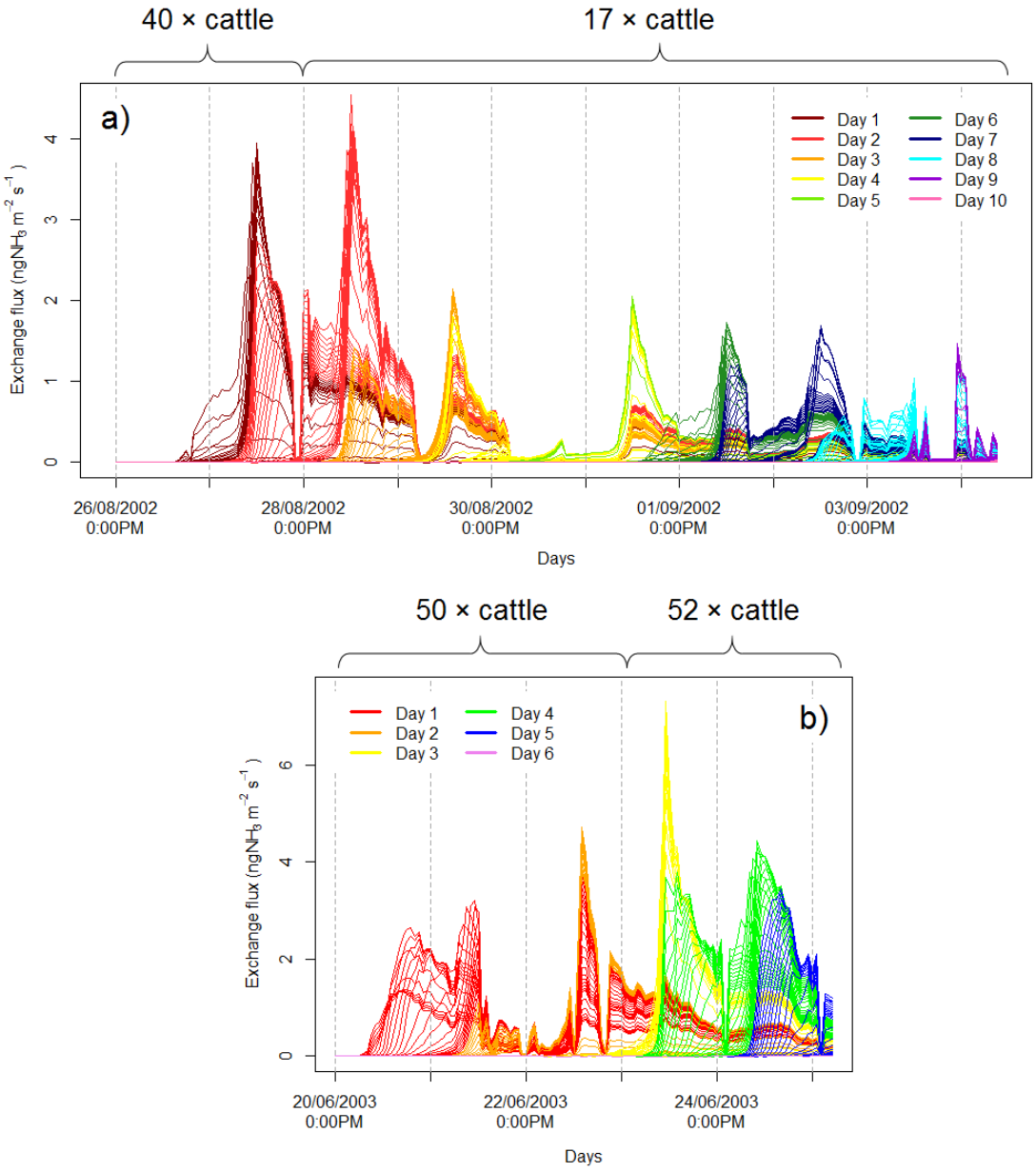

Figure 4.8. Simulated NH_3 fluxes from urine patches deposited in the same time step in the modelling periods P2002 (a) and P2003 (b). Each line indicates NH_3 fluxes from urine patches deposited in a given time step (expressed for the whole field), while the different colours indicate the days of the urination events. The number above the plots show how many cattle were grazing in the given time intervals.

This confirms the considerable effect of the presence of grazing animals on NH_3 exchange over grasslands.

The contribution to the NH_3 exchange flux was also investigated for the groups of patches deposited in the different time steps (Fig. 4.8). The ensemble of the fluxes from the different patches show a clear daily variation with NH_3 emission peaks at midday in both modelling periods. In P2002, these peaks became lower from the fourth day because after the third day instead of the initial 40 animals, only 17 cattle were grazing on the field, depositing fewer urine patches.

In the baseline experiment with GAG_patch, the first and highest peak in NH_3 emission occurred about 12 hours after the urine application (Fig. 3.1 a). By contrast, in the current results (Fig. 4.8) it can be observed that in some cases the highest peak over an individually deposited urine patch emerges later, only a day or two days after the urination event. For example, in P2002 (Fig. 4.8 a) from the urine patches deposited on the third day (orange lines) the highest emission occurred on the fourth day, or from the patches deposited on the fourth day (yellow green lines) the maximal flux was observed two days later. Further examples from P2003 (Fig. 4.8 b) are the urination events on the second day (orange lines) from which the highest flux can be observed a day after.

It has to be also noted that NH_3 emission fluxes in a given day can be substantially affected by urine patches deposited several days earlier. For instance, in Fig. 4.8 a), on 02/09 the fluxes originating from the urination events six days before (red lines) are comparable with those from urine patches deposited two days before (dark green lines).

4. 6. Sensitivity analysis to the regulating model parameters

In the following, first, a description is provided how a general sensitivity analysis was carried out concerning the regulating model parameters, and how these results can be compared with those from the sensitivity analysis of GAG_patch (Section 4.6.1). The results (Table 4.4.) of the perturbation experiments with GAG_field are discussed in Sections 4.6.2-4.6.4. Secondly, in Section 4.6.5 the uncertainty associated with the

urinary N content (c_N), A_{patch} and *UF* is investigated. Finally, model experiments are presented in which GAG_field was tested with different constant values of soil pH (Section 4.6.6).

Table 4.4. Change in the total NH_3 flux over the field as a response to a change (±10% and ±20%) in the listed model parameters, expressed as the percentage of the total NH_3 exchange in the baseline simulations with GAG_field. Results are listed for both modelling periods, P2002 and P2003. It is also indicated how the given parameters affect total NH_3 exchange in GAG_field: through the urine patches (P) or the clean area (C).

Constants	**Effect**	**Period**	**Change in the total net flux in response to a change of the constants by**			
			-20%	**-10%**	**+10%**	**+20%**
Δz (thickness of the source layer)	P	P2002	-14%	-6%	+5%	+8%
		P2003	-8	-4%	+2%	-2%
REW (readily evaporable water)	P	P2002	0	0	0	0
		P2003	-3%	-1%	+1%	+2%
$pH(t_0)$ (initial soil pH)	P	P2002	-57%	-30%	+32%	+66%
		P2003	-79%	-42%	+48%	+100%
Γ_{sto} (stomatal emission potential)	C	P2002	-1%	-0.4%	+0.4%	+1%
		P2003	-1%	-0.3%	+0.3%	+1%
Γ_g (soil emission potential)	C	P2002	-17%	-0.8%	+0.8%	+17%
		P2003	-12%	-6%	+6%	+12%
β (soil buffering capacity)	P	P2002	+32%	+15%	-14%	-28%
		P2003	+50%	+24%	-22%	-41%
θ_{fc} (field capacity)	P	P2002	-119%	-63%	+70%	+148%
		P2003	-153%	-85%	+96%	+191%
θ_{pwp} (permanent wilting point)	P	P2002	+120%	+57%	-52%	-96%
		P2003	+157%	+76%	-65%	-118%

4. 6. 1. Methods used in the general sensitivity analysis

Similarly to the perturbation model experiments carried out with GAG_patch (Section 3.4), the sensitivity analysis of GAG_field to the regulating model parameters was

performed as follows: the investigated parameter was modified with the other parameters kept the same. At the end of every simulation, the total NH_3 exchange was calculated by summing the modelled hourly NH_3 fluxes in the given modelling period. The difference compared with the baseline simulations was expressed as the percentage of the total NH_3 exchange in the baseline model integrations (428 g N and 403 g N for the whole field in the baseline simulations for P2002 and P2003, respectively). The results for the examined parameters are listed in Table 4.4.

When the results from the sensitivity analysis for GAG_field and GAG_patch is compared, two types of lessons can be learned from the differences: 1) how the total NH_3 exchange responds to the perturbation of the regulating parameters on different scales, and 2) how the sensitivity of total NH_3 exchange to these parameters differ in the case of a single urine patch (simulated by GAG_patch) and multiple urine patches (simulated within GAG_field). For the first point, answers can be obtained with a simple comparison of the results from the two different scales (Table 3.4 and Table 4.4). In the case of the second point, it has to be considered that the modelling approach for NH_3 exchange is different in the case of the clean area and the urine patches deposited on the field (Section 4.3).

As a consequence, the parameters that are used only in the formulation of GAG_field for the urine patches have an effect on the NH_3 exchange for the whole field only through the NH_3 emission from the urine patches. These parameters are Δz, β, REW (readily evaporable water), θ_{fc} (field capacity), θ_{pwp} (permanent wilting point), and pH(t_0) (initial soil pH). The value of Δz, REW, θ_{fc}, and θ_{pwp} influence the water budget which is considered in the calculation of the stomatal resistance for both the clean area and the patches. However, this effect is negligibly small compared to that through the soil resistance applied in the model only for the urine patches. This dual effect of the water budget on soil resistance and stomatal resistance is discussed in more detail in Section 5.3. To conclude, the effect of Δz, REW, θ_{fc} and θ_{pwp} on the total NH_3 exchange over the whole field through the clean area can be neglected.

Since the net NH_3 exchange over the whole field equals to the sum of the NH_3 emission from the urine patches and the NH_3 exchange over the clean area (Fig. 4.3),

the total NH_3 exchange over the whole field (ΣF_{net}, Eq. (4.16)) over a time interval is equal to the sum of the total NH_3 exchange over the clean area (ΣF_{clean}) and the total NH_3 emission from the urine patches (ΣF_{patch}). Therefore, based on Eq. 4.16, when a urine-patch-related parameter is perturbed, the resulting differences in ΣF_{patch} and ΣF_{net} will be the same.

$$\sum F_{net} = \sum F_{clean} + \sum F_{patch} \tag{4.16}$$

Based on this difference (ΔF), the sensitivity in the total NH_3 exchange can be expressed for the urine patches ($Sens_{patch}$) and the whole field ($Sens_{net}$) as:

$$Sens_{patch} = \frac{\Delta F}{\sum F_{patch}} \tag{4.17}$$

$$Sens_{net} = \frac{\Delta F}{\sum F_{net}} \tag{4.18}$$

As over the clean area net deposition occurred (ΣF_{clean} is negative as suggested also by Fig. 4.7), ΣF_{net} in the baseline simulation was smaller than ΣF_{patch}. This results in higher $Sens_{net}$ than $Sens_{patch}$. In order to convert the values of $Sens_{net}$ reported in Table 4.4 to $Sens_{patch}$, based on Eq. 4.17 and Eq. 4.18, $Sens_{net}$ has to be multiplied by the ratio of ΣF_{net} and ΣF_{patch}. These ratios were approximately 0.5 in the baseline simulations with GAG_field (0.54 and 0.48 in P2002 and P2003, respectively).

Therefore, in order to investigate the difference in the response of ΣF_{patch} in the case of the multiple patches simulated within GAG_field and the single urine patch simulated by GAG_patch, this value of 0.5 should be applied to the percentage differences in Table 4.4 as a multiplying factor.

4. 6. 2. Sensitivtiy to Δz, REW, pH(t_0), Γ_{sto} and Γ_{soil}

According to Table 4.4, compared with the other parameters, ΣF_{net} turned out to be the least sensitive to the changes in Δz and *REW*. These percentage differences were similarly low in the case of the perturbation experiments with GAG_patch (Table 3.4), with an overall, slightly weaker sensitivity than was found in the case of GAG_patch.

In the case of pH(t_0), ΣF_{net} was found to be very sensitive to the ±10% and ±20% modifications (Table 4.4) in this parameter. However, it has to be pointed out that these changes in the value of pH(t_0) (±0.5 unit for a ±10% modification and ±1 unit for ±20%), can be considered as a large increase in the soil pH, taking into account that during intensive urea hydrolysis 2-3 units change can be expected (Fig. 4.9).

The constant Γ_{sto} and Γ_{soil} affect NH_3 exchange over the whole field exclusively through its effect on the NH_3 exchange over the clean area. As the results show (Table 4.4), the model is only slighltly sensitive to Γ_{sto}, whilst Γ_g can have a considerable effect on NH_3 exchange.

4. 6. 3. Sensitivity to β

In the case of β, strong sensitivity was detected in ΣF_{net} (Table 4.4). Since β is not used in the parametrization of the NH_3 exchange over the clean area, it affects ΣF_{net} exclusively through the urine patches. Therefore, the response of the total NH_3 exchange to the perturbation of β over the multiple patches in the two baseline simulations with GAG_field and the single urine patch in GAG_patch (Table 3.4) can be compared. To this, as explained in Section 4.6.1, the multiplying factor of 0.5 has to be applied to the percentage differences derived for β in Table 4.4. The values resulting in this way are significantly larger than those reported for GAG_patch (Table 3.4), suggesting a stronger sensitivity of ΣF_{patch} to the variation of β for the multiple patches than for the single patch. The reasons for this large difference between the two cases in the response of ΣF_{patch}, in a series of model experiments were investigated (Table 4.5).

The effect of buffering on the H^+ ion budget (Eq. 2.66) in the NH_3 source layer can be expressed with the term (pH(t_i)-pH(t_{i-1})) × β_{patch}, where $\beta_{patch} = \beta \times A_{patch} \times \Delta z$ (Section 2.8). Based on these, the main factors that can regulate the governing role of buffering in the evolution of soil pH in the model soil pore and subsequently, NH_3 exchange, are

1) pH(t_i)-pH(t_{i-1}), and

2) β_{patch}.

Considering point 1), if pH(t_0) is lower, i.e. [H^+] is higher, during urea hydrolysis more H^+ ion can be consumed, resulting in a larger increase in soil pH shortly after the urine patch deposition. This can be observed on Fig. 4.9, where in most of the urine patches deposited in the baseline simulations with GAG_field, the difference between the initial and maximum soil pH was about 3 units, whilst in the case of the baseline experiment with GAG_patch (Fig. 3.1 b), it was only 2.

Table 4.5. Results from simulations with GAG_patch, testing the effect of pH(t_0) (initial soil pH), θ_{fc} (field capacity) and θ_{pwp} (permanent wilting point) on the sensitivity of the total NH_3 emission to β. Input data were applied from the baseline simulation with GAG_patch, except for the investigated parameters, which were modified in the simulations as stated below. Bold values are taken from the input data for the baseline simulations with GAG_field, and italics denote a situation when the water content was assumed to be halfway between the field-scale values of θ_{fc} and θ_{pwp}. The sensitivity was expressed as the percentage difference in the original NH_3 emission (listed also in the table for every model experiment).

Model experiment	**Model settings**			**Original emission**	**Response of emission to a change in β by**			
	pH(t_0)	**θ_{fc}**	**θ_{pwp}**	**(g N)**	**-20%**	**-10%**	**+10%**	**+20%**
A	**4.95**	0.40	0.10	1.5 g	+5%	+2%	-2%	-5%
B	6.65	**0.37**	**0.19**	0.9 g	+3%	+1%	-1%	-2%
C	**4.95**	**0.37**	**0.19**	0.6 g	+11%	+5%	-5%	-10%
D	**4.95**	**0.37**	***0.28***	0.1 g	+42%	+18%	-16%	-30%

These larger changes in soil pH generate a larger buffering effect ((pH(t_i)-pH(t_{i-1})) × β_{patch}), i.e. a larger term in the H^+ budget, which makes the system more sensitive to a modification of β ($\beta_{patch} = \beta \times A_{patch} \times \Delta z$). This was confirmed in the model experiment A (Table 4.5). In this simulation GAG_patch was run with the initial pH of 4.95 used in the baseline simulation with GAG_field, which is lower than the initial pH of 6.65 in the baseline experiment with GAG_patch. Although the response of NH_3 exchange was relatively weak to the modifications of β, it was stronger than in the perturbation experiment for GAG_patch (Table 3.4).

Regarding point 2), the definition of β_{patch} expresses the buffering effect of the solid material of the soil on the liquid content. Since β_{patch} is independent of the liquid content of the soil, within the source layer the same buffering effect takes place even

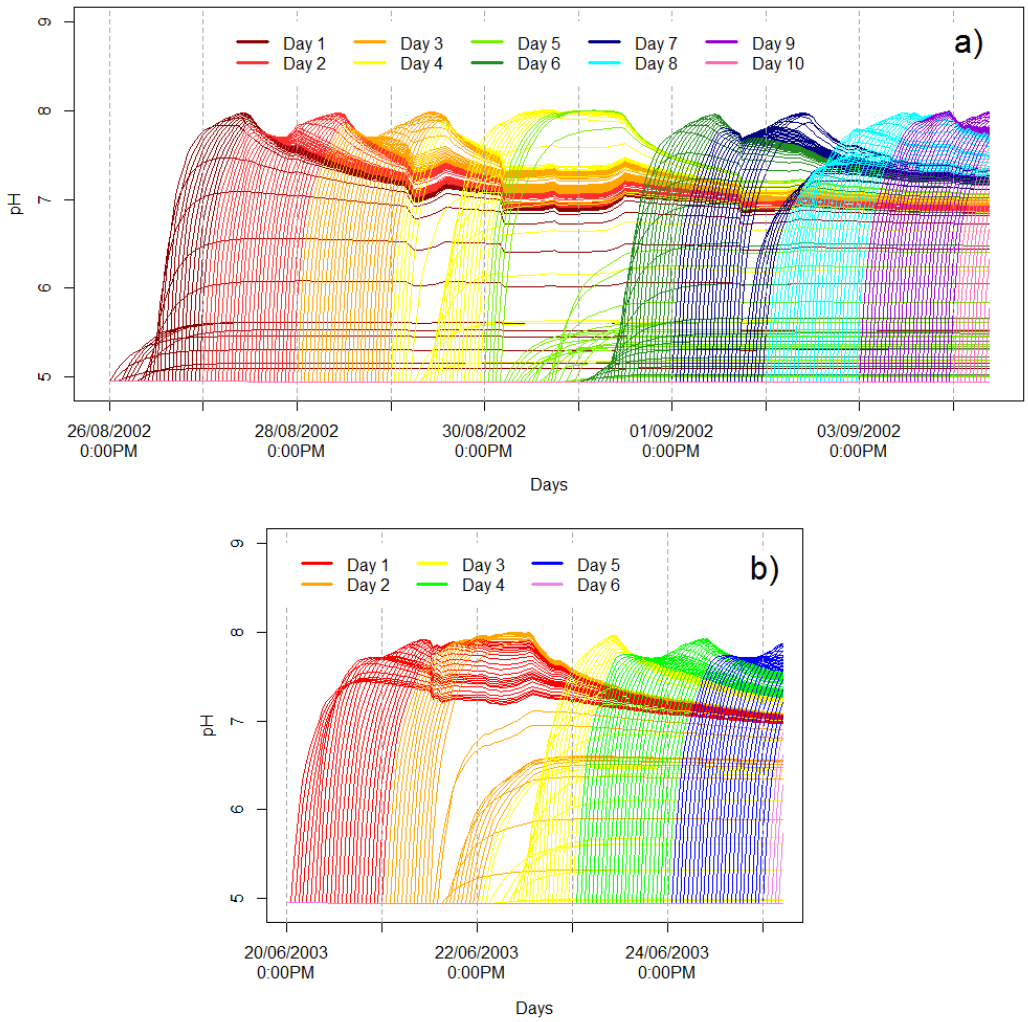

Figure 4.9. Simulated soil pH in the NH_3 source layer under urine patches deposited in the same time step in the modelling periods, P2002 (a) and P2003 (b) in the baseline experiments with GAG_field. The different colours indicate the days of the urination events. Each line indicates soil pH under urine patches deposited in a given time step, while the different colours indicate the days of the urination events.

if less urine stored in it. In a smaller amount of urine, the H^+ ion budget (Eq. 2.66) and the variations in it are proportionally smaller too. Therefore, the governing role of the same buffering capacity in the case of a smaller amount of urine becomes stronger, resulting in a stronger model sensitivity to β.

The maximum volume of urine that can be stored in the NH_3 source layer (θ_{urine}) is determined by the difference of θ_{fc} and θ_{pwp} (Eq. 3.2). The value of θ_{urine} in the baseline

experiments with GAG_field and GAG_patch were 0.18 and 0.3, respectively. This, based on the above consideration, suggests a stronger response in ΣF_{patch} to the perturbation of β for GAG_field than GAG_patch. This effect was explored in the model experiment B (Table 4.5), in which the baseline simulation with GAG_patch was performed with θ_{fc} and θ_{pwp} applied from the baseline experiment with GAG_field (Table 4.3). The results show a small difference in ΣF_{patch} in response to the change of β, but it is still larger than in the sensitivity analysis carried out for the baseline simulation with GAG_patch (Table 3.4), supporting the effect described above.

When the influence of pH(t_0) and the soil water content characteristics were examined together (model experiment C, Table 4.5), their effect added up, reaching a ±10% difference in ΣF_{patch} when β was modified by ±20%. The model was tested also with a higher θ_{pwp} (model experiment D, Table 4.5), assuming that half of the available space for urine in the model soil pore is filled with water, allowing only half of the maximum urine to infiltrate. This can represent a situation on the field when a urine patch is deposited after a rain event, when only half of the soil pore is empty. As expected, with this modification, the sensitivity to β became even stronger.

If the percentage differences for β in GAG_field reported in Table 4.4 are multiplied by 0.5, the resulting values (the percentage differences in ΣF_{patch} over the field) are smaller than was observed in the above perturbation experiments with GAG_patch (Table 4.5). This suggests that over the field scale, the sensitivity of ΣF_{patch} to β over the individual urine patches, deposited in the different time steps, can vary between wide ranges, depending on pH(t_0) and the water content of the soil at the time of the urination event. This varying sensitivity among the urine patches determines the overall sensitivity to β over the field.

4. 6. 4. Sensitivity to θ_{fc} and θ_{pwp}

In the case of θ_{fc} and θ_{pwp}, the perturbation experiments suggested an extremely strong sensitivity of ΣF_{net} (Table 4.4). Some of the changes in these parameters resulted in a ΣF_{net} that was double or almost triple (+191% in P2003 when θ_{fc} was changed by +20%) of the ΣF_{net} for the baseline simulation. Furthermore, in P2003 when θ_{pwp} was

modified by +20% the originally positive exchange turned to deposition (-118% less ΣF_{net} than in the baseline experiment).

Neglecting the effect of θ_{fc} and θ_{pwp} on NH_3 exchange through the stomatal resistance (Section 4.6.1) in the clean area, these parameters influence ΣF_{net} mostly through the urine patches. Therefore, the sensitivity to these parameters over the urine patches in the field-scale experiments is comparable with that over the single urine patch in the baseline simulation with GAG_patch (Table 3.4). In order to do the comparison, the multiplying factor of 0.5 has to be applied to the percentage differences in Table 4.4 (as explained in Section 4.6.1). Although, in this way, the resulting percentages became less extreme, they still suggest a substantially stronger sensitivity of ΣF_{patch} to the modifications of θ_{fc} and θ_{pwp} in GAG_field than GAG_patch.

As it was shown in Section 3.4.4, θ_{fc} and θ_{pwp} influence NH_3 exchange over a urine patch predominantly through θ_{urine} (Eq. 3.2), affecting the amount of urea available for hydrolysis in the NH_3 source layer. Therefore, the difference in the response of ΣF_{patch} to the changes in θ_{fc} and θ_{pwp} over the two scales, might be caused by the difference in the values of θ_{fc} and θ_{pwp} used in the baseline simulations with GAG_field and GAG_patch.

As it was pointed out in Section 4.6.3, in the baseline simulation with GAG_patch θ_{urine} = 0.3, and over the field scale θ_{urine} = 0.18. In the perturbation experiments, when θ_{fc} and

Table 4.6. The maximum space in the NH_3 source layer that can be filled by the incoming liquid (θ_{urine}) in the baseline experiments with GAG_patch and GAG_field, and the percentage it changes when θ_{fc} (field capacity) and θ_{pwp} (permanent wilting point) are modified by ±10% and ±20%.

Scale	**θ_{urine}**	**Percentage difference in θ_{urine} as a response to a change in**			
		θ_{pwp}		**θ_{fc}**	
		±10%	**±20%**	**±10%**	**±20%**
GAG_patch	0.3	±3%	±6%	±13%	±26%
GAG_field	0.18	±11%	±22%	±21%	±42%

θ_{pwp} are modified this fillable space in the source layer is also affected. As it can be seen in Table 4.6, the ±10% and ±20% modifications of θ_{fc} and θ_{pwp} resulted in proportionally smaller differences in θ_{urine} in the case of GAG_patch than GAG_field.

This effect was explored within a model experiment with GAG_patch (Table 4.7), in which the θ_{fc} and θ_{pwp} used in the baseline simulation with GAG_patch (0.4 and 0.1, respectively) were changed to those applied in the baseline simulation with GAG_field (0.37 and 0.192, respecively). All the other parameters and input variables were kept the same as in the baseline simulation with GAG_patch. The experiments were carried out in two cases for both θ_{fc} and θ_{pwp}: 1) when the initial water content of the soil ($\theta(t_0)$) was assumed to be the θ_{pwp} ($\theta(t_0) = 0.19$) and 2) when half of the available space was filled by liquid ($\theta(t_0) = 0.28$), e.g. by rain water from a preceding rainfall.

Table 4.7. Model results from model experiments with GAG_patch, testing the effect of the initial water content of the soil ($\theta(t_0)$) on the model sensitivity to θ_{fc} (field capacity) and θ_{pwp} (permanent wilting point). Input data were applied from the baseline simulation with GAG_patch, except for θ_{fc} and θ_{pwp}, which were applied from the baseline simulation with GAG_field, and $\theta(t_0)$, which was modified in the simulations as stated below. The sensitivity was expressed as a percentage difference in the original NH_3 emission (listed also in the table for every model experiment).

Parameter tested (x)	**Model setting $\theta(t_0)$**	**Original emission (g N)**	**Response of emission to a change in x by**			
			-20%	**-10%**	**+10%**	**+20%**
θ_{fc}	θ_{pwp}	0.9 g	-41%	-20%	+18%	+31%
	0.28	0.4 g	-90%	-47%	+45%	+81%
θ_{pwp}	θ_{pwp}	0.9 g	+33%	+16%	-16%	-31%
	0.28	0.4 g	+67%	+33%	-31%	-58%

As it can be seen in Table 4.7, with the $\theta(t_0) = \theta_{pwp}$ model setting, the sensitivity to both θ_{fc} and θ_{pwp} became higher than in the case of the perturbation experiment with GAG_patch (Table 3.4). This sensitivity became even stronger when urine was deposited to a half-filled source layer ($\theta(t_0) = 0.28$). If the values from Table 4.7 are up-scaled to field-scale (dividing them by the factor of 0.5 defined in Section 4.6.1),

the resulted percentage differences are similarly high to those observed in the sensitivity test for GAG_field (Table 4.4).

These results suggest that depending on the rain events and how they modify the initial water budget in the soil before a urine patch is deposited, the sensitivity of NH_3 exchange to the perturbations of θ_{fc} and θ_{pwp} over the individual urine patches deposited in the modelling period can vary widely. This varying response to θ_{fc} and θ_{pwp} amongst the urine patches deposited in the field will determine the overall sensitivity to θ_{fc} and θ_{pwp} over the whole field.

4. 6. 5. Sensitivity to c_N, A_{patch} and UF

As explained in Section 4.1, for c_N, A_{patch} and UF constant, average values were applied in the baseline simulations with GAG_field. However, in reality these parameters can vary amongst different animals, and amongst different urination events as well. To examine the model uncertainty caused by these model assumptions, firstly, a sensitivity analysis was carried out applying the minimum and the maximum of these parameters as suggested in the literature (Table 4.1 and 2 – 20 g N l^{-1} for c_N from Whitehead, 1995).

According to Table 4.8, whilst the uncertainty originating from the choice of a constant A_{patch} and UF is considerable, the uncertainty coupled with the value of c_N is extremely large. Although the model shows a large uncertainty associated with c_N, the reasonable agreement between GAG_field and the measurements (Fig. 4.5 b and Fig. 4.6) suggests that using the same average value in every time step well represents reality. In the following, the reasons of this high uncertainty associated with c_N is further examined.

In natural conditions, in an hour several, different urine patches are deposited over the field. For example, calculating with the lowest animal number on the field in the baseline experiment with GAG_field (17 from Table 4.3) and the minimal UF (8 urination day^{-1} $cattle^{-1}$, from Table 4.1), there were at least 5 urine patches deposited in an hour. When the number of urine patches is high enough, it can be assumed that the overall c_N of all the urine deposited in a given hour is characterized by the average

Table 4.8. Results from the baseline simulations with GAG_field when the maximum and minimum was applied of the investigated parameters. In every simulation the difference in the total NH_3 exchange was derived, expressed as the percentage of the total exchange in the baseline simulations with GAG_field.

Parameters	**Min/Max**	**Change in the total NH_3 exchange**	
		P2002	**P2003**
A_{patch} (dm^2)	38	-9%	+11%
	40	+9%	-11%
c_N (g N dm^{-3})	2	-187%	-211%
	20	+292%	+403%
UF (urination $animal^{-1}$ day^{-1})	8	-38%	-42%
	12	+38%	+42%

of the c_N values related to the individual urination events. This can be expressed by Eq. 4.19, in which $c_N^{Ave}(t_j)$ represents the average N concentration in the time step t_j, $c_N^k(t_j)$ stands for the N content associated with the k^{th} urine patch in t_j, and $n(t_j)$ is the number of urine patches deposited in t_j.

In the baseline simulations with GAG_field, c_N^{Ave} was assumed to be 11 g N dm^{-3} over the whole modelling period. In the following it is examined how the model responds to a value of c_N^{Ave}, which is calculated in every time step according to Eq. 4.19. To approach this task, firstly c_N^k values have to be randomized for every urination event from an estimated statistical distribution of c_N.

$$c_N^{Ave}(t_j) = \frac{\sum_{k=1}^{n(t_j)} c_N^k(t_j)}{n(t_j)}. \qquad (4.19)$$

Li et al. (2012) fitted a log-normal distribution (Eq. 4.20) to a c_N dataset, originating from the observation of two Aberdeen Angus steers over three 24 hour periods (Betteridge et al., 1986). In Eq. 4.20 σ and μ are the scale parameters of the distribution. These, in the fitted distribution by Li et al (2012), were σ = 0.786 and μ = 1.154. The mean of c_N calculated from these values (Eq. 4.21) was 4.33 g N dm^{-3}. In the study of Li et al. (2012), the findings were applied for cows, assuming that the

distribution of c_N is similar with the same σ, but a higher mean c_N. Based on these, from Eq. 4.21, Li et al. (2012) derived μ of the new distribution and from this they generated a series of samples for c_N.

$$D(c_N) = \frac{1}{c_N \sigma \sqrt{2\pi}} e^{-\frac{(\ln c_N - \mu)^2}{2\sigma^2}} \tag{4.20}$$

$$mean(c_N) = e^{\mu + \frac{\sigma^2}{2}} \tag{4.21}$$

To test the uncertainty coupled to c_N in the field-scale version of the GAG model, the following steps were carried out. Firstly, following the method described by Li et al. (2012), based on Eq. 4.21, a new distribution of c_N was obtained assuming a mean c_N of 11 g N dm^{-3}, and σ = 0.786. In this way, the scale parameter μ was found to be 2.089, and the resulted distribution of c_N is depicted in Fig. 4.10. Secondly, in every time step c_N^k values were randomized from the resulted distribution, and from these, c_N^{Ave} was derived based on Eq. 4.19. This resulted in a time series of c_N^{Ave} values. In total, 30 c_N^{Ave} time series were generated for both experimental periods (P2002 and P2003) and simulations were performed with GAG_field, for all of these time series.

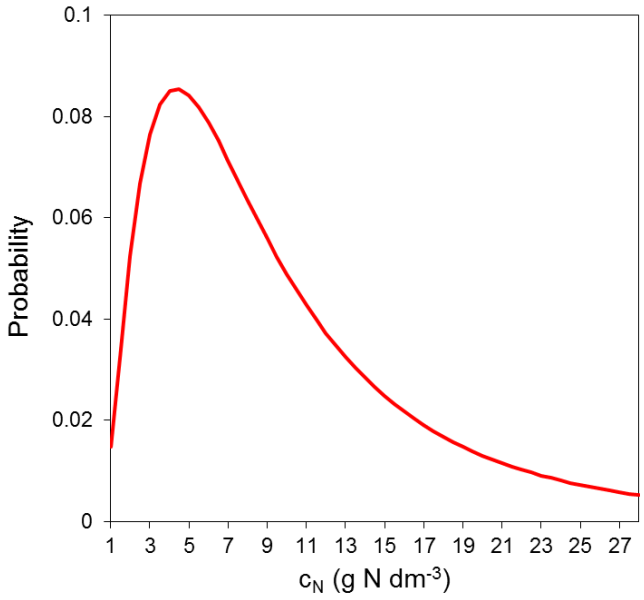

Figure 4.10. Probability density function of the log-normal distribution generated for the distribution of c_N, with scale parameters σ = 0.786 and μ = 2.089.

The ensemble of the simulations derived in this way can be seen in Fig. 4.11. In both years the largest uncertainty occurred at the peaks of the NH_3 fluxes. Overall, however, the uncertainties observed in Fig. 4.11 are much smaller than was suggested by the sensitivity analysis presented above (Table 4.8). This is because in the sensitivity analysis the two extremes of c_N were tested, whilst the c_N^{Ave} values generated from the log-normal distribution of c_N resulted in a value close to 11 g N dm^{-3} applied in the baseline simulation with GAG_field.

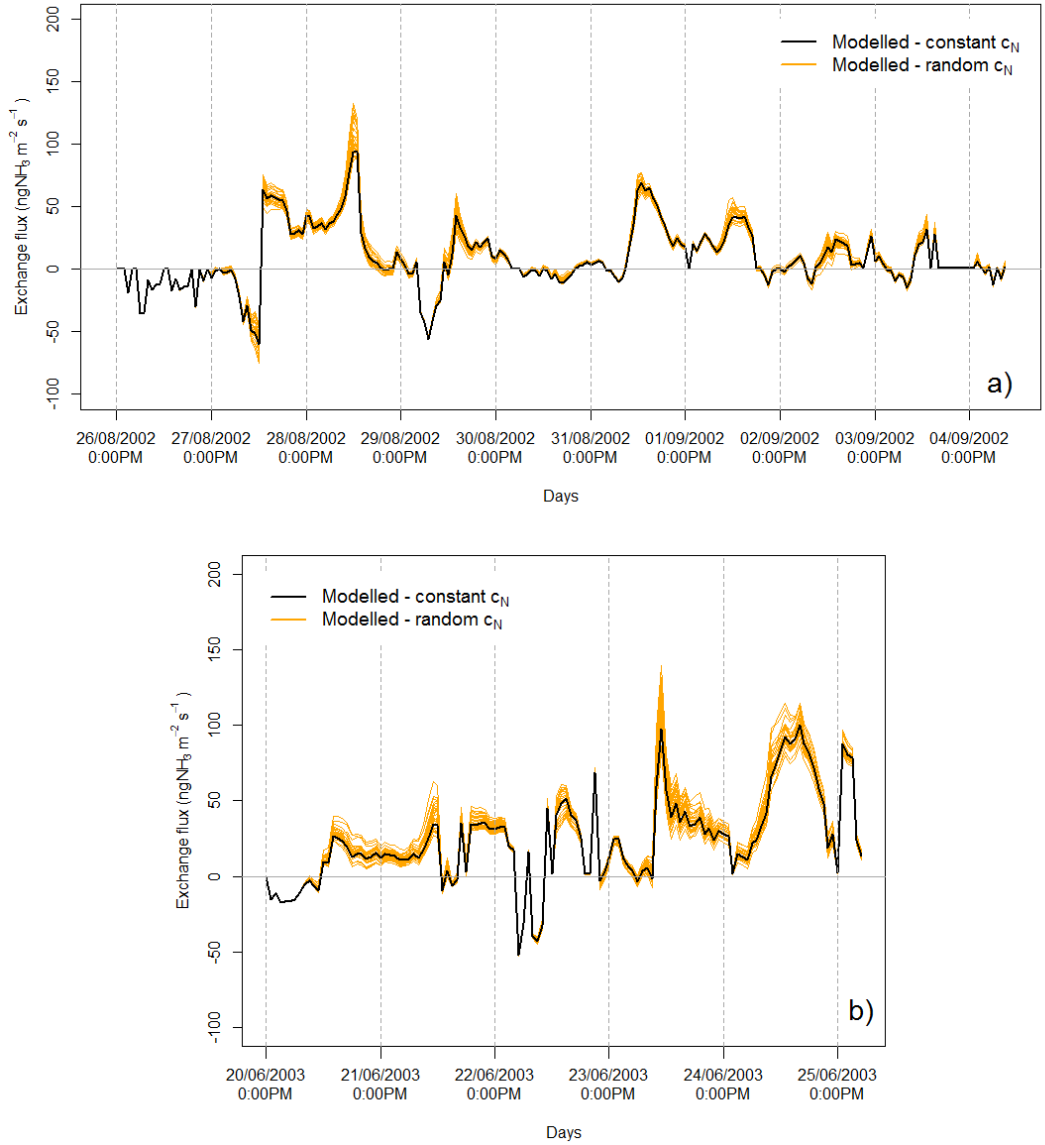

Figure 4.11. Simulated NH_3 exchange fluxes from the basewline simulation with GAG_field with a constant c_N (black line), and 30 model experiments in which c_N was randomized for every time step (orange lines) for the modelling periods P2002 (a) and P2003 (b).

4. 6. 6. Sensitivity to a constant soil pH

From the point of view of future application of the model for regional scale, computational time could be saved if a constant soil pH over the whole time period could be assumed instead of simulating soil pH dynamically for every urine patch deposited in the different time steps. To investigate the effect of such a simplification the baseline simulation with GAG_field was performed with a constant soil pH of 7.5 (GAGf_pH7.5). This value was selected, as it is the approximate value where the curve of soil pH flattens out in the case of every urine patch deposited in the baseline simulations in GAG_field (Fig. 4.10).

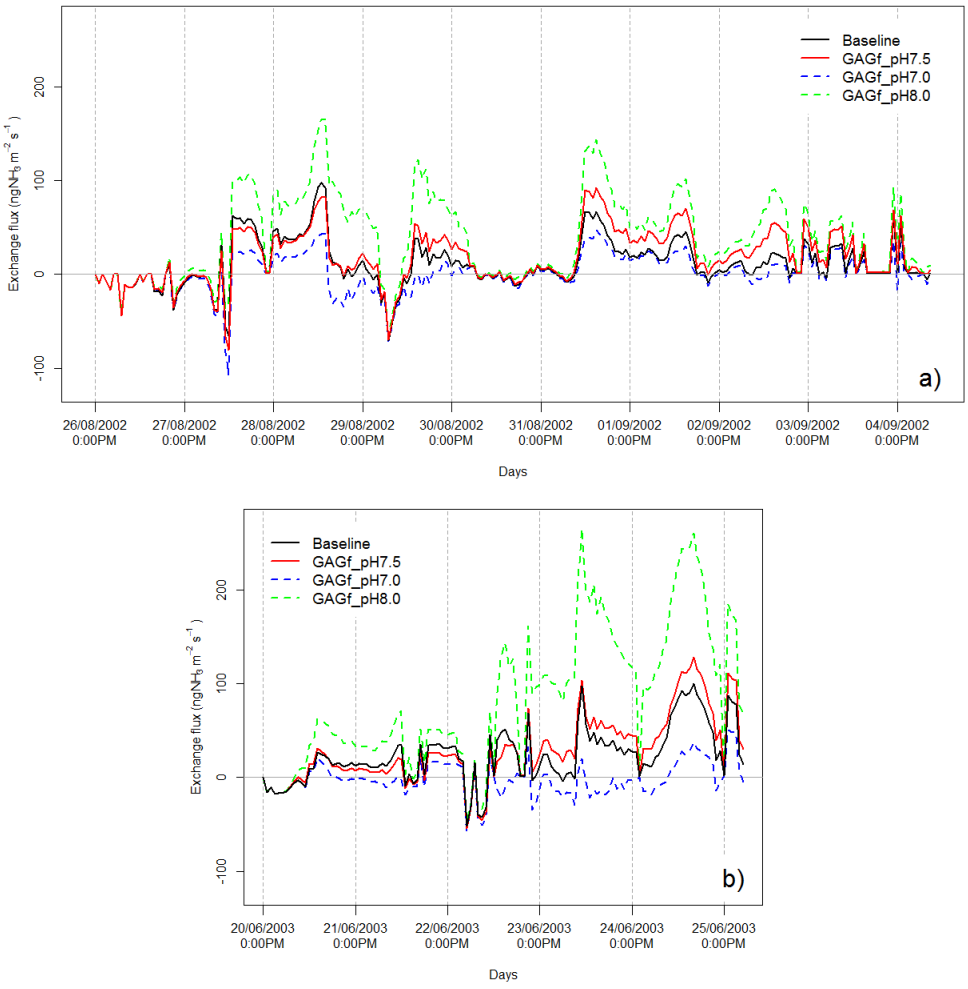

Figure 4.12. NH_3 exchange fluxes simulated by GAG_field with the original dynamic approach for soil pH (Baseline), and when constant values of soil pH were assumed: pH 7.5 (GAGf_pH7.5), pH 7.0 (GAGf_pH7.0) and pH 8.0 (GAGf_pH8.0). Simulations were carried out for both modelling periods, P2002 and P2003.

With a fix value of pH 7.5 the model produced a similar temporal variation in NH_3 flux as with the dynamically changing soil pH in the baseline simulation with GAG_field (Fig. 4.12), following relatively closely the fluxes in the baseline simulations. The model was tested with further two constant soil pH values, 7.0 and 8.0 in the experiments GAGf_pH7.0 and GAGf_pH8.0, respectively. These simulations resulted in highly different NH_3 exchange fluxes compared to those in the baseline simulations, especially in the case of GAGf_pH8.0.

Although the results from GAGf_pH7.5 suggest a possible simplification of the model for larger scale application, GAGf_pH8.0 and GAGf_pH7.0 implied that the NH_3 exchange fluxes are sensitive to the chosen constant value of soil pH. In GAGf_pH7.5 that value was applied where the soil pH stabilized under a patch after the intense urea hydrolysis stopped. However, this value might not be the same in every situation. For example, in the case of the baseline experiment with GAG_patch (Fig. 3.1 b) the curve of soil pH flattened out around pH 7. Therefore, further considerations are needed regarding the choice of a constant soil pH, which may also be expected to vary with soil type.

4. 7. Conclusions

In this chapter the NH_3 emission model developed for a single urine patch (GAG_patch) was applied for field scale. The new, field-scale model (GAG_field) was tested over two modelling periods, using NH_3 flux measurements conducted at Easter Bush, UK. Although there are uncertainties in the observational dataset, it was concluded that the model represents well the observed fluxes. It was found that the temporal evolution of the NH_3 exchange flux over a grazed field is dominated by the NH_3 emission from the urine patches, which is substantially decreased by the simultaneous NH_3 deposition to the clean area. The results presented also showed that the evolution of NH_3 emission from urine patches deposited in different time steps can be substantially different and that NH_3 fluxes in a given day can be considerably affected by urine patches deposited several days earlier.

The findings, resulting from the sensitivity analysis to the regulating model parameters, showed that GAG_field was highly sensitive to the buffering capacity (β), the field capacity (θ_{fc}) and the permanent wilting point (θ_{pwp}). The observed sensitivities turned out to be much higher than was found in the case of GAG_patch. The different sensitivities over the two scales can be explained by the different initial soil pH and the different soil physical characteristics which determine the maximum volume of urine that can be stored in the NH_3 source layer. It was found that in the case of a higher initial soil pH and higher initial soil water content, the sensitivity of NH_3 exchange to β was stronger. Also, in the case of a higher initial soil water content, NH_3 exchange was more sensitive to the changes in θ_{fc} and θ_{pwp}.

The sensitivity analysis also showed that the nitrogen content of urine (c_N) is coupled with an extreme uncertainty. However, model experiments based on c_N values randomized from an estimated statistical distribution, implied that this uncertainty might considerably smaller in practice than it was suggested by the sensitivity analysis.

Finally, GAG_field was tested with a constant soil pH of 7.5 to see how well a simpler model structure could perform, such for a regional scale application. The variation of NH_3 fluxes simulated in this way showed a good agreement with those from the baseline simulations with GAG_field that accounts for a dynamically changing soil pH. These results suggest a way for model simplification when GAG_field is applied later for regional scale. However, since the NH_3 exchange fluxes showed a large sensitivity to the value of the applied constant soil pH, further examinations are needed, concerning the choice of the this constant value.

Chapter 5

Investigation of the influence of meteorological variables, in particular temperature on NH_3 exchange over grazed fields

5. 1. Introduction

The exchange of NH_3 between the surface and atmosphere is affected by meteorological variables in many ways, as reviewed in Chapter 1. Accounting for these effects, meteorlogy-driven models for NH_3 exchange above a urine patch (Chapter 2) and grazed fields (Chapter 4) were constructed. As such, these tools can be used to explore the influence of meteorology on the process of NH_3 exchange at both patch and field scale.

This chapter focuses on the influence of meteorology on the simulated NH_3 fluxes at both the patch and field scale. Firstly, a sensitivity analysis is carried out for both the patch- and field-scale version of the model and a detailed investigation of the effect of the different meteorological variables on NH_3 exchange is presented (Section 5.2). The next section of this chapter focuses in particular on the influence of temperature. This section considers both the temperature-dependency of NH_3 exchange over the different scales, and the applicability of the widely-used metric for the strength of temperature-dependency, Q_{10} is examined (Section 5.3).

5. 2. Sensitivity analysis to meteorological variables

In the following subsections the results of a comprehensive sensitivity analysis of the patch-scale (GAG_patch) and field-scale version (GAG_field) of the GAG model is

presented (Sections 5.2.1 and 5.2.2, respectively), which is followed by a comparison of the outcomes of the perturbation experiments for the two scales (Section 5.2.3).

5. 2. 1. Sensitivity analysis to meteorological variables over a urine patch

As discussed in Chapter 1, NH_3 emission fluxes over a urine patch are influenced by a number of different meteorological variables. In Fig. 5.1 the measured time series of these variables are plotted for the baseline simulation with GAG_patch (Section 3.3), together with the measured and simulated NH_3 fluxes. The NH_3 emission flux peaked every day shortly after midday, when soil temperature reached its maximum. The only exception was the third day after urine application when the curve of emission flux stayed flat in the simulation, which was linked to the rain event as discussed in Section 3.4.3.

To test the sensitivity of the total NH_3 emission to the change of a given meteorological variable, the variable was modified, and while keeping all the other parameters the same, a simulation was carried out with GAG_patch. At the end of every simulation the total NH_3 emission was calculated over the period, and expressed as the percentage difference compared to the total emission in the baseline simulation with GAG_patch (1.78 g N). The original meteorological datasets were modified in every case by $\pm \Delta x$, calculated as 10% of the difference between the measured minimum and maximum value of the given variable over the modelling period.

Table 5.1 shows that the total NH_3 emission was the most sensitive to the change in relative humidity (*RH*) (the differences in total emission were +9.1% and -8.6%) and wind speed (u) (the differences were -5.5% and 4.7%). In addition, a relatively high difference (+4.1%) was observed in the case of global radiation (R_{glob}) when its values were raised by Δx. The effect of R_{glob} on the total NH_3 exchange is discussed in more detail in Section 5.2.3.

When soil (T_{soil}) and air temperatures (T_{air}) were modified separately, relatively small anomalies were observed in the total NH_3 emission (less than 3% in absolute value for both T_{soil} and T_{air}). However, when T_{air} and T_{soil} were adjusted together (assuming that the change of these two temperature variables occurs parallel), the

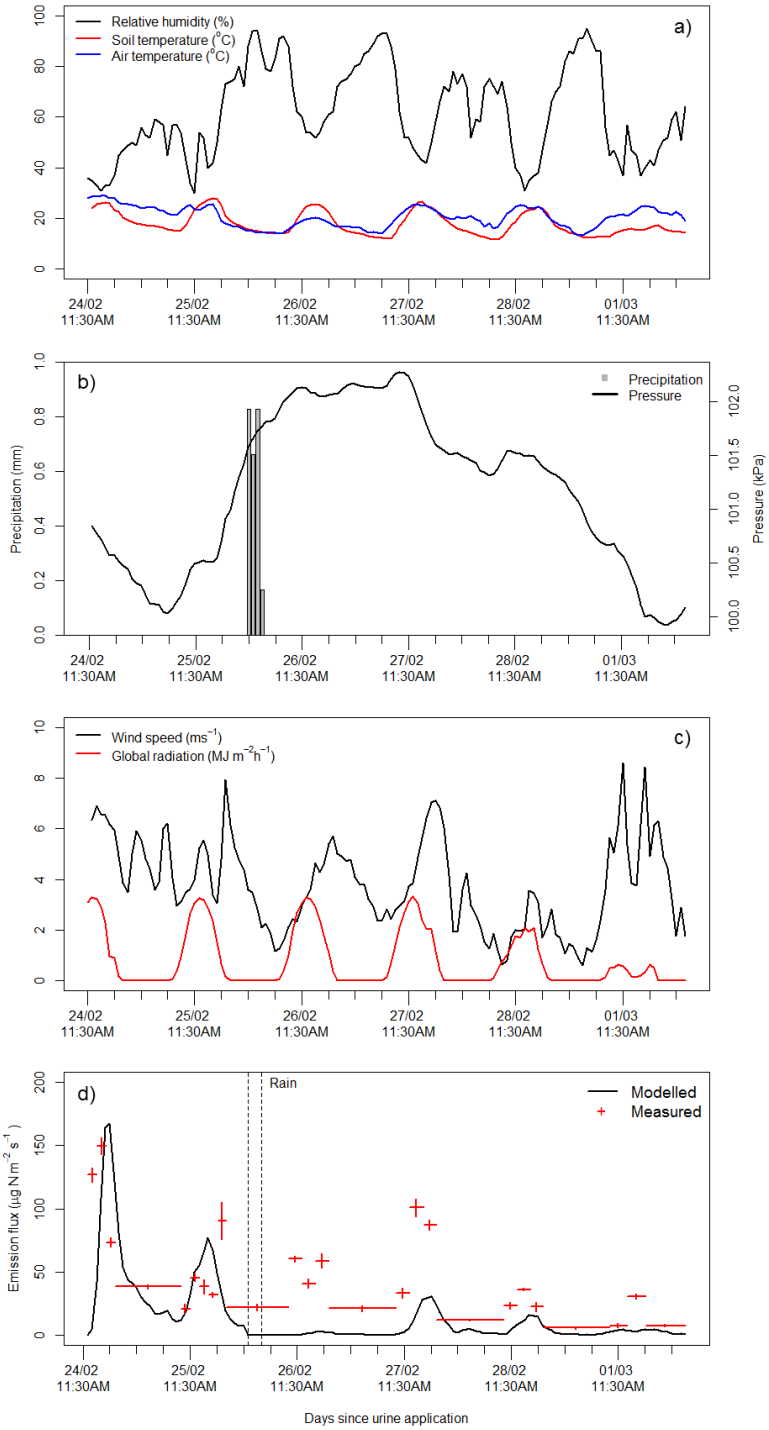

Figure 5.1. The investigated meteorological variables at Lincoln, New-Zealand (relative humidity, soil and air temperature (a), precipitation and surface pressure (b), wind speed and global radiation (c)) and the hourly NH_3 fluxes measured at the site and simulated by GAG_patch as shown in Fig. 3.1. a.

Table 5.1. The results of the sensitivity analysis to the changes of the different meteorological variables for GAG_patch. The variables were changed by ± Δx derived based on the minimum and the maximum of the given variable over the modelling period (Δx = (Max-Min)/10), and the difference in the total NH_3 emission over the modelling period compared to the baseline simulation was calculated.

Variable	**Min**	**Max**	**Δx**	**Total NH_3 emission change in response to change in parameter by**	
				- Δx	**+ Δx**
u (ms^{-1})	0.62	8.59	0.80	-5.5%	+4.7%
T_{soil} (^0C)	11.6	27.9	1.64	-2.6%	+2.7%
p (kPa)	99.9	102.3	0.24	+0.0%	-0.0%
T_{air} (^0C)	13.5	29.0	1.56	-2.4%	2.9%
R_{glob} (MJ m^2 h^{-1}) [a]	0.00	3.32	0.33	-2.0%	+4.1%
RH (%) [b]	30	95	6.50	+9.1%	-8.6%
RH (%) [b]	only for evaporation [c]			+3.2%	-2.8%
P(mm) [d]	0.00	0.83	0.08	-0.7%	+0.8%
T_{air} and T_{soil} (^0C)	-	-	-	-4.9%	+5.7%

[a]When changed by -Δx, negative values were replaced by 0.
[b]When changed by + Δx, values greater than 100% were reduced to 100%.
[c]In this test RH was modified by the same extent but only in the evaporation module.
[d]The hourly precipitation sum was changed only in the hours when there was precipitation originally.

differences were larger (see Table 5.1). Only weak sensitivity was detected in the case of atmospheric pressure and hourly precipitation.

The results for *u* and the different temperature variables can be explained as follows. Wind speed plays a governing role in turbulent mixing of the quasi-laminar and turbulent layer (Section 2.4); consequently, it has a considerable effect on the vertical atmospheric transfer of NH_3. Regarding temperature, urea hydrolysis as well as the compensation point, both in the stomata and the soil pores, follow an exponential function of temperature (Sections 2.6, and 2.4, and 2.5, respectively).

Relative humidity has a dual effect on the total NH_3 emission. Firstly, it plays a vital role in the water budget through soil evaporation and secondly, it influences the

deposition of NH_3 to the leaf surface. To asses the effect of these processes on the total NH_3 emission flux, a further simulation was performed, where *RH* was modified only in soil evaporation. This perturbation experiment resulted in only a +3.2% difference for - Δx and -2.8% for +Δx change, whilst in the original sensitivity test these changes in the total NH_3 emission were +9.1% and -8.6%, respectively. Since in GAG_patch *RH* affects NH_3 emission only through soil evaporation and the NH_3 deposition to the leaf surface, the above results suggest that the effect of *RH* on NH_3 emission in GAG_patch is stronger through NH_3 deposition to leaf surfaces than through soil evaporation.

The physical explanation for the inverse relationship between *RH* and total NH_3 emission is that at higher values of *RH* the formation of a water film on the leaf surface is more likely (Burkhardt et al., 1999). As a result, deposition to the leaf surface is more effective, which will tend to reduce the net emission flux (including the exchange with soil and stomata as well as the deposition to cuticle) over the urine patch.

The total NH_3 emission over the period was not strongly sensitive to a change of ±10% in the hourly amount of precipitation (±0.08 mm) (Table 5.1). This is a result of the model formulation that 1) allows only a ($\Delta z \times (\theta_{fc} - \theta_{pwp})$=) 1.2 mm of maximum liquid content in the model soil pore and 2) does not allow TAN to be washed out from the source layer. Therefore, in GAG_patch even a heavy rain event (> 6 mm / hr) – apart from a slight effect on evaporation – has the same effect as a modest 1.2 mm / hr of precipitation. In the baseline simulation during the rain event, the soil reached its maximum water content, which was assumed to be the at field capacity (θ_{fc}) (Section 2.7). It was found that by decreasing the amount of total precipitation so that the soil does not reach θ_{fc}, the maximum difference in total emission was +3%.

In addition to a modification in the amount of precipitation, the timing of the rain event can also lead to a difference in the total NH_3 emission. To test the model sensitivity to this effect, the exact same hourly precipitation values were assumed and only the starting time of the rain event was modified. Fig. 5.2 (a) shows that the change of the timing of the rain event can lead to up to a 6% reduction or 2% increase in the total NH_3 emission.

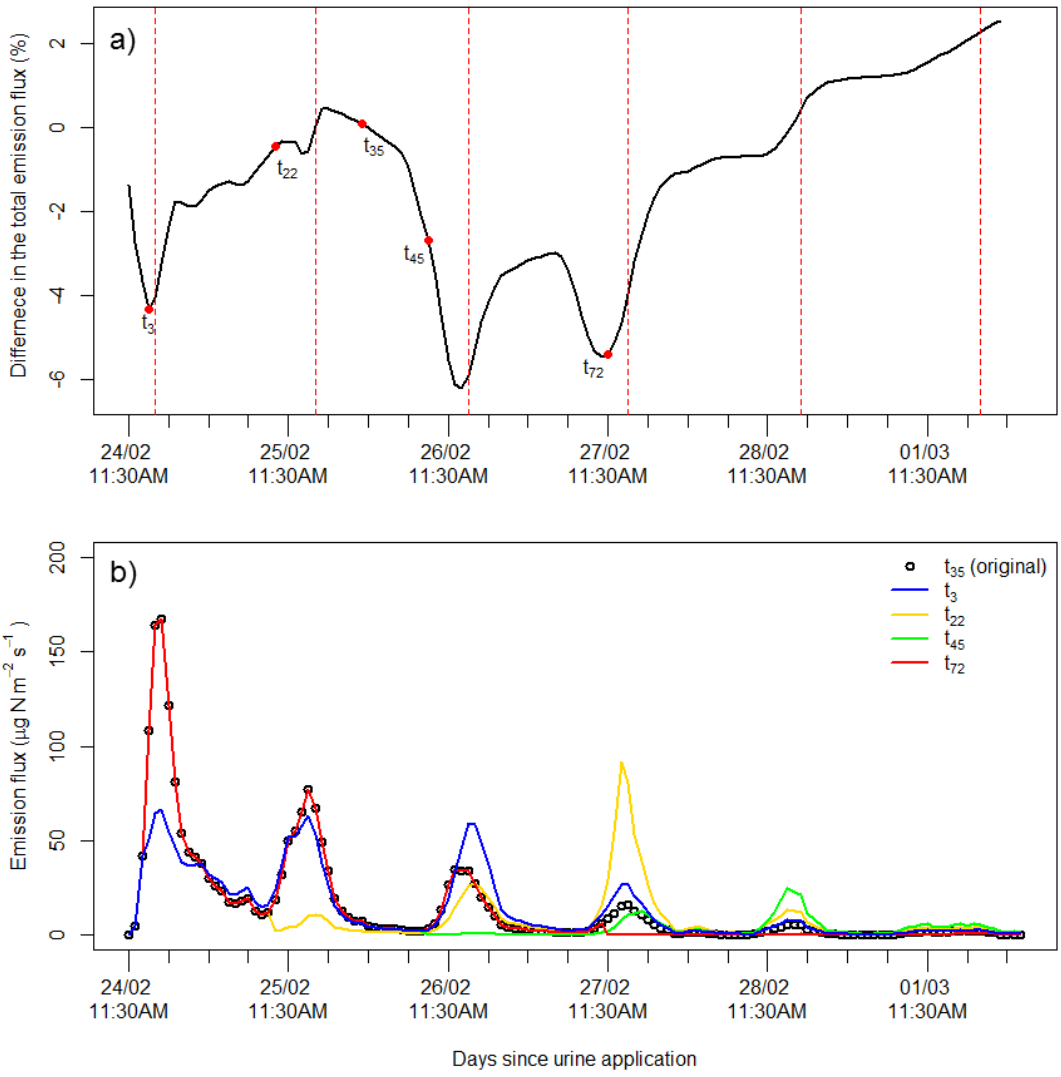

Figure 5.2. (a): The difference in total NH_3 emission over the modelling period compared with the baseline simulation (t_{35}) for a given starting time of the rain event. Dashed red lines indicate the time of the daily maxima of soil temperature. (b): Hourly ammonia emission for the time steps indicated on panel (a) with red dots. Before the lines become visible, they follow the values in the baseline simulation ("t_{35}, original").

If it starts raining close to the time of urine application, at the beginning of the modelling period, the larger soil resistance (R_{soil}) reduces the total NH_3 emission by suppressing the first peak of emission (see Fig. 5.2 b, time step t_3). Further local minima occur in the total emission two and three days after urine application (Fig. 5.2 a). At these times the rain event coincided the daily maxima of T_{soil}, which are when the daily peak of NH_3 emission is expected. In these cases the increased R_{soil} also

inhibits volatilization. For example, in the 45th time step (Fig. 5.2 b) the third peak of emission disappeared. If the rain event occurs after the daily maximum of T_{soil}, the prevented peak appears (as it can be seen Fig. 5.2 b, time step 72), and at the same time an increase in the total NH_3 emission can be observed.

Nevertheless, if precipitation infiltrates into the soil, when there is still enough TAN available for volatilization, apparently the "trapped" TAN can be emitted later when R_{soil} declines due to evaporation. This will lead to a larger minimum in the total NH_3 emission. An example can be seen for this process in Fig. 5.2 (b), when it started raining in the 22nd time step (t_{22}), supressing the second NH_3 emission peak but enhancing the fourth peak two days later, when the soil dried out.

On the other hand, if precipitation occurs several days after the deposition of the urine patch (e.g. four or five days after urine application) total emission does not decline. This is because, after the third day the increased R_{soil} prevents all the NH_3 emissions after rainfall until the end of the period (Fig. 5.2 (b), t_{72}). The reason for this is that in this later period only a small amount of TAN remains in the soil, which is not able to overcome the effect of the R_{soil}. Later, as the rain event passes the daily maximum temperatures on the 4th and 5th day, emission peaks appear, leading to an increase in total NH_3 emission.

Although the total NH_3 emission in GAG_patch can be be influenced by the timing of the rain event, it must be emphasized that in reality NH_3 can escape from wet soil not only through gaseous diffusion in the empty soil pores. Dissolved NH_3 may reach the soil surface also through the solution and can be volatilized from there (Cooter et al., 2010). This is not taken into account in the present R_{soil} parametrisation. Therefore, the effect of rainfall on the temporal evolution of NH_3 emission may not be as strong as this experiment showed. In contrast, as mentioned in Section 3.3, during a dry period urea hydrolysis may slow or stop in absence of water. If the rainfall begins after such a dry period, by restarting urea hydrolysis, it can even enhance NH_3 emission rather than suppress it (as also showed in a model experiment in Section 3.4.3).

5. 2. 2. Sensitivity analysis to meteorological variables over a grazed field

In the case of GAG_field, the sensitivity of the simulated total NH_3 exchange was tested to the same meteorological variables that were investigated for GAG_patch in Section 5.2.1. In Section 4.5 two baseline simulations were carried out with GAG_field for two modelling periods: 26/08/2002 00:00 - 04/09/2002 09:00 (P2002) and 20/06/2003 00:00 - 25/06/2003 05:00 (P2003). All the meteorological variables for both P2002 and P2003, are depicted in Fig 5.3 and 5.4, respectively together with the measured and simulated NH_3 fluxes.

In both periods a clear diurnal variation can be observed in the air temperature (T_{air}), relative humidity (RH) and global radiation (R_{glob}). In contrast to the patch-scale results, where a well-defined daily cycle emerged in the NH_3 flux (Fig. 5.1 d), here a less sharp daily cycle occurs in the NH_3 fluxes. In P2002 a daily pattern can be distinguished between 31/08 and 03/09, with daily peaks in both the modelled and measured dataset. In P2003 only the last two days have a clear daily variation, with midday peaks in both the modelled NH_3 fluxes and the measurements.

The perturbation experiments for the meteorological variables used in the baseline simulations of GAG_fied (Section 4.5) were performed following the same methodology as in Section 5.2.1 for GAG_patch with the same $\pm\Delta x$ perturbations (see the fourth column of Table 5.1). The total NH_3 exchange over the field in the baseline simulations (calculated by summing the simulated hourly NH_3 fluxes over the modelling periods) were 428 g N and 403 g N in P2002 and P2003, respectively. The percentage differences in these totals in response to the perturbations in the meteorological variables are shown in Table 5.2.

As explained in Section 4.2.3, over a grazed field a part of the surface is covered by urine patches and the rest of it is not affected by urine ("clean area", see Fig. 4.3). The governing processes of NH_3 exchange are different in the case of these two surface types; therefore, to gain a clearer understanding of the results derived in the sensitivity analysis, the meteorological effects were examined also separately over the urine patches and the clean area. Thus, in addition to the results in Table 5.2, the

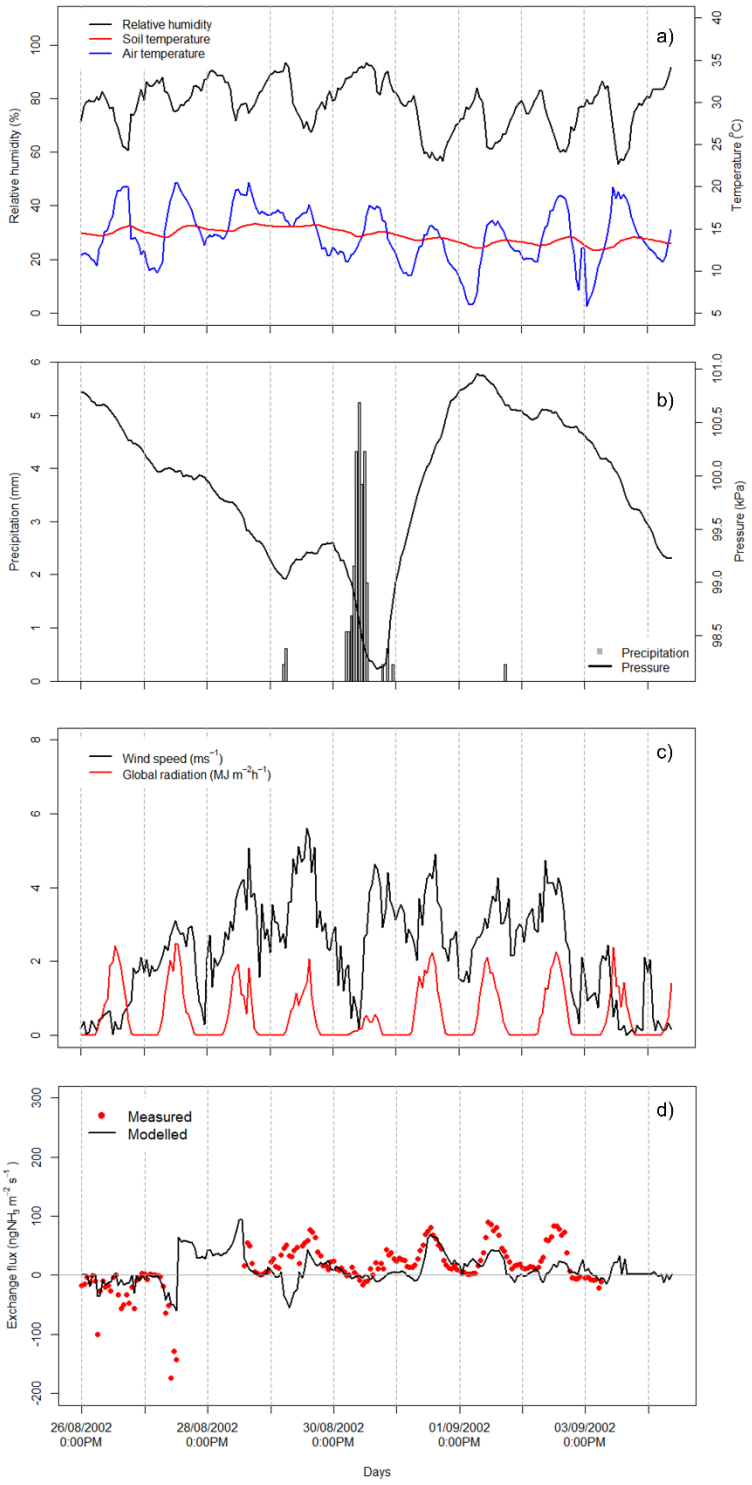

Figure 5.3. Measured meteorological variables (relative humidity, soil and air temperature (a), precipitation and surface pressure (b), wind speed and global radiation (c)), and the measured and simulated hourly NH_3 fluxes (d) in P2002 in Easter Bush. In the bottom panel those measured fluxes were plotted that were considered to represent the real NH_3 fluxes the best.

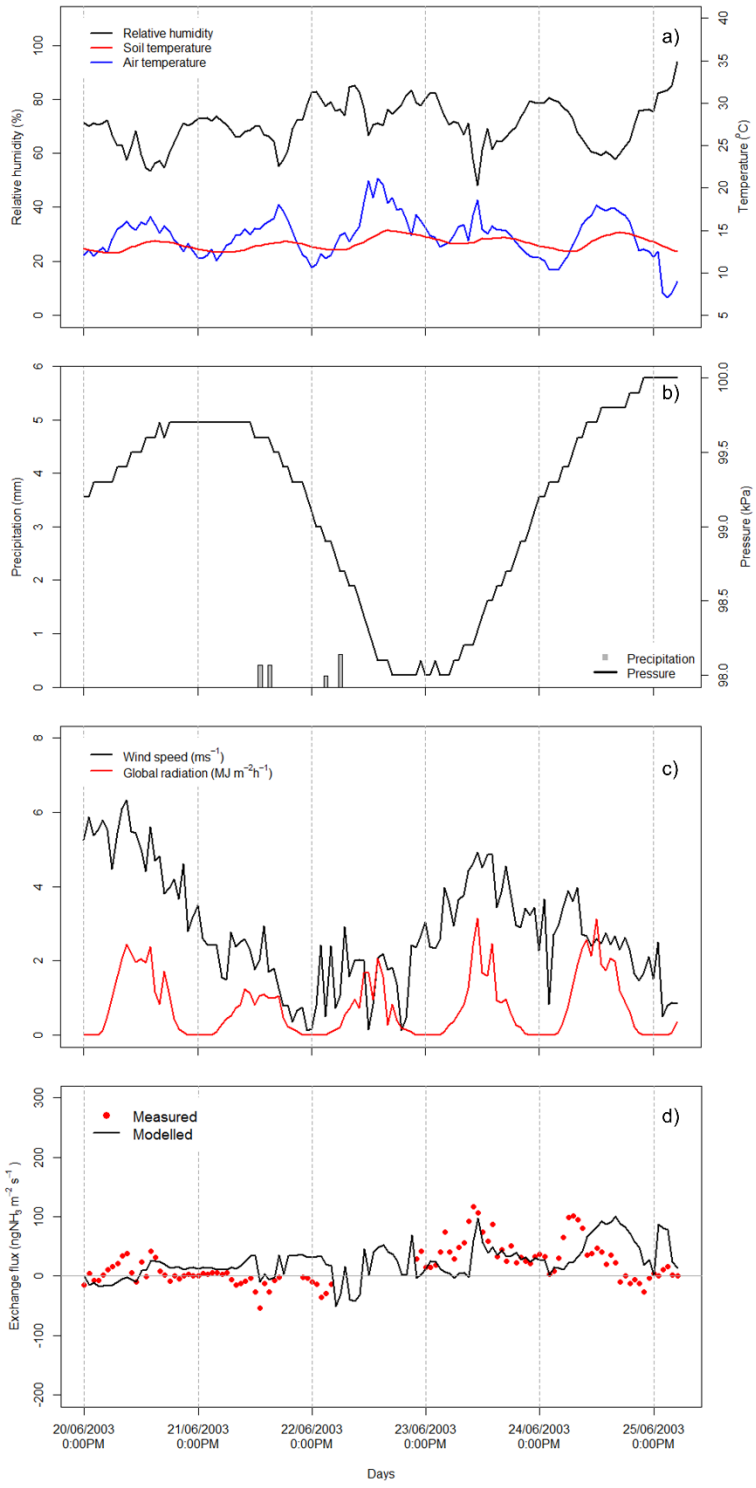

Figure 5.4. Measured meteorological variables (relative humidity, soil and air temperature (a), precipitation and surface pressure (b), wind speed and global radiation (c)), and the measured and simulated hourly NH_3 fluxes (d) in P2003 in Easter Bush. In the bottom panel those measured fluxes were plotted that were considered to represent the real NH_3 fluxes the best.

Table 5.2. The results of the sensitivity analysis to the different meteorological variables for GAG_field for the modelling periods P2002 and P2003. The variables were changed by ± Δx (defined for the patch-scale model experiment in Table 5.1), and the difference in the total NH_3 emission over the modelling period compared to the baseline simulations with GAG_field was calculated.

Meteorological variables (x)	**Change in x**	**Change in the total net flux**	
		P2002	**P2003**
u ($m\ s^{-1}$)	-Δx	+0.3%	+1.0%
	+Δx	-12.3%	-8.2%
T_{soil} (^0C)	-Δx	-30.2%	-32.4%
	+Δx	+34.0%	+35.6
p (kPa)	-Δx	+0.0%	+0.0%
	+Δx	-0.0%	-0.0%
T_{air} (^0C)	-Δx	-1.5%	-1.2%
	+Δx	+1.2%	+1.2%
R_{glob} ($MJ\ m^2\ h^{-1}$)	-Δx	-14.7%	-26.0%
	+Δx	+10.8%	+9.3%
RH (%)	-Δx	+36.5%	+41.8%
	+Δx	-30.0%	-35.3%
P (mm)	-Δx	+3.6%	+7.0%
	+Δx	-2.9%	-0.9%
T_{air} and T_{soil} (^0C)	-Δx	-31.6%	-33.5%
	+Δx	+35.3%	+36.9%

following were derived (Table 5.3): 1) the difference in the total NH_3 emission (in g N) over the whole field as a response to the perturbed meteorological variables, 2) the contribution of the urine patches and the clean area to this difference, and 3) the difference in the total exchange over the patches expressed as the percentage of total NH_3 exchange over the patches in the baseline simulations with GAG_field.

Table 5.3. The results of the sensitivity analysis to the different meteorological variables for GAG_field for the two modelling periods, P2002 and P2003. The variables were changed by ± Δx (defined for the patch-scale model experiment in Table 5.1). The differences in the total NH_3 exchange (g N) are determined for the whole field as well as the clean area and the urine patches separately. The percentage in brackets is the percentage difference in NH_3 exchange over the urine patches.

Meteorological variables (x)	**Change in x**	**Change in total net flux (g N)**					
		P2002			**P2003**		
		Whole	**Clean**	**Patch**	**Whole**	**Clean**	**Patch**
u ($m\ s^{-1}$)	-Δx	1.4	108.9	-107.5 *(-13.5%)*	4.0	121.5	-117.5 *(-13.9%)*
	+Δx	-52.7	-162.1	109.4 *(+13.7%)*	-32.9	-114.5	81.7 *(+9.7%)*
T_{soil} (^{0}C)	-Δx	-129.1	-70.0	-59.1 *(-7.4%)*	-130.7	-45.9	-84.8 *(-10%)*
	+Δx	145.3	85.4	59.9 *(+7.5%)*	143.4	55.5	87.9 *(+10.4%)*
p (kPa)	-Δx	0.0	0.0	0.0 *(0.0%)*	0.1	0.01	0.05 *(0.0%)*
	+Δx	0.0	0.0	0.0 *(0.0%)*	-0.1	-0.01	-0.05 *(0.0%)*
T_{air} (^{0}C)	-Δx	-6.5	0.1	-6.5 *(-0.8%)*	-4.9	0.0	-4.9 (-0.6%)
	+Δx	5.2	-0.1	5.2 *(+0.7%)*	4.7	0.0	4.7 *(+0.6%)*
R_{glob} ($MJ\ m^2\ h^{-1}$)	-Δx	-63.0	0.4	-63.4 *(-7.9%)*	-104.6	0.0	-104.6 *(-12.4%)*
	+Δx	46.3	-0.4	46.7 *(+5.9%)*	37.4	0.0	37.4 *(+4.4%)*
RH (%)	-Δx	155.8	86.3	69.5 *(8.7%)*	168.3	90.6	77.7 *(+9.2%)*
	+Δx	-128.2	-68.6	-59.6 *(-7.5%)*	-142.4	-78.0	-64.4 *(-7.6%)*
P (mm)	-Δx	15.2	0.0	15.2 *(1.9%)*	28.2	0.0	28.2 *(+3.3%)*
	+Δx	-12.6	0.0	-12.6 *(-1.6%)*	-3.5	0.0	-3.5 *(-0.4%)*
T_{air} and T_{soil} (^{0}C)	-Δx	-135.2	-70.0	-65.2 *(-8.2%)*	-135.1	-45.9	-89.2 *(-10.5%)*
	+Δx	150.7	85.2	65.5 *(+8.2%)*	148.6	55.5	93.2 *(+11%)*

Table 5.2 shows that the meteorological variables with the strongest influence on the total NH_3 exchange were *u*, *RH* and the simultaneously changed temperature values ("T_{air} + T_{soil}"). Although these variables had a dominant effect on the total NH_3 exchange also in the case of GAG_patch (Table 5.1), the resulted percentage

differences for GAG_field and GAG_patch were significantly different. These differences are further discussed in Section 5.2.3. Compared with the above-mentioned meteorological variables, the sensitivity of NH_3 exchange over the field to atmospheric pressure (p) and precipitation (P) was relatively low (Table 5.2).

Examining the differences in the results for the two field-scale modelling periods (Table 5.2), it can be seen that the sensitivity of the total NH_3 exchange to the perturbations of the meteorological variables for P2002 and P2003 were similar in magnitude in most of the cases, implying a similar sensitivity to meteorology in the two years. The largest difference between the two modelling periods was observed in the results for R_{glob}, when changed by $-\Delta x$ (the percentage difference in the total NH_3 exchange was -14.7% in P2002 and -26% in P2003). It can be seen in Table 5.3 that in both P2002 and P2003, the difference in the total NH_3 exchange as response to the perturbations of R_{glob}, was mainly associated with the urine patches. Above the urine patches in P2002 and P2003 the percentage differences in the total NH_3 emission in response to the changes in R_{glob} (-7.9% in P2002 and -12.4% in P2003) were closer to each other than over the whole field.

This dominant influence of R_{glob} through the urine patches can be explained by its direct impact on soil evaporation which affects the water budget. In the case of the clean area, the water budget influences only the stomatal resistance (R_{sto}), while in the case of the urine patches, it has an additional effect on R_{soil} (no R_{soil} is assumed over the clean area, see Section 4.3).

Lower global radiation ($-\Delta x$) leads to weaker soil evaporation, that in turn leads to more water to be stored in the soil. This opens the stomata (R_{sto} becomes smaller), which allows stronger stomatal NH_3 emission, and consequently, a positive change in the total exchange over the clean area (+0.4 gN in P2002, in Table 5.3). Higher soil water content is also coupled with larger R_{sto} that has a larger constraint on NH_3 emission from the soil, leading to a negative change in the total emission over the urine patches (-63 g N in P2002 and - 104.6 g N in P2003 in Table 5.3). In the case of a higher R_{glob} ($+\Delta x$), the opposite of the described processes take place.

The negligible contribution of the clean area to the difference in the total NH_3 exchange over the whole field (±0.4 g N and ±0.0 g N in P2002 and P2003, respectively in Table 5.3) suggests that the effect of R_{glob} on NH_3 exchange through the R_{soil} is significantly stronger than through R_{sto}.

5. 2. 3. Comparison of the model sensitivity over the patch and the field scale

As mentioned in Section 5.2.2, both for GAG_patch (Table 5.1) and GAG_field (Table 5.2), *u*, *RH* and the simultaneously changed temperature values ("$T_{air} + T_{soil}$" in Table 5.1) were found to be the meteorological variables with the strongest influence on the total NH_3 exchange. However, the strength and the direction of their effects were significantly different over the two scales. Also, in the case of GAG_field R_{glob} emerged as an additional strong influencing factor. In the following, the reasons of these differences over the two scales are examined.

The effect of *u* was found to be the opposite of that was observed in the patch scale: in GAG_field a $+\Delta x$ change in *u* resulted in lower total NH_3 exchange (Table 5.2), whilst in GAG_patch the same perturbation led to higher total emission (Table 5.1). Over the field scale, examining the contribution of the clean area and the urine patches (Table 5.3), it can be seen that the effect of *u* over the two different surface types were the opposite, and in absolute value the changes were larger over the clean area than over the patches. As a consequence, the sign of the difference in the total NH_3 exchange over the whole field was determined by the difference over the clean area.

The opposite tendency in *u* and the total NH_3 exchange over the clean area (Table 5.3) can be explained by that the total exchange over this part of the field was negative, that is, deposition occurred in total. As explained in Section 5.2.1, larger *u* ($+\Delta x$) results in stronger turbulent mixing, facilitating NH_3 exchange. As over the clean field originally deposition occurred, the higher *u* led to intensified deposition flux and as a result, lower total NH_3 exchange. In the case of a smaller *u* ($-\Delta x$), through weaker turbulent mixing, the opposite occurred.

In addition to the opposite sign of the response of the total NH_3 exchange to the perturbations of *u* for GAG_patch and GAG_field, in Table 5.3 it can be also seen that

the total NH_3 emission from the urine patches in the field experiment was more sensitive to *u* than in the case of GAG_patch (e.g. for $-\Delta x$ the difference in the total NH_3 exchange was -5.5% for GAG_patch (Table 5.1), and -13.5% and -13.9% in P2002 and P2003, respectively in the field-scale experiment (Table 5.3)). This might be a consequence of the fact that the change in *u* (Δx = 0.8 m s^{-1}) was proportionally bigger in the case of the GAG_field than in GAG_patch (see the average *u* values in Table 5.4). Since the atmospheric resistances are inversely proportional to *u*, this relatively larger modification in *u* in GAG_field could lead to a larger difference in the NH_3 exchange than in the case of GAG_patch.

Relative humidity affected NH_3 exchange in GAG_field (Table 5.2) substantially more strongly than in GAG_patch (Table 5.1). However, the percentage differences in the total NH_3 exchange over the patches deposited on the field (Table 5.3) were similar to those observed in the case of GAG_patch for the single urine patch (Table 5.1). As shown in Table 5.3, the contribution of the clean area to the difference in NH_3 exchange over the whole field was similar to that of the urine patches in sign. This suggests that the effect of *RH* on NH_3 exchange in the case of the clean area, is similar to that explained in the case of GAG_patch (Section 5.2.1): at higher relative humidity ($+\Delta x$), there is a higher chance for the formation of a water film on the leaf surface that helps the absorption of NH_3, leading to a stronger deposition and consequently, a lower total NH_3 exchange. Lower relative humidity ($-\Delta x$) has the opposite effect.

The combined effect of T_{soil} and T_{air} on NH_3 exchange was stronger for GAG_field (Table 5.2) than GAG_patch (Table 5.1). The underlying reasons are examined in more detail in Section 5.2. However, here it has to be noted that while in the case of GAG_patch, the sensitivity to T_{soil} and T_{air} was similar (Table 5.1), over the urine patches deposited in GAG_field, the combined temperature effect was dominated by the influence of T_{soil} (Table 5.3).

In the case of GAG_field, compared to the results for GAG_patch (Table 5.1), R_{glob} was an additional substantial influencing variable (Table 5.2). As explained in Section 5.2.2, R_{glob} affects NH_3 exchange over the field mostly through the urine patches. The percentage differences in NH_3 exchange over the urine patches deposited in

GAG_field (Table 5.3) were notably larger than in the case of the single urine patch simulated by GAG_patch (Table 5.1). Global radiation, as mentioned earlier, influences NH_3 exchange indirectly via soil evaporation; therefore, the reason for the weaker response of NH_3 exchange to the change of R_{glob} observed for GAG_patch should be find in the relationship between R_{glob} and the soil evaporation.

As shown in Table 5.4, the meteorological conditions did not favour evaporation in the baseline simulations with GAG_field: in both years T_{air} was significantly lower, u was lower and RH was higher than in the baseline experiment with GAG_patch. Consequently, the regulating effect of T_{air}, u and RH on soil evaporation was more dominant than in the case of GAG_field. Therefore, the influence of the same change in R_{glob} on soil evaporation most probably could not be as strong as in the experiments with GAG_field, as shown by Table 5.5. As a result, this stronger effect of R_{glob} on soil evaporation, through the water budget as well as R_{soil}, could possibly lead to a larger influence of R_{glob} on NH_3 exchange in GAG_field than GAG_patch.

Table 5.4. Meteorological statistics in the three baseline simulations: with GAG_patch, and the simulations with GAG_field in the modelling periods, P2002 and P2003.

Statistics	**Model experiment**		
	GAG_patch	**GAG_field P2002**	**GAG_field P2003**
mean u (m s^{-1})	3.8	2.3	2.8
mean T_{air} (°C)	20.6	14.2	14.3
mean RH (%)	61.4	77.3	70.7
mean R_{glob} (MJ m^{-2} h^{-1})	0.8	0.5	0.7
sum P (mm)	2.5	27.1	1.6

In addition to soil evaporation, rain events can also substantially affect the water budget. Precipitation represents – apart from the water content of the urine – the main input to the water budget. As such, it can outweigh the effect of soil evaporation and through it, R_{glob} on the water budget, resulting in a modified influence of R_{glob} on NH_3 exchange. As Table 5.4 shows, there was a substantial difference in the total amount

Table 5.5. The change in the total soil evaporation in response to a change in R_{glob} of ±Δx as defined in Table 5.1. The resulted differences are expressed relative to the original total soil evaporation.

Experiment	**Change in soil evaporation in response to a change in R_{glob} of**	
	-Δx	**+Δx**
GAG_field, P2002	-30%	+35%
GAG_field, P2003	-19%	+21%
GAG_patch	-9%	+15%

of precipitation in the baseline experiments, and according to Fig. 5.1, Fig 5.3 and Fig 5.4, the temporal distribution of precipitation was also considerably different in the three simulations.

The interaction between soil evaporation and precipitation differs among the urine patches. After the deposition of a urine patch the soil begins drying out gradually (Fig. 5.1 d). This means that over the field scale, where urine patches are deposited in every time step, the same rain event affects every urine patch in a different stage of this drying process. This varying interaction between soil evaporation and precipitation adds a further level of complexity to the effect of R_{glob} on NH_3 exchange over the field scale.

5. 3. Investigation of the temperature-dependence

As indicated by the perturbation experiments carried out in Section 5.2.1 and Section 5.2.2, the sensitivity of the total NH_3 exchange to the modification of the temperature variables (perturbing T_{air} and T_{soil} togehter) was different for GAG_patch and GAG_field. In this section the reasons behind this different temperature-response of the total NH_3 exchange are discussed in detail. As a starting point of the investigations, the Q_{10} values were calculated. Q_{10} is a metric to express the relative increase of the emission of a trace gas over a range of 10 °C. It is widely used for various trace gases, for instance, for N_2O by Grant and Pattey (2008) or for CO_2 by Gritsch et al. (2015). For NH_3 a series of Q_{10} values were calculated and reported by Sutton et al. (2013).

Table 5.6 shows the Q_{10} values calculated for GAG_patch, and the simulations with GAG_field for both modelling periods, P2002 and P2003. In the latter case, Q_{10} values were derived separately for the whole field, the clean area and the urine patches. The values in Table 5.6 were calculated following two different methods. For both methods, firstly the baseline simulations with GAG_patch and GAG_field were carried out with a 10 °C higher T_{air} and T_{soil}. Secondly, in the first method (Q_{10}^{Ex} Eq. 5.1) the resulting NH_3 exchange fluxes were summed for the modelling periods in both the baseline simulations ($\Sigma Ex(\Delta T$ = 0°C)) and in the +10 °C higher temperature simulation ($\Sigma Ex(\Delta T$ = +10°C)), then the ratio of the two was calculated. In the second method (Q_{10}^{Em} Eq. 5.2), from the hourly NH_3 exchange fluxes, resulting from the model simulations, only the positive hourly fluxes were summed (ΣEm), i.e. only those time steps were taken into account in which net NH_3 emission occurred.

$$Q_{10}^{Ex} = \frac{\sum Ex\left(\Delta T = +10°C\right)}{\sum Ex\left(\Delta T = 0°C\right)}, \tag{5.1}$$

$$Q_{10}^{Em} = \frac{\sum Em\left(\Delta T = +10°C\right)}{\sum Em\left(\Delta T = 0°C\right)}, \tag{5.2}$$

The resulted Q_{10}^{Em} and Q_{10}^{Ex} values in Table 5.6 show that if all of the fluxes are taken into account, in the case of GAG_field, Eq. 5.1 results in negative values over the clean area. This is because in the baseline experiments, over the clean area total NH_3 deposition ($\Sigma Ex(\Delta T$ = 0°C) < 0) occurred. These negative Q_{10} values are not meaningful, and thus, the Q_{10}^{Ex} values are not comparable for every situation outlined in Table 5.6. Therefore, in the following, in the examination of the temperature-dependence of NH_3 exchange, the Q_{10}^{Em} values are used as the focus of comparisons.

This choice does not affect the results over the urine patches, since Q_{10}^{Ex} and Q_{10}^{Em} are practically the same, suggesting that the hourly NH_3 fluxes were dominated by net emission. The consequences of the choice to focus on Q_{10}^{Em} instead of Q_{10}^{Ex} for the clean area and the whole field are further discussed in Sections 5.3.3 and 5.3.4, respectively.

Table 5.6. Q_{10} values calculated based on simulation with GAG_field (for the modelling periods, P2002 and P2003) and GAG_patch. In the case of the GAG_field Q_{10} values were calculated separately for the NH_3 emission originating from the urine patches and the clean area as well as the total emission from the whole field. Q_{10}^{Ex} is calculated based on the sum of all of the NH_3 exchange fluxes in the period, whilst in Q_{10}^{Em} only the positive fluxes were taken into account.

Source	**GAG_field P2002**		**GAG_field P2003**		**GAG_patch**	
	$\mathbf{Q_{10}^{Ex}}$	$\mathbf{Q_{10}^{Em}}$	$\mathbf{Q_{10}^{Ex}}$	$\mathbf{Q_{10}^{Em}}$	$\mathbf{Q_{10}^{Ex}}$	$\mathbf{Q_{10}^{Em}}$
Urine patches	1.51	1.51	1.72	1.71	1.26	1.26
Clean area	-1.34	7.65	-0.29	18.21	-	-
Whole field	4.00	3.10	3.94	3.39	-	-

Based on the Q_{10}^{Em} values in Table 5.6, the following questions can be raised, concerning the temperature-dependence of NH_3 emission over the different surface types (urine patch, clean area, whole field):

1. Why is there a difference in the temperature response of NH_3 emission over the single urine patch (GAG_patch) and the multiple patches in the field-scale experiments (GAG_field)? (Discussed in Section 5.3.1.)
2. Why is NH_3 emission much more sensitive to temperature (higher Q_{10}^{Em}) over the clean area than the urine patches? (Discussed in Section 5.3.2.)
3. Why is there a large difference in the temperature-dependency of NH_3 emission over the clean area between the two modelling periods? (Discussed in Section 5.3.3.)
4. What is the relationship between the temperature-response of NH_3 emission over the urine patches, clean area and the whole field? (Discussed in Section 5.3.4.)

Preliminary model simulations suggested that the value of Q_{10}^{Em} can be influenced by an assumed TAN sink/source in the NH_3 source layer, the length of the period that Q_{10}^{Em} is calculated for, and the temperature at which the denominator of Q_{10}^{Em} (Eq. 5.2) is calculated. Therefore in the following subsections the above four questions are addressed together with an additional fifth one:

5. What other factors can influence Q_{10}^{Em}? [Discussed in Sections 5.3.5-5.3.6.]

In the following subsections Q_{10}^{Em} is simply referred to as Q_{10}, unless it is stated otherwise.

5. 3. 1. Difference between the single patch and the multiple patch simulations

To gain further insights into the variability of Q_{10} among the urine patches deposited in GAG_field, Q_{10} was also calculated for each of the individual patches deposited over P2002 and P2003. The results are shown in Fig. 5.5. In both periods there is a constant level in Q_{10} around Q_{10}=1.3 (close to the Q_{10} calculated for the single patch case, Q_{10}=1.26, Table 5.6). There are also some intermittent values, peaking in some cases above 40 or even 80 in P2003. Also, a gradual, exponential growth can be observed in Q_{10} in the last day of both modelling periods.

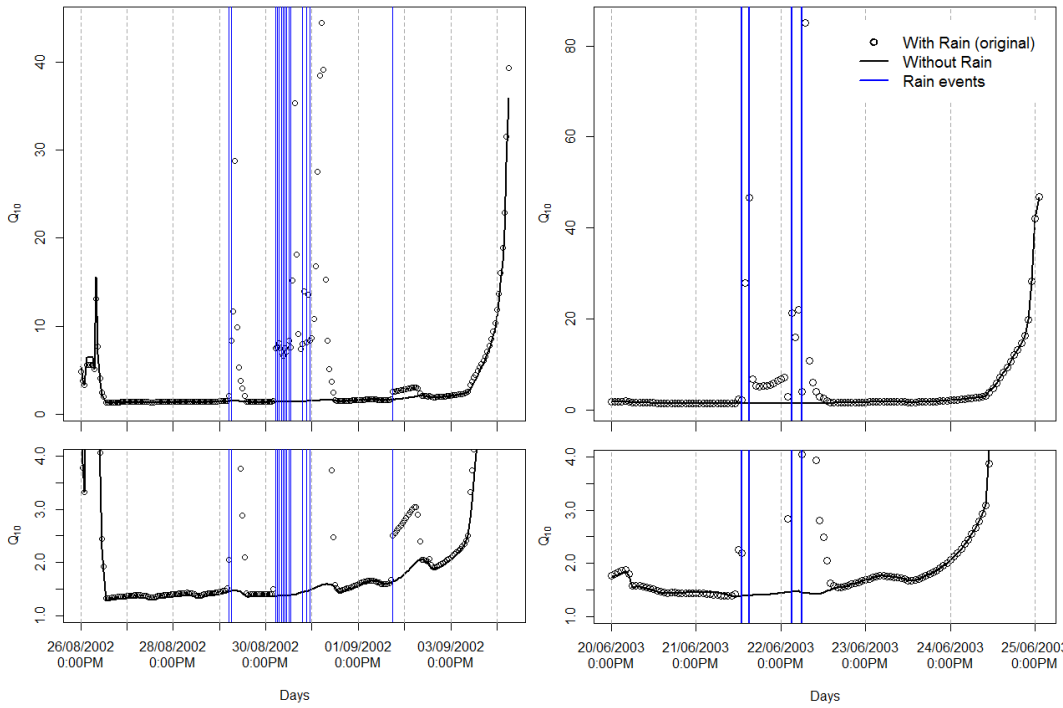

Figure 5.5. Q_{10} values for the NH_3 emission originating from the individual patches deposited in GAG_field in the modelling periods P2002 (left panels) and P2003 (right panels). The two bottom panels shows the same values on a narrower range of Q_{10} (from 1 to 4). Each black dot represents a Q_{10} calculated for the urine patch deposited in GAG_field in the given time step. The black line represents Q_{10} values derived from model simulations with GAG_field in which no rain was assumed. Vertical blue lines indicate the time steps with precipitation.

The scattered spikes in Q_{10} suggest that the reason behind them might be in relation to the rain events during the modelling periods. To test this hypothesis, the baseline simulations with GAG_field were carried out, assuming no precipitation for both the ΔT = 0°C and ΔT = +10°C case. In the Q_{10} dataset, calculated for these experiments, the spikes in Q_{10} disappeared (black line in Figure 5.5), resulting in a close to constant level of Q_{10}. Only the first peak remained in the results in P2002, which was caused by a slight dew fall in the morning of 26/08.

The effect of rain events on Q_{10} can be explained by the influence of T_{air} on soil evaporation. When T_{air} is raised by 10 °C, soil evaporation becomes stronger, resulting in a lower water budget. This effect is more prominent after a rain event, when there is evaporable water in the NH_3 source layer.

If the initial water content of the NH_3 source layer is lower, more urine is allowed to infiltrate to the soil, therefore, more urea is available for hydrolysis. As shown in Section 4.6.4 the total NH_3 emission is strongly influenced by the available space for urine in the source layer (θ_{urine}). In the sensitivity analysis of GAG_field, the 10-20% perturbations of the field capacity (θ_{fc}) and the permanent wilting point (θ_{pwp}) were equal to a 2-8% difference in θ_{urine} (Table 4.6). When T_{air} was increased by 10 °C in the present model experiments with GAG_field, the largest differences in θ_{urine} between the wetter soil in the ΔT = 0°C simulation and the drier soil in the ΔT = +10°C simulation were 11% and 23%, in P2002 and P2003, respectively. These large changes in θ_{urine} could strongly affect the total NH_3 emission in the ΔT = +10°C simulation.

The same effect does not occur in the urine patches deposited before the rain events or a day after them. This is because in these urine patches the source layer was dried out, therefore, the soil evaporation could not further decrease the water budget in the ΔT = +10°C simulation, allowing the same amount of urine to penetrate at both ΔT = 0°C and ΔT = +10°C.

To conclude, in the urine patches deposited on the field after the rain events, in the ΔT = +10°C simulation, the total NH_3 emission was larger, not just because of the effect of T_{soil} on the compensation point in the soil pore, but also because a larger amount of urea could be stored in the source layer, and was available for hydrolysis

and subsequent NH_3 emission. This led to a higher Q_{10} than in the case of the urine patches that were deposited before the rain events or a day after them.

The gradual increase in Q_{10} toward the end of the modelling period (Fig. 5.5) is caused by the length of time of NH_3 emission. If a urine patch is deposited in GAG_field in the last day of the modelling period, it has less time to volatilize NH_3, than a urine patch deposited in the beginning of the modelling period. For example, P2003 was 126 hours long in total; if a urine patch is deposited in P2003 in the 22nd hourly time step, it has 104 hours to emit NH_3, whereas if a urine patch is deposited in the 120th time step, it has only 6 hours to emit NH_3. That is, according to Fig. 5.5, the longer time a urine patch has to emit NH_3, the lower Q_{10} it has. This is in accordance with the finding that Q_{10} decreases exponentially with the increase of the length of the time period it is calculated for (Section 5.3.6). The reason behind this behaviour of Q_{10} in relation to the length of the modelling period is mathematical (see in more detail in Section 5.3.6).

To conclude, the answer for the first question is: the overall Q_{10} over the urine patches deposited in GAG_field, is determined by the variation of Q_{10} values associated with the individual urine patches. It was found that a rain event can increase the Q_{10} of the urine patches deposited in GAG_field shortly after the rain event. This could lead to a larger overall Q_{10} for the multiple patch experiment (GAG_field) than the single patch experiment (GAG_patch). Furthermore, the overall Q_{10} for the urine patches can be also enhanced by the large, individual Q_{10} values of the urine patches deposited toward the end of the modelling period. This latter effect can be considered as an artefact of the calculation approach, rather than a real influence on the temperature-dependency of NH_3 exchange.

5. 3. 2. Difference between the patch and the clean field simulations

In order to gain a better understanding of the mechanism behind the large difference in Q_{10} between the simulations for the urine patches and GAG_field for the *clean area* (GAG_field^{clean}), additional model experiments were performed with both GAG_patch, and GAG_field for P2002 and P2003, where T_{soil} and T_{air} were changed

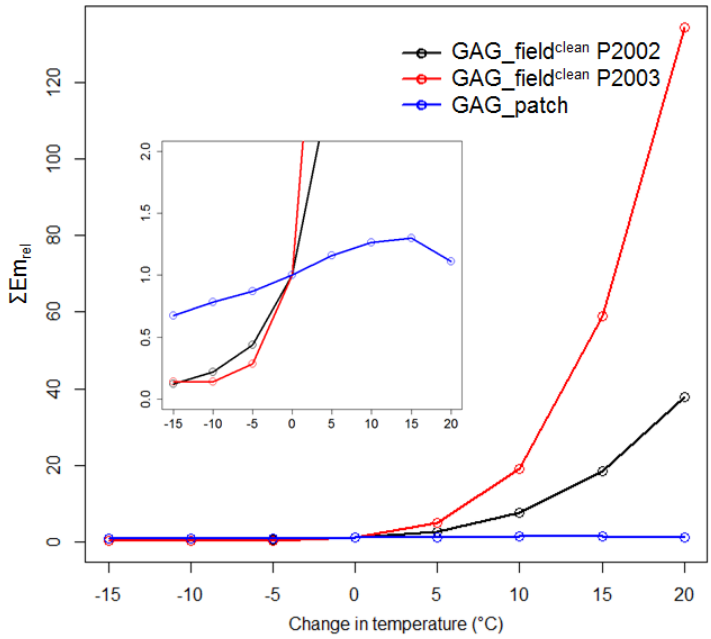

Figure 5.6. Total NH_3 emission (ΣEm_{rel}) as a function of the change in temperature (in 5°C increments) relative to the total NH_3 emission in the baseline experiments (ΔT= 0°C). Model experiments were performed for the clean area in the two modelling periods, P2002 and P2003 (GAG_field^{clean}) and the single urine patch (GAG_patch). The small plot shows the same variable but on a narrower range of ΣEm_{rel} (from 0 to 2).

by ΔT= -15°C – +20°C, in increments of 5°C. For all simulations ΣEm was calculated, which are illustrated in Fig. 5.6, expressed relative to $\Sigma Em(\Delta T=0°C)$ (ΣEm_{rel}). As it can be seen, ΣEm grew exponentially in both simulations with GAG_field^{clean}, whilst in GAG_patch the temperature response was rather modest.

Ammonia exchange over the canopy is the sum of the soil emission (F_g) and exchange above the canopy (F_f). Therefore, to explain the difference in the temperature response of ΣEm in GAG_patch and GAG_field^{clean}, the total soil emission (ΣF_g Fig. 5.7 a) and the total deposition to the canopy were also examined (ΣF_f, Fig. 5.7 b). In ΣF_g and ΣF_f all of the hourly fluxes were taken into account. In Fig. 5.7, for GAG_field^{clean}, similarly to ΣEm, an exponential increase can be observed for both ΣF_g and ΣF_f. Whereas in the case of the single patch the function is almost a constant value of 1 for ΣF_g, and it oscillates around 1 for ΣF_f. (The difference in the temperature-dependence of ΣEm in GAG_field^{clean} for P2002 and P2003 is investigated in Section 5.3.3.)

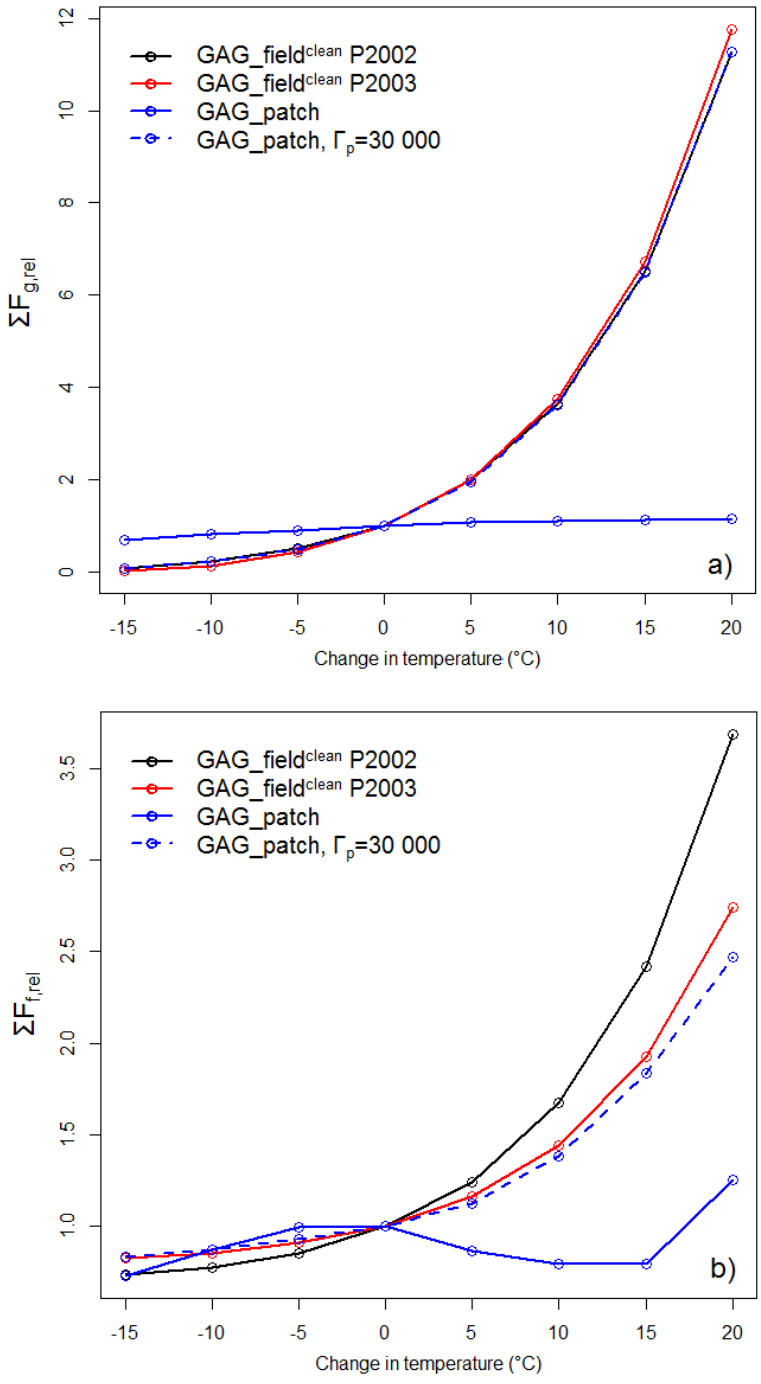

Figure 5.7. The total NH_3 emission from the soil ($\Sigma F_{g,rel}$), and the total NH_3 deposition to the canopy ($\Sigma F_{f,rel}$) as a function of the change in temperature (in 5°C increments) relative to the total NH_3 emission in the baseline experiments (ΔT= 0°C). Model experiments were performed for the clean area in the two modelling periods, P2002 and P2003 (GAG_field^{clean}) and the single urine patch (GAG_patch). GAG_patch was also tested with a constant soil emission potential in the model soil pore (Γ_p) of 30 000.

The main difference in the modelling of NH_3 exchange over the clean field parts and the urine patches is that over the clean area a constant soil emission potential is applied, whilst in the case of the urine patches the emission potential of the soil pore (Γ_p) is dynamically simulated. To test how ΣF_g and ΣF_f changes over a single urine patch with a constant Γ_p, simulations were carried out with GAG_patch with a Γ_p of 30,000. The results indicate that in both ΣF_g and ΣF_f a similar, exponential function occurred in this way ($\Sigma F_{g,rel}$ and $\Sigma F_{f,rel}$ in Fig. 5.7), supporting the significant role of dynamic chemistry in the temperature-response of ΣF_g and ΣF_f and consequently, ΣEm.

The compensation points for the soil pore (χ_p) and the soil surface (χ_g) (Eq. 2.39 and Eq. 4.7, respectively) are calculated as the product of an exponential function of temperature and the corresponding emission potential (Γ). On one hand, this explains the exponential increase of ΣF_g in the constant Γ experiments with GAG_patch (Fig. 5.7). On the other hand, this implies that the dynamically simulated Γ_p in the urine patches overcomes the effect of the exponential temperature function of χ_p.

This moderating effect of the dynamically changing Γ_p on χ_p in GAG_patch can be partly explained by the limited TAN budget under the urine patch that is increasingly depleted as temperature is raised. However, the effect of temperature can also be detected in the evolution of Γ_p (Fig. 5.8). This effect was explored in a series of model experiments with GAG_patch, in which at different temperature the same amount of urea was assumed to be hydrolysed in the soil pore (i.e. the same amount of TAN was added to the soil pore), filled with an aqueous solution with an initial pH of 6.65, the initial pH in the baseline simulation with GAG_patch (i.e. initially $[H^+]=10^{-6.65}$ in every case). The experiments were carried out twice, with an assumed amount of TAN input of 0.79 g N (the TAN input in the patch-scale experiment in the first time step) and 2.11 g N (the highest TAN budget in the patch-scale experiment). In every model run the instantaneous, equilibrium Γ_p was derived, and expressed relative to the Γ_p value for the ΔT=0°C model integration ($\Gamma_{p,rel}$; Fig. 5.8).

Fig. 5.8 shows a decreasing tendency in $\Gamma_{p,rel}$ with increasing temperature. This is because at higher temperature more NH_4^+ dissociates to H^+ and $NH_{3(aq)}$, resulting in a lower $[NH_4^+]/[H^+]$ ratio, i.e. Γ_p. This temperature-response of Γ_p is stronger if larger

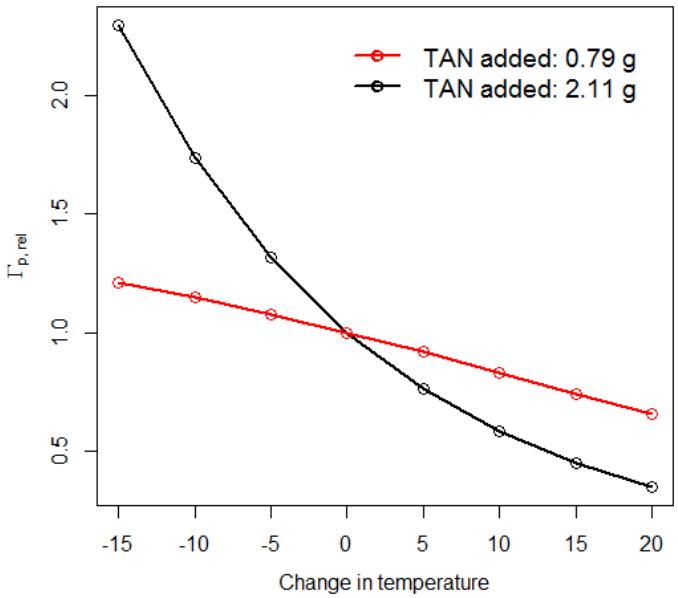

Figure 5.8. Instantaneous emission potentials ($\Gamma_{p,rel}$) in GAG_patch in the function of the change in temperature, resulting from different TAN inputs to the same solution in the soil pore (initially pH=6.65, B_{TAN}=0). The values are expressed relative to Γ_p in the ΔT = 0 °C simulation.

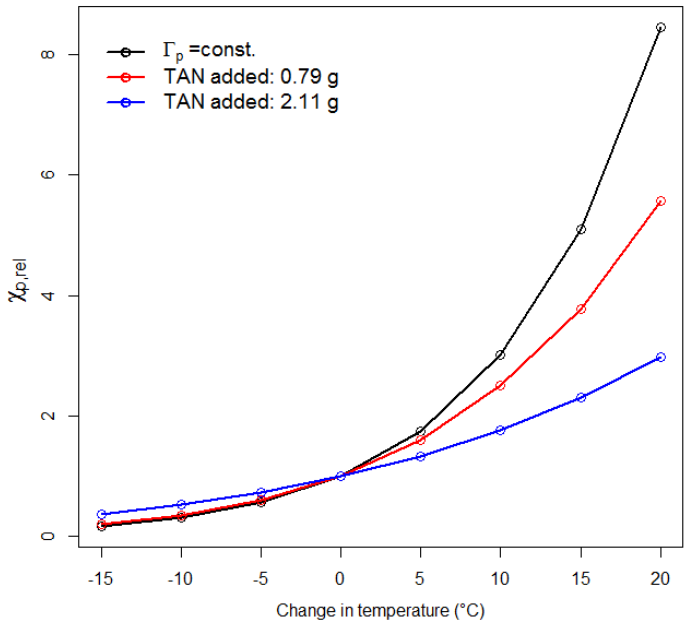

Figure 5.9. Instantaneous compensation points in the soil pore ($\chi_{p,rel}$) calculated by GAG_patch in the function of the change in temperature, when different amount of TAN was added to the solution in the soil pore (initially pH=6.65, B_{TAN}=0) and when the emission potential in the soil pore was assumed to be constant (Γ_p=30 000). The values are expressed relative to the χ_p in the ΔT= 0°C simulation.

amount of urea is assumed to be hydrolysed in the experiments. Furthermore, Fig 5.9 shows that this declining tendency in $\Gamma_{p,rel}$ has a mitigating effect on the exponential growth of the compensation point in the soil pore ($\chi_{p,rel}$ expressed relative to the χ_p in the ΔT=0°C simulation). This effect is stronger in the case of the larger TAN input.

In every model integration for a given TAN input, the initial chemical composition of the solution was the same (the same amount of urea is assumed to be hydrolysed in an aqueous solution with the same $[H^+]$), only the temperature varied. In essence, the same equilibrium system was investigated in every experiment at different temperatures. From this aspect, the difference between the experiments with the different TAN inputs is that in the "low TAN input" case the initial Γ_p was lower (given $[H^+]$ in the solution with low $[NH_4^+]$) and it was higher in the "high TAN input" case (given $[H^+]$ in the solution with high $[NH_4^+]$). Overall, three main conclusions can be drawn: 1) according to the model results, in a urine patch Γ_p is temperature-dependent; 2) this temperature-dependence is stronger if the initial Γ_p is higher; 3) the change of Γ_p in relation to temperature moderates the temperature-dependency of χ_p.

Based on the above findings the answer to the second question is: the weaker temperature-dependency of NH_3 emission (low Q_{10}) in the case of the urine patches compared to the clean area, can be explained by the dynamically changing Γ_p in the urine affected soil. The changes are driven by the gradually running out TAN budget under the urine patches and the temperature-dependence of Γ_p. As a result, the change in Γ_p moderates the exponential temperature-response of χ_p, leading to a weaker temperature-dependence in the total NH_3 emission, i.e. a lower Q_{10} than for a urine patch than the clean area.

5. 3. 3. Difference between the clean field simulations

A large difference in Q_{10} was found for the clean area in GAG_field between the modelling periods P2002 and P2003 (Table 5.6, Q_{10}^{Em}). This is a consequence of the calculation method of Q_{10}^{Em} described by Eq. 5.2. As explained in the introduction of Section 5.3, in this approach, ΣEm includes only the time steps over P2002 and P2003, where net NH_3 emission occurred in GAG_field^{clean}. Therefore, Q_{10}^{Em} expresses two

sources of increase in ΣEm in relation to rising temperature: 1) NH_3 emission grows in the time steps in which originally emission occurred (e.g. in Fig. 5.10 in t_2, t_3, t_6…), and 2) there are time steps with NH_3 emission in the ΔT = +10°C simulation, in which deposition occurred in the ΔT = 0°C simulation, i.e. there was a switch from deposition to emission at the +10°C higher temperature (e.g. in Fig. 5.10 in t_4 and t_7). This latter effect on ΣEm, hereby is referred to as "deposition-emission switch", is investigated in the following.

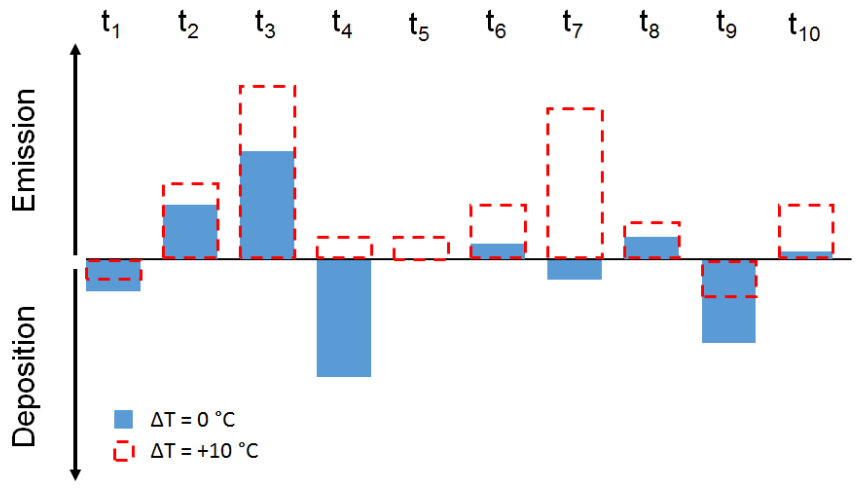

Figure 5.10. Schematic of how NH_3 exchange over a modelling period changes between two simulation with ΔT=0°C and ΔT=10°C.

In the ΔT = +10°C simulation with GAG_field^{clean}, in P2002 the number of time steps with NH_3 emission doubled compared to the simulation for ΔT = 0°C, whereas in P2003 it became almost 4 times higher than in the ΔT = 0°C experiment (Table 5.7). This significant change in the number of "emitting time steps" in P2003 resulted also in a higher contribution to the increase ΣEm (Table 5.8): 4.8 – 1.9 = 2.9 mg N m^{-2} was originating from the "deposition-emission switch", which is 64% of the total increase in ΣEm (4.8 – 0.3 = 4.5 mg N m^{-2}). The same contribution was 51% in P2002. The higher contribution of the "deposition-emisison switch" to the increase of ΣEm in P2003 can explain the higher Q_{10} calculated for GAG_clean^{field} in P2003 than in P2002.

Table 5.7. The number of time steps in which NH_3 emission was detected in GAG_clean^{field} for the two modelling periods, P2002 and P2003 at the original temperature ($\Delta T = 0$ °C) and when it was raised by 10 °C ($\Delta T = +10$ °C). In the brackets the same number is expressed as the percentage of the total number of time steps.

Modelling period (total number of time steps)	**Number of time steps with emission**	
	$\Delta T = 0$ °C	**$\Delta T = +10$ °C**
P2002 (226)	77 (34%)	176 (78%)
P2003 (126)	18 (14%)	68 (54%)

Table 5.8. Total NH_3 emission (ΣEm) in GAG_field^{clean} for the two modelling periods, P2002 and P2003 at the original temperature ($\Delta T = 0$ °C) and when it was raised by 10 °C ($\Delta T = +10$ °C). In the brackets ΣEm is calculated only for the time steps in which emission occurred at $\Delta T = 0$ °C.

Modelling period	**ΣEm (mg N m^{-2})**	
	$\Delta T = 0$ °C	**$\Delta T = +10$ °C**
P2002	1.5	11.2 (emission time steps: 6.3)
P2003	0.3	4.8 (emission time steps: 1.9)

Although the larger effect of "deposition-emission switch" on ΣEm could explain the difference in Q_{10} for GAG_field^{clean} in P2002 and P2003, these values of Q_{10} are not in accordance with the real effect of temperature on NH_3 exchange over the clean field. This is suggested by Fig. 5.11, where the total NH_3 exchange (ΣEx) was plotted for the same simulations performed in Section 5.3.2 with the different ΔT scenarios. Fig. 5.11 implies that the temperature-response of ΣEx was stronger in P2002 than P2003, which is in contradiction with that implied by the larger Q_{10} calculated for P2003. Therefore, in order to obtain a more realistic picture about the temperature-dependence of NH_3 exchange over the clean field, the temperature dependence of the component fluxes were also examined.

These component fluxes are illustrated in Fig. 5.12. Over the clean area in GAG_field, the component fluxes are determined by the ambient NH_3 air concentration (χ_a), the compensation point on the soil surface (χ_g) and in the stomata

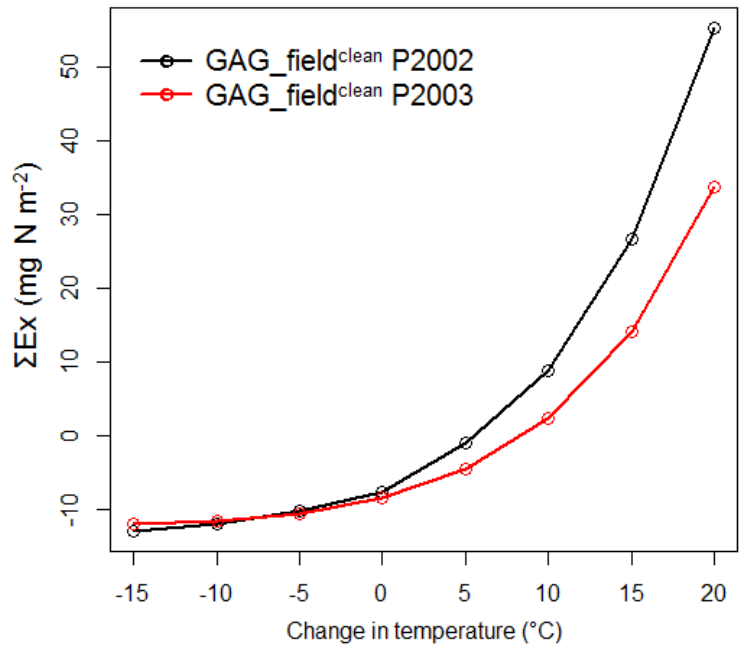

Figure 5.11. Total NH_3 exchange flux (ΣEx) above the clean area in GAG_field^{clean} for P2002 and P2003, as a function of the change in temperature.

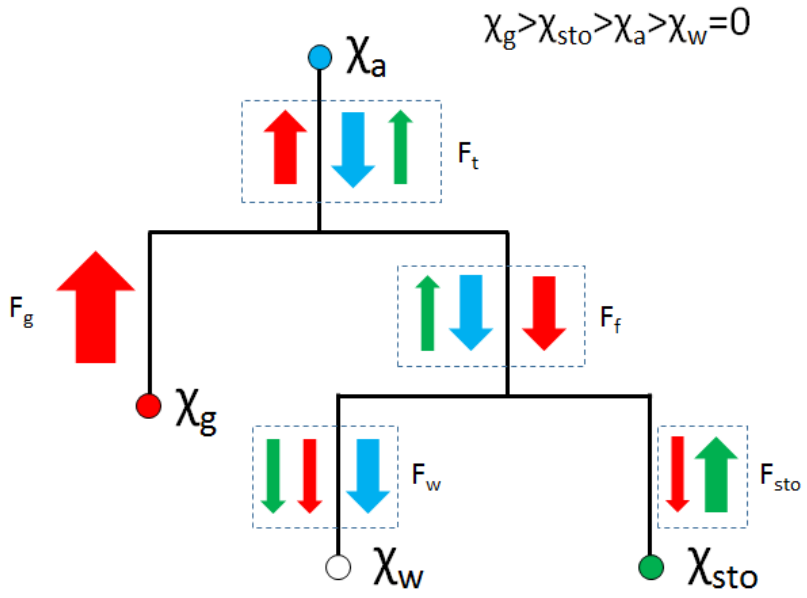

Figure 5.12. Schematic of NH_3 flows (arrows) as regulated by the different NH_3 concentrations within the two-layer canopy compensation point model used in GAG_field^{clean}: soil compensation point (χ_p), ambient air concentration (χ_a) stomatal compensation point (χ_{sto}) and the compensation point above the leaf surface (χ_w=0). The descending order of these concentrations occurred most of the time in GAG_field^{clean} is also indicated. An NH3 flow with a given colour originates from the point with the same colour.

(χ_{sto}), as well as the compensation point over the cuticle (χ_w), which is 0, since to the cuticle only NH_3 deposition was assumed in the model (Section 2.3). Based on the difference between these concentrations, NH_3 flows from the larger concentrations toward the smaller ones. In most of the time, in GAG_field^{clean} the descending order of this concentrations were $\chi_g > \chi_{sto} > \chi_a > \chi_w = 0$.

Among the NH_3 flows between the concentrations, the ones starting from χ_g (red arrows in Fig. 5.12) and χ_{sto} (green arrows in Fig. 5.12) are regulated by temperature through these two compensation points. Therefore, both in ΣF_g and the total stomatal NH_3 flux (ΣF_{sto}) for GAG_field^{clean}, a strong and very similar response can be observed to the changes of temperature (Fig. 5.7 a, and Fig. 5.13, respectively). The explanation for the slightly weaker agreement between P2002 and P2003 in $\Sigma F_{sto,rel}$ (Fig. 5.13) than $\Sigma F_{g,rel}$ (Fig. 5.7 a) is that at lower temperature also $\chi_a > \chi_{sto}$ can occur. In this case, F_{sto} is also influenced by the atmospheric deposition (blue arrows, Fig. 5.12). This effect, however, diminishes with the increase of temperature, and completely ceases when χ_{sto} becomes larger than χ_a.

In contrast to F_{sto} and F_g, the net NH_3 exchange over the surface (F_t), the exchange above the canopy (F_f) and the deposition to the leaf surface (F_w) are always affected by the atmospheric deposition (blue arrows in Fig. 5.12), since $\chi_a > \chi_w$=0 in every time step. Atmospheric deposition is independent of temperature in the model in this situation and governed by χ_a, which in GAG_field^{clean} is an input variable. Examining how the sums of F_t, F_f and F_w over P2002 and P2003 change when the temperature is perturbed ($\Sigma F_t = \Sigma Ex$: Fig. 5.11, ΣF_f: Fig. 5.14, and ΣF_w: Fig. 5.15), in all three cases a weaker temperature dependency can be observed for P2003.

These differences between P2002 and P2003 can be explained as follows. Let F_1 and F_2 be single fluxes which are determined by a temperature-driven NH_3 component, F^{temp}, as well as F_1^{ind} and F_2^{ind} components that are independent of temperature:

$$F_1 = F^{temp} + F_1^{ind}, \tag{5.3}$$

$$F_2 = F^{temp} + F_2^{ind}. \tag{5.4}$$

When the temperature is raised by 10 °C, F^{temp} becomes:

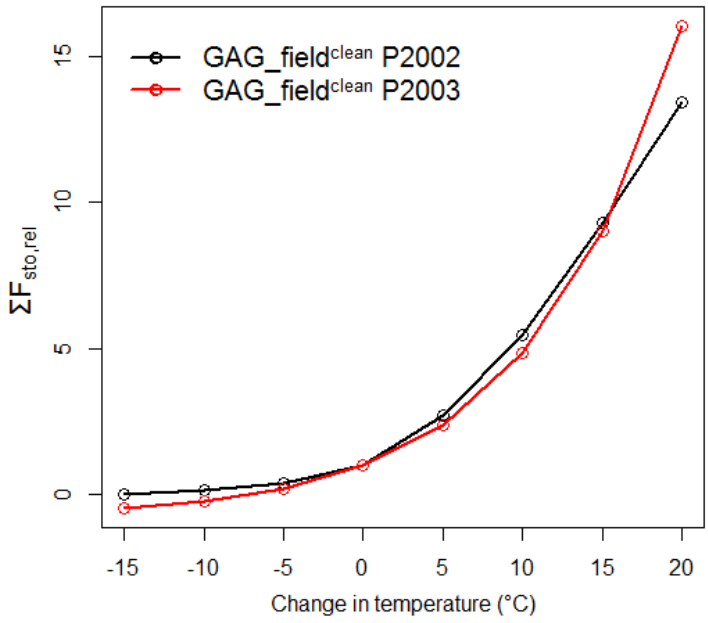

Figure 5.13. Total stomatal NH_3 emission flux ($\Sigma F_{sto,rel}$) above the clean area in GAG_field^{clean} for P2002 and P2003, as a function of the change in temperature. The values are expressed relative to ΣF_{sto} for the simulations with $\Delta T = 0°C$.

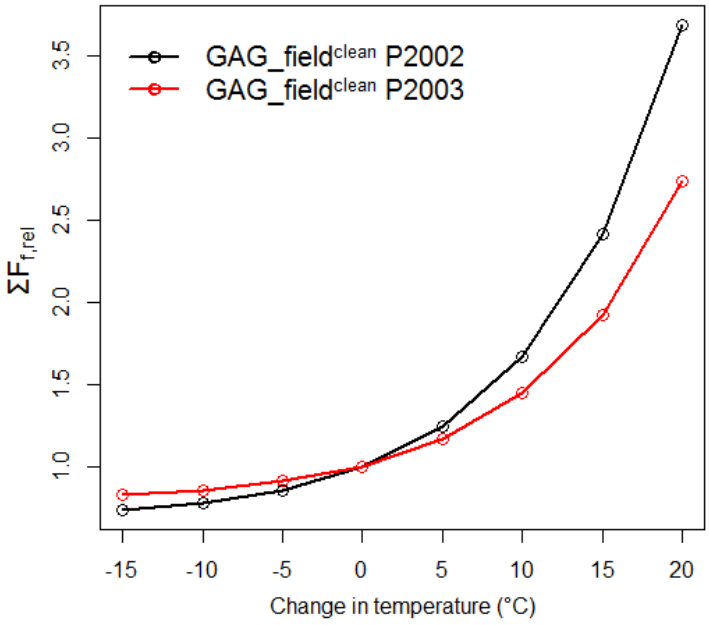

Figure 5.14. Total NH_3 exchange flux over the canopy ($\Sigma F_{f,rel}$) above the clean area in GAG_field^{clean} for P2002 and P2003, as a function of the change in temperature. The values are expressed relative to ΣF_f for the simulations with $\Delta T = 0°C$.

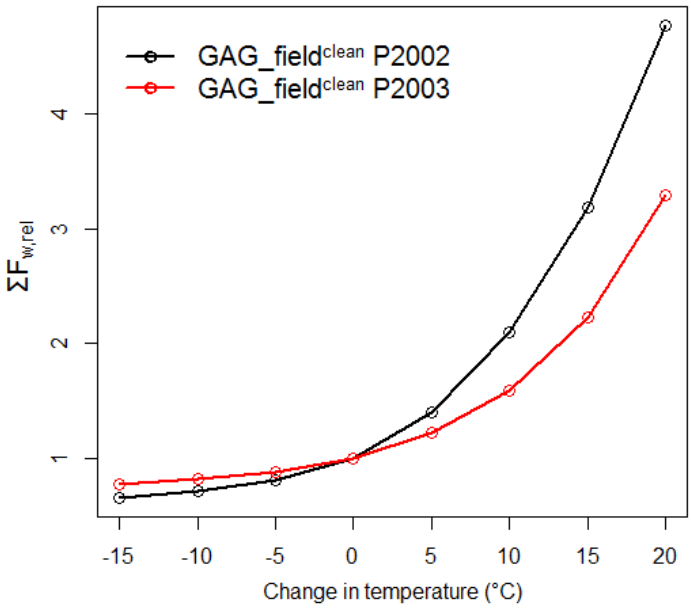

Figure 5.15. Total cuticular deposition flux of NH_3 ($\Sigma F_{w,rel}$) above the clean area in GAG_field^{clean} for P2002 and P2003, as a function of the change in temperature. The values are expressed relative to ΣF_w for the simulations with ΔT = 0°C.

$$F^{temp}\left(\Delta T = 10°C\right) = Q_{10}{}^{temp} F^{temp}. \tag{5.5}$$

Based on this, the Q_{10} values for F_1 and F_2 can be expressed as:

$$Q_{10}^{1} = \frac{Q_{10}^{temp} F^{temp} + F_1^{ind}}{F^{temp} + F_1^{ind}}, \tag{5.6}$$

$$Q_{10}^{2} = \frac{Q_{10}^{temp} F^{temp} + F_2^{ind}}{F^{temp} + F_2^{ind}}. \tag{5.7}$$

Let $Q_{10}{}^1$ be larger than $Q_{10}{}^2$. This, after reorganizing Eqs. 5.6 and 5.7, can be written as:

$$\left(Q_{10}^{temp} - 1\right)\frac{F^{temp}}{F_1^{ind} + F^{temp}} + 1 > \left(Q_{10}^{temp} - 1\right)\frac{F^{temp}}{F_2^{ind} + F^{temp}} + 1, \tag{5.8}$$

which after the simplification becomes:

$$\frac{1}{F_1^{ind} + F^{temp}} > \frac{1}{F_2^{ind} + F^{temp}}. \tag{5.9}$$

This can be reorganized and simplified as:

$$F_2^{ind} > F_1^{ind} . \quad (5.10)$$

To conclude, this result shows that if an NH_3 flux is determined by a temperature dependent and a non-dependent component, the larger is the non-dependent component, the weaker will be the temperature-response of the given NH_3 flux (smaller Q_{10}). Applying this finding to the results from GAG_field^{clean}, the difference in the temperate-response of ΣF_t, ΣF_f and ΣF_w, might have been weaker in P2003 than in P2002 because the atmospheric deposition component (blue arrows, Fig. 5.12) was larger in F_t, F_f and F_w in P2003. Since this component is larger if χ_a is larger, and in P2003 the average χ_a was higher by 0.4 µg m^{-3} (the average χ_a was 1.0 µg m^{-3} and 1.4 µg m^{-3} in P2002 and P2003, respectively), this can be considered as a feasible explanation for the difference in the temperature response of ΣF_t in the two modelling periods.

Finally, the following answer can be provided to the third question: the reason for the large difference in Q_{10} for GAG_field^{clean} in P2002 and P2003 is the "deposition-emission swtich", which is an artefact of the calculation method that was applied to derive Q_{10}. However, these Q_{10} values were not in accordance with the real temperature-response of the net NH_3 exchange flux over the clean area. Examining the differences of the temperature-dependence of ΣEx, it was found that in P2003 the temperature-response was weaker than in P2002, which is most likely caused by the larger χ_a measured over P2003.

5. 3. 4. Difference between the whole field simulations

According to Table 5.6, in P2003, ΣEm for the clean area was much more sensitive to temperature (Q_{10} = 18.21) than in P2002 (Q_{10} = 7.65), whilst the Q_{10} values for the urine patch emissions showed only a small difference (Q_{10} = 1.51 in P2002 and Q_{10} = 1.72 in P2003). Since NH_3 emission is determined by the coupled effect of the clean area and the urine patches, the difference in Q_{10} calculated for the clean area in the two modelling periods may apply to the Q_{10} values over the whole field. Based on this, a high difference could be expected in the temperature-sensitivity over the whole field,

similarly to the results for the clean area. However, the difference in Q_{10} for the whole field was in fact relatively small (Q_{10} = 3.10 and Q_{10} = 3.39 for P2002 and P2003, respectively).

The fact that the Q_{10} values calculated for the whole field were not in accordance with the expectations can be explained by the higher average urination frequency in P2003 (21 patches / hour) compared to P2002 (9 patches / hour), that decreased the area of the clean field (and increased the area covered by urine patches) twice as quickly in P2003 as in P2002 (Fig. 5.16). Therefore, a possible answer for the fourth question can be: the temperature-dependency of ΣEm over the whole field is determined by the coupled effect of the temperature-response of ΣEm over the urine patches and the clean area. The more urine patches are deposited on the field, the closer will be the Q_{10} for the whole field to the Q_{10} over the urine patches.

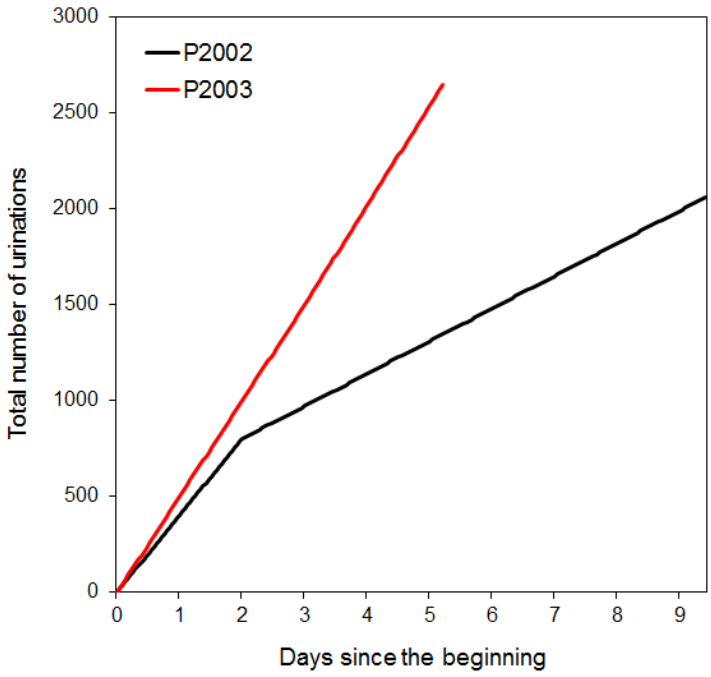

Fig. 5.16. Total urination number over the field in the baseline simulations with GAG_field for P2002 and P2003.

Nevertheless, it has to be noted that in the case of the whole field, Q_{10} can be calculated using not only ΣEm (Q_{10}^{Em}, Eq. 5.1) but also ΣEx (Q_{10}^{Ex}, Eq. 5.2). The values of Q_{10}^{Ex} are larger (4.00 and 3.93 in 2002 and 2003, respectively in Table 5.6)

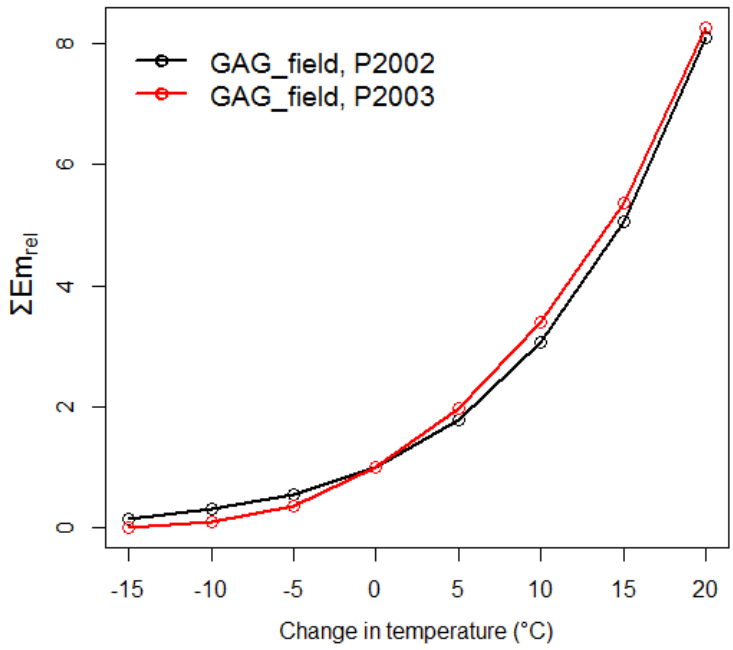

Figure 5.17. The sum of the NH_3 emission (positive exchange) fluxes (ΣEm_{rel}) above the whole field in GAG_field for P2002 and P2003, as a function of the change in temperature. The values are expressed relative to ΣEm at ΔT=0°C.

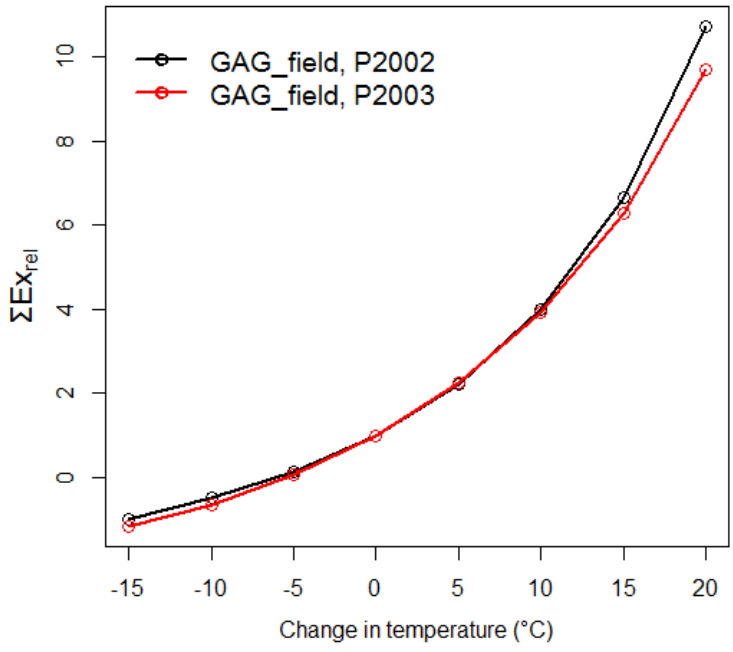

Figure 5.18. Total NH_3 exchange flux (ΣEx_{rel}) above the whole field in GAG_field for P2002 and P2003, as a function of the change in temperature. The values are expressed relative to ΣEm at ΔT=0°C.

and suggest a slightly stronger temperature-dependency of ΣEx (Fig. 17) for P2002 than P2003, which is the opposite of that Q_{10}^{Em} implied for ΣEm (Fig. 18). The larger values for Q_{10}^{Ex} than Q_{10}^{Em}, can be explained by that ΣEm and ΣEx differ in the deposition terms that are not included in ΣEm (see Fig 5.10.). The larger the deposition term, the larger the difference between ΣEm and ΣEx. As at higher temperature the deposition terms are weaker (due to larger χ_{sto}), the difference between ΣEm and ΣEx is smaller in warmer conditions. This means that comparing Eq. 5.1 and 5.2, the difference in the numerator is smaller than in the denominator, resulting in a higher ratio, i.e. a higher Q_{10}^{Ex} than Q_{10}^{Em} (summarized in Eq. 5.11).

$$\left.\begin{array}{l}\sum Em(\Delta T=+10°C) > \sum Ex(\Delta T=+10°C) \\ \sum Em(\Delta T=0°C) >> \sum Ex(T=0°C)\end{array}\right\} \Rightarrow Q_{10}^{Em} < Q_{10}^{Ex} \qquad (5.11)$$

5. 3. 5. The effect of the change of the TAN budget on Q_{10}

Previously, in Section 3.4.2, it was shown that a daily loss or gain in the TAN budget can influence the temporal variation of the NH_3 emission flux over a urine patch. In Table 5.9 it can be seen that not only the temporal variation of NH_3 emission, but also Q_{10} can be influenced by a possible daily change in the TAN budget. The tendency of the change was the same in all three simulations (GAG_patch and GAG_field for P2002 and P2003): in the case of TAN loss, Q_{10} became larger in all simulations, whilst with additional TAN, Q_{10} became lower. The results also show that the influence on Q_{10} for the simulations with GAG_field is stronger than for GAG_patch.

Table 5.9. Q_{10} values calculated in the simulation with GAG_patch and GAG_field for P2002 and P2003 with three scenarios: with unchanged TAN budget (baseline simulations) and with a 10% daily loss and gain in it

Modelling period	**Q_{10}**		
	-10% TAN	**Base**	**+10% TAN**
GAG_field, P2002	4.64	3.10	2.09
GAG_field, P2003	6.28	3.39	2.40
GAG_patch	1.39	1.26	1.18

In order to find an explanation for the findings in Table 5.9, the results for GAG_patch were examined in more detail (Table 5.10). Table 5.10 indicates all

pathways of NH_3 exchange over the urine patch (columns A-D), the remaining TAN in the model soil pore (column E) and the actual TAN loss/gain in the given simulation with GAG_patch (column F). First of all, it can be concluded that there is no TAN leakage within the model, as the lost/gained TAN and the amount remaining in the soil pore are equal (within a 0.33% error interval) to the initial, 3 g TAN input (column A + E – F = 3).

In Table 5.10 it can be also seen that with TAN loss the net NH_3 exchange becomes lower, whilst with a TAN gain it becomes higher. This might lead to a larger number of time steps with deposition over the field scale in the ΔTAN=-10% model runs and a smaller number of them in the opposite case. As it was shown in Section 5.3.3, when time steps with deposition are present over a modelling period, at the +10 °C higher temperature a large increase can occur in the total NH_3 emission due to the new "emitting time steps". This can be a possible explanation for the large difference in the effect of ±TAN on Q_{10} between the patch and field-scale simulations (Table 5.9).

Table 5.10. Model results from the sensitivity test to an assumed daily TAN loss or gain (ΔTAN) in GAG_patch. The table indicates the total emitted and deposited NH_3 (g N) in the different pathways over the urine patch, the TAN remaining at the end of the modelling period in the soil pore and the total TAN lost/gained over the simulation. Simulations were carried out at the original temperature (ΔT = 0 °C) and when the temperature was raised by 10 °C.

	A	B	C	D	E	F
Model experiment	**Soil Emission**	**Exchange with the canopy**		**Net exchange**	**Remaining TAN in the soil pore**	**Total TAN loss/gain**
		Stomata	**Cuticle**			
ΔTAN = 0% ΔT = 0 °C	2.59	-0.81 -0.24	-0.57	1.77	0.41	0
ΔTAN = 0% ΔT = +10 °C	2.89	-0.64 -0.10	-0.55	2.24	0.11	0
ΔTAN = -10% ΔT = 0 °C	2.11	-0.65 -0.21	-0.44	1.45	0.36	-0.52
ΔTAN = -10% ΔT = +10 °C	2.62	-0.57 -0.09	-0.48	2.06	0.10	-0.28
ΔTAN = +10% ΔT = 0 °C	2.99	-0.95 -0.28	-0.67	2.04	0.58	+0.57
ΔTAN = +10% ΔT = +10 °C	3.11	-0.71 -0.11	-0.60	2.41	0.18	+0.29

This is, however, not the only reason for the change in Q_{10} in relation to the change in the TAN budget. In the case of the TAN loss experiment, at higher temperature, because of the stronger NH_3 emission, the TAN budget runs out more quickly, and as a result less TAN could be lost via the competing processes in the soil (-0.28 g, Table 5.10) than at the original temperature (-0.52 g, Table 5.10), where the NH_3 emission is slower, leaving more TAN in the TAN budget available for the soil loss processes. In essence, if a TAN consuming process is present in the soil pore, more TAN is available for NH_3 emission than in cooler conditions. Compared to the ΔTAN=0 experiments this will result in:

$$\begin{array}{l} \sum Em^{\Delta TAN=-10\%}\left(\Delta T=+10°C\right) < \sum Em^{\Delta TAN=0}\left(\Delta T=+10°C\right) \\ \sum Em^{\Delta TAN=-10\%}\left(\Delta T=0°C\right) << \sum Em^{\Delta TAN=0}\left(\Delta T=0°C\right) \end{array}, \qquad (5.12)$$

which suggests a stronger temperature-dependence in ΣEm, i.e. a larger Q_{10} for the ΔTAN = -10% case than for the ΔTAN = 0 simulations.

In the case of the ΔTAN = +10% scenario, the explanation is similar: since at higher temperature less TAN is available, the proportional daily growth in it is smaller (+0.29 g, Table 5.10) than at ΔT = 0°C (+0.57, Table 5.10). This means that at higher temperature there will be more TAN available for NH_3 emission. Compared to the ΔTAN = 0 simulations, this can be expressed by the opposite of the relationship in Eq. 12:

$$\begin{array}{l} \sum Em^{\Delta TAN=+10\%}\left(\Delta T=+10°C\right) > \sum Em^{\Delta TAN=0}\left(\Delta T=+10°C\right) \\ \sum Em^{\Delta TAN=+10\%}\left(\Delta T=0°C\right) >> \sum Em^{\Delta TAN=0}\left(\Delta T=0°C\right) \end{array}, \qquad (5.13)$$

which implies a weaker temperature-response of ΣEm, *i.e.* a smaller Q_{10} for ΔTAN = +10% simulation than for the ΔTAN= 0 one.

It also has to be pointed out that ΣEm over the urine patch (column D in Table 5.10), which is used to calculate the Q_{10} values, is also dependent on the deposition to the canopy (column B + C). Nevertheless, the percentage of soil NH_3 emission that is depositing back to the canopy (column (B+C) / A) is not affected by the TAN loss or gain. In the case of every ΔTAN simulation, at the original temperature about 31% of

the NH_3 emitted from the soil is recaptured by the canopy, whilst in the ΔT = +10 °C simulations this percentage amounts about 22%. This suggests that the difference in ΣEm with a TAN loss or gain is clearly an effect of the modified soil emission, through the changes in the TAN budget.

5. 3. 6. The effect of the length of the modelling period on Q_{10}

To investigate the temporal development of Q_{10}, for GAG_patch and GAG_field for both P2002 and P2003, the cumulative NH_3 emissions were derived in every time step. The cumulative NH_3 emission in a certain time step indicates the sum of the NH_3 emission between the beginning of the modelling period and the investigated time step (Fig. 5.19). To derive a Q_{10} time series, the cumulative NH_3 emissions at ΔT = +10 °C were divided by the cumulative emissions at ΔT = 0 °C.

Fig 5.20 shows that in every simulation, at the beginning of the modelling period there was an overall exponential decrease in Q_{10} that flattened out after the third day and became similar for the three model experiments. Nevertheless, the inset in Fig 5.20 indicates that in the small numbers in the later stage of the modelling period, still relatively big changes could be observed in the two field-scale simulations. This led to various differences between the Q_{10} values for the P2002 and P2003 modelling period: for example, on day 3 there was a difference of 2 between the Q_{10} values, whilst two days later they were almost the same.

Móring et al. (2016) explained that in GAG_patch the peak at the beginning of the modelling period is caused by the higher temperature-sensitivity of NH_3 emission in the beginning. According to this study, in the first couple of hours after the deposition of the urine patch, not just NH_3 exchange but also the urea breakdown is governed by temperature. This effect diminishes after the first 24 hour when all the urea is hydrolysed. In the case of GAG_field, urine patches are deposited in every time step, consequently, there are urine patches in every time step that are in the stage of the intensive urea-hydrolysis. Therefore, if the mechanism described by Móring et al. (2016) was be the only reason for the temporal development of Q_{10}, in the field scale

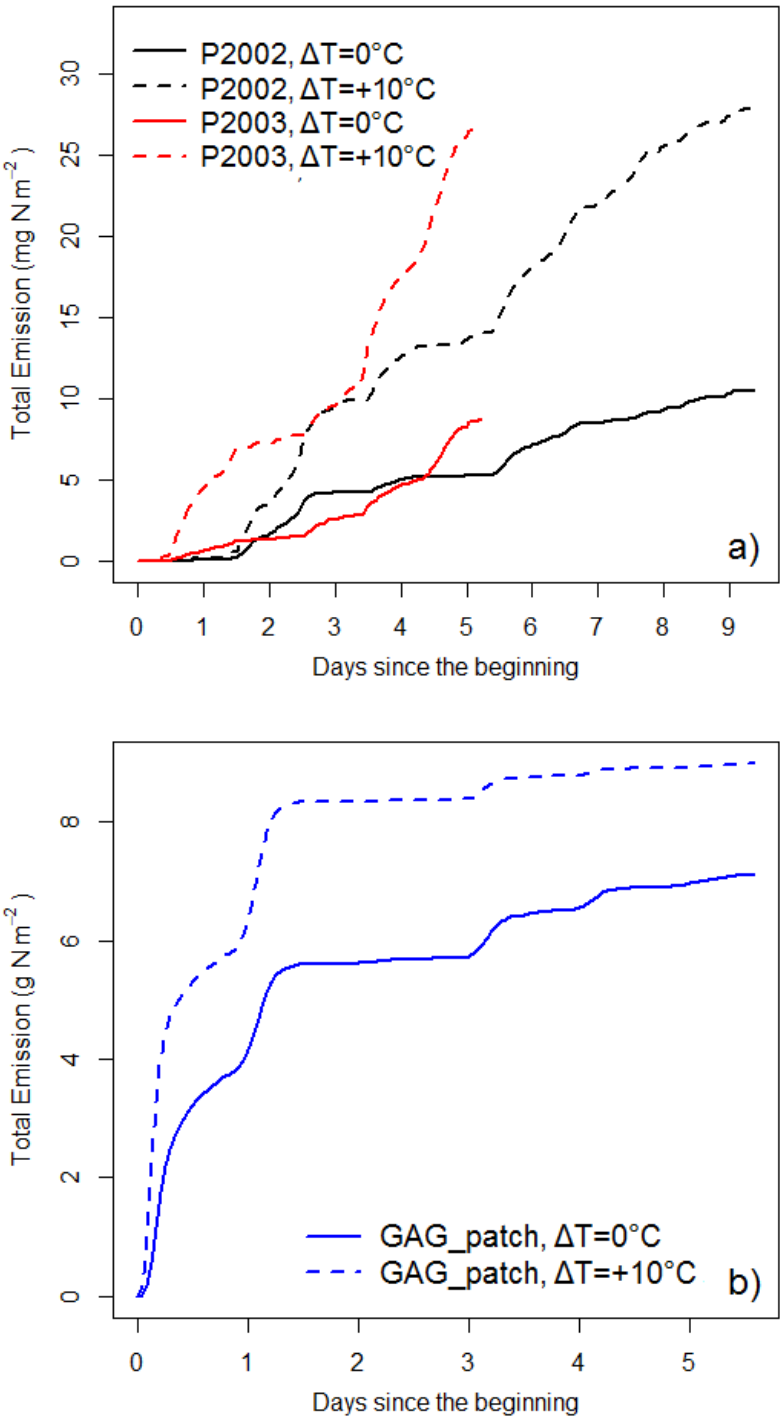

Figure 5.19. Cumulative NH_3 emission (the total emission between the beginning and the given time step) in the simulations with GAG_field for P2002 and P2003 (a) and in the simulation with GAG_patch (b). On both panels solid lines and dashed lines denote the baseline simulations (ΔT=0°C), and the simulations with an assumed +10°C increase (ΔT=+10°C), respectively.

a constant, high Q_{10} value would be seen. According to the current findings, however, this is not the case.

The similar temporal development of Q_{10} in the different simulations implies that the reason is mathematical: at the beginning, very small NH_3 emissions are divided by even smaller ones (Fig. 5.19), resulting in apparently high Q_{10} values. Then, as the cumulative emissions grow, their ratio, Q_{10} stabilises.

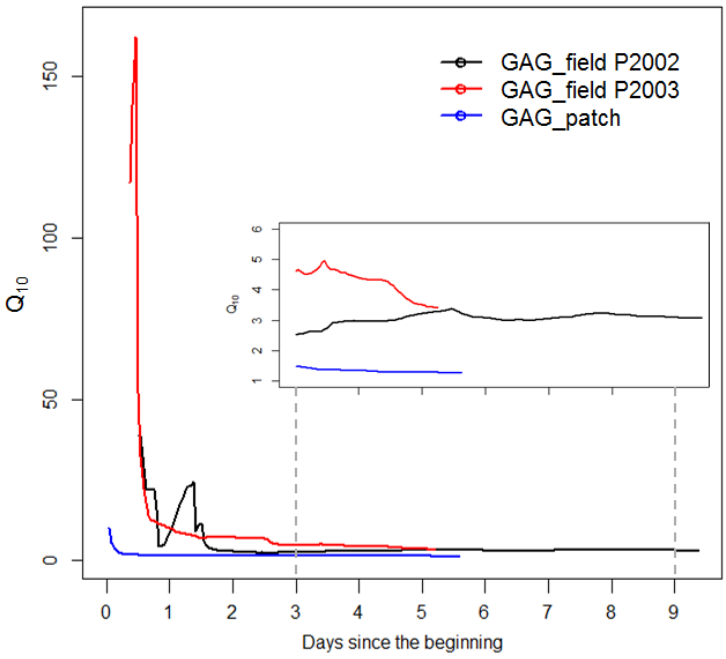

Figure 5.20. The temporal evolution of Q_{10} calculated for the cumulative NH_3 emissions (the sum of NH_3 emission between the beginning of the period and the given time step). The small panel shows the same Q_{10} values from the 3rd day on a smaller scale (Q_{10}=1-6).

5. 3. 7. The effect of the initial temperature on Q_{10}

In order to investigate the effect of the initial temperature (at which the +10°C increase starts) on the calculation of Q_{10}, in the model simulations with GAG_field and GAG_patch for the different ΔT modifications (Section 5.3.2), values of Q_{10} were calculated for every pair of simulations with a difference of 10 °C for the whole field and for the single urine patch. The simulation pairs were denoted by A-F (Table 5.11). The results (Fig. 5.21) show that the initial temperature had the strongest effect on Q_{10} in the case of GAG_field for P2003. Whilst in the field-scale simulation for P2002 and

Table 5.11. Simulation pairs denoted as A-F to calculate Q_{10} based on different ΔT scenarios.

Simulation pairs	ΔT scenarios used	
	Start	End
A	-15 °C	-5 °C
B	-10 °C	0 °C
C	-5 °C	+5 °C
D	0 °C	+10 °C
E	+5 °C	+15 °C
F	+10 °C	+20 °C

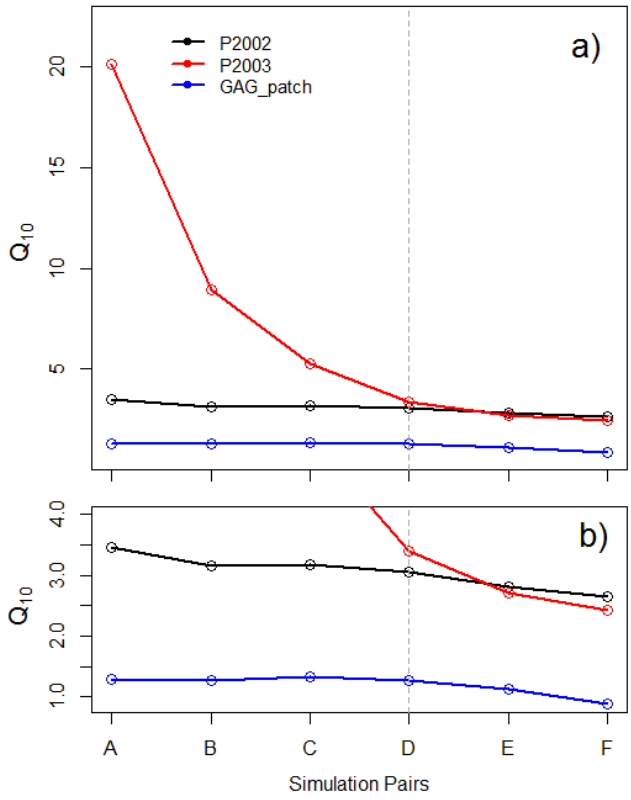

Figure 5.21. Values of Q_{10} calculated based on total emissions for the whole field simulated by GAG_field for P2002 and P2003, and the single urine patch derived by GAG_patch, using the different ΔT scenarios listed in Table 5.10. The bottom panel shows the same Q_{10} values but on a narrower range (Q_{10} = 1-4). The vertical dashed line denotes the basic simulation pairs, in which the original temperature (ΔT=0°C) was raised by 10°C.

GAG_patch only a weak influence of the initial temperature was detected, which resulted in a moderate decrease of Q_{10} in these two cases.

The reason for the large difference in the Q_{10} for the two field-scale simulations can be explained by the more intense increase of the number of the time steps with NH_3 emission in P2003 than in P2002, i.e. the stronger effect of the "deposition-emission switch" on Q_{10} in P2003 (Fig. 5.22). As explained in Section 5.3.3, this effect is an

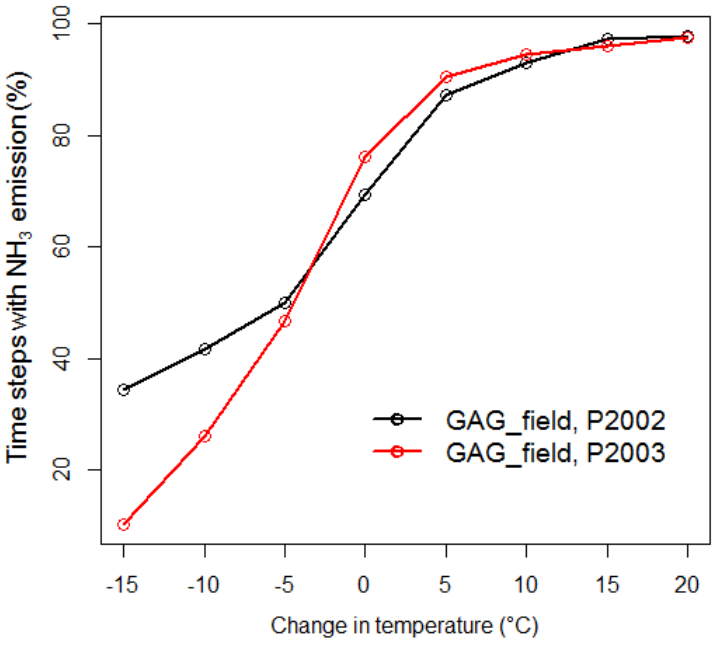

Figure 5.22. Time steps within GAG_field over the modelling periods P2002 and P2003 in which NH_3 emission occurred. The numbers are expressed relative to the total number of time steps, 226 and 126 in P2002 and P2003, respectively.

Table 5.12. Values of Q_{10}^{Ex} calculated based on Eq. 5.1, for the whole field simulated by GAG_field for the modelling periods, P2002 and P2003, using the different ΔT scenarios listed in Table 5.11. In the simulation pairs A and B negative Q_{10}^{Ex} negative values occurred which are not considered meaningful, therefore, these were not indicated here.

Modelling period	**Q_{10}^{Ex} in the simulation pairs**			
	C	**D**	**E**	**F**
P2002	16.4	4.0	3.0	2.7
P2003	34.5	3.9	2.8	2.5

artefact of the calculation method of Q_{10} (Eq. 5.2). However, the Q_{10} values calculated based on ΣEx (Q_{10}^{Ex}, *Eq. 5.1)* also show a substantial variability in Q_{10} in relation to the initial temperature (Table 5.12). These results suggest that Q_{10} should be used with caution, since for the same system different Q_{10} values can be derived, depending on the range of temperature for which it is calculated for.

Finally, it has to be noted that a slight decrease in Q_{10} can be expected with a higher temperature even if in all time steps emission occurs at both the initial and the modified temperature. Fig 5.23 illustrates a situation in which NH_3 exchange is driven clearly by the soil compensation point (χ_g). This condition can occur, if χ_a and the other NH_3 exchange fluxes within the canopy are negligibly small. As a result, in these circumstances, χ_g is regulated only by the temperature-dependent chemical equilibria in the surface soil solution. The modest decrease in Q_{10}, resulting in this way (Fig. 5.23), is a consequence of the temperature-dependence of χ_g, as it is not a clear exponential function of temperature (Eq. 4.7), but also includes a multiplying factor that is an inversely proportional function of T_{soil} (161500 / T_{soil}).

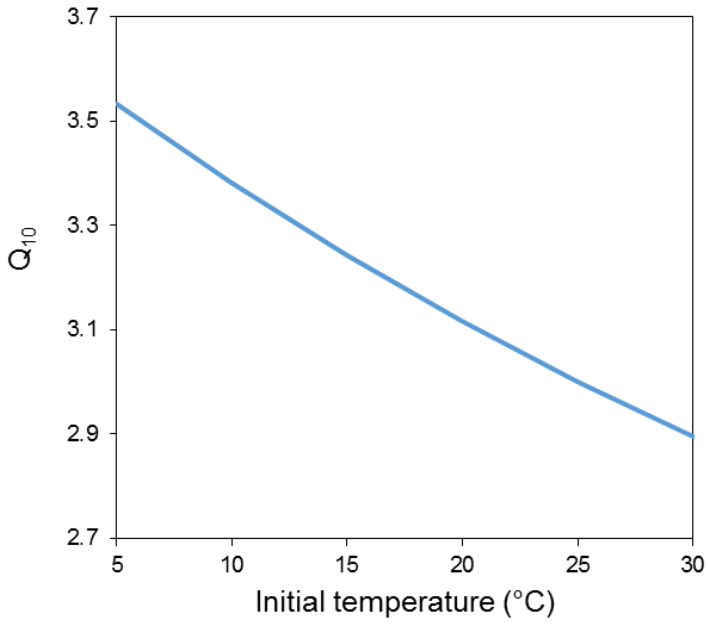

Figure 5.23. Q_{10} values calculated for a simplified modelling situation in which the total NH_3 exchange over the canopy is clearly governed by the compensation point on the soil surface (χ_g). In this case the ambient NH_3 air concentration and the other NH_3 exchange fluxes within the canopy are negligibly small, i.e. χ_g is regulated by the temperature-dependent chemical equilibria in the soil solution on the surface.

5. 4. Discussion and conclusions

In this chapter simulations were performed with GAG_field and GAG_patch to test the sensitivity of the total NH_3 exchange and emission to the different meterological variables, with a special focus on temperature. In the case of GAG_patch, NH_3 emission was found to be sensitive to temperature (considering air and soil temperature together), wind speed (u) and relative humidity (RH). In the case of RH a dual effect was observed through affecting the modelled soil evaporation and the deposition to leaf surfaces, with the latter being the dominant term for the simulation with GAG_patch. The model did not show high sensitivity to the amount of precipitation, but it was found that the total NH_3 emission and the temporal development of NH_3 volatilization can be affected by the timing of the rain event.

Temperature, u and RH considerably influenced NH_3 exchange also in GAG_field. However, the resulted changes in the total NH_3 exchange over the field were substantially different from those found for GAG_patch. Whilst in the case of u in GAG_field and GAG_patch the opposite change was observed in the total exchange, the effect of RH on NH_3 exchange was similar, but stronger. In the field-scale simulation global radiation (R_{glob}) was detected as an additional strong influencing meteorological variable. The results suggested that in meteorological circumstances that do not favour soil evaporation, R_{glob} can have a larger effect on NH_3 exchange than in conditions that facilitate soil evaporation.

For the in-depth investigation of the temperature-dependence of NH_3 exchange, a metric was used, Q_{10}, that describes the relative increase in the total emission over a range of 10 °C. Based on this investigation two types of conclusions can be distinguished: 1) conclusions for the real temperature-dependence of NH_3 exchange, 2) conclusions for the applicability of Q_{10} for NH_3 exchange.

As for the real temperature-dependence of NH_3 exchange, the following can be concluded. The temperature-response of the total NH_3 emission from the urine patches can be considerably affected by precipitation. After rain events, in warmer conditions the stronger evaporation from the soil allows more urine to infiltrate, which can lead to higher NH_3 emission and as a results, higher Q_{10} than in dry conditions, where in

both the cooler and warmer conditions the same amount of urine can penetrate to the NH_3 source layer.

Substantially weaker temperature-dependence was found for GAG_patch than for the clean area in GAG_field. This can be explained by the dynamically changing soil emission potential under the urine patches that moderates the exponential temperature-response of the soil compensation point, leading to a weak temperature-dependence in NH_3 emission. A slight difference was also detected in the temperature-response of the clean area in GAG_field, in the case of the two modelling periods. The results indicated that the weaker temperature-response of the total NH_3 exchange in the modelling period for 2003 was a consequence of the higher ambient NH_3 air concentration. This could moderate the effect of the temperature-dependent fluxes in the net NH_3 exchange through the non-temperature-dependent atmospheric deposition.

It was shown that over the whole field the temperature-response of the total NH_3 exchange is determined by the temperature-sensitivity of NH_3 emission over the clean area and the urine patches. The relative contribution of these two surface types is dependent on the average urination frequency.

Finally, it was found that the temperature-dependency of NH_3 emission from a urine patch can become stronger in the case of an assumed TAN loss in the soil, and become weaker in the case of TAN gain.

Concerning the applicability of Q_{10}: because in a modelling period total NH_3 deposition can occur, it cannot be universally used for NH_3 exchange fluxes, except if Q_{10} is derived based only on the period of NH_3 emission fluxes (e.g. hourly values with emission). However, due to the increasing number of hourly NH_3 emission fluxes with warming, this can lead to Q_{10} values that are not in accordance with the real temperature-response of the NH_3 exchange. Furthermore, it was found that the value of Q_{10} can be affected by the length of the period for which it is calculated and the initial temperature, that is, the temperature at which the original total NH_3 emissions are derived. All these results suggest that Q_{10} can be used only with caution for NH_3 exchange, and supports the need for a suitable metric or a set of metrics that can be used for such situations with bi-directional fluxes.

Chapter 6

Discussion and conclusions

6. 1. Introduction

This chapter provides an overview and a synthesis of the findings presented in this thesis. In the first section, the results are discussed from the evaluation of both the patch- and field-scale version of the GAG model (Section 6.2). This is followed by the review of the effects of meteorology on NH_3 exchange reported in Chapter 5 (Section 6.3). The next section, based on the lessons learned during this thesis, outlines the possible directions of future work (Section 6.4). The chapter and the whole thesis concludes with a summary (Section 6.5) in the form of concise answers to the research questions formulated in Chapter 1.

6. 2. Modelling ammonia exchange over grazed fields

6. 2. 1. Construction and evaluation of a patch-scale and a field-scale model

The main source of NH_3 emission from grazed fields is the urine patches (Laubach et al., 2013, Petersen et al., 1998). Therefore, to simulate NH_3 exchange between the atmosphere and the surface, in the first stage, a new NH_3 emission model (GAG) was constructed for a single urine patch (Chapter 2). The GAG model is capable of simulating the TAN and the water content of the soil under a urine patch and the variation of soil pH. At a larger scale, over a grazed field NH_3 exchange is determined by the coupled effect of NH_3 emission from the urine patches and NH_3 exchange with the area of the field that is not affected by urine ("clean area"). Therefore, in the second

stage, the GAG model was applied at the field scale, by employing it for the urine patches and using a modified version of it for the clean area (Chapter 4).

Both the patch- and the field-scale versions of the model have been evaluated based on measurements, with both model versions turning out to be in broad agreement with the observations, being able to simulate both the temporal variability of NH_3 emission and its magnitude over the measurement periods (Section 3.3 and Section 4.5). At the patch scale, the difference between the simulated and measured values suggested that the model could be improved by including the effect of a possible restart of urea hydrolysis with rain events. In Section 3.4.3 a simulation was presented showing the potential of such a model extension. However, the assumptions made for this particular simulation were hypothetical and specific for the site. Therefore, it was concluded that to generalize and operationally include this effect in the model, further investigation was needed regarding, e.g. how much urine can be retained on the leaf surface, what are the circumstances needed to completely stop the hydrolysis, and how much urine captured by the vegetation can be washed into the soil from the leaf surface with precipitation.

The formulation of the field-scale version of the GAG model enabled the investigation of NH_3 exchange separately for the urine-affected and unaffected areas, as well as for groups of patches deposited in different time intervals. It was found that the temporal evolution of the total net NH_3 exchange flux over a grazed field was dominated by the NH_3 emission from the urine patches, which was significantly reduced by simultaneous NH_3 deposition to the clean parts of the same field (Section 4.5.3). The results also showed that the temporal evolution of NH_3 emission from urine patches deposited in different time steps could be substantially different (Figure 4.8). Moreover, NH_3 fluxes over the whole field in a given day could be considerably affected by the emission from urine patches deposited several days earlier (Section 4.5.3).

The GAG model, in contrast to the NH_3 volatilization models published earlier for urea affected soils (Sherlock and Goh, 1985, Rachhpal and Nye, 1986), incorporating a canopy compensation point model, accounts for the effect of meteorology on net

canopy exchange of NH_3. A similar type of model was constructed by Laubach et al. (2012). Compared with this model, GAG is capable of simulating the influence of vegetation on NH_3 exchange. In addition, GAG also simulates soil pH, the TAN and the water content of the soil, allowing GAG to predict net NH_3 exchange, instead of operating only in "inverse" mode, calculating soil parameters based on flux measurements.

Rachhpal and Nye (1986) suggested a solution for dynamic modelling of soil pH with a set of continuity equations. However, in their approach the dissociation coefficients, as well as the urea hydrolysis rate were independent of temperature. Although the GAG model accounts for the same chemical reactions, it incorporates a different mathematical description and additionally, accounts for the missing temperature dependencies.

Dynamic simulation of soil pH as described in the GAG model is novel among the NH_3 exchange models on the ecosystem scale. In the PaSim ecosystem model (Riedo et al., 2002) pH is treated as a constant, and the same is true for the VOLT'AIR model (Génermont and Cellier, 1997) developed for simulating NH_3 emission related to fertilizer and manure application. Furthermore, the framework of GAG is simpler and requires less input data than the VOLT'AIR model. Therefore, for grazing situations, it is much easier to adapt GAG on both field and regional scale.

6. 2. 2. Uncertainties in the ammonia fluxes simulated by GAG

In the GAG model, the main uncertainties in the simulation of the NH_3 flux originate from the estimation of the TAN budget, the soil pH, and the water budget. In the following subsections an overview of these uncertainties is provided.

6. 2. 2. 1. TAN budget

The main model uncertainties originating from the simulation of the TAN budget are associated with the thickness of the source layer (Δz), the exclusion of the vertical movement of TAN within the soil, and the N content as well as the chemical composition of the urine.

In the case of Δz, NH_3 exchange was found to be sensitive to this parameter in both the patch-scale and the field-scale experiments (Section 3.4.2 and Section 4.6.2). However, the fact that the modelled NH_3 fluxes were in good agreement with the measurements in three different model simulations using the same value of Δz, suggests that the main governing processes of NH_3 emission from urine patches might occur in this thin top soil layer and that the natural variability of Δz is much possibly within the ±20% changes that were assumed in the sensitivity analysis in this thesis (Table 3.4 and Table 4.4). Nevertheless, future work is needed to confirm this hypothesis, considering how further datasets can help characterize the appropriate thickness of the effective soil emission layer.

Since any downward or upward vertical movement of TAN within the soil was excluded (Section 2.2), the sensitivity of the model to a hypothetical TAN loss and gain within the source layer was examined. TAN could be lost via TAN immobilization, plant uptake or runoff, whilst TAN gain could take place due to capillary rise or mineralization of soil organic matter. It was found that the model is more sensitive to these when TAN production from urea hydrolysis subsided, so that an additional TAN sink or source can become more effective (Section 3.4.2). It was also shown that an extra TAN sink in the NH_3 source layer can strengthen the effect of temperature on NH_3 emission from urine patches whilst a TAN source can weaken it (Chapter 5.3.5).

The ultimate goal of the development of GAG was to construct a modelling tool that could be applied to regional (i.e. national or continental) scale. Thus, simplicity was a key aspect of the model development, avoiding extra steps of model simplification during the up-scaling. For this reason, the exchange of TAN between the soil layers was excluded and a single soil layer was assumed. Although this is a simpler approach compared to some of the models mentioned in Section 6.2.1 (Rachhpal and Nye, 1986, Génermont and Cellier, 1997, Riedo et al., 2002), the model code of GAG enables the addition of new modules in the future, for instance a multi-layer approach for simulating the TAN budget or the water budget in the source layer.

Over the field scale, the sensitivity analysis also showed that the N content of urine is coupled with an extreme uncertainty. However, model simulations with randomized N concentrations implied that this uncertainty might be considerably smaller than it was suggested by the sensitivity analysis (Section 4.6.5).

Regarding the effect of the chemical composition of urine, it was assumed that the urinary N consists entirely of urea. Further constituents that can contribute to NH_3 emission through their decomposition, such as allantoin, creatine and creatinine (Whitehead et al., 1989), were neglected. Since the patch-scale version of GAG was compared with measurements taken over artificial urine patches enriched with urea, the error originating from this assumption might be negligibly small. However, it could be still relevant if the model is applied to a real grazing situation.

Hippuric acid, apart from its decomposition, also affects NH_3 emission through its triggering effect on urea hydrolysis. Whitehead et al. (1989) studied this effect in laboratory experiments, and expressed the detected NH_3 volatilization as the percentage of the total nitrogen content of urine. Based on this, their results showed that the absence of hippuric acid in artificial urine (such as used by Laubach et al., 2012) can lead to up to -10% difference in the cumulative NH_3 volatilization compared to real urine containing the same amount of urinary N. On the other hand, the same study reported that assuming an average N concentration of 8 g l^{-1}, can result in a 10% overestimation in the cumulative volatilization of ammonia if the real nitrogen concentration was as low as 2 g l^{-1}. Furthermore, Whitehead et al. (1989) also suggested that if an average ratio of hippuric acid N is assumed in the total urinary N (ca. 0.8% based on Dijkstra et al., 2013), the overestimation of the cumulative NH_3 emission can be 10% if the proportion of hippuric acid was minimal in reality.

Considering these experimental results by Whitehead et al. (1989), it can be concluded that the possible underestimation of NH_3 emission over the field scale due to the exclusion of the influence of hippuric acid and the further urinary N components, may be partly balanced by the sources of overestimation in the model.

6. 2. 2. 2. Soil pH

In the case of the soil pH, the effect of the soil buffering capacity (β) and the exclusion of CO_2 emission on the simulated NH_3 flux was investigated (Sections 3.4.3 and 4.6.3). In the patch-scale model experiment, β was determined during preliminary simulations (Section 2.8). The sensitivity analysis, carried out for the patch-scale version of GAG, showed that the simulated NH_3 flux is hardly sensitive even to a ±20% change in β (Section 3.4.3). The exact same value of β was used also in the field-scale experiments for both modelling periods, however, in these cases NH_3 exchange was found to be highly sensitive to the same changes in β (Section 4.6.3).

It was shown that the dependence of NH_3 exchange on β is influenced by the soil pH before urine deposition and also by the maximum amount of urine that can be stored in the source layer (Section 4.6.3). According to the results, in the case of higher initial soil pH and higher initial soil water content, the sensitivity of the total net NH_3 exchange to β is stronger. However, the good agreement found on the field scale between the modelled and the observed NH_3 fluxes in both modelling periods, suggests that the natural variability of β might be less than the perturbation applied in the sensitivity analysis. Nevertheless, this requires further experimental investigation.

During the analysis of the patch-scale version of GAG, it was also found that incorporating a simple estimation of CO_2 emission from the source layer allows the model to reproduce the measured soil pH values more accurately than neglecting CO_2 emissions (3.4.3). Future work should therefore consider how CO_2 fluxes could be incorporated more systematically into the GAG model.

Finally, in the case of the patch-scale model, it was shown that the dynamic simulation of soil pH was necessary to represent the first, highest peak in NH_3 emission after the deposition of the urine patch (Section 3.4.3). In addition, over the field scale, strong sensitivity was detected in the NH_3 exchange associated with the value of soil pH before the deposition of the urine patch (Section 4.6.2). However, the results over the field scale implied that with a well-chosen constant soil pH, the simulated NH_3 fluxes could be similar to those derived with the dynamic chemistry approach (Section 4.6.6). This suggests a way for model simplification when it is applied later at a

regional scale. Nevertheless, further considerations are needed to find a generalized approach that determines the applicable value of a constant soil pH.

6. 2. 2. 3. Water budget

The sensitivity analysis for both the patch-scale and field-scale version of the model showed that the highest uncertainties are associated with the water content of soil at field capacity (θ_{fc}) and permanent wilting point (θ_{pwp}) (Sections 3.4.4 and 4.6.4). Over the field scale the response of the NH_3 fluxes was extremely strong to the perturbation of these parameters. This high sensitivity was attributed to the maximum amount of urine that the NH_3 source layer can hold, which depends on θ_{fc} and θ_{pwp}, or if the soil volumetric water content is higher than θ_{pwp} before a urination event, the initial water content of the soil ($\theta(t_0)$). It was found that in the case of a higher initial soil water content (i.e. less urine in the source layer), NH_3 exchange was more sensitive to the changes in θ_{fc} and θ_{pwp}.

The broad agreement between the simulated and measured NH_3 fluxes (Sections 3.3 and 4.5) suggests that the uncertainty of the measurement of θ_{fc} and θ_{pwp} might be less than the perturbations applied in the sensitivity analysis (±10%, ±20%). However, a regional scale model application would require θ_{fc} and θ_{pwp} values over a high-resolution grid, which is likely to be coupled with higher uncertainties. Therefore, at regional scale model application, the uncertainty of the input θ_{fc} and θ_{pwp} datasets has to be assessed when the model results are evaluated.

6. 2. 2. 4. Further remarks

A further, more general, but important conclusion can be drawn from the analysis of the model uncertainties: the sensitivity of the simulated NH_3 flux to the perturbation of a given model constant can depend on the value of another parameter. Therefore, on one hand, when the response of the simulated NH_3 flux is tested to a given parameter in any kind of an NH_3 emission model, it is suggested to investigate how the response of the flux to the tested parameter changes with a modified set of input parameters. On the other hand, the varying response of the NH_3 flux to the governing parameters also suggests that the response of NH_3 exchange to certain environmental characteristics might be different in different circumstances, not just in the model but also in the reality.

6. 3. Effects of meteorology on ammonia exchange over a grazed field

6. 3. 1. General effects of meteorological variables on ammonia exchange

It was found on both the patch and the field scale that the main meteorological variables, governing NH_3 exchange, are temperature (considering soil and air temperature together), wind speed and relative humidity (*RH*) (Sections 5.2.1 and 5.2.2). In the case of *RH* a dual effect was shown due to a) its effect on the modelled soil evaporation and b) the deposition to leaf surfaces, with the latter being the dominant term.

The model did not show high sensitivity to the total amount of precipitation, but it was found that the total NH_3 emission and the temporal development of NH_3 volatilization could be affected by the timing of the rain event (Section 5.2.1). This leads to a more complicated effect on the NH_3 exchange over the field scale, since the urine patches deposited in different time steps are affected by the same rain event in a different stage of NH_3 ammonia volatilization, resulting in various response in the patch emissions.

Whilst in the patch scale simulation global radiation had only a weak effect on NH_3 emission (Section 5.2.1), in the case of the field scale it emerged as a strong influencing variable (Section 5.2.2). The results suggested that in meteorological circumstances that do not favour evapotranspiration global radiation could have a larger effect on NH_3 exchange than in opposite conditions (Section 5.2.3). This is because if the soil evaporation is strongly driven by high air temperature, wind speed or *RH* (favouring soil evaporation), the same changes in global radiation can have only a weaker effect on soil evaporation and consequently, NH_3 emission, than in the case of lower air temperature, wind speed and *RH*.

6. 3. 2. The effect of temperature on ammonia exchange

The in-depth investigation of the temperature-dependence of NH_3 exchange over a grazed field clearly suggested that the temperature response can be affected by precipitation (Section 5.3.1). After rain events, in warmer conditions the stronger evaporation from the soil allows more urine to infiltrate, which can lead to higher NH_3

emission and as a results, higher Q_{10} than in dry conditions, where in both the cooler and warmer conditions the same amount of urine can penetrate to the NH_3 source layer.

Based on this finding, further effects of other meteorological variables on the temperature-response of NH_3 exchange can be anticipated, especially those of wind speed and relative humidity. These variables, similarly to precipitation, can affect the water content of the soil through their influence on soil evaporation. This implies that the sensitivity of NH_3 exchange to temperature might be different in different climatic regions with stronger temperature-response in wetter climatic conditions than in drier ones. In addition, this also means that when the influence of climate change on NH_3 emission is investigated, a more realistic picture can be obtained if the effect of changing temperature is investigated together with the change of the other meteorological variables.

The results also showed that the temperature-response of NH_3 emission is significantly different in the case of the urine patches and the clean field (Section 5.3.2). This difference is a consequence of the different modelling approaches for these two surface types. Whilst under the urine patches the available TAN is limited, over the clean field it was assumed to be infinite. Furthermore, in the case of the urine patches, a dynamic approach was applied to simulate the relevant soil chemical processes, whereas over the clean field the soil chemistry was assumed to be undisturbed (no considerable N input). The consequence of these assumptions was a weak temperature-response over the patches and a strong, exponential response in the case of the clean area.

It was found that in the dynamic soil chemistry approach the exponential increase of the compensation point of the soil pore with increasing temperature – apart from the gradually depleting TAN budget - is moderated by the simultaneous decrease of the emission potential. It was shown that the same equilibrium system of the solution in the soil pore has a lower emission potential at higher temperature. The strength of the process was found to be stronger, when the initial emission potential at the unchanged, original temperature was higher.

This result suggests that the temperature-dependence of the emission potential can be generalized for any NH_3 source, since NH_3 volatilization is governed by the same basic chemical equilibria of NH_3 and NH_4^+. This means that some NH_3 sources probably cannot realistically be represented by a single, constant emission potential even in the absence of a substantial N input (e.g. see the compilation of such constant vales by Massad et al., 2010b). Therefore, the challenge of the future NH_3 emission models is to decide which NH_3 sources require a dynamic chemical approach, and which sources can be modelled assuming permanent chemical conditions, using a constant emission potential.

Finally, a more general conclusion can be drawn for the temperature-dependence of NH_3 exchange over grazed fields. In Section 5.3.3 it was shown that if an NH_3 flux is determined by a temperature dependent and a non-dependent component, the smaller is the non-dependent component, the stronger will be the temperature-response of the given NH_3 flux. The finding for the effect of the TAN loss/gain processes (also mentioned in Section 6.2.2.1) is parallel with this, if these process are considered as "virtual flux components".

In the original GAG model there is no term for TAN loss or gain, therefore the "virtual flux component" here equals to 0. Whereas for TAN loss this "virtual flux component" is negative (smaller non-temperature-dependent component), resulting in a stronger temperature-dependence and for TAN gain it is positive (larger non-temperature-dependent component), leading to a weaker temperature-dependence. Therefore, in general, it can be concluded that in a system stronger temperature-response of NH_3 exchange can be expected if the non-temperature-dependent NH_3 loss processes are stronger (e.g. TAN loss in the soil or recapture of the NH_3 from the soil by the overlaying vegetation).

6. 3. 3. Applicability of Q_{10}

To quantify the temperature-dependence of NH_3 exchange, as a starting point, a metric, Q_{10} was used, which expresses the relative increase of NH_3 emission over a range of 10°C. In a review of existing observations, Sutton et al. (2013) reported a Q_{10}

of 4.7 for fields grazed by sheep. Whilst the Q_{10} values derived from the simulations with GAG (Table 5.6) were considerably smaller for urine patches (Q_{10} = 1.26-1.72), for the whole field the values (Q_{10} = 4.0 and 3.9, respectively) were much closer to the Q_{10} published by Sutton et al. (2013). The reason for the difference in Q_{10} between the patch-scale and the field-scale is that the weak temperature dependence over the urine patches is enhanced by the strong temperature-response over the clean area.

Although the calculation of Q_{10} enables the temperature-dependence of NH_3 exchange from different sources to be compared, it was shown that it can be used only with caution. First of all, because of its definition (relative increase of NH_3 *emission*) it cannot be applied to measured nor modelled datasets, where the total NH_3 exchange summed for a given period is negative, i.e. net deposition occurred. Furthermore, it was showed that the value of Q_{10} is also affected by the length of the investigated period (Section 5.3.6). The value of Q_{10} provides a reliable estimation for the temperature-dependence of NH_3 exchange only after 4-5 days from the beginning of the investigated period. Moreover, it was shown that Q_{10} also depends on the initial value of the 10°C temperature range (Section 5.3.6). Ultimately, these results highlight the need for a universal metric or a set of metrics that is capable of quantifying the temperature-dependence of the different NH_3 sources, independently of the initial temperature or the length of the period.

6. 4. Future work

In the following six topics are outlined for future research with the GAG model.

1) Up-scaling the GAG model for larger scale

The main goal of the development of GAG was to construct an NH_3 emission model from grazing that can be applied for larger scale, such as national or continental scale. Therefore, the next stage of this research will be the up-scaling of the GAG model for larger scale. With such a model application lessons could be learned about how a dynamic approach for NH_3 emission can affect the simulated nitrogen deposition, dispersion and ultimately, the formation of particulate matter (Section 1.2). Since all the input data can be obtained for larger scales, considering the possible errors, GAG

is concluded to be suitable for implementation in an atmospheric chemistry transport model (ACTM).

In the case of such a large scale model application – independently from the target region or the chosen ACTM - two large challenges will have to be considered: a) the optimal level of simplification of the GAG model has to be found so that the coupled model framework is computationally efficient; b) whilst meteorological data is readily available, a gridded dataset, based on a comprehensive review of the existing data sources, would have to be compiled for the field-specific input parameters (especially data for initial soil pH, θ_{fc}, and θ_{pwp}).

2) Investigating the effect of climate change on NH_3 exchange over grazed fields

Since GAG is dynamically driven by meteorology, studies on climate-dependency of NH_3 exchange, based on future climate scenarios could be performed in order to assess how climate change impacts the process of NH_3 exchange. Such model experiment would require a meteorological input dataset for both the present and the future. To this, the available datasets for regional future climate projections will need to be reviewed, e.g., those published in the last IPCC Assessment Report, AR5 (Stocker et al., 2013).

3) Refining the modelling approach of GAG for field scale

The code of GAG enables further modules to be added to the GAG model to simulate certain variables (e.g. TAN budget or water budget) in a more sophisticated way. As such, it would be highly interesting to explore how GAG would benefit from a multilayer soil approach to simulate the vertical movement of water and the diffusion of N compounds in it. A possible option would be for example, to implement the model by Shorten and Pleasants (2007) that is capable of simulating urinary N and water flows in grasslands.

Moreover, the results reported in Section 3.4.3 implied further possible ways to improve the model performance: future research should investigate the options of the implication of a module for dynamic CO_2 emission from the soil, as well as the operational handling of the possible restart of urea hydrolysis within the GAG model.

4) Evaluation of the GAG model with further measurements

In addition to the national/continental scale application, discussed in point 1), among the future plans further field-scale experiments are considered as priorities. Therefore, after examining what further observational datasets are available for grazed fields, the GAG model is planned to be applied to further measurement campaigns. By applying GAG to grazed fields in different climatic regions, further insights could be gained on the relationship between the meteorological variables and the NH_3 exchange over a grazed field.

5) Applying the GAG model for urea based fertilizers

Since the model describes NH_3 emission from a solution of urea, the GAG model can be modified and applied also for fields fertilized with urea. Such a modification could largely widen the applicability of the model, which also means further opportunities for model evaluation and investigation of the meteorological dependencies of NH_3 exchange above agricultural lands.

6) Developing ammonia emission models for further agricultural sources, based on the philosophy of GAG

The GAG model represents an example of a process-based NH_3 exchange model that is capable of simulating the key budgets (TAN, water and H^+) and the key processes regulating them. As argued also by Sutton et al. (2013), in order to get a full picture about how NH_3 exchange is dependent on meteorology, and how it will be modified under climate change, it would be necessary to construct process-based, meteorology-driven models for every agricultural NH_3 source. This could be achieved by using a similar approach to that developed for the GAG model.

Based on the lessons learned from GAG, it is believed that by identifying the TAN, water and H^+ budgets and their key driving processes, the construction of the envisaged set of process-based NH_3 emission models is achievable. Therefore, the ultimate plan for long-term is to construct and support the construction of further NH_3 emission models based on the philosophy of GAG.

6. 5. Summary

As a summary, the main findings of this thesis are presented below in the form of answers for the research questions formulated in Chapter 1.

1. How can an ammonia exchange model be constructed for a urine patch that accounts for the regulating effect of temperature (and other meteorological factors) and changing emission potential of the soil, while being applicable at field scale?

The patch-scale version of the GAG (Generation of Ammonia from Grazing) model, constructed in Chapter 2, simulates NH_3 emission from a urine patch. NH_3 fluxes are modelled by a canopy compensation point model, adjusted for this particular NH_3 source. This canopy compensation point model takes into account the influence of meteorology on NH_3 emission, including temperature. Soil chemistry also regulates NH_3 emission. To capture this effect, a dynamic approach was developed that is able to simulate the variations in the TAN content of the soil and the soil pH. In addition to these features, the water budget is also simulated by GAG. In order to develop a model that is also applicable for the field scale, simplicity and the low number of input parameters and variables was a key aspect of the model development. For this reason, the model operates with a single layer ("NH_3 source layer") approach, and takes into account only basic soil physical and chemical characteristics, such as field capacity, permanent wilting point, porosity and the initial soil pH before urine patch deposition.

It was shown that NH_3 emission from a urine patch can be affected by the simultaneous CO_2 emission from the soil, as well as a possible restart of the urea hydrolysis after a rain event. Since these processes are not well-documented enough in the literature for a general model application, they were not included into the field-scale version of GAG.

2. How can such a urine patch model be applied to the scale of a grazed field, so that it still accounts for the main emission drivers, while being applicable for the regional scale (i.e. in ACTMs)?

Over a grazed field NH_3 exchange is affected by the NH_3 emission from the urine patches and the NH_3 exchange with the area of the field that is not affected by urine ("clean area"). To simulate NH_3 fluxes over the whole field, the GAG model was applied to every urine patch deposited on the field, and a modified version of GAG was employed over the clean area. The model, constructed in this way, enabled the investigation of NH_3 exchange separately for the urine affected and the unaffected area as well as for the groups of patches deposited in the different time steps.

The model was designed so that all its inputs could also be obtained when moving to larger scale. However, when the regional scale application of the GAG model is evaluated, the possible errors have to be considered. Urination frequency and constant N content was found to be associated with a large uncertainty in the modelled NH_3 fluxes. Nevertheless, the results suggested that with average, constant values of these parameters NH_3 exchange could be represented reasonably well.

A large uncertainty was found to be associated also with field capacity, permanent wilting point and the initial soil pH. Although these parameters might be measured with a high accuracy over a field, a gridded dataset required for a regional scale model application, can be associated with a high level of uncertainty. Therefore, to assess the model results of a regional scale application, the accuracy of the applied input datasets has to be identified. For a computationally efficient regional scale model application the options of possible model simplifications have to be also investigated. It was found that one these simplifications could be the usage of a constant soil pH instead of its dynamic simulation.

3. How do the different meteorological variables (e.g. temperature, wind, relative humidity, precipitation… etc.) affect ammonia exchange over a grazed field?

The main meteorological variables, governing NH_3 exchange are temperature (considering soil and air temperature together), wind speed and relative humidity. In the case of relative humidity a dual effect was observed: through its effect a) on the modelled soil evaporation, and b) the deposition to leaf surfaces, with the latter being

the dominant term. The model did not show high sensitivity to the amount of precipitation. However, it was found that the total NH_3 emission and the temporal development of NH_3 volatilization from a urine patch can be affected by the timing of the rain event, increasing the soil resistance after the rain event and as a result, supressing NH_3 emission from the source layer.

The results also suggested that the temperature-dependence of NH_3 exchange over a grazed field is stronger if precipitation occurs. This is because after the rain event temperature also affects soil evaporation, allowing more urine to infiltrate to the source layer, and consequently, more NH_3 to be emitted at higher temperature. Furthermore, in general, it was concluded that the temperature-dependence of NH_3 emission is stronger if the NH_3 sinks are stronger, such as, the recapture of NH_3 volatilized from the soil on the surface of the overlaying vegetation, or the TAN loss processes in the soil (e.g. runoff, immobilization, or plant uptake).

Finally, it was found that the Q_{10} metric, expressing the relative increase of NH_3 emission over a range of 10°C, should be used only with caution for situations with bi-directional exchange. The model results indicated that the value of Q_{10} can be affected by the length of the investigated period, and it can provide a reliable estimation for the temperature-dependence of NH_3 exchange only after 4-5 days after the beginning of the investigated period. Moreover, it was shown that the initial value of the 10°C temperature range can also influence the value of Q_{10}. These findings highlight that it is necessary to find a universal metric or a set of metrics that can be used to quantify the temperature-dependence of NH_3 exchange, independently of the initial temperature or the length of the period.

References

Allen, R. G., Pereira, L. S., Raes, D. and Smith, M.: Crop evapotranspiration-Guidelines for computing crop water requirements, FAO Irrigation and drainage paper 56, FAO, Rome, Italy, 1998.

Asman, W. A. H., Sutton, M. A. and Schjoerring, J. K.: Ammonia: emission, atmospheric transport and deposition, New Phytologist, 139**,** 27-48, 1998.

Bash, J. O., Cooter, E. J., Dennis, R. L., Walker, J. T. and Pleim, J. E.: Evaluation of a regional air-quality model with bi-directional NH_3 exchange coupled to an agro-ecosystem model, Biogeosciences Discuss., 9**,** 11375-11401, 2012.

Bates, R. G. and Pinching, G. D.: Acidic dissociation constant of ammonium ion at 0-degrees-C to 50-degrees-C, and the base strength of ammonia, Journal of Research of the National Bureau of Standards, 42**,** 419-430, 1949.

Betteridge, K., Andrewes, W. G. K. and Sedcole, J. R.: Intake and excretion of nitrogen, potassium and phosporus by grazing steers, The Journal of Agricultural Science, 106**,** 393-404, 1986.

Betteridge, K., Hoogendoorn, C., Costall, D., Carter, M. and Griffiths, W.: Sensors for detecting and logging spatial distribution of urine patches of grazing female sheep and cattle, Computers and Electronics in Agriculture, 73**,** 66-73, 2010.

Bobbink, R., Hicks, K., Galloway, J., Spranger, T., Alkemade, R., Ashmore, M., Bustamante, M., Cinderby, S., Davidson, E., Dentener, F., Emmett, B., Erisman, J. W., Fenn, M., Gilliam, F., Nordin, A., Pardo, L. and De Vries, W.: Global assessment of nitrogen deposition effects on terrestrial plant diversity: a synthesis, Ecological Applications, 20**,** 30-59, 2010.

Burkhardt, J., Kaiser, H., Goldbach, H. and Kappen, L.: Measurements of electrical leaf surface conductance reveal re-condensation of transpired water vapour on leaf surfaces, Plant, Cell and Environment, 22**,** 189-196, 1999.

Burkhardt, J., Flechard, C. R., Gresens, F., Mattsson, M., Jongejan, P. A. C., Erisman, J. W., Weidinger, T., Meszaros, R., Nemitz, E. and Sutton, M. A.: Modelling the dynamic chemical interactions of atmospheric ammonia with leaf surface wetness in a managed grassland canopy, Biogeosciences, 6**,** 67-84, 2009.

Butterbach-Bahl, K., Nemitz, E., Zaehle, S., Billen, G., Boeckx, P., Erisman, J. W., Garnier, J., Upstill-Goddard, R., Kreuzer, M., Oenema, O., Reis, S., Schaap, M., Simpson, D., Vries, W. d., Winiwarter, W. and Sutton, M. A.: Nitrogen as a threat to the European greenhouse balance, in*:* The European Nitrogen Assessment: Sources, Effects and Policy Perspectives, Sutton, M. A., Howard, C. M., Erisman, J. W., Billen, G., Bleeker, A., Grennfelt, P., van Grinsven, H. and Grizzetti, B. (Eds.), Cambridge University Press, Cambridge**,** 434-462, 2011.

Cape, J. N., Eerden, L. J. v. d., Sheppard, L. J., Leith, I. D. and Sutton, M. A.: Reassessment of critical levels for atmospheric ammonia, in*:* Atmospheric Ammonia: Detecting emission changes and environmental impacts. Results of an Expert Workshop under the Convention on Long-range Transboundary Air Pollution, Sutton, M. A., Reis, S. and Baker, S. M. H. (Eds.), Springer**,** 15-40, 2009.

Cooter, E. J., Bash, J. O., Walker, J. T., Jones, M. R. and Robarge, W.: Estimation of NH_3 bi-directional flux from managed agricultural soils, Atmospheric Environment 44**,** 2107-2115, 2010.

Cooter, E. J., Bash, J. O., Benson, V. and Ran, L.: Linking agricultural crop management and air quality models for regional to national-scale nitrogen assessments, Biogeosciences, 9**,** 4023-4035, 2012.

Cowling, E. B., Erisman, J. W., Smeulders, S. M., Holman, S. C. and Nicholson, B. M.: Optimizing air quality management in Europe and North America: Justification for integrated management of both oxidized and reduced forms of nitrogen, Environmental Pollution, 102**,** 599-608, 1998.

Dasgupta, P. K. and Dong, S.: Solubility of ammonia in liquid water and generation of trace levels of standard gaseous ammonia, Atmospheric Environment, 20**,** 565-570, 1986.

David, M., Loubet, B., Cellier, P., Mattsson, M., Schjoerring, J. K., Nemitz, E., Roche, R., Riedo, M. and Sutton, M. A.: Ammonia sources and sinks in an intensively managed grassland canopy, Biogeosciences, 6**,** 1903-1915, 2009.

DEFRA: Emissions of air pollutants in the UK, 1970 to 2014, available: https://www.gov.uk/government/uploads/system/uploads/attachment_data/file/486085/Emissions_of_air_pollutants_statistical_release_2015_-_Final__2_.pdf, last access: 18 February 2016, 2015.

Dennis, S. J., Moir, J. L., Cameron, K. C., Edwards, G. R. and Di, H. J.: Measuring excreta patch distribution in grazed pasture through low-cost image analysis, Grass and Forage Science, 68**,** 378-385, 2013.

Dentener, F. and Crutzen, P.: A three-dimensional model of the global ammonia cycle, Journal of Atmospheric Chemistry, 19**,** 331-369, 1994.

Dijkstra, J., Oenema, O., van Groenigen, J. W., Spek, J. W., van Vuuren, A. M. and Bannink, A.: Diet effects on urine composition of cattle and N2O emissions, animal, 7**,** 292-302, 2013.

Doak, B. W.: Some chemical changes in the nitrogenous constituents of urine when voided on pasture, The Journal of Agricultural Science, 42**,** 162-171, 1952.

EC: Eurostat Satistics Explained. Agri-environmental indicator - livestock patterns, available: http://ec.europa.eu/eurostat/statistics-explained/index.php/Agri-environmental_indicator_-_livestock_patterns, last access: 04. 11. 2015, 2015.

EDGAR: Emissions Database for Global Atmospheric Research v4.2, available: http://edgar.jrc.ec.europa.eu/, last access: 20 May 2014, 2011.

Emberson, L., Simpson, D., Tuovinen, J.-P., Ashmore, M. and Cambridge, H.: Towards a model of ozone deposition and stomatal uptake over Europe, EMEP MSC-W Note 6/2000, The Norwegian Meteorological Institute, Oslo, Norway, 2000.

Erisman, J. W., Sutton, M. A., Galloway, J., Klimont, Z. and Winiwarter, W.: How a century of ammonia synthesis changed the world, Nature Geosci, 1**,** 636-639, 2008.

Farquhar, G. D., Firth, P. M., Wetselaar, R. and Weir, B.: On the Gaseous Exchange of Ammonia between Leaves and the Environment: Determination of the Ammonia Compensation Point, Plant Physiology, 66**,** 710-714, 1980.

Flechard, C. R. and Fowler, D.: Effects of Changing Temperature on Leaf Surface Water-Film Chemistry and Trace Gas Exchange Processes over Terrestrial Vegetation, in: The Impact of Climate Change on Air Quality, The 4th ACCENT Barnsdale Expert Workshop, Builtjes, P., Fowler, D., Feichter, J., Lewis, A., Monks, P. and Borrell, P. (Eds.), ACCENT Secretariat, Urbino, Italy, 155–161, 2008.

Flechard, C. R., Fowler, D., Sutton, M. A. and Cape, J. N.: A dynamic chemical model of bi-directional ammonia exchange between semi-natural vegetation and the atmosphere, Quarterly Journal of the Royal Meteorological Society, 125**,** 2611-2641, 1999.

Flechard, C. R., Massad, R. S., Loubet, B., Personne, E., Simpson, D., Bash, J. O., Cooter, E. J., Nemitz, E. and Sutton, M. A.: Advances in understanding, models and parameterizations of biosphere-atmosphere ammonia exchange, Biogeosciences, 10**,** 5183-5225, 2013.

Foley, K. M., Roselle, S. J., Appel, K. W., Bhave, P. V., Pleim, J. E., Otte, T. L., Mathur, R., Sarwar, G., Young, J. O., Gilliam, R. C., Nolte, C. G., Kelly, J. T., Gilliland, A. B. and Bash, J. O.: Incremental testing of the Community Multiscale Air Quality (CMAQ) modeling system version 4.7, Geosci. Model Dev., 3**,** 205-226, 2010.

Galloway, J. N., Aber, J. D., Erisman, J. W., Seitzinger, S. P., Howarth, R. W., Cowling, E. B. and Cosby, B. J.: The Nitrogen Cascade, Bioscience, 53**,** 341-356, 2003.

Galloway, J. N., Townsend, A. R., Erisman, J. W., Bekunda, M., Cai, Z., Freney, J. R., Martinelli, L. A., Seitzinger, S. P. and Sutton, M. A.: Transformation of the Nitrogen Cycle: Recent Trends, Questions, and Potential Solutions, Science, 320**,** 889-892, 2008.

Garland, J. A.: The Dry Deposition of Sulphur Dioxide to Land and Water Surfaces, Proceedings of the Royal Society of London A: Mathematical, Physical and Engineering Sciences, 354**,** 245-268, 1977.

Génermont, S. and Cellier, P.: A mechanistic model for estimating ammonia volatilization from slurry applied to bare soil, Agricultural and Forest Meteorology 88**,** 145-167, 1997.

Gilliland, A. B., Wyat Appel, K., Pinder, R. W. and Dennis, R. L.: Seasonal NH_3 emissions for the continental united states: Inverse model estimation and evaluation, Atmospheric Environment 40**,** 4986-4998, 2006.

Grant, R. F. and Pattey, E.: Temperature sensitivity of N2O emissions from fertilized agricultural soils: Mathematical modeling in ecosys, Global Biogeochemical Cycles, 22**,** n/a-n/a, 2008.

Gritsch, C., Zimmermann, M. and Zechmeister-Boltenstern, S.: Interdependencies between temperature and moisture sensitivities of CO2 emissions in European land ecosystems, Biogeosciences, 12**,** 5981-5993, 2015.

Hamaoui-Laguel, L., Meleux, F., Beekmann, M., Bessagnet, B., Génermont, S., Cellier, P. and Létinois, L.: Improving ammonia emissions in air quality modelling for France, Atmospheric Environment, 2012.

Harned, H. S. and Scholes, S. R.: The Ionization Constant of HCO3- from 0 to 50°, Journal of American Chemical Society, 63, 1706-1709, 1941.

Harned, H. S. and Davis, R.: The Ionization Constant of Carbonic Acid in Water and the Solubility of Carbon Dioxide in Water and Aqueous Salt Solutions from 0 to 50°, Journal of American Chemical Society, 65, 2030-2037, 1943.

Hellsten, S., Dragosits, U., Place, C. J., Misselbrook, T. H., Tang, Y. S. and Sutton, M. A.: Modelling Seasonal Dynamics from Temporal Variation in Agricultural Practices in the UK Ammonia Emission Inventory, Water, Air, and Soil Pollution: Focus, 7**,** 3-13, 2007.

Hellsten, S., Dragosits, U., Place, C. J., Vieno, M., Dore, A. J., Misselbrook, T. H., Tang, Y. S. and Sutton, M. A.: Modelling the spatial distribution of ammonia emissions in the UK, Environmental Pollution, 154**,** 370-379, 2008.

Hicks, B. B., Baldocchi, D. D., Meyers, T. P., Hosker, R. P., Jr. and Matt, D. R.: A preliminary multiple resistance routine for deriving dry deposition velocities from measured quantities, Water, Air, and Soil Pollution, 36**,** 311-330, 1987.

Hoogendoorn, C. J., Betteridge, K., Costall, D. A. and Ledgard, S. F.: Nitrogen concentration in the urine of cattle, sheep and deer grazing a common

ryegrass/cocksfoot/white clover pasture, New Zealand Journal of Agricultural Research, 53**,** 235-243, 2010.

Horváth, L., Asztalos, M., Führer, E., Mészáros, R. and Weidinger, T.: Measurement of ammonia exchange over grassland in the Hungarian Great Plain, Agricultural and Forest Meteorology 130**,** 282-298, 2005.

Itier, B. and Perrier, A.: Presentation dune etude analytique de I'advection: I. Advection like aux variations horizontales de concentration et de temp6rature., Annales Agronomiques, 27**,** 11 l- 140, 1976.

Kielland, J.: Individual Activity Coefficients of Ions in Aqueous Solutions, Journal of the American Chemical Society 59**,** 1675-1678, 1937.

Laubach, J., Taghizadeh-Toosi, A., Sherlock, R. R. and Kelliher, F. M.: Measuring and modelling ammonia emissions from a regular pattern of cattle urine patches, Agricultural and Forest Meteorology 156**,** 1-17, 2012.

Laubach, J., Taghizadeh-Toosi, A., Gibbs, S. J., Sherlock, R. R., Kelliher, F. M. and Grover, S. P. P.: Ammonia emissions from cattle urine and dung excreted on pasture, Biogeosciences, 10**,** 327-338, 2013.

Leuning, R., Freney, J. R., Denmead, O. T. and Simpson, J. R.: A sampler for measuring atmospheric ammonia flux, Atmospheric Environment, 19**,** 1117-1124, 1985.

Li, F. Y., Betteridge, K., Cichota, R., Hoogendoorn, C. J. and Jolly, B. H.: Effects of nitrogen load variation in animal urination events on nitrogen leaching from grazed pasture, Agriculture, Ecosystems and Environment, 159**,** 81-89, 2012.

Lin, X., Wang, S., Ma, X., Xu, G., Luo, C., Li, Y., Jiang, G. and Xie, Z.: Fluxes of CO_2, CH_4, and N_2O in an alpine meadow affected by yak excreta on the Qinghai-Tibetan plateau during summer grazing periods, Soil Biology and Biochemistry 41**,** 718-725, 2009.

Ma, X., Wang, S., Wang, Y., Jiang, G. and Nyren, P.: Short-term effects of sheep excrement on carbon dioxide, nitrous oxide and methane fluxes in typical grassland of Inner Mongolia, New Zealand Journal of Agricultural Research 49**,** 285-297, 2006.

Massad, R. S., Loubet, B., Tuzet, A. and Cellier, P.: Relationship between ammonia stomatal compensation point and nitrogen metabolism in arable crops: Current status of knowledge and potential modelling approaches, Environmental Pollution 154**,** 390-403, 2008.

Massad, R.-S., Tuzet, A., Loubet, B., Perrier, A. and Cellier, P.: Model of stomatal ammonia compensation point (STAMP) in relation to the plant nitrogen and carbon metabolisms and environmental conditions, Ecological Modelling, 221**,** 479-494, 2010a.

Massad, R. S., Nemitz, E. and Sutton, M. A.: Review and parameterisation of bi-directional ammonia exchange between vegetation and the atmosphere, Atmospheric Chemistry and Physics, 10**,** 10359-10386, 2010b.

Mattsson, M., Herrmann, B., David, M., Loubet, B., Riedo, M., Theobald, M. R., Sutton, M. A., Bruhn, D., Neftel, A. and Schjoerring, J. K.: Temporal variability in bioassays of the stomatal ammonia compensation point in relation to plant and soil nitrogen parameters in intensively managed grassland, Biogeosciences, 6**,** 171-179, 2009.

Milford, C., Theobald, M. R., Nemitz, E. and Sutton, M. A.: Dynamics of Ammonia Exchange in Response to Cutting and Fertilising in an Intensively-Managed Grassland, Water, Air and Soil Pollution: Focus, 1**,** 167-176, 2001.

Millington, R. J. and Quirk, J. P.: Permeability of porous solids, Transactions of the Faraday Society, 57**,** 1200-1207, 1961.

Misselbrook, T. H., Van Der Weerden, T. J., Pain, B. F., Jarvis, S. C., Chambers, B. J., Smith, K. A., Phillips, V. R. and Demmers, T. G. M.: Ammonia emission factors for UK agriculture, Atmospheric Environment 34**,** 871-880, 2000.

Misselbrook, T. H., Gilhespy, S. L., Cardenas, L. M., Chambers, B. J., Williams, J. and Dragosits, U.: Inventory of Ammonia Emissions from UK Agriculture 2012, DEFRA, NAEI, 2013.

Moir, J. L., Cameron, K. C., Di, H. J. and Fertsak, U.: The spatial coverage of dairy cattle urine patches in an intensively grazed pasture system, The Journal of Agricultural Science, 149**,** 473-485, 2011.

Móring, A., Vieno, M., Doherty, R. M., Laubach, J., Taghizadeh-Toosi, A. and Sutton, M. A.: A process-based model for ammonia emission from urine patches, GAG (Generation of Ammonia from Grazing): description and sensitivity analysis, Biogeosciences, 13**,** 1837-1861, 2016.

Móring, A., Vieno, M., Doherty, R. M., Milford, C., Nemitz, E., Twigg, M. M. and Sutton, M. A.: Process-based modelling of NH_3 exchange over a grazed field, in: Proceeding of the 7th International Nitrogen Initiative Conference, Melbourne, Australia, 04-08 December 2016, in review.

Nemitz, E., Sutton, M. A., Schjoerring, J. K., Husted, S. and Paul Wyers, G.: Resistance modelling of ammonia exchange over oilseed rape, Agricultural and Forest Meteorology, 105**,** 405-425, 2000.

Nemitz, E., Milford, C. and Sutton, M. A.: A two-layer canopy compensation point model for describing bi-directional biosphere-atmosphere exchange of ammonia, Quarterly Journal of the Royal Meteorological Society, 127**,** 815-833, 2001.

NIWA: The National Climate Database, available: http://cliflo.niwa.co.nz/, last access: 2 December 2013, 2015.

Owen, P. R. and Thomson, W. R.: Heat transfer across rough surfaces, Journal of Fluid Mechanics 15**,** pp 321-33, 1963.

Pakrou, N. and Dillon, P. J.: Leaching losses of N under grazed irrigated and non-irrigated pastures, The Journal of Agricultural Science, 142**,** 503-516, 2004.

Paulson, C. A.: The Mathematical Representation of Wind Speed and Temperature Profiles in the Unstable Atmospheric Surface Layer, Journal of Applied Meteorology, 9, 857-861, 1970

Personne, E., Loubet, B., Herrmann, B., Mattsson, M., Schjoerring, J. K., Nemitz, E., Sutton, M. A. and Cellier, P.: SURFATM-NH3: a model combining the surface energy balance and bi-directional exchanges of ammonia applied at the field scale, Biogeosciences, 6**,** 1371-1388, 2009.

Petersen, R. G., Lucas, H. L. and Woodhouse, W. W.: The Distribution of Excreta by Freely Grazing Cattle and Its Effect on Pasture Fertility: I. Excretal Distribution, Agronomy Journal, 48**,** 440-444, 1956.

Petersen, S. O., Sommer, S. G., Aaes, O. and Søegaard, K.: Ammonia losses from urine and dung of grazing cattle: effect of N intake, Atmospheric Environment 32**,** 295-300, 1998.

Pleasants, A. B., Shorten, P. R. and Wake, G. C.: The distribution of urine deposited on a pasture from grazing animals, The Journal of Agricultural Science, 145**,** 81-86, 2007.

R Core Team: R: A language and environment for statistical computing, R Foundation for Statistical Computing, Vienna, Austria, 2012.

Rabalais, N. N.: Nitrogen in Aquatic Ecosystems, AMBIO: A Journal of the Human Environment 31**,** 102-112, 2002.

Rachhpal, S. and Nye, P. H.: A model of ammonia volatilization from applied urea. I. Development of the model, Journal of Soil Science, 37**,** 9-20, 1986.

Riddick, S. N.: Global ammonia emissions from seabird colonies, Ph.D. thesis, Kings College, London, UK, 2012.

Riedo, M., Milford, C., Schmid, M. and Sutton, M. A.: Coupling soil–plant–atmosphere exchange of ammonia with ecosystem functioning in grasslands, Ecological Modelling, 158**,** 83-110, 2002.

Romera, A., Levy, G., Beukes, P., Clark, D. and Glassey, C.: A urine patch framework to simulate nitrogen leaching on New Zealand dairy farms, Nutrient Cycling in Agroecosystems 92**,** 329-346, 2012.

Schaap, M., Timmermans, R. M. A., Michiel Roemer, Boersen, G. A. C. and Builtjes, P. J. H.: The LOTOS–EUROS model: description, validation and latest developments, International Journal of Environment and Pollution, 32**,** 270-290, 2008.

Schuepp, P.: Turbulent transfer at the ground: On verification of a simple predictive model, Boundary-Layer Meteorology 12**,** 171-186, 1977.

Seinfeld, J. H. and Pandis, S. N.: Atmospheric Chemistry and Physics: From Air Pollution to Climate Change, John Wiley and Sons, New York, USA, 2006.

Sherlock, R. R. and Goh, K. M.: Dynamics of ammonia volatilization from simulated urine patches and aqueous urea applied to pasture I. Field experiments, Fertilizer Research, 5, 181-195, 1984.

Sherlock, R. R. and Goh, K. M.: Dynamics of ammonia volatilization from simulated urine patches and aqueous urea applied to pasture. II. Theoretical derivation of a simplified model, Fertilizer Research, 6**,** 3-22, 1985.

Shorten, P. R. and Pleasants, A. B.: A stochastic model of urinary nitrogen and water flow in grassland soil in New Zealand, Agriculture, Ecosystems and Environment, 120**,** 145-152, 2007.

Simpson, D., Benedictow, A., Berge, H., Bergström, R., Emberson, L. D., Fagerli, H., Flechard, C. R., Hayman, G. D., Gauss, M., Jonson, J. E., Jenkin, M. E., Nyíri, A., Richter, C., Semeena, V. S., Tsyro, S., Tuovinen, J. P., Valdebenito, Á. and Wind, P.: The EMEP MSC-W chemical transport model; technical description, Atmospheric Chemistry and Physics, 12**,** 7825-7865, 2012.

Skjøth, C. A., Geels, C., Berge, H., Gyldenkærne, S., Fagerli, H., Ellermann, T., Frohn, L. M., Christensen, J., Hansen, K. M., Hansen, K. and Hertel, O.: Spatial and temporal variations in ammonia emissions – a freely accessible model code for Europe, Atmospheric Chemistry and Physics, 11**,** 5221-5236, 2011.

Sorteberg, A. and Hov, Ø.: Two parametrizations of the dry deposition exchange for SO_2 and NH_3 in a numerical model, Atmospheric Environment 30**,** 1823-1840, 1996.

Spiller, L. L.: Determination of Ammonia/Air Diffusion Coefficient Using Nafion Lined Tube, Analytical Letters 22**,** 2561-2573, 1989.

Stocker, T. F., Qin D., Plattner, G.-K., Tignor, M., Allen, S. K., Boschung, J., Nauels, A., Xia, Y., Bex, V. and Midgley, P. M.: Climate Change 2013: The Physical Science Basis. Contribution of Working Group I to the Fifth Assessment Report of the Intergovernmental Panel on Climate Change, IPCC, Cambridge University Press, Cambridge, United Kingdom and New York, NY, USA, 2013.

Sutton, M. A. and Fowler, D.: A model for inferring bi-directional fluxes of ammonia over plant canopies, in*:* WMO Conference on the Measurement and Modeling of Atmospheric Composition Changes including Pollution Transport. WMO/GAW-91, WMO, Geneva**,** 179-182, 1993.

Sutton, M. A., Schjorring, J. K. and Wyers, G. P.: Plant-Atmosphere Exchange of Ammonia Philosophical Transactions of the Royal Society A-Mathematical Physical and Engineering Sciences, 351**,** 261-276, 1995.

Sutton, M. A., Burkhardt, J. K., Guerin, D., Nemitz, E. and Fowler, D.: Development of resistance models to describe measurements of bi-directional ammonia surface–atmosphere exchange, Atmospheric Environment, 32**,** 473-480, 1998.

Sutton, M. A., Tang, Y. S., Dragosits, U., Fournier, N., Dore, A. J., Smith, R. I., Weston, K. J. and Fowler, D.: A Spatial Analysis of Atmospheric Ammonia and Ammonium in the U.K., The Scientific World JOURNAL, 1**,** 275-286, 2001.

Sutton, M. A., Nemitz, E., Theobald, M. R., Milford, C., Dorsey, J. R., Gallagher, M. W., Hensen, A., Jongejan, P. A. C., Erisman, J. W., Mattsson, M., Schjoerring, J. K., Cellier, P., Loubet, B., Roche, R., Neftel, A., Hermann, B., Jones, S. K., Lehman, B. E., Horvath, L., Weidinger, T., Rajkai, K., Burkhardt, J., Löpmeier, F. J. and Daemmgen, U.: Dynamics of ammonia exchange with cut grassland: strategy and implementation of the GRAMINAE Integrated Experiment, Biogeosciences, 6**,** 309-331, 2009.

Sutton, M. A., Howard, C. M., Erisman, J. W., Billen, G., Bleeker, A., Bouwman, A. F., Grennfelt, P., van Grinsven, H. and Grizzetti, B.: Assessing our nitrogen inheritance, in*:* The European Nitrogen Assessment: Sources, Effects and Policy Perspectives, Sutton, M. A., Howard, C. M., Erisman, J. W., Billen, G., Bleeker, A., Grennfelt, P., van Grinsven, H. and Grizzetti, B. (Eds.), Cambridge University Press, Cambridge, UK**,** 1-6, 2011.

Sutton, M. A., Reis, S., Riddick, S. N., Dragosits, U., Nemitz, E., Theobald, M. R., Tang, Y. S., Braban, C. F., Vieno, M., Dore, A. J., Mitchell, R. F., Wanless, S., Daunt, F., Fowler, D., Blackall, T. D., Milford, C., Flechard, C. R., Loubet, B., Massad, R., Cellier, P., Personne, E., Coheur, P. F., Clarisse, L., Van Damme, M., Ngadi, Y., Clerbaux, C., Skjøth, C. A., Geels, C., Hertel, O., Wichink Kruit, R. J., Pinder, R. W., Bash, J. O., Walker, J. T., Simpson, D., Horváth, L., Misselbrook, T. H., Bleeker, A., Dentener, F. and de Vries, W.: Towards a climate-dependent paradigm of ammonia emission and deposition, Philosophical Transactions of the Royal Society B: Biological Sciences, 368, 2013.

Tetens, O.: Über einige meteorologische Begriffe, Zeitschrift für Geophysik, 6**,** 297-309, 1930.

van Breemen, N., Burrough, P. A., Velthorst, E. J., van Dobben, H. F., de Wit, T., Ridder, T. B. and Reijnders, H. F. R.: Soil acidification from atmospheric ammonium sulphate in forest canopy throughfall, Nature, 299**,** 548-550, 1982.

Walter, I., Allen, R., Elliott, R., Jensen, M., Itenfisu, D., Mecham, B., Howell, T., Snyder, R., Brown, P., Echings, S., Spofford, T., Hattendorf, M., Cuenca, R., Wright, J. and Martin, D.: ASCE's Standardized Reference Evapotranspiration Equation, in*:* Watershed Management and Operations Management 2000, American Society of Civil Engineers**,** 1-11, 2001.

Wang, X., Huang, D., Zhang, Y., Chen, W., Wang, C., Yang, X. and Luo, W.: Dynamic changes of CH_4 and CO_2 emission from grazing sheep urine and dung patches in typical steppe, Atmospheric Environment 79**,** 576-581, 2013.

Webb, E. K.: Profile relationships: The log-linear range, and extension to strong stability, Quarterly Journal of the Royal Meteorological Society, 96, 67-90, 1970.

Whitehead, D. C., Lockyer, D. R. and Raistrick, N.: Volatilization of ammonia from urea applied to soil: Influence of hippuric acid and other constituents of livestock urine, Soil Biology and Biochemistry, 21**,** 803-808, 1989.

Whitehead, D. C.: Grassland Nitrogen, CAB International, Wallingford, United Kingdom, 1995.

Wichink Kruit, R. J., Schaap, M., Sauter, F. J., van Zanten, M. C. and van Pul, W. A. J.: Modeling the distribution of ammonia across Europe including bi-directional surface–atmosphere exchange, Biogeosciences, 9**,** 5261-5277, 2012.

Wilhelm, E., Battino, R. and Wilcock, R. J.: Low-pressure solubility of gases in liquid water, Chemical Reviews, 77, 219-262, 1977.

Williams, P. H. and Haynes, R. J.: Comparison of initial wetting pattern, nutrient concentrations in soil solution and the fate of ^{15}N-labelled urine in sheep and cattle urine patch areas of pasture soil, Plant and Soil, 162**,** 49-59, 1994.

Wolfe, A. H. and Patz, J. A.: Reactive Nitrogen and Human Health:Acute and Long-term Implications, AMBIO: A Journal of the Human Environment 31**,** 120-125, 2002.

Wu, Y., Walker, J., Schwede, D., Peterslidard, C., Dennis, R. and Robarge, W.: A new model of bi-directional ammonia exchange between the atmosphere and biosphere: Ammonia stomatal compensation point, Agricultural and Forest Meteorology, 149**,** 263-280, 2009.

Wyers, G. P., Otjes, R. P. and Slanina, J.: A continuous-flow denuder for the measurement of ambient concentrations and surface-exchange fluxes of ammonia, Atmospheric Environment. Part A. General Topics, 27**,** 2085-2090, 1993.

Appendix

Related publication

Móring, A., Vieno, M., Doherty, R. M., Laubach, J., Taghizadeh-Toosi, A. and Sutton, M. A.: A process-based model for ammonia emission from urine patches, GAG (Generation of Ammonia from Grazing): description and sensitivity analysis, Biogeosciences, 13**,** 1837-1861, 2016.

Biogeosciences, 13, 1837–1861, 2016
www.biogeosciences.net/13/1837/2016/
doi:10.5194/bg-13-1837-2016

Biogeosciences Open Access EGU

A process-based model for ammonia emission from urine patches, GAG (Generation of Ammonia from Grazing): description and sensitivity analysis

Andrea Móring[1,2,3], Massimo Vieno[2], Ruth M. Doherty[1], Johannes Laubach[4], Arezoo Taghizadeh-Toosi[5], and Mark A. Sutton[2]

[1]School of GeoSciences, University of Edinburgh, Crew Building, Alexander Crum Brown Road, Edinburgh, EH9 3FF, UK
[2]NERC, Centre for Ecology & Hydrology, Edinburgh, Bush Estate, Midlothian, Penicuik, EH26 0QB, UK
[3]Hungarian Meteorological Service, Kitaibel P. u. 1, 1024 Budapest, Hungary
[4]Landcare Research, P.O. Box 69040, Lincoln 7640, New Zealand
[5]Department of Agroecology, Aarhus University, Blichers Allé 20, 8830 Tjele, Denmark

Correspondence to: Andrea Móring (a.moring@sms.ed.ac.uk)

Received: 29 May 2015 – Published in Biogeosciences Discuss.: 8 July 2015
Revised: 18 January 2016 – Accepted: 14 February 2016 – Published: 29 March 2016

Abstract. In this paper a new process-based, weather-driven model for ammonia (NH_3) emission from a urine patch has been developed and its sensitivity to various factors assessed. The GAG model (Generation of Ammonia from Grazing) is capable of simulating the TAN (total ammoniacal nitrogen) and the water content of the soil under a urine patch and also soil pH dynamics. The model tests suggest that ammonia volatilization from a urine patch can be affected by the possible restart of urea hydrolysis after a rain event as well as CO_2 emission from the soil. The vital role of temperature in NH_3 exchange is supported by our model results; however, the GAG model provides only a modest overall temperature dependence in total NH_3 emission compared with the literature. This, according to our findings, can be explained by the higher sensitivity to temperature close to urine application than in the later stages and may depend on interactions with other nitrogen cycling processes. In addition, we found that wind speed and relative humidity are also significant influencing factors. Considering that all the input parameters can be obtained for larger scales, GAG is potentially suitable for field and regional scale application, serving as a tool for further investigation of the effects of climate change on ammonia emissions and deposition.

1 Introduction

The consequences of strong emission of reactive nitrogen compounds (N_r), dominated by the emission of ammonia (NH_3), are widely discussed: threatening air, water and soil quality, it endangers also ecosystems as well as human health in many ways (Sutton et al., 2011; Galloway et al., 2008; Fowler et al., 2013). Globally 70 % of NH_3 released to atmosphere originates from agricultural sources, such as livestock housing, manure management, and fertilizer spreading on fields (EDGAR, 2011). According to the latest available report of the UK government agency DEFRA (Department for Environment, Food and Rural Affairs), in the UK grazing accounts for ca. 11 % of the total NH_3 emission (Misselbrook et al., 2012). Although this proportion in the total national emission is rather small, since two thirds of the grasslands are estimated to be grazed (Hellsten et al., 2008), NH_3 emission from grazing affects a significant percentage of the country.

As demonstrated by both laboratory and field experiments (Farquhar et al., 1980; Sutton et al., 1995), ammonia exchange between atmosphere and surface is a bidirectional process and dependent largely on meteorological factors, especially temperature. The direction of the net NH_3 exchange at any time depends on the relative magnitude of the ambient air concentration of NH_3 high above the surface and the concentration of NH_3 right above the surface (referred to as the "compensation point"). If the air concentration is the larger

of the two, deposition occurs; whilst in the opposite case, emission takes place.

During grazing, the dominant NH_3 source is urine, rather than dung (Petersen et al., 1998; Laubach et al., 2013). In a urine patch ammonium (NH_4^+) is produced by urea hydrolysis. Because of the equilibrium between NH_4^+ and NH_3, increasing NH_4^+ concentration results in an NH_3 compensation point that is usually higher than the ambient air concentration above the urine patch. This generally leads to NH_3 emission from a urine patch. According to the literature (e.g. Sherlock and Goh, 1985; Laubach et al., 2012 and the references therein) the period with significant NH_3 emission lasts about 4–8 days after urine deposition.

The state-of-the-art NH_3 exchange models for vegetated surfaces (e.g. Burkhardt et al., 2009; Flechard et al., 2013), called canopy compensation point models, use the analogy of electrical circuits. In these, electrical current and potential difference represent NH_3 fluxes and the difference between the NH_3 concentrations at the different levels of the canopy, respectively. The model resistances capture the influence of meteorological factors and the canopy on NH_3 transfer. The first "canopy compensation point" model (Sutton et al., 1995) took into account the net NH_3 exchange with vegetation (a single-layer model), considering exchange with stomata and leaf surfaces. Later the canopy compensation point approach was developed by including NH_3 exchange also with soil surface (a two-layer model by Nemitz et al., 2001) and different parts of the plant, such as siliques and foliage (a three-layer model by Nemitz et al., 2000).

An example for estimating emissions from an excretal source that applies a simple compensation point model is the GUANO model (Riddick, 2012; Sutton et al., 2013), which simulates the processes leading to NH_3 emission from seabird excreta. In this model the compensation point is calculated based on Henry's law (for partitioning of NH_3) and the dissociation of NH_4^+ over a hypothetical surface covered by guano. In calculating the compensation point, the effect of meteorological factors (temperature, wind speed, solar radiation, relative humidity, and precipitation) are represented, furthermore, it accounts for the total ammoniacal nitrogen ($TAN = NH_4^+ + NH_{3(aq)}$) budget on the surface simulating the conversion of uric acid content of guano to ammoniacal nitrogen. In addition, it also calculates the water budget on the surface using the Pennman equation for evaporation.

Several attempts have been made to simulate NH_3 emission from urine patches as well as grazed fields. Laubach et al. (2012) published an NH_3 volatilization model from urine patches which was run in an "inverse" mode to calculate soil resistance, applying also a simple compensation point model. The equilibrium gaseous NH_3 concentration in the soil pores was considered as a compensation point, and three resistances (a soil, an aerodynamic, and a quasi-laminar resistance) were assumed between the soil and air concentration. Running the model in predictive mode, simulating NH_3 emission, requires soil sampling and measurement of pH and NH_4^+ concentration of soil water.

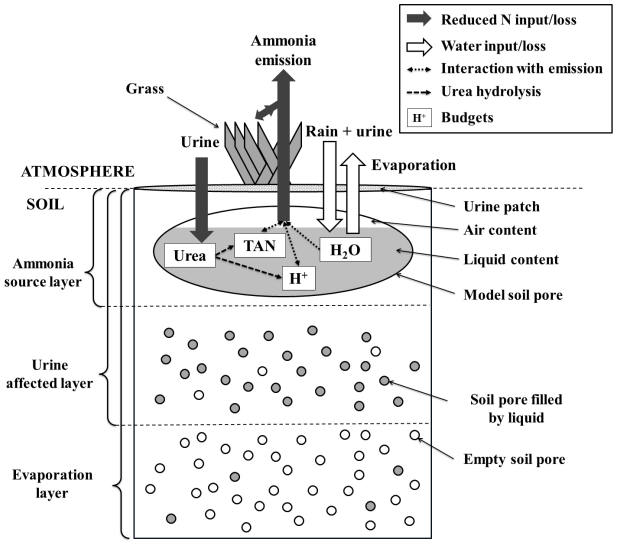

Figure 1. Schematic of major relationships in the GAG model. Empty soil pores in the middle layer represents that the maximum water content in the model is field capacity instead of being saturated. Whilst in the bottom layer the soil pores filled by liquid represents that the lowest water content is at the permanent wilting point instead of being completely dry. For more details on schematic see the text of Sect. 2.

The approach for the process of urea hydrolysis in the above-mentioned model by Laubach et al. (2012) is based on the earlier model of Sherlock and Goh (1985), which accounts for the NH_3 volatilization from urine patches and aqueous urea. This model for describing the transfer of NH_3 between surface and atmosphere operates with a constant "volatilization exchange coefficient", rather than a system of dynamically changing resistances. Rachhpal and Nye (1986) made an attempt to simulate NH_3 emission from applied urea. Although this model employed a constant "transfer coefficient" for NH_3 volatilization as well as a constant rate of urea hydrolysis were applied, the study gives an alternative for modelling the chemistry of a urine patch, as well as the vertical distribution of the different nitrogen compounds under the urine patch.

The present paper reports our work to construct and test a process-based, weather-driven model for NH_3 emission from a urine patch, which can be applied on both field and regional scales. On a field scale our approach is to apply the model for every urine patch deposited over the modelling period (involving statistical consideration), whilst for regional scale we are currently working to incorporate the field scale model into the EMEP4UK atmospheric chemistry transport model (Vieno et al., 2010, 2014). As such, the development represents a contribution toward developing a comprehensive suite of weather-dependent ammonia exchange models, as a

necessary basis for assessing the effects of climate change on ammonia emissions and deposition (Sutton et al., 2013). As soil measurements are not widely available – especially for a high-resolution grid that would be required for regional scale application – we had to account for the relevant processes in the soil, such as the change of concentration of the different reduced nitrogen compounds, pH, and water content. On the other hand, bearing in mind our final goal – a detailed investigation of weather dependency of NH_3 emission from grazing – we focused predominantly on the parametrization of the effect of meteorological variables, keeping the simulation of physical and chemical soil processes as simple as possible.

As our future aim is to apply the model to regional scale, simplicity to enhance scalability is a key aspect of the model development. For example, from a theoretical perspective, it could be attractive to explicitly model the 3-dimensional dispersion of ammonia between urine patches and adjacent vegetation within the canopy. However, this would be a much more complex task, which would also require major simplification when developing an upscaled regional application.

In this paper we firstly provide the description of our model of Generation of Ammonia from Grazing (GAG). Then we present the results from the test simulation based on the measurements by Laubach et al. (2012). Finally, we report the results of a sensitivity analysis in relation to the uncertain model parameters as well as several meteorological variables.

2 Description of the GAG model

To simulate NH_3 emission over a urine patch the GAG model calculates the TAN budget and the water budget, as well as the soil pH (hydrogen ion, H^+, budget) under the patch. For this purpose, firstly, we assume that, during urination and rain events, the incoming liquid infiltrates the soil to fill soil pores until the wetted soil layer reaches its field capacity. After this point we neglect any further downward or upward motion (capillary rise) in the soil. On Fig. 1 this depth in the soil is the bottom of the layer referred to as "urine affected layer".

We also make the assumption that soil NH_3 emission occurs only from the "source layer", the very top layer of the wetted soil column (similarly to Riedo et al., 2002, who also assumed a source layer on the top of their multilayer system), while reduced nitrogen (here the sum of NH_x and urea) that infiltrates beneath this layer is assumed to be nitrified "and no longer available to NH_3 emission. This assumption allows us to handle the numerous soil pores in the source layer as a single big pore – referred hereafter as "model soil pore" – the liquid content of which represents the soil pores filled by liquid, while its gaseous section represents the air-filled soil pores in the source layer (Fig. 1). We assume that all the liquid content is at the bottom of the model soil pore and/or source layer.

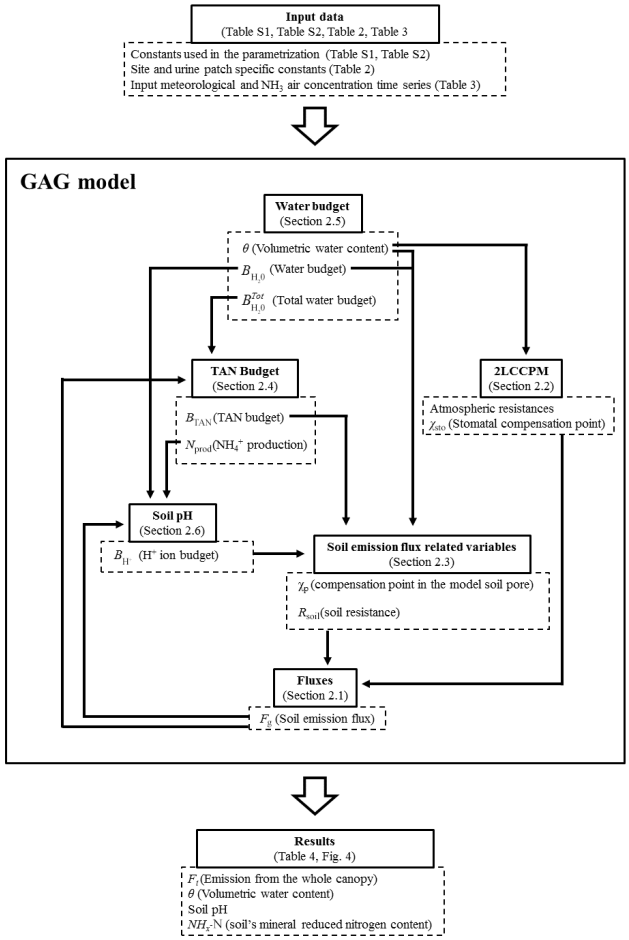

Figure 2. A flowchart depicting the steps of the calculation in the GAG model (middle panel), processing the input data (top panel) to the results that were compared with measurements in this study (bottom panel). The figure indicates the key variables that are carried from one module to another module(s). The figure, table, and section numbers referred in the figure show where further description of the different model parts can be found in this paper. (2LCCPM stands for Two-Layer Canopy Compensation Point Model.)

The input to the TAN budget is generated by hydrolysis of the urea contained within incoming urine, while NH_3 emission acts as a loss from the TAN budget. Soil pH is also regulated by urea hydrolysis, which is a proton (H^+) consuming process, and by NH_3 emission which is a proton producing process. The water budget is increased by rain water and the liquid content of urine, whilst it is decreased by soil evaporation. We assume that water evaporates from the "evaporation layer" (as defined by Allen et al. (1998), see in more details in Sect. 2.5), and the soil dries from the top, that is, during evaporation a dry front moves downwards in the soil. The model was coded in R, version 3.1.2 (31 October 2014; R Core Team, 2012) and the steps of the calculation are shown in Fig. 2.

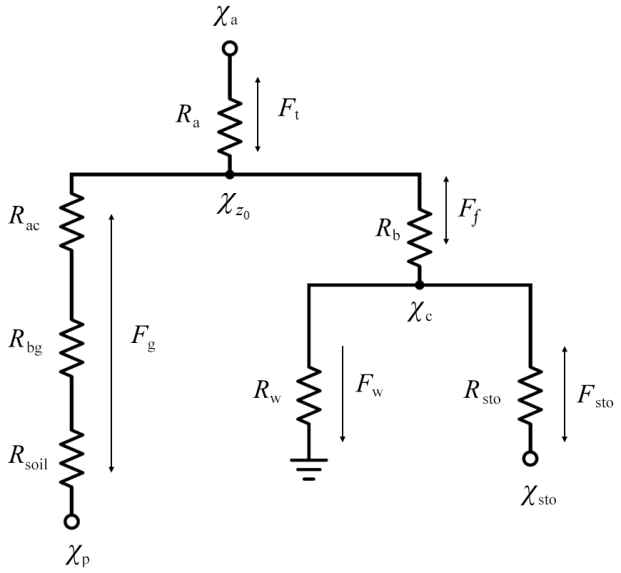

Figure 3. The network of gaseous resistances (R), ammonia concentrations (χ), and ammonia fluxes (F) used in the GAG model, which is based on the two-layer canopy compensation point model of Nemitz et al. (2001) incorporating concentration of the soil pore (χ_p) and soil resistance (R_{soil}). For the description of the other parameters in the framework see the text of this section.

2.1 Simulation of ammonia exchange flux

As urine deposition by grazing animals typically happens on vegetated surfaces of grassland we need to take into account the effect of vegetation on the total net NH_3 flux (F_t, calculated as emission minus deposition) over a urine patch. Therefore, an ideal model should capture not just the ground flux at the soil surface (F_g; referred hereafter as "soil emission"), but also the exchange with foliage (F_f), including NH_3 deposition to water and waxes on the leaf surface (F_w) and the NH_3 exchange with stomata (F_{sto}).

To achieve this, we extended the framework of the two-layer canopy compensation point model (abbreviated in this paper to 2LCCPM) of Nemitz et al. (2001) as shown in Fig. 3. The original exchange model calculates F_g assuming a bulk soil compensation point on the soil surface. Instead of calculating this compensation point, we derive the compensation point for our model soil pore (χ_p). To capture the constraint due to soil particles on NH_3 exchange with the soil, we added a soil resistance (R_{soil}) to the original framework.

Based on the analogy of electrical circuit, seven equations (Eqs. 1–7) can be derived to determine the five unknown fluxes (F_t, F_g, F_f, F_w, F_{sto}) and the two unknown compensation points (over the vegetation, χ_c, and over the whole canopy, χ_{z0}). Parameterizing the resistances – aerodynamic (R_a) and quasi-laminar resistance (R_b) over the canopy, aerodynamic resistance within the canopy (R_{ac}), quasi-laminar resistance (R_{bg}) at the ground, soil resistance, resistance to water and wax on the leaf surface (R_w) and stomatal resistance (R_{sto}) – as well as calculating the compensation point in the soil pore and in the stomata (χ_{sto}), we get a solvable linear system of equations.

$$F_t = F_g + F_f \quad (1)$$

$$F_f = F_w + F_{sto} \quad (2)$$

$$F_t = \frac{\chi_{z_0} - \chi_a}{R_a} \quad (3)$$

$$F_g = \frac{\chi_p - \chi_{z_0}}{R_{ac} + R_{bg} + R_{soil}} \quad (4)$$

$$F_f = \frac{\chi_c - \chi_{z_0}}{R_b} \quad (5)$$

$$F_w = \frac{-\chi_c}{R_w} \quad (6)$$

$$F_{sto} = \frac{\chi_{sto} - \chi_c}{R_{sto}} \quad (7)$$

Assuming that the changes are close to linear within a time step (1 h), and taking the air concentration of ammonia high above the canopy (χ_a) from measurements, the system of equations was solved for every time step by using the solve function of R programming language.

2.2 Parametrization of the resistances and stomatal compensation point (R_a, R_b, R_{ac}, R_{bg}, R_w, R_{sto}, χ_{sto})

The detailed parametrization of the resistances and the stomatal compensation point can be found in Sect. S1 in the Supplement together with all the model constants (Table S1 in the Supplement). Here we focus on the modifications and model assumptions we made for applying the 2LCCPM of Nemitz et al. (2001) in the GAG model.

Atmospheric resistances (R_a, R_b, R_{ac}, R_{bg}) are usually derived for homogenous (virtually infinite) surfaces, which is in apparent contradiction with the current application for a single, finite urine patch. In ongoing and future work we will apply the GAG model to field and regional scales, where the meteorological measurements and the canopy specific parameters, required to calculate these resistances, can be obtained for overall canopy types. To apply atmospheric resistances to urine patches, we assume that all the required variables and parameters to calculate them are representative for the whole experimental site including every single urine patch on the field (we also compared the results from GAG with measurements from a field experiment, as detailed in Sect. 4).

In the original description of the 2LCCPM, Nemitz et al. gave a parametrization for R_a as a function of u_* (friction velocity) and L (Monin-Obukhov length), which were measured in the original modelling study. In the absence of measurements to obtain u_* and L, parametrization should be used (Eqs. S7 and S8 in the Supplement, respectively). As these

two parameters depend on each other, we applied iteration to calculate both. For R_b we applied the formula suggested by Nemitz et al., expressed by Eq. (S12).

Following Nemitz et al., R_{ac} was assumed to be inversely proportional to u_* ($R_{ac} = \alpha u_*^{-1}$). Massad et al. (2010b) recommended values for parameter α for many surface types – including grass – as well as for all of the four seasons (Table S1). Nemitz et al. applied a parametrization for R_{bg} ($s\,m^{-1}$) for oilseed rape (Eq. S13). As the approach for calculation of this resistance for grasslands is not widely discussed in the literature, we adapted the one for oilseed rape for grassland. In our model, soil emission is dependent also on R_{soil}, which is larger at least by one order of magnitude than any of the atmospheric resistances. Thus, our model is not highly sensitive to this approximation for R_{bg} (for detailed analysis of the model sensitivity see Sect. 5).

The cuticular exchange of ammonia is strongly linked to the presence of a water film on the waxy leaf surface (Flechard et al., 1999). This can form even below the saturation point for pure water vapour, as a result of condensation facilitated by hygroscopic particles on the plant surface (Burkhardt et al., 1999). Therefore, the cuticular resistance (R_w) describes the effect of this water film on NH_3 absorption. The extent to which such a thin water layer is present affects the value of R_w; however, NH_3 absorption is also dependent on the air concentration of the acidic components (especially SO_2). These compounds, decreasing the pH of the water film, favour NH_3 deposition (Flechard et al., 1999). The process is referred to as co-deposition of the different components.

The modelling of this phenomenon requires the knowledge of the chemical composition of the atmosphere and substantially increases model complexity. For a simpler approach, R_w ($s\,m^{-1}$, Eq. 8) can be estimated as a function of relative humidity (RH, %). For this purpose – similarly also to Nemitz et al. (2001) – we used the formula from Massad et al. (2010b) based on Sutton and Fowler (1993) with the recommended parameters in the same study ($R_{w(min)}$ minimal cuticular resistance and a for grassland as reported by Horváth et al., 2005):

$$R_w = R_{w(min)} \times \exp\left(a\,(100 - RH)\right). \quad (8)$$

In the original description of the 2LCCPM R_{sto} is parametrized based on Hicks et al. (1987). Instead of this, we used a more state-of-the-art approach. As in Massad et al. (2010b), the value of R_{sto} ($s\,m^{-1}$, Eq. 9) was derived from the stomatal resistance to ozone ($R_{sto}\,(O_3)$, $s\,m^{-1}$), taking into account the difference between the diffusivity of the two gases ($D_{O_3}/D_{NH_3} = 1/1.6$). On the other hand, in Eq. (10), we parametrized R_{sto} (where 41 000 is the conversion from mmol $O_3\,m^{-2}$ to $m\,s^{-1}$) based on LAI (values are recommended by Massad et al. (2010b) for grass if not measured) applying the stomatal conductance (g_s, mmol $O_3\,m^{-2}$) model of Emberson et al. (2000).

$$R_{sto} = R_{sto}\,(O_3) \times \frac{D_{O_3}}{D_{NH_3}} \quad (9)$$

$$R_{sto}\,(O_3) = \left(\frac{g_s \times LAI}{41\,000}\right)^{-1} \quad (10)$$

Stomatal conductance Eq. (11) is defined based on the relative conductances that express how the openness of the stomata changes in the function of the phenological state of the plant (g_{pot}; assuming that grass could grow equally over the year, $g_{pot} = 1$), light (g_{light}), temperature (g_{temp}), vapour pressure deficit (g_{VPD}) and soil water potential (g_{SWP}). The combined effect of these, through the openness of stomata, controls g_s between its maximal value (g_{max}) and its minimal value ($g_{max} \times g_{min}$):

$$g_s = g_{max}\ g_{pot} \max\left\{g_{min}, \left(g_{light}\, g_{temp}\, g_{VPD}\, g_{SWP}\right)\right\}. \quad (11)$$

We followed the suggested parametrization by Emberson et al. for g_{light}, g_{temp}, and g_{VPD} (see in Sect. S1), but applied a different approach for g_{SWP} (Eq. 12). As the GAG model simulates the volumetric water content of the soil (θ, $m^3\,m^{-3}$; see the formulation in Sect. 2.5) for estimating g_{SWP} – instead of using the original parametrization depending on the soil water potential – we adapted the approach by Simpson et al. (2012), who defined a soil moisture index (S_{MI} Eq. 13), based on θ, influenced also by the soil's permanent wilting point (θ_{pwp}) and field capacity (θ_{fc}).

$$g_{SWP} = \begin{cases} 1 & \text{if} \quad S_{MI} \geq 0.5 \\ 2 \times S_{MI} & \text{if} \quad S_{MI} < 0.5 \end{cases} \quad (12)$$

$$S_{MI} = \frac{\theta - \theta_{pwp}}{\theta_{fc} - \theta_{pwp}} \quad (13)$$

The stomatal compensation point, as the equilibrium gaseous NH_3 concentration in the stomata, can be derived from the temperature-dependent form of Henry's law for dissolution of NH_3 (Reaction (R1) in Table 1) and the dissociation coefficient of NH_4^+ (Reaction (R4) in Table 1). Nemitz et al. (2000) derived χ_{sto} (Eq. 14) as a function of temperature (K) and the emission potential of the stomata (Γ_{sto}), which equals to the ratio of the NH_4^+ and H^+ concentrations (mol dm^{-3}) in the apoplastic fluid in the stomatal cavity.

$$\chi_{sto} = \frac{161\,500}{T} \times \exp\left(\frac{-10\,380}{T}\right) \times \Gamma_{sto} \quad (14)$$

In the original 2LCCPM Γ_{sto} is an input parameter from measurements. Since the measurement of Γ_{sto} is very difficult, in models it is usually handled as a constant, parametrized or simulated by a sub-model (e.g. Massad et al., 2010a; Wu et al., 2009). As there were no Γ measurements

Table 1. Chemical equations – indicated by Reactions (R0)–(R5) – simulated within the model, (where applicable) their equilibrium coefficient according to definition (K for dissociation and H for dissolution) and the coefficients expressed as the function of soil temperature (T_{soil}, K) and their references (squared brackets denotes that the concentration of every compound is in mol dm^{-3}).

Chemical equation	Equilibrium coefficient	Equilibrium coefficient as a function of temperature		Reference
R0: $CO(NH_2)_2 + 2H_2O + H^+ \rightarrow 2NH_4^+ + HCO_3^-$	–	–		–
R1: $NH_4^+ \Leftrightarrow NH_{3(aq)} + H^+$	$K\left(NH_4^+\right) = \frac{[NH_{3(aq)}][H^+]}{[NH_4^+]}$	$K\left(NH_4^+\right) = 5.67 \times 10^{-10} \exp\left(-6286\left(\frac{1}{T_{\mathrm{soil}}} - \frac{1}{298.15}\right)\right)$		Bates and Pinching (1949)
R2: $HCO_3^- \Leftrightarrow CO_3^{2-} + H^+$	$K\left(HCO_3^-\right) = \frac{[H^+]\left[CO_3^{2-}\right]}{[HCO_3^-]}$			
		$\lg(K(X)) = -\left(\left(\frac{a}{T_{\mathrm{soil}}}\right) + (b \times T_{\mathrm{soil}}) - c\right)$	$a = 2902.39$ $b = 0.02379$ $c = 6.4980$	Harned and Scholes (1941)
R3: $H_2CO_3 \Leftrightarrow HCO_3^- + H^+$	$K(H_2CO_3) = \frac{[HCO_3^-][H^+]}{[H_2CO_3]}$		$a = 3404.71$ $b = 0.032786$ $c = 14.8435$	Harned and Davis (1943)
R4: $NH_{3(aq)} \Leftrightarrow NH_{3(g)}$	$H(NH_{3(g)}) = \frac{[NH_{3(aq)}]}{[NH_{3(g)}]}$	$H(NH_{3(g)}) = 56 \times \exp\left(4092 \times \left(\frac{1}{T_{\mathrm{soil}}} - \frac{1}{298.15}\right)\right) \times c_{\mathrm{con}}$		Dasgupta and Dong (1986)
R5: $H_2CO_3 \Leftrightarrow CO_{2(g)}$	$H(CO_{2(g)}) = \frac{[H_2CO_3]}{[CO_{2(g)}]}$	$H(CO_{2(g)}) = 0.034 \times \exp\left(2400 \times \left(\frac{1}{T_{\mathrm{soil}}} - \frac{1}{298.15}\right)\right) \times c_{\mathrm{con}}$		Wilhelm et al. (1977)
		where $c_{\mathrm{con}} = \left(\frac{0.001 \frac{\mathrm{m}^3}{\mathrm{dm}^3}}{8.314 \frac{\mathrm{J}}{\mathrm{Kmol}}} \times \frac{1.013 \times 10^5 \frac{\mathrm{Pa}}{\mathrm{atm}}}{T_{\mathrm{soil}}}\right)^{-1}$ is the conversion from atm $(\mathrm{mol\,dm^{-3}})^{-1}$ to $(\mathrm{mol\,dm^{-3}})$ $(\mathrm{mol\,dm^{-3}})^{-1}$		

in the experiment we used in the test simulation (nor would such measurements be available for regional scale application) and over a urine patch NH_3 exchange is dominated by soil emission, we chose the parametrization recommended by Massad et al. (2010b) for grazed fields. Equation (15) assumes that Γ_{sto} reaches its maximum Γ_{sto} (max) right after N application (in this case after urine deposition), and then decays exponentially with time (t_i indicates the time step, the hours spent after urine deposition, with a decay parameter τ set at 2.88×24 h).

$$\Gamma_{\mathrm{sto}}(t_i) = \Gamma_{\mathrm{sto}}(\mathrm{max}) \times \exp\left(-\frac{t_i - 1}{\tau}\right) \quad (15)$$

Massad et al. (2010b) proposed a parametrization, describing an empirical relationship (Eq. 16) between the total N applied to the ecosystem (N_{app} in kg N ha^{-1}, see Eq. 17) and the observed maximal stomatal NH_3 emission potential (Γ_{sto} (max)). To apply the formula for a urine patch, we calculated N_{app} as the total N content of the urine – the volume of urine (W_{urine}, dm^3) multiplied by its nitrogen content (c_{N}, gN dm^{-3}) – divided by the area of the urine patch (A_{patch}, m^2; with 10 as a conversion factor between the different units).

$$\Gamma_{\mathrm{sto}}(\mathrm{max}) = 12.3 \times N_{\mathrm{app}} + 20.3 \quad (16)$$

$$N_{\mathrm{app}} = \frac{W_{\mathrm{urine}} \times c_{\mathrm{N}}}{A_{\mathrm{patch}}} \times 10 \quad (17)$$

2.3 Simulation of the soil pore (χ_{p}) compensation point and the soil resistance (R_{soil})

The simulation of χ_{p} (mol dm^{-3}) is very similar in theory to that of χ_{sto}, being derived from Henry's law for NH_3 dissolution and the dissociation coefficient of NH_4^+. In this way (following Nemitz et al., 2000) we get Eq. (18), where T_{soil} is the soil temperature (K) and Γ_{p} is the ratio of the NH_4^+ and H^+ concentration in the model soil pore. In Eq. (19) Γ_{p} is expressed as a function of TAN concentration ([TAN] = [NH_4^+] + [$NH_{3(aq)}$]) based on the definition of dissociation constant (K(NH_4^+), second column of Table 1 and its temperature-dependent form in the third column).

$$\chi_{\mathrm{p}} = \frac{161\,500}{T_{\mathrm{soil}}} \times \exp\left(\frac{-10\,380}{T_{\mathrm{soil}}}\right) \times \Gamma_{\mathrm{p}} \quad (18)$$

$$\Gamma_{\mathrm{p}} = \frac{[\mathrm{TAN}]}{K\left(NH_4^+\right) + \left[H^+\right]} \quad (19)$$

TAN and H^+ concentration (both in mol dm^{-3}) are derived from TAN budget (B_{TAN}, g N) and H^+ budget ($B_{\mathrm{H+}}$, mol), according to their mass ratio with water budget ($B_{\mathrm{H_2O}}$, dm^3), as shown in Eqs. (20)–(21), respectively, (where 14 is the molar mass of nitrogen). All budgets are simulated within GAG (see B_{TAN}: Sect. 2.4, $B_{\mathrm{H+}}$: Sect. 2.6, and $B_{\mathrm{H_2O}}$: Sect. 2.5).

$$[\mathrm{TAN}] = \frac{\frac{B_{\mathrm{TAN}}}{14}}{B_{\mathrm{H_2O}}} \quad (20)$$

$$\left[H^+\right] = \frac{B_{H^+}}{B_{\mathrm{H_2O}}} \quad (21)$$

For R_{soil} (s m^{-1}) we applied the approach by Laubach et al. (2012), as expressed in Eq. (22). This captures the effect of soil depth (Δz), that is, from how deep the soil NH_3 emission occurs on average. In the study of Laubach et al. Δz is referred as "source depth", and in GAG model we consider it as the thickness of the source layer. The model experiments by Laubach et al. suggested that the distribution of Δz has a median of 0.002 m with an uncertainty factor of 2

and a similar value (0.003 m) was used in the study of Riedo et al. (2002) as well. In reality the thickness of the source layer changes parallel with the moisture content of the top soil layer; however, its approximation, due to the thinness of the layer, is difficult. Therefore, at the moment our model operates with a constant Δz of 0.004 m. In Sect. 5.2 we tested the model sensitivity also to Δz.

$$R_{\text{soil}} = \frac{\Delta z}{\xi D_{\text{g}}} \tag{22}$$

According to this approach, R_{soil} is inversely proportional to soil tortuosity (ξ) and diffusivity of NH_3 (D_{g}). For ξ, Laubach et al. (2012) suggested the parametrization by Millington and Quirk (1961), based on the volumetric water content as well as porosity (θ_{por}):

$$\xi = \frac{\left(\theta_{\text{por}} - \theta\right)^{\frac{10}{3}}}{\theta_{\text{por}}^2}. \tag{23}$$

2.4 Simulation of the TAN budget under the urine patch (B_{TAN})

The amount of TAN in the model soil pore in a given time step t_i ($B_{\text{TAN}}(t_i)$, g N), depends on its value in the previous time step ($B_{\text{TAN}}(t_{i-1})$, g N) and is controlled by the amount of TAN produced during urea hydrolysis (N_{prod}, g N) and soil NH_3 emission (F_{g}, g N m^{-2}) calculated in the previous time step (Eq. 24). We assume that B_{TAN} before urine deposition is negligibly small (compared to that of after urine deposition). Therefore, its initial value is set to 0. The model does not allow to emit more NH_3 than TAN is available in the source layer, as it is described by Eq. (25).

$$B_{\text{TAN}}(t_i) = \text{N}_{\text{prod}}(t_i) + B_{\text{TAN}}\left(t_{i-1}\right) - F_{\text{g}}\left(t_{i-1}\right) \times A_{\text{patch}} \tag{24}$$

$$F_{\text{g}} = \begin{cases} \dfrac{B_{\text{TAN}}(t_{i-1})}{A_{\text{patch}}} & \text{if } \left(B_{\text{TAN}}(t_{i-1}) - F_{\text{g}}(t_{i-1}) \times A_{\text{patch}}\right) < 0 \\ \dfrac{\chi_{\text{p}} - \chi_{z_0}}{R_{\text{ac}} + R_{\text{bg}} + R_{\text{soil}}} & \text{otherwise} \end{cases} \tag{25}$$

TAN production depends on the current amount of urea nitrogen within the model soil pore (B_{urea}, g N), as well as soil temperature (T_{soil}, °C). For N_{prod} Sherlock and Goh (1985) suggested an empirical formula (Eq. 26), with a temperature-dependent parameter (A_{h}, Eq. 27) and a hydrolysis constant (k_{h}, see Table 2).

$$N_{\text{prod}}(t_i) = B_{\text{urea}}(t_i)\left(1 - \exp\left(A_{\text{h}}(t_i) \times k_{\text{h}}\right)\right) \tag{26}$$

$$A_{\text{h}}(t_i) = 0.25 \times \exp\left(0.0693 \times T_{\text{soil}}(t_i)\right) \tag{27}$$

Table 2. Urine patch details from the experiment of Laubach et al. (2012) or from other sources as listed in the footnote and site specific model constants.

Model constants	Value
Urine patch specific constants	
A_{patch} (area of a urine patch)[1]	0.25 m^2
c_{N} (N content of the urine)	10 g N dm^{-3}
W_{urine} (volume of urine)	1.5 dm^3
Δz (thickness of the source layer)[2]	4 mm
k_{h} (urea hydrolysis constant)[3]	0.23
Site specific constants	
Longitude	172°27.34′ E
Latitude	43°38.56′ S
Height above sea level	11 m
θ_{pwp} (permanent wilting point)[4]	0.1
θ_{fc} (field capacity)[4]	0.4
θ_{por} (porosity)	0.62
f_{c} (vegetation coverage)	35 %
z_{w} (height of wind measurement)	2.1 m

[1] In the experiment the expansion of the patches was observed up to 0.5 m^2. For model sensitivity to A_{patch} see Sect. 5.2. [2] Assumed in this study. [3] For summer (Sherlock and Goh, 1984) [4] Assumed based on the provided measured volumetric water content data set.

Urea nitrogen content in a given time step (Eq. 28) is determined by its value in the previous time step, the loss as conversion to TAN ($-N_{\text{prod}}$) and, in the first time step, the amount of urea nitrogen added (U_{add}, g N) with the incoming urine. In U_{add} (Eq. 29) we take into account the dilution effect of rain and soil water on the nitrogen concentration of urine (c_{n}). We assume that right after urine deposition the urea nitrogen content of urine, diluting in the total soil water ($B_{\text{H}_2\text{O}}^{\text{Tot}}$, Eq. 29), forms a homogenous soil solution with a concentration of $c_{\text{n}}^{\text{Tot}}$ (Eq. 30). Finally, U_{add} is calculated as the product of $c_{\text{n}}^{\text{Tot}}$ and the water content of the emission layer. This will equal to $B_{\text{H}_2\text{O}}^{\text{Tot}}$ unless there is more water in the soil than can be stored in the emission layer, as indicated by $B_{\text{H}_2\text{O}}$ (max), which is specified in the following section, see Eq. (36).

$$B_{\text{urea}}(t_i) = B_{\text{urea}}(t_{i-1}) - N_{\text{prod}}(t_{i-1}) + U_{\text{add}}(t_i) \tag{28}$$

$$U_{\text{add}} = c_{\text{n}}^{\text{Tot}} \min\left\{B_{\text{H}_2\text{O}}(\max), B_{\text{H}_2\text{O}}^{\text{Tot}}\right\} \tag{29}$$

$$c_{\text{n}}^{\text{Tot}} = c_{\text{n}} \frac{W_{\text{urine}}}{B_{\text{H}_2\text{O}}^{\text{Tot}}} \tag{30}$$

2.5 Simulation of the water budget under the urine patch ($B_{\text{H}_2\text{O}}^{\text{Tot}}$, θ, $B_{\text{H}_2\text{O}}$, $B_{\text{H}_2\text{O}}$(max))

The soil moisture content affects NH_3 emission in several ways. In the first time step when the urine is deposited, both the water content of the model soil pore and the water content

of the whole urine-affected soil layer ($B^{\mathrm{Tot}}_{\mathrm{H_2O}}$, Eq. 31) have an effect on emission. The thickness of the urine-affected soil layer depends on the amount of incoming liquids: urine (considering its whole volume as water) and rain (W_{rain}, dm^3). The more water is added, the more empty soil pore it can fill up and consequently, the deeper it will infiltrate.

We made the assumption for our model that the lowest possible volumetric water content in the soil is at permanent wilting point (θ_{pwp}) and the highest is at the field capacity (θ_{fc}), where both θ_{pwp} and θ_{fc} are expressed as fractions of total soil volume. Assuming that the initial soil water content is at θ_{pwp}, and after infiltration it rises to θ_{fc}, the volume fraction taken up by the incoming water will be $\theta_{\mathrm{fc}} - \theta_{\mathrm{pwp}}$. Finally, we get the total water content (incoming + soil water) in the urine-affected layer (having a volumetric water content of θ_{fc}) as

$$B^{\mathrm{Tot}}_{\mathrm{H_2O}} = \left(W_{\mathrm{rain}}\left(t_1\right) + W_{\mathrm{urine}}\right)\frac{\theta_{\mathrm{fc}}}{\theta_{\mathrm{fc}} - \theta_{\mathrm{pwp}}}. \tag{31}$$

After urine deposition, actual volumetric water content (θ, Eq. 32) of the source layer can be expressed as the volume of the water in the layer ($\mathrm{B_{H_2O}}$, dm^3) divided by the volume of the soil column under the urine patch with a surface area of A_{patch} (m^2). In Eq. (32) 1000 is the conversion from m^3 to dm^3).

$$\theta = \frac{B_{\mathrm{H_2O}}}{1000 \times \Delta z \times A_{\mathrm{patch}}} \tag{32}$$

The actual water content of the soil at any time step ($B_{\mathrm{H_2}0}$‘(t_i), Eq. 33) depends on the water content in the previous time step, soil evaporation (W_{evap}, dm^3), rain events (W_{rain}, dm^3), and in the very first time step the volume of urine (e.g. if the volume of the urine is $1.5\,\mathrm{dm}^3$ then W_{urine} $(t_1) = 1.5\,\mathrm{dm}^3$, otherwise 0). Both the volume of evaporation from the source layer and incoming rain to this layer are derived as the product of A_{patch} and soil evaporation (with E ($\mathrm{dm}^3\,\mathrm{m}^{-2}$): $W_{\mathrm{evap}} = E \times A_{\mathrm{patch}}$) as well as precipitation (with P ($\mathrm{dm}^3\,\mathrm{m}^{-2}$): $W_{\mathrm{rain}} = P \times A_{\mathrm{patch}}$) for a m^2, respectively.

$$B'_{\mathrm{H_2O}}(t_i) = \begin{cases} B_{\mathrm{H_2O}}(\mathrm{min}) + W_{\mathrm{rain}}(t_i) + W_{\mathrm{urine}}(t_i) \\ \quad \text{if } \left(B_{\mathrm{H_2O}}(t_{i-1}) - W_{\mathrm{evap}}(t_{i-1})\right) < B_{\mathrm{H_2O}}(\mathrm{min}) \\ B_{\mathrm{H_2O}}(t_{i-1}) - W_{\mathrm{evap}}(t_{i-1}) + W_{\mathrm{rain}}(t_i) + \quad \text{otherwise} \\ \quad W_{\mathrm{urine}}(t_i) \end{cases} \tag{33}$$

It is not possible for more water to be evaporated from the source layer than the minimal water content (water content of the layer at θ_{pwp}: $B_{\mathrm{H_2O}}(\mathrm{min})$ (dm^3), Eq. 34). On the other hand, (as is shown in Eq. 35) this layer cannot store more water than the maximal water content (water content of the layer at θ_{fc}: $B_{\mathrm{H_2O}}(\mathrm{max})$ (dm^3), Eq. 36). The excess water is assumed to infiltrate to the deeper soil layers. In Eqs. (34) and (36) 1000 is the conversion from m^3 to dm^3.

$$B_{\mathrm{H_2O}}\left(\mathrm{min}\right) = 1000 \times \Delta z \times A_{\mathrm{patch}} \times \theta_{\mathrm{pwp}} \tag{34}$$

$$B_{\mathrm{H_2O}}\left(t_i\right) = \min\left\{B'_{\mathrm{H_2O}}\left(t_i\right), B_{\mathrm{H_2O}}\left(\mathrm{max}\right)\right\} \tag{35}$$

$$B_{\mathrm{H_2O}}\left(\mathrm{max}\right) = 1000 \times \Delta z \times A_{\mathrm{patch}} \times \theta_{\mathrm{fc}} \tag{36}$$

Instead of constructing a comprehensive energy balance model for GAG (driving NH_3 and water vapour flux in the same time), for simplicity's sake, to estimate the soil evaporation we adapted the dual crop method of Allen et al. (1998). The approach firstly calculates the reference evapotranspiration ($\mathrm{ET_0}$, evaporation from soil + transpiration by plants) for a reference surface (a surface covered by grass with a height of 0.12 m, a fixed surface resistance to water exchange of $70\,\mathrm{s\,m}^{-1}$ and albedo of 0.23). Then, defining a "crop coefficient" (K_{c}) for the actual surface, it gives an estimation for the actual evapotranspiration ($\mathrm{ET} = K_{\mathrm{c}} \times \mathrm{ET_0}$). In the final step K_{c} is split to a coefficient for transpiration and a coefficient for soil evaporation ($K_{\mathrm{c}} = K_{\mathrm{cb}} + K_{\mathrm{e}}$).

In our model for $\mathrm{ET_0}$ we incorporated a slightly modified form of the Penman-Monteith equation (Eq. 37, Walter et al., 2001) compared with that of Allen et al. (1998). In this way the model accounts for the effect of change of day and night on evapotranspiration (C_{d}, Eq. 38). For the formulation of Δ (the slope of the saturation vapour pressure temperature relationship), R_{n} (net radiation), G (soil heat flux) and γ (psychrometric constant), see the details in Allen et al. (1998).

$$\mathrm{ET_0} = \frac{0.408 \times \Delta\left(R_{\mathrm{n}} - G\right) + \gamma \frac{37}{T+273.15} u\left(e_{\mathrm{s}} - e_{\mathrm{a}}\right)}{\Delta + \gamma\left(1 + C_{\mathrm{d}} u\right)} \tag{37}$$

$$C_{\mathrm{d}} = \begin{cases} 0.24 & \text{if} \quad R_{\mathrm{n}} > 0 \quad \text{(daytime)} \\ 0.96 & \text{otherwise} \quad \text{(nighttime)} \end{cases} \tag{38}$$

When calculating soil evaporation ($E = K_{\mathrm{e}} \times \mathrm{ET_0}$) we made the following assumptions:

- According to Allen et al., soil evaporation occurs from the wetted, uncovered soil fraction (f_{w}). Applying the evapotranspiration model for a urine patch, the whole modelled soil will be wet. In addition, we assumed that the percentage of the whole field covered by vegetation (f_{c}) is the same over a urine patch. In this way $f_{\mathrm{w}} = (1 - f_{\mathrm{c}})$ for a urine patch.

- Following the recommendations of Allen et al., we assumed that there is no runoff, no transpiration from the evaporation layer (including the NH_3 source layer) and no "deep percolation" (which occurs when θ exceeds θ_{fc}, but in our model θ_{fc} is assumed to be the maximum of θ).

– In the original approach it is assumed that soil evaporation attenuates when more water is evaporated from the soil evaporation layer (characterized by a thickness of Δz_E) than the amount of "readily evaporable water" (REW). The study of Allen et al. recommends REW values for different soil types defined by their θ_{fc} and θ_{pwp}. However, for the site whose measurement we used in the test simulation (see Sect. 4.), with a sandy loam soil, these θ_{fc} and θ_{pwp} values were not in accordance with the measurements. Therefore, we calculated REW as the water content of the evaporation layer halfway between θ_{fc} and θ_{pwp}:

$$\mathrm{REW} = 1000\left(\theta_{fc} - 0.5\left(\theta_{fc} - \theta_{pwp}\right)\right) \times \Delta z_E. \quad (39)$$

The model constants used in the soil evaporation estimation are listed in Table S2.

2.6 Simulation of soil pH (B_{H+})

After urine deposition, soil pH is affected by two main reactions: urea hydrolysis and NH_3 emission. When a urea molecule is decomposed (based on Reaction (R0) in Table 1) an H^+ ion is consumed, producing two NH_4^+ ions and a bicarbonate ion (HCO_3^-). In the early stages of urea hydrolysis, when a large amount of urea is hydrolysed, a large amount of H^+ is required, resulting in a peak of soil pH (minimum of soil H^+ concentration). This triggers the dissociation of the produced NH_4^+ and consequently the formation of gaseous ammonia, which also leads to an emission peak shortly after urine deposition. Once the majority of urea has been hydrolysed, ammonia emission may still be continuing. To balance the lost gaseous ammonia, more NH_4^+ dissociates, resulting in H^+ production, which tends to compensate the H^+ consumption associated with urea hydrolysis.

According to Sherlock and Goh (1985) after a rapid increase, soil pH usually peaks around 6–48 h after urine deposition (referred to as "first stage" of emission). Subsequently, the pH tends to drop for the reasons explained above over a period of about 2–8 days (second stage). Sherlock and Goh also identified two further stages: a 1–3 week long constant phase (third stage) when soil pH does not change considerably and, finally, a phase (fourth stage) with a moderate decline in soil pH, regulated by the nitrification of TAN.

As Sherlock and Goh (1985) pointed out that the bulk of TAN is volatilized over the first and second periods, and nitrification is a sufficiently slower process than NH_3 volatilization (see the cited references in the study of Sherlock and Goh), in the GAG model we neglect the effect of nitrification. On the other hand, we make the assumption that the solid material of soil is chemically inert, and consequently, NH_3 emission from soil is only affected by the composition of urine solution.

Whitehead et al. (1989) showed that not only urea but other urinary nitrogen components, such as allantoin, creatine and creatinine, can contribute to NH_3 emission through their decomposition. However, Whitehead et al. found that only allantoin can have a comparable influence on NH_3 volatilization (from the solutions of these compounds with the same N concentration, over 8 days 15 % of the applied N was emitted from urea and 11 % from the allantoin); that of the other two components, creatine and creatinine, is rather small (over 8 days 4 % and less than 1 % of the applied N was emitted as NH_3, respectively). In addition, according to Dijkstra et al. (2013) the proportion of allantoin in urinary nitrogen is considerably lower than that of urea, 2.2–14.2 compared to 57.8–93.5 % and the proportions for creatine and creatinine are even lower. Therefore, to further focus our model onto the key reactions, we simulate urine chemistry considering only the water and urea available in the beginning, and the products of urea breakdown afterwards.

As urine is a relatively concentrated solution, non-ideal ionic behaviour may have an effect on the chemical equilibria. To test this in the model, we did a test run with the maximum activity coefficients derived for the highest ion concentrations (0.2 mol dm^{-3}) published by Kielland (1937; the highest ionic concentration in the modelled solution was 0.14 mol dm^{-3}). With this modification, the difference, in the total NH_3 emission was −4.7 % and the average change in pH was −0.019. Considering that the ion concentration decreases toward the end of the modelling period, and consequently, the activity coefficients converge to 1, we neglect the effect of non-ideal behaviour in the solution.

In this way, we consider the reactions for change of soil pH listed in Table 1: urea hydrolysis (Reaction R0), NH_4^+ dissociation (R1), dissociation of HCO_3^- and H_2CO_3 (carbonic acid; Reactions (R2) and (R3), respectively), formation of gaseous NH_3 and CO_2 (carbon dioxide; Reactions (R4) and (R5), respectively). However, considering that soil is a buffered system, we also incorporate a soil buffering capacity (β mol H^+ (pH unit)$^{-1}$ dm^{-3}). Buffering capacity moderates the change of H^+ ion concentration. When H^+ ions are produced in the system during urea hydrolysis and the related equilibrium processes, to balance this change H^+ ions are consumed by buffers, and similarly, when H^+ ions are consumed in the system, buffers release H^+ ions. In the model this buffering effect is expressed by the term of β_{patch} (pH(t_i)-pH(t_{i-1})) in Eq. (46). This term is positive when the H^+ ion concentration decreases (pH increases), and it is negative in the opposite case.

Whitehead and Raistrick (1993) found a strong correlation between the cation exchange capacity (CEC) and NH_3 volatilization as well as a weaker correlation with organic matter, clay, and sand content of the soil. However, we are not aware of a specific quantitative relationship between buffering capacity and CEC, or the clay content or the organic matter content. Therefore, we address this issue through a sensitivity analysis on the model performance (Sect. 5.3).

Regarding the effect of the potassium content of urine on buffering capacity and indirectly, NH_3 emission, Whitehead et al. (1989) showed that the potassium salts of urine have a rather small influence on NH_3 volatilization. Based on these, we used a constant buffering capacity in the model. We defined β during test simulations with GAG. We found that the model represents the measured pH well with a β of 0.021 mol H^+ (pH unit)$^{-1}$ dm^{-3}. To get the buffering effect in the volume of our model soil pore we calculated $\beta_{\text{patch}} = \beta \times A_{\text{patch}} \times \Delta z$. For a sensitivity analysis to β see Sect. 5.3.

We defined 13 equations to calculate soil pH (Eqs. 40–52), eight of which are predictive equations, Eqs. (40)–(47), where B_X (mol) is the budget of the component X in the urine solution and r_{Rx} (mol) is the production or consumption of the compound predicted by the given equation in the reaction X (following the numbering of reactions in Table 1). Variables i_{N} and i_{C} indicate the nitrogen and carbon input generated during urea hydrolysis, respectively. The nitrogen input is the same as N_{prod} but in mol ($i_{\text{N}} = N_{\text{prod}}/14$) and based on R0, $i_{\text{C}} = i_{\text{N}}/2$.

The other five equations describe the equilibrium in every time step (Eqs. 48–52). These were derived by reorganizing the equations in the second column in Table 1, where, for a dissolved component X: $[X] = B_x/B_{\text{H}_2\text{O}}$ and for a gaseous component $X_{(\text{g})}$: $[X_{(\text{g})}] = B_{X(g)}/V_{\text{air}}$. V_{air} is the volume of the air in the model soil pore, which can be calculated as the volume of the space in the model soil pore that is not taken up by the liquid content ($V_{\text{air}} = \theta_{\text{por}} A_{\text{patch}} \Delta z \times 1000 - B_{\text{H}_2\text{O}}$, where 1000 is the conversion between m^3 and dm^3).

Variables B_{C} and B_{N} represent the total inorganic carbon and nitrogen budget in the urine solution, respectively. Both can be derived as a sum of the different components and their input (by urea breakdown) and loss via emission as gas (Eqs. 53 and 54).

$$B_{\text{H}_2\text{CO}_3}(t_i) = B_{\text{H}_2\text{CO}_3}(t_{i-1}) + (-r_{\text{R5}} + r_{\text{R3}}) \quad (40)$$

$$B_{\text{HCO}_3^-}(t_i) = B_{\text{HCO}_3^-}(t_{i-1}) + (-r_{\text{R2}} - r_{\text{R3}} + i_{\text{C}}(t_i)) \quad (41)$$

$$B_{\text{CO}_3^{2-}}(t_i) = B_{\text{CO}_3^{2-}}(t_{i-1}) + r_{\text{R2}} \quad (42)$$

$$B_{\text{CO}_{2(\text{g})}}(t_i) = B_{\text{CO}_{2(\text{g})}}(t_{i-1}) + r_{\text{R5}} \quad (43)$$

$$B_{\text{NH}_4^+}(t_i) = B_{\text{NH}_4^+}(t_{i-1}) + (-r_{\text{R1}} + i_{\text{N}}(t_i)) \quad (44)$$

$$B_{\text{NH}_{3(\text{aq})}}(t_i) = B_{\text{NH}_{3(\text{aq})}}(t_{i-1}) + (r_{\text{R1}} - r_{\text{R4}}) \quad (45)$$

$$B_{\text{NH}_{3(\text{g})}}(t_i) = B_{\text{NH}_{3(\text{g})}}(t_{i-1}) + \left(r_{\text{R4}} - \frac{F_{\text{g}}(t_{i-1}) \times A_{\text{patch}}}{14}\right) \quad (46)$$

$$B_{\text{H}^+}(t_i) = B_{\text{H}^+}(t_{i-1}) - i_{\text{C}}(t_i) + (-r_{\text{R3}} + r_{\text{R2}} + r_{\text{R1}}) + \beta_{\text{patch}}(\text{pH}(t_i) - \text{pH}(t_{i-1})) \quad (47)$$

$$K\left(\text{NH}_4^+\right)(t_i)\, B_{\text{H}_2\text{O}}(t_i)\, B_{\text{NH}_4^+}(t_i) - B_{\text{H}^+}(t_i)\, B_{\text{NH}_{3(\text{aq})}}(t_i) = 0 \quad (48)$$

$$K\left(\text{CO}_3^-\right)(t_i)\, B_{\text{H}_2\text{O}}(t_i)\, B_{\text{HCO}_3^-}(t_i) - B_{\text{H}^+}(t_i)\, B_{\text{CO}_3^{2-}}(t_i) = 0 \quad (49)$$

$$K\left(\text{H}_2\text{CO}_3\right)(t_i)\, B_{\text{H}_2\text{O}}(t_i)\, B_{\text{H}_2\text{CO}_3}(t_i) - B_{\text{H}^+}(t_i)\, B_{\text{HCO}_3^-}(t_i) = 0 \quad (50)$$

$$\left(H\left(\text{CO}_{2(\text{g})}\right)(t_i)\frac{B_{\text{H}_2\text{O}}(t_i)}{V_{\text{air}}(t_i)} + 1\right) B_{\text{H}_2\text{CO}_3}(t_i) + H\left(\text{CO}_{2(\text{g})}\right)(t_i)\frac{B_{\text{H}_2\text{O}}(t_i)}{V_{\text{air}}(t_i)} B_{\text{HCO}_3^-}(t_i) + \text{H}\left(\text{CO}_{2(\text{g})}\right)(t_i)\frac{B_{\text{H}_2\text{O}}(t_i)}{V_{\text{air}}(t_i)} B_{\text{CO}_2}(t_i) = H\left(\text{CO}_{2(\text{g})}\right)(t_i)\frac{B_{\text{H}_2\text{O}}(t_i)}{V_{\text{air}}(t_i)} B_{\text{C}}(t_i) \quad (51)$$

$$\left(H\left(\text{NH}_{3(\text{g})}\right)(t_i)\frac{B_{\text{H}_2\text{O}}(t_i)}{V_{\text{air}}(t_i)} + 1\right) B_{\text{NH}_{3(\text{aq})}}(t_i) + H\left(\text{NH}_{3(\text{g})}\right)(t_i)\frac{B_{\text{H}_2\text{O}}(t_i)}{V_{\text{air}}(t_i)} B_{\text{NH}_4^+}(t_i) = H\left(\text{NH}_{3(\text{g})}\right)(t_i)\frac{B_{\text{H}_2\text{O}}(t_i)}{V_{\text{air}}(t_i)} B_{\text{N}}(t_i) \quad (52)$$

$$B_{\text{C}}(t_i) = B_{\text{H}_2\text{CO}_3}(t_{i-1}) + B_{\text{HCO}_3^-}(t_{i-1}) + B_{\text{CO}_3^{2-}}(t_{i-1}) + B_{\text{CO}_2}(t_{i-1}) + i_{\text{C}}(t_i) \quad (53)$$

$$B_{\text{N}}(t_i) = B_{\text{NH}_{3(\text{aq})}}(t_{i-1}) + B_{\text{NH}_4^+}(t_{i-1}) + B_{\text{NH}_{3(\text{g})}}(t_{i-1}) + i_{\text{N}}(t_i) - \frac{F_{\text{g}}(t_{i-1}) \times A_{\text{patch}}}{14} \quad (54)$$

Although references can be found in the literature for measurements of CO_2 emission from urine patches (e.g. Wang et al., 2013; Ma et al., 2006; Lin et al., 2009), we considered that the driving processes behind them are not described well enough for an hourly model application. Therefore, in the case of the carbon budget (Eq. 53) we did not assume a term for CO_2 emission in the basic GAG model, but we tested the effect of CO_2 emission in Sect. 5.3. The dissociation coefficients ($K(X)(t_i)$) and Henry constants ($H(X(g))(t_i)$) for the given t_i time step were derived as a function of actual soil temperature (third column of Table 1).

For a given $B_{\text{H}+}(t_i)$ Eqs. (40)–(46) and (48)–(52) constitute a linear system of equations (12 equations, and seven $B_X(t_i)$ budgets and five r_{Rx} consumptions and/or productions as unknowns). As $B_{\text{H}+}(t_i)$ is unknown, we are looking for a solution with a particular $B^*_{\text{H}+}$ for this equation system, whose roots also satisfy Eq. (47), giving back $B^*_{\text{H}+}$. For this purpose, we used the uniroot function of programming language R (version 3.1.2; 31 October 2014), which is able to find this $B^*_{\text{H}+}$. $B^*_{\text{H}+}$ provides the H^+ budget in the given time step and finally, pH can be calculated as $\text{pH} = -\log_{10}(B^*_{\text{H}+}/B_{\text{H}_2\text{O}})$.

3 Measurement data used in the test simulation

The GAG model described in the preceding sections was developed to simulate NH_3 emission from a single urine patch. However, for testing the model we chose a field experiment where the NH_3 emission flux was measured from several urine patches deposited relatively close in time. The only experiment we are aware of with these features was conducted

by Laubach et al. (2012), who measured the NH_3 fluxes over a field covered with a regular pattern of urine patches.

In the experiment, 156 artificial urine patches were deposited within 45 min (see an overview of urine patch characteristics in Table 2) over a circular plot at an experimental site, in Lincoln New Zealand. In the middle of the plot NH_3 concentration was measured at five heights with Leuning samplers (Leuning et al., 1985) from which the fluxes were derived by different methods. For this study we used the fluxes calculated by Laubach et al. according to the mass balance (MB) method.

Soil samples were taken from 24 patches on the edge of the plot to measure soil pH, volumetric water content and mineral N content. Soil temperature was measured at two heights, and meteorological measurements were also carried out (from which we used wind speed, temperature, photosynthetically active radiation (PAR), sensible heat flux and atmospheric pressure data). For more details on measurements and flux calculation, see Laubach et al. (2012).

In addition to the available measurements, we also needed meteorological data that were not measured in the experiment: global radiation (R_{glob}) and RH. We obtained these data from the National Climate Database for New Zealand (NIWA, 2015).

We compared our model results with measurements of F_{t}, soil pH, and θ for the measurement period between 24 February 11:30 and 1 March 2010 01:30 a.m. UTC +13 hours. In the case of F_{t}, the length of the collecting period of each measurement varied mostly between 1–1.5 h for daytime measurements, and 7–7.5 h for the night-time measurements. As the time step of our model is 1 h and emission fluxes were not expected to change considerably over the night, we assumed that the measured average NH_3 flux over the collecting period is representative for the midpoint of the period, and we compared these to our model values in the time step closest to the midpoint of the corresponding measurements.

In addition, assuming that the change of the soil's mineral reduced nitrogen content (NH_x-N) is parallel with the B_{TAN} in the model soil pore, we also compared these two parameters. All of the input data, as well as the measurement data we used to compare our model results, together with their modification for our hourly model run, are listed in Table 3.

To compare the measured and modelled F_{t} for a single urine patch, we assumed that the great majority of NH_3 in the experiment of Laubach et al. (2012) was emitted from the urine patches. Therefore, we multiplied the observed fluxes by the effective source area (804.9 m^2 as calculated by Laubach et al., 2012), then divided it by the total area of the deposited 156 patches (Eq. 55; where $F_{\mathrm{t}}^{\mathrm{single}}$ stands for the converted measured flux).

$$F_{\mathrm{t}}^{\mathrm{single}} = \frac{F_{\mathrm{t}} \times 804.9}{156 \times A_{\mathrm{patch}}} \tag{55}$$

To compare θ with the observations, we had to consider that the θ measurements were taken by using a sharp-edged metal ring that was pushed to about 5mm to the soil. As the model simulates the water content of a 4 mm thick layer, the same water loss via evaporation would not result in the same volumetric water content as was measured in the 5 mm depth sample. Since none of the other soil modules have an effect on the water budget, we ran the model also with a Δz of 5 mm to get results that are comparable with the measurements.

4 Test simulation

The results of the test simulation are summarized in Fig. 4 and Table 4. GAG captures the emission relatively well. Considering that compared to the complexity of the phenomena, we use a simple model, the Person's correlation coefficient (hereafter referred to as "correlation") for NH_3 flux, can be considered as relatively high ($r = 0.54$, $p = 0.01$). The model slightly overestimates the fluxes before the rain event on the second day and it rather underestimates the measured values after it. The total emissions over the whole period from a single patch (modelled: 1.78 g N, measured: 3.88 g N) was underestimated. However, the model is still capable of reproducing the daily pattern of emissions with the mid-day peaks (except on the second day).

Soil pH is well simulated before the rain event, but similarly to the emission fluxes, it is underestimated afterwards. Overall there was a high and significant correlation ($r = 0.75$), between the model and the measurements. The sudden pH drop at the beginning of the rain event is thought to be caused by the lack of handling of CO_2 emission in the basic version of the model (see Sect. 5.3 for further examination of this effect).

Despite the large error bars on the measured mineral reduced soil N, its tendency is fairly similar to that of the TAN budget simulated by GAG. This is supported also by the significant correlation ($r = 0.63$) between the two variables. The model performance in terms of volumetric water content is very good with a slight underestimation from the fourth day after urine application. The statistical analysis showed a high correlation of 0.92 at a 0.001 significance level.

Analysing the NH_3 emission, pH and TAN budget together, it can be concluded that the rain event affected all three variables considerably. As it can be seen in the measured NH_x-N and pH data set (Fig. 4), their values right after the rain event peaked close to the level (or even higher) of the first peaks, which were generated by urea hydrolysis. This suggests that urea breakdown might restart after the rain event, explaining the difference between the modelled and measured values.

The GAG model used here does not account for any retention of urine by vegetation; however, it is possible that this occurs in reality. For example, Doak (1952) found that the urine held on the leaf surfaces was 36 % of fresh herbage

Table 3. Measured data used as input and the base of comparison with the model results, together with their original time resolution and their conversion to hourly time resolution.

Variable	Original time resolution	Adaptation to hourly time resolution
Input data		
χ_a ($\mu g\,N\,m^{-3}$)	Various (2–10 hourly)	Interpolated for the required hours.
u ($m\,s^{-1}$) – at 2.1 m PAR ($\mu mol\,m^{-2}\,s^{-1}$) T_{soil} (°C) – at 2 cm p (kPa) H ($MJ\,m^{-2}\,h^{-1}$)	Half hourly	Averaged for the given hour.
P (mm)	Half hourly	Summed up for the given hour.
T (°C) – at 3.85 m	Half hourly	Averaged for the given hour then calculated to 2 m height considering the average temperature gradient 6.5 °C km^{-1}: T (2 m) = T (3.85 m)–0.0065 × 1.85
R_{glob} ($MJ\,m^{-2}\,h^{-1}$)* RH (%)*	Hourly	–
Data used in the comparison		
F_t ($\mu g\,N\,m^{-2}\,s^{-1}$)	Various (2–10 hourly)	Measurements in the midpoints of the collection periods were considered as representative hourly averages.
θ ($m^3\,m^{-3}$) pH NH_x-N ($\mu g\,N\,(g\,soil)^{-1}$)	Various (2–19 hourly)	Measurements in the given hour were considered as representative hourly averages.

* From the National Climate Database for New Zealand (NIWA, 2015), all the other parameters were measured at the site.

Table 4. Statistics calculated for the comparison of the modelled and measured variables: root mean square error (RMSE), Pearson's correlation coefficient (r), the equation of the fitted least-squares equation (x – observation, y – model) and the level of significance of the correlation.

Variable*	RMSE	Equation	r	Level of significance
Ammonia emission flux	43.06 $\mu g\,N\,m^{-2}g^{-1}$	$y = 34.63+0.50x$	0.54	0.01
Soil pH	0.56	$y = 3.04+0.64x$	0.75	0.001
Model TAN budget vs. measured soil NH_x-N	–	–	0.63	0.01
Volumetric water content	0.05 $m^3\,m^{-3}$	$y = 0.10+0.67x$	0.92	0.001

* All the modelled and measured variables are the same as shown in Fig. 4. In the case of the emission flux, we compared the measured flux in the given measurement period with the value simulated at the time of the midpoint of the corresponding measurement period as explained in Table 2.

weight. In addition, the model assumptions do not allow the model soil pore to dry out (the minimum water content is at the permanent wilting point). In reality, however, the moisture content of urine retained on the leaf surfaces can evaporate easily and also some soil pores can completely dry out leaving behind the urine components undissolved. In such dry conditions, in lack of water urea hydrolysis stops. Then, after a rainfall, urea gets dissolved (as well as from the leaf surface it is washed into the soil) and hydrolysis can begin again, leading to a high peak in pH, TAN budget and consequently, NH_3 emission (see the further model results presented in Sect. S4).

5 Sensitivity analysis for non-meteorological parameters

In the following subsections we investigated module by module (2LCCPM, TAN budget, soil pH and water budget), how the model responds if we change the most critical model fea-

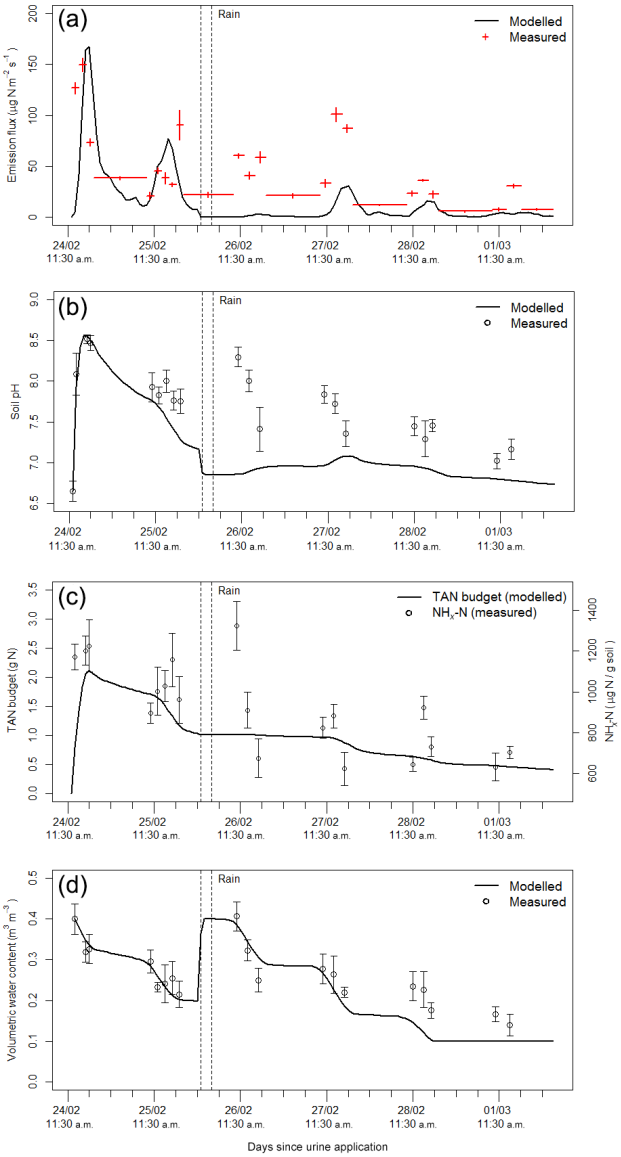

Figure 4. Comparison of modelled and measured values for NH_3 emission flux with the corresponding sampling periods of the measurements **(a)**, soil pH **(b)**, TAN budget and NH_x-N **(c)**, and volumetric water content of the top 5 mm layer of the soil **(d)**. The vertical error bars stand for the standard deviation in the measurements.

tures. In the case of the model constants, we tested how the modelled total emitted NH_3 (1.78 g N from a urine patch) changes over the modelling period by increasing and decreasing the given assumed model constant by 10 and 20 %. An overview of the results can be seen in Table 5. Comments on this table are provided in the following subsections.

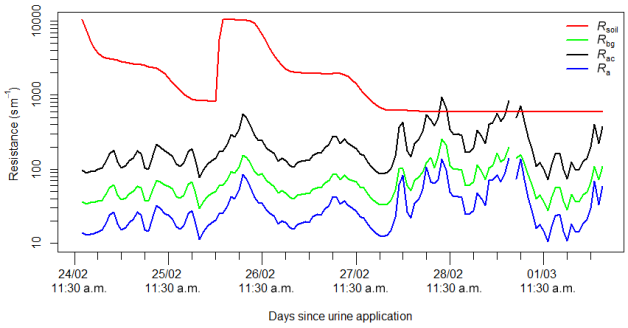

Figure 5. The atmospheric and the soil resistances over the modelling period. At the time of the missing values in R_{bg}, R_{ac} and R_a u_* was 0, for which resistances are infinite. In these cases emission flux was assumed to be 0.

5.1 Sensitivity to atmospheric resistances

As the net NH_3 flux is dominated by the soil emission flux (shown in Fig. S1 in the Supplement) we investigated here only the influence of the atmospheric resistances that affect the soil emission: R_{soil}, R_{bg}, R_{ac} and R_a. In Fig. 5, on the logarithmic scale it can be clearly seen that R_{ac} is the only atmospheric resistance that reaches the magnitude of the estimated R_{soil}.

For the simulation the main driver in temporal variation in R_{soil} is the actual volumetric water content (see Fig. 4). In the case of R_a, R_b, and R_{bg} there is at least one order of magnitude difference compared to the soil resistance, illustrating how the model performance is much less sensitive to the exact values of R_a, R_{ac}, and R_{bg}. The close temporal correlation of all these atmospheric resistances illustrates how they are all controlled by variations in wind speed and stability for a single canopy type. All the atmospheric resistances are the closest to the soil resistance when weak wind (large atmospheric resistances) is coupled to dry soil conditions (small soil resistance).

Among R_{bg}, R_{ac} and R_a, the parametrization of R_{bg} is the most uncertain. As Table 5 shows, the model is hardly sensitive to the value of z_1. In addition, u_{*g}, as formulated by Nemitz et al. (2001; Eq. S15), can also change in wide ranges without significantly affecting soil emission: R_{bg} could overcome the effect of R_{soil} on NH_3 emission only with a 10 times higher value of u_{*g}.

5.2 Sensitivity to the estimation of the TAN budget

The two uncertain factors in the estimation of the TAN budget are the thickness of the source layer (Δz) and the area of the patch (A_{patch}). Originally the model was run with a Δz of 4 mm; however, the sensitivity analysis showed (Table 5) that the change in total emission is approximately half of the change in Δz. Therefore, this source of error must be considered when model results are evaluated.

Table 5. The percentage of the change in total emitted NH_3 compared to the original run after modifying the different model constants by -20, -10, $+10$ and $+20$ %.

Module	Parameters	Total NH_3 emission change in response to change if parameter by			
		-20 %	-10 %	$+10$ %	$+20$ %
2LCCPM	z_l (height of the top of logarithmic wind profile)	$+0.02$ %	$+0.01$ %	-0.01 %	-0.02 %
TAN budget	Δz (thickness of NH_3 emission layer)	-11.7 %	-5.57 %	$+5.07$ %	$+10.5$ %
	A_{patch} (area of a urine patch)	$+1.39$ %	$+0.67$ %	-0.58 %	-1.61 %
Soil pH	β (soil buffering capacity)	$+1.29$ %	$+0.64$ %	-0.62 %	-1.22 %
Water budget	REW (readily evaporable water)	-2.98 %	-1.69 %	$+2.06$ %	$+4.32$ %
	θ_{fc} (field capacity)	-18.4 %	-6.63 %	$+6.34$ %	$+9.12$ %
	θ_{pwp} (permanent wilting point)	$+9.48$ %	$+4.60$ %	-4.42 %	-8.85 %

We also tested the model with Δz values between the ranges reported by Laubach et al. (2012; Fig. 6), and we found that the smaller the value of Δz, the higher the emission peak after urine application and the smaller the emission peaks in the following days. Firstly, this is caused by a smaller value of R_{soil}, due to the thinner source layer. Secondly, since the thinner layer can store less TAN in total, the source layer runs out of TAN more quickly leading to lower peaks in the later part of the modelling period.

In addition, we carried out a simulation with the maximum value of Δz, the penetration depth of incoming urine. Considering a soil layer with a thickness of y (dm), its water content can be expressed as $A_{\text{patch}} \times y \times (\theta_{\text{fc}} - \theta_{\text{pwp}})$. In this way, the urine deposited in a single patch (W_{urine}) in this experiment will fill up a $y = 0.2\,\text{dm} = 20\,\text{mm}$ thick soil layer. In this case, R_{soil} is at least 5 times higher than in the original run (or even bigger as there is more water in the source layer and, consequently, the layer dries out more slowly), that prevents NH_3 from escaping from the soil shortly after urine deposition. However, from the second day due to the higher available TAN budget, the fluxes are closer to the measurements.

In contrast to Δz, the model does not appear to be very sensitive to A_{patch}, with even a $+20$ % change causing less than 2 % change in total emission (Table 5). Laubach et al. (2012) estimated that the patches gradually grew by lateral diffusion, so that the area of the patches had doubled over the modelling period at the measurement site. Therefore, we conducted a simulation with GAG with a gradually growing patch, whose area doubles by the end of the period. In Fig. 7 we show the measured emission fluxes in relation to constant and gradually increasing values of A_{patch}, with the model results expressed for the whole area (converted based on the reorganized form of Eq. 55).

The largest difference with the growing patches, compared with the original run, occurred over the first 2 days. Then, the emission rates became smaller for the growing patches than with the constant patch area. The difference is a consequence of the combined effect of the growing source area ($156 \times A_{\text{patch}}(t_i)$) and the changing emission flux from a single patch.

In our model if a urine patch grows, it means physically that the initial liquid content is diffusing in the soil horizontally, leading to gradually declining volumetric water content. In addition, the evaporating area grows simultaneously, further intensifying the decrease of water content. Thus, R_{soil} will be smaller, allowing stronger NH_3 emissions in the first 2 days. This leads to lower TAN budget in the second half of the period, resulting in slightly smaller emissions than in the original run.

Finally, it has to be pointed out that we neglect an effect where the presence of hippuric acid in urine may increase urea hydrolysis and consequently, NH_3 emission (Whitehead et al., 1989). Whitehead et al. found that ignoring this triggering effect can lead to up to -10 % difference in the cumulative NH_3 volatilization (expressed as the proportion of the total nitrogen content of urine) compared to real urine containing the same amount of urinary N.

In the measurement campaign (Laubach et al., 2012) an artificial urine solution was spread on the experimental plot that was enriched with additional urea, so we compared a urea based model with a concentrated urea solution. Therefore, the difference in modelled and measured NH_3 fluxes, originating from this simplification, is possibly negligible, though it could be relevant if the model is applied in a real grazing situation. However, Whitehead et al. (1989) reported comparable differences in NH_3 emissions when they compared urea+hippuric acid solutions with different total N contents as well as different hippuric acid ratios.

The N content of urine ranges widely, not just amongst different animals, but also for different urination events by the same animal (Betteridge et al., 1986; Hoogendoorn et

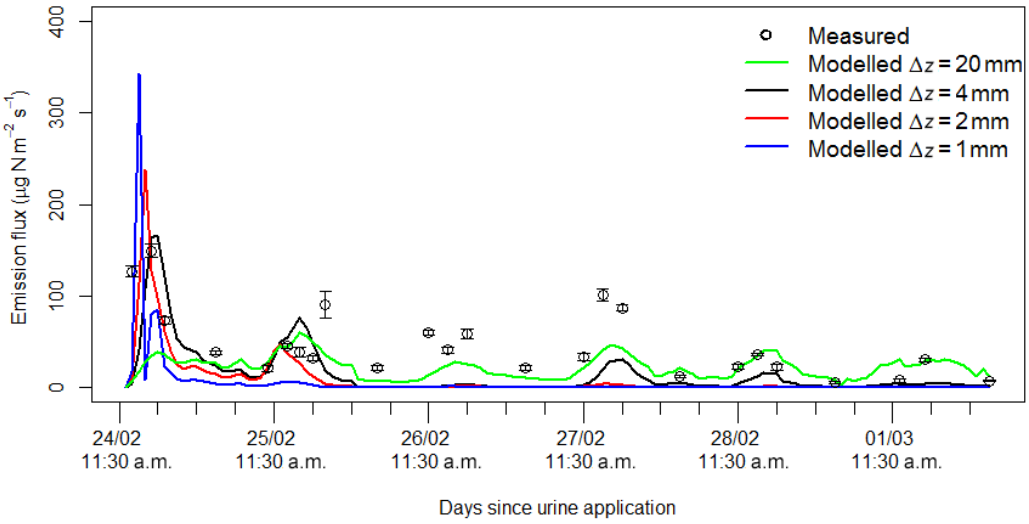

Figure 6. NH_3 fluxes from a urine patch with different Δz values.

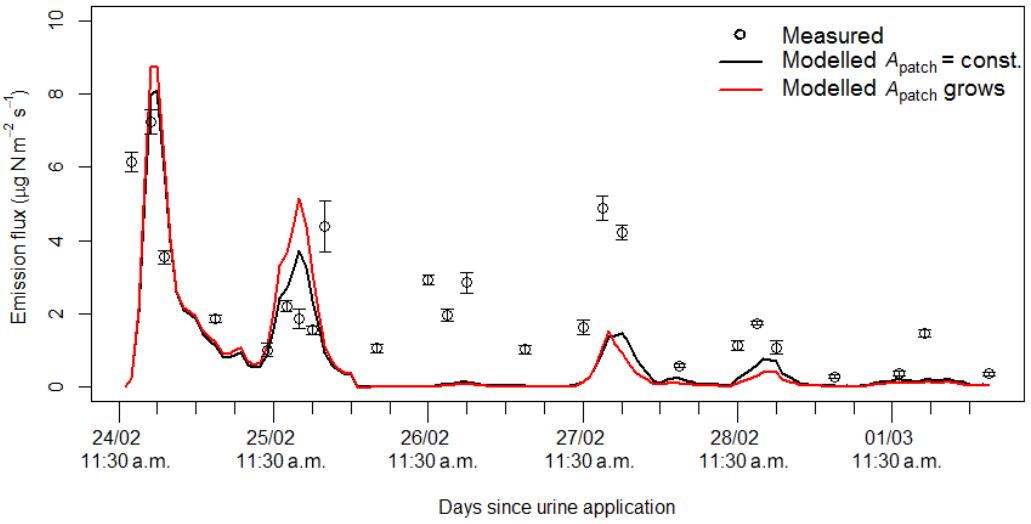

Figure 7. NH_3 fluxes from the whole experimental area with constant and with gradually growing urine patches.

al., 2010). This means that assuming an average N concentration of 8 g, according to Whitehead et al. (1989) can result in a 10 % overestimation in the cumulative volatilization of ammonia if the real nitrogen concentration was as low as $2\,g\,L^{-1}$. Similarly, in the case of the different ratios of hippuric acid and urea: if we assume that the hippuric acid N is an average of 0.8 % of the urea N (based on the data published by Dijkstra et al. (2013) this proportion varies between 1.4–0.36 %), according to Whitehead et al. (1989), the overestimation of the cumulative ammonia emission can be 10 % if the proportion of hippuric acid was minimal in reality.

As the effect of hippuric acid on urea hydrolysis is not widely investigated in the literature, at the moment the current approach is the best we can achieve to simulate the decomposition chemistry in urine. Although the field scale model would most likely underestimate ammonia emission due to the exclusion of the effect influence of hippuric acid, this underestimation may be partly balanced by the sources of overestimation in the model. Nonetheless, this uncertainty should be addressed when the model is applied on field scale.

5.3 Uncertainties in the estimation of soil pH

The main uncertainty in the model pH calculation is the applied buffering capacity (β). Apparently, the model is not highly sensitive to the tested changes of β; however, using the same β for every soil type could lead to errors in NH_3 emission estimation. Therefore, we tested the model with two

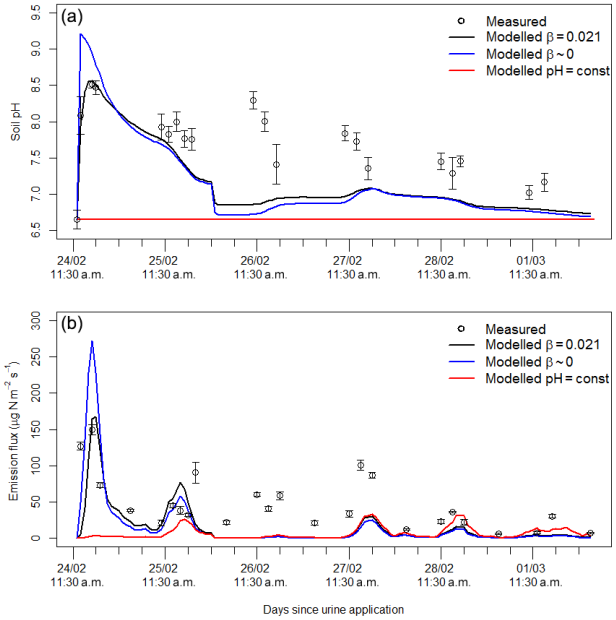

Figure 8. Soil pH under a urine patch **(a)** and NH_3 emission from it **(b)** with the currently applied buffering capacity ($\beta = 0.021$, original run), with no buffering ($\beta = 0$) and with constant pH, together with the measured values.

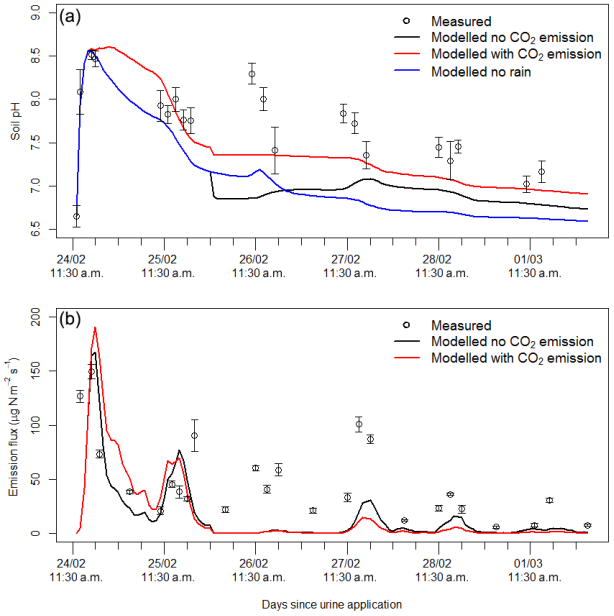

Figure 9. Soil pH under a urine patch **(a)** and NH_3 emission from it **(b)** without CO_2 emission (original run) and with an assumed CO_2 emission. On panel **(a)** the original run without rain is also plotted.

contrasting assumptions about buffering capacity: (a) when the system is totally buffered (pH is constant) and (b) when there is no buffering effect ($\beta = 0$). For the constant pH scenario, we chose the soil pH measured before the deposition of the urine patches (pH = 6.65).

The results show (Fig. 8) that with a constant soil pH, GAG fails to capture the first, dominant peak in emission. This suggests that dynamic modelling of pH is necessary for a proper estimation of NH_3 emission. By contrast, with $\beta = 0$ the model overestimates the first emission peak, while there is little difference in NH_3 fluxes in the rest of the period. Thus, with $\beta = 0$ the model is still capable of reproducing the daily cycle of NH_3 emission.

Another feature of the model which affects the pH as well as the emission flux calculation is the handling of CO_2 emission following urine deposition (as discussed in Sect. 2.6). A sudden drop can be seen in the simulated pH at the beginning of the rain event (Fig. 4b), which tends to disappear if there is no rainfall over the modelling period (Fig. 9a, blue line).

At the beginning of the rainfall the volume of the gaseous part of the model soil pore suddenly shrinks as the liquid part grows with the incoming water. As a result (given that the base model does not allow CO_2 emission), gaseous CO_2 accumulates in the soil pore and is forced to dissolve into the liquid phase. This intensifies the formation of carbonic acid and its subsequent dissociation, leading to a significant drop in pH.

In the experiment by Wang et al. (2013) CO_2 emission over urine patches peaked within 8 h after urine application, while both Ma et al. (2006) and Lin et al. (2009) found that the first peak of CO_2 emission occurred on the first day. In addition, Lin et al. (2009) reported a high correlation ($r = 0.63$) between CO_2 emission and soil temperature, suggesting a strong temperature dependency (similarly, we found a correlation of 0.58 for NH_3, see Table 6).

Based on the above similarities between the temporal development of NH_3 and CO_2 emission, to test the effect of CO_2 emission on the GAG simulations, we assumed that the amount of emitted CO_2 is half of the emitted NH_3 in moles (similarly to urea hydrolysis where from one urea molecule two NH_4^+ and one HCO_3^- ions are produced). Even if this is a simplification for CO_2 emission, the results show the potential of future more comprehensive incorporation of the process into the model. By accounting for CO_2 emission the modelled pH values were found to be closer to the measured ones, while the sudden drop at the start of the rain event also largely disappeared (Fig. 9). As a consequence of these changes, the NH_3 emission fluxes were larger before the second day and – due to the larger loss in TAN budget – were smaller in the latter part of the experiment.

The apparently contradictory results with the assumed CO_2 emission above – better agreement in pH and poorer agreement in the NH_3 fluxes – suggest that the TAN in the model soil pore is depleted too early, leading to a significant underestimation of the emission fluxes in the second part of the modelling period. Two scenarios can be envisaged that

Table 6. The results of the sensitivity analysis to the different meteorological variables. We changed these by $\pm\Delta x$ derived based on the minimum and the maximum of the given parameter over the modelling period ($\Delta x = (\text{Max–Min})/10$), and calculated the difference in the total emission over the modelling period compared to the original run. We also calculated the correlation (r) between the original input variables and the modelled hourly NH_3 emission fluxes.

Variable	Min	Max	Δx	Total NH_3 emission change in response to change in parameter by		
				$-\Delta x$	$+\Delta x$	r
u (ms^{-1})	0.62	8.59	0.80	−5.5 %	+4.7 %	0.40
T_{soil} (°C)	11.6	27.9	1.64	−2.6 %	+2.7 %	0.58
p (kPa)	99.9	102.3	0.24	+0.0 %	−0.0 %	−0.33
T_{air} (°C)	13.5	29.0	1.56	−2.4 %	2.9 %	0.60
R_{glob} ($MJ\,m^2\,h^{-1}$)[a]	0.00	3.32	0.33	−2.0 %	+4.1 %	0.32
RH (%)[b]	30	95	6.50	+9.1 %	−8.6 %	−0.49
RH (%)[b]	only for evaporation[c]			+3.2 %	−2.8 %	–
P (mm)[d]	0.00	0.83	0.08	−0.7 %	+0.8 %	–
T_{air} and T_{soil} (°C)	–	–	–	−4.9 %	+5.7 %	–

[a] When changed by $-\Delta x$, negative values were replaced by 0. [b] When changed by $+\Delta x$, values greater than 100 % were reduced to 100 %. [c] In this test RH was modified by the same extent but only in the evaporation module. [d] The hourly precipitation sum was changed only in the hours when there was precipitation originally.

could cause this effect: scenario (1) the simulated rate of urea hydrolysis is higher than it is in reality, or scenario (2) at the experimental site fresh urea that had been intercepted by leaves and dried onto leaf surfaces, was washed to the soil during the rain event, thereby maintaining NH_3 emission afterwards.

As we discussed in Sect. 4, the measurement data also suggest the feasibility of scenario (2). Therefore, we tested the model – assuming that 10 % of the applied urine was intercepted on the leaf surface – with 1.5 g of urea washed in during the rain event (see Sect. S4). With this assumption the modelled values were in better agreement with observations not only in the case of NH_3 exchange flux (Fig. 10d) but also the TAN budget and soil pH (see both at Fig. S2). These results clearly support the idea of the possible restart of breakdown of the fresh urea penetrating to the soil dissolved in rain water.

5.4 Uncertainties in the estimation of the water budget

The GAG model is found to be sensitive to model constants related to the water budget, especially field capacity, θ_{fc} (Table 5). The high sensitivity to a low value of θ_{fc} appears to be because this limits the amount of urine which remains available for hydrolysis and NH_3 emission from the source layer. In addition, we also found large differences in total ammonia emission when we modified the permanent wilting point. On regional scale it is not likely to have a database of measured θ_{fc} and θ_{pwp} values over a dense grid. It is more feasible that a soil texture map can be used for this purpose with recommended values of θ_{fc} and θ_{pwp} values for different soil types. Both θ_{fc} and θ_{pwp} can have an uncertainty of ±20 % (e.g. in Allen et al., 1998 for sandy loam $\theta_{fc} = 0.18$–0.28), similarly to the extent of modification in the current sensitivity test. Therefore, at regional application, this uncertainty has to be considered when interpreting the model results.

In addition, a limitation of the calculation of the water budget is that GAG does not account for the water movement in the soil, including the effect of capillary force, diffusion of water in the soil as well as the concentration of TAN and urea within the moving liquid. However, the simulation of these processes is very complex. Shorten and Pleasants (2007) published a system of partial differential equations describing these processes, which could be a basis for further development of GAG.

6 Sensitivity to meteorological factors

For quantitative comparison, we show a variety of meteorological factors and the hourly NH_3 emission fluxes in Fig. 10. The NH_3 emission flux peaks almost every day shortly after midday, when soil temperature reaches its maximum. The only exception is the second day after urine application when the curve of emission flux stayed flat in the simulation, which was linked to the rain event as discussed in the previous sections.

The close relationship between the soil as well as the air temperature and NH_3 emission fluxes can be also seen in the calculated high correlations ($r = 0.58$ and $r = 0.60$, respectively). Compared with the other meteorological factors (Table 6) the relationship with these two seems to be the strongest. Relative humidity apparently has a slightly weaker, but still considerable role in the simulated NH_3 volatilization ($r = -0.49$). Based on the correlation values, there was a weaker relationship with wind speed ($r = 0.40$), which may

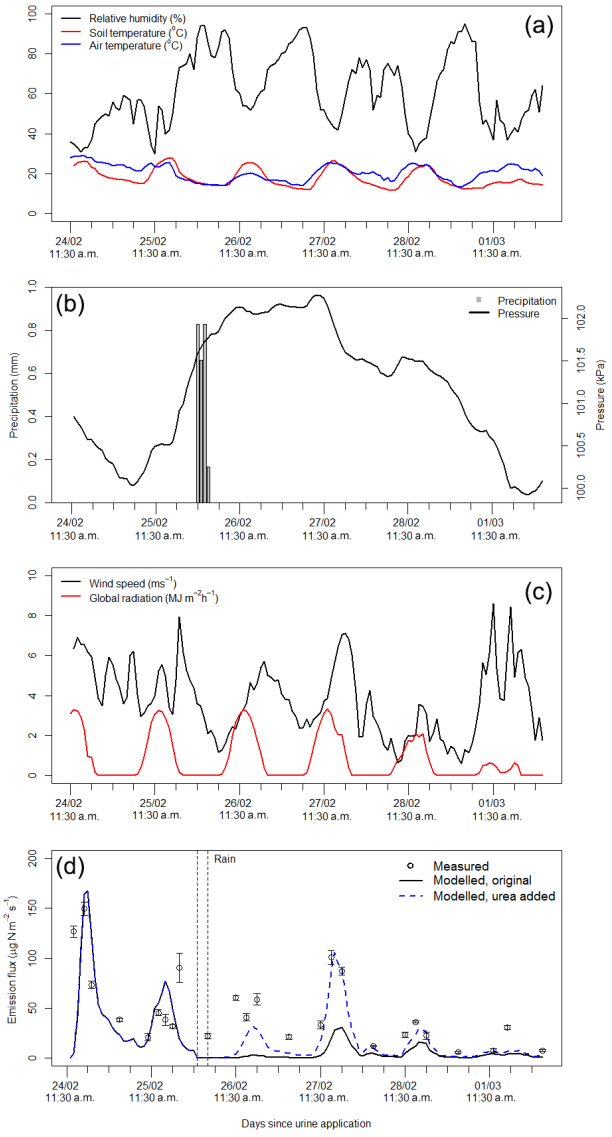

Figure 10. The investigated meteorological variables (relative humidity, soil, and air temperature **(a)**, precipitation and surface pressure **(b)**, wind speed and global radiation **c**) and the hourly NH_3 fluxes **(d)** simulated by the original model (black line) and the modified model (dashed blue line), in which fresh urea was assumed to be washed into the soil during the rain event.

be related to the fact that simulated R_{soil} provided a much larger constraint on NH_3 soil emission than the atmospheric resistances (Fig. 5). Global radiation as well as atmospheric pressure indicated a weaker influence (lower than $r = 0.40$ in absolute value) on the simulated NH_3 emission.

We also carried out a sensitivity analysis to the different meteorological parameters. To test the sensitivity to a given parameter, we modified it, while keeping all the other parameters the same, and we ran a simulation with GAG. At the end of every simulation we calculated the total ammonia emission over the period, and expressed it as the percentage difference compared to the total emission in the original run. To get comparable results, we modified the original data sets in every case by $\pm\Delta x$, calculated as 10 % of the difference between the measured minimum and maximum value of the given parameter over the modelling period.

Table 6 shows that NH_3 emission is the most sensitive to relative humidity (the differences in total emission were +9.1 and −8.6 %) and wind speed (the differences were −5.5 and 4.7 %). In addition, a relatively high difference (+4.1 %) was observed in the case of global radiation when its values were raised by Δx.

In spite of the high correlations, when soil and air temperature were modified separately, we got relatively small anomalies in the total emissions (less than 3 % in absolute value for both soil and air temperature). However, when air and soil temperature were adjusted together (assuming that the change of these two temperature parameters is parallel), the differences were larger (see Table 6). Only low sensitivity was detected in the case of atmospheric pressure and hourly precipitation.

The results for wind speed and the different temperature parameters can be easily explained. Wind plays a governing role in turbulent mixing of the quasi-laminar and turbulent layer; consequently, it has a considerable effects on the vertical atmospheric transfer of ammonia. Regarding temperature, urea hydrolysis as well as the compensation point both in the stomata and the soil pores follow an exponential function of temperature.

Sutton et al. (2013) used a metric, Q_{10}, to express the relative increase in NH_3 emission over a range of 10 °C. We derived Q_{10} by running the model with 10 °C higher air and soil temperature. The resulted value of 1.26 compared to that reported by Sutton et al. for grazing (4.7 for sheep sites) suggest a rather modest temperature sensitivity. The model showed similarly modest sensitivity when we tested it with three and five times higher N concentration in urine (allowing more TAN in the later stages of the modelling period; Table 7). Based on this results it can be concluded that the lower Q_{10} values are not a consequence of the limited TAN available in the later stages of the modelling period.

A possible explanation for the difference between the reported and the simulated temperature sensitivity can be the temporal development of Q_{10} over time (Fig. 11). We calculated the Q_{10} values for every time step as the ratio of the cumulative emissions from the higher temperature model version and the original one, and we found that NH_3 emission is more sensitive to temperature in the first 6 h than in the later stages. Considering that over a grazed field urine patches are deposited in every time step, creating a peak in the individual patch emissions, the total emission for the whole field will be presumably more sensitive to temperature than that for a single urine patch.

RH has a dual effect on NH_3 emission. Firstly, it plays a vital role in the water budget and secondly, it also influences

Table 7. Comparison of the total emission (g N) from a single urine patch from the model runs assuming different N content of the urine deposited with the original temperature and +10 °C (both in air and the soil temperature) scenario. We also calculated Q_{10} as the ratio of the total emission for the original and the amended temperature scenario.

	Total emission (g N)		
	Original	+10 °C	Q_{10}
Base run	95.8	121.0	1.26
3 × N content	290.4	370.8	1.28
5 × N content	489.7	613.8	1.25

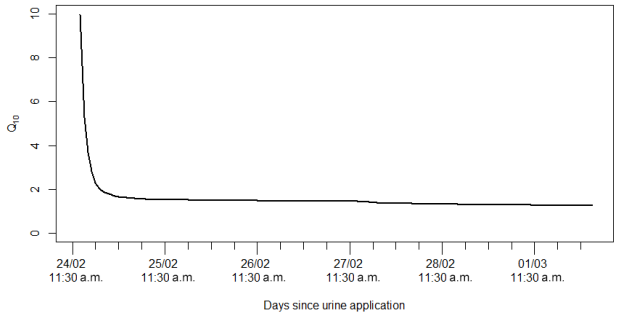

Figure 11. Calculated Q_{10} values for the cumulative NH_3 emissions between urine application and the given time step.

the deposition of ammonia to the leaf surface. We tested the sensitivity in a model scenario where relative humidity was modified only in evaporation, and we observed only a +3.2 % difference for $-\Delta x$ and −2.8 % for $+\Delta x$ change. This clearly suggests that the effect of RH on NH_3 emission in GAG is stronger through deposition to leaf surfaces than through soil evaporation.

The physical explanation for the opposite change in RH and the total emission is that at higher values of relative humidity the formation of a water film on the leaf surface is more likely. As a result, deposition is more effective (see the different fluxes in Fig. S1), which will generate a loss in the net emission flux over the whole system (including the exchange with soil and stomata as well as the deposition to cuticle).

Although precipitation was shown to suppress modelled emission, the total emission over the period was not strongly sensitive to a change of ±10 % (±0.08 mm; Table 6). This is a result of the model features that (1) allow only a $(\Delta z \times (\theta_{fc} - \theta_{pwp}) =)$ 1.2 mm of maximum liquid content in the model soil pore and (2) do not allow wash out TAN from the source layer. Therefore, in the GAG model even a heavy rain event (> 6 mm h^{-1}) – apart from the slight effect on evaporation – has the same effect as a modest 1.2 mm h^{-1} of precipitation. In the test simulation during the rain event the soil reached its maximum water content (θ_{fc}). We found that by decreasing the amount of total precipitation so that the soil does not reach θ_{fc}, the maximum difference in total emission was +3 %.

In addition, the timing of the rain event can also lead to a difference in total NH_3 emission due to the associated increase in R_{soil} which tends to suppress the rate of volatilization. We found that the timing of the rain event affects the NH_3 emission, with up to a 6 % reduction or 2 % increase in the total NH_3 emission (see the model results in Sect. S5). Nevertheless, it must be emphasized that in reality NH_3 can escape from wet soil not only through gaseous diffusion in the empty soil pores. Dissolved NH_3 may get to the soil surface also through the solution and can be volatilized from there (Cooter et al., 2010). This is not taken into account in the present soil resistance parametrization. Therefore, the effect of rainfall might not be as strong as this experiment showed. On the other hand, as we mentioned earlier, during a dry period urea hydrolysis may slow or stop in the absence of water. If the rainfall begins after such a dry period, by restarting urea hydrolysis, it can even enhance ammonia emission rather than suppress it.

7 Discussion

We constructed a novel NH_3 emission model for a urine patch (GAG) that is capable of simulating the TAN and the water content of the soil under a urine patch and also soil pH (see the list of all the model parameters and variables together with their abbreviations in Table 8). The difference between the simulated and measured values suggested that to improve the model, further investigation is needed regarding the effect of a possible restart of urea hydrolysis with rain events also soil pH.

The sensitivity analysis to the uncertain parameters showed that soil resistance had more than an order of magnitude stronger effect on soil NH_3 emission than the atmospheric resistances. An exceptional case is when weak wind is coupled with dry soil, in which case atmospheric and soil resistances may become comparable.

Our sensitivity analysis also showed that if the thickness of the source layer (Δz) is modified by a given percentage, the difference in the resulting total ammonia emission over the modelling period will be half of this percentage. Therefore, this source of error must be considered when model results are evaluated. Future work should also consider how independent data sets can help characterize the depth of the effective soil emission layer, as well as consider how both downward and upward migration of TAN with deeper soil layers can be addressed.

In the case of pH we showed that process-based modelling of pH is necessary to reproduce the very first high peak in NH_3 emission. The simulations were carried out with an assumed soil buffering capacity. While this affects the timing of emissions, we found that the total emission is not sensitive

Table 8. Abbreviations.

Abbreviation (unit)	Model variable
$\frac{D_{O_3}}{D_{NH_3}}$	Ratio of diffusivity of O_3 and NH_3
$[X]$ (mol dm^{-3})	Concentration of compound X
A	Parameter for calculating R_w
A_h	Parameter for urea hydrolysis simulation
A_{patch} (m^2)	Area of a urine patch
B_C (mol)	Carbon content of the source layer (originating from urea)
B_{H_2O} (dm^3)	Water budget in the source layer
B_{H_2O}(max) (dm^3)	Maximal water amount in the source layer
B_{H_2O}(min) (dm^3)	Minimal water amount in the source layer
B_{H_2O}' (dm^3)	Precalculated water budget in the source layer
$B^{Tot}_{H_2O}$ (dm^3)	Total water budget under a urine patch
B_N (mol)	TAN + gaseous ammonia content in the source layer
B_{TAN} (g N)	TAN budget in the source layer
B_{urea} (g N)	Urea budget under a urine patch
B_X (mol) ($X = H_2CO_3$, HCO_3^-, CO_3^{2-}, $CO_{2(g)}$, NH_4^+, $NH_{3(aq)}$, $NH_{3(g)}$, H^+)	Budget of a chemical compound X under the urine patch
C_d	Effect of day and night on evapotranspiration
c_N (N dm^{-3})	N content of the urine
c^{Tot}_N (g N dm^{-3})	Urine N content after dilution in the soil
D_g (m^2 s^{-1})	Diffusivity of NH_3 in air
E (mm h^{-1})	Soil evaporation rate
e_a (kPa)	Actual water vapour pressure
e_s (kPa)	Saturated water vapour pressure
ET (mm h^{-1})	Actual evapotranspiration rate
ET_0 (mm h^{-1})	Reference evapotranspiration rate
f_c (m^2 m^{-2})	Vegetation coverage
F_f (µg N m^{-2} s^{-1})	NH_3 exchange flux with the foliage
F_g (µg N m^{-2} s^{-1})	NH_3 exchange flux over the ground
F_{sto} (µg N m^{-2} s^{-1})	NH_3 exchange flux with stomata
F_t (µg N m^{-2} s^{-1})	Total NH_3 exchange flux over the canopy
f_w (m^2 m^{-2})	Wetted uncovered soil fraction
F_w (µg N m^{-2} s^{-1})	NH_3 deposition flux to water and waxes on the leaf surface
G (MJ m^2 h^{-1})	Soil heat fux
g_{light}	Relative conductance for the effect of light on g_s
g_{max} (mmol O_3 m^{-2})	Maximal stomatal conductance
g_{min}	Minimal relative stomatal conductance
g_{pot}	Relative stomatal conductance for the effect of plant phenological state on g_s
g_s (mmol O_3 m^{-2})	Stomatal conductance for O_3
g_{SWP}	Relative conductance for the effect of soil water on g_s
g_{temp}	Relative conductance for the effect of temperature on g_s
g_{VPD}	Relative conductance for the effect of vapour pressure deficit on g_s
$H(X)$ (mol dm^{-3} (mol dm^{-3})$^{-1}$)	Henry coefficient for the given gas X
i_C (mol)	Carbon input to the urine patch
i_N (mol)	TAN input to the urine patch (TAN production in moles)
$K(X)$ (mol dm^{-3})	Dissociation constant for the given compound X
K_c	Crop coefficient
K_{cb}	Transpiration coefficient
K_e	Soil evaporation coefficient
k_h	Urea hydrolysis constant
L (m)	Monin-Obukhov length
LAI (m^2 m^{-2})	Leaf area index
N_{app} (kg N ha^{-1})	Nitrogen applied over a urine patch
N_{prod} (g N)	TAN production

Table 8. Continued.

Abbreviation (unit)	Model variable
P (mm)	Precipitation
PAR (μmol m^2 s^{-1})	Photosynthetically active radiation
Q_{10}	Relative increase in NH_3 emission over a range of 10 °C
R_a (s m^{-1})	Aerodynamic resistance over the canopy
R_{ac} (s m^{-1})	Aerodynamic resistance in the canopy
R_b (s m^{-1})	Resistance of the quasi-laminar layer over the canopy
R_{bg} (s m^{-1})	Resistance of the quasi-laminar layer in the canopy
REW (mm)	Readily evaporable water in the soil
R_{glob} (MJ m^2 h^{-1})	Global radiation/solar radiation
RH (%)	Relative humidity
R_n (MJ m^2 h^{-1})	Net radiation
r_{RX} (mol)	Consumption or production of a given compound in reaction X.
R_{soil} (s m^{-1})	Soil resistance
R_{sto} (s m^{-1})	Stomatal resistance
R_{sto} (O_3)(s m^{-1})	Stomatal resistance for O_3
R_w (s m^{-1})	Cuticular resistance
R_w (min) (s m^{-1})	Minimal cuticular resistance
S_{MI}	Soil moisture index
T (°C)	Air temperature at 2 m
t_i	ith time step
T_{soil} (°C)	Soil temperature
u (m s^{-1})	Wind speed
u_* (m s^{-1})	Friction velocity
u_{*g}	Friction velocity at ground level in the canopy
U_{add} (g N)	Urea added to the source layer
V_{air} (dm^3)	Volume of the air in the source layer
W_{evap} (dm^3)	Water loss as soil evaporation from the urine patch
W_{rain} (dm^3)	Water input as rain water over the urine patch
W_{urine} (dm^3)	Volume of urine
z_l (m)	Height of the top of logarithmic wind profile
z_w (m)	Height of wind measurement
α	Parameter for calculating R_{ac}
β (mol H$^+$ (pH unit)$^{-1}$ dm^{-3})	Soil buffering capacity
β_{patch} (mol H$^+$ (pH unit)$^{-1}$)	Buffering capacity of the source layer
γ (kPa °C^{-1})	Psychometric constant
Γ_p	NH_3 emission potential in the soil pore
Γ_{sto}	NH_3 emission potential from the stomata
Γ_{sto}(max)	Maximal NH_3 emission potential from the stomata
Δ (kPa °C^{-1})	Slope of saturation vapour pressure curve
Δz (mm)	Thickness of the source layer
Δz_E (m)	Thickness of the evaporation layer
θ (m^3 m^{-3})	Volumetric water content
θ_{fc} (m^3 m^{-3})	Field capacity
θ_{por} (m^3 m^{-3})	Porosity
θ_{pwp} (m^3 m^{-3})	Permanent wilting point
ξ	Soil tortuosity
τ (days)	Decay parameter
χ_a (μg N m^{-3})	Air concentration of NH_3
χ_c (μg N m^{-3})	Compensation point above the vegetation
χ_p (μg N m^{-3})	Compensation point in the soil pores
χ_{sto} (μg N m^{-3})	Stomatal compensation point
χ_{z0} (μg N m^{-3})	Canopy compensation point

to the value of β and it is able to represent the main temporal development of ammonia emission even with 0 buffering capacity.

On the other hand, we found that incorporating a simple estimation of CO_2 emission allows the model to reproduce the measured soil pH values more accurately than neglecting CO_2 emissions. Future work should therefore consider how CO_2 fluxes could be incorporated more systematically into the GAG model.

The model turned out to be sensitive to the value of soil water content at field capacity (θ_{fc}) and at permanent wilting point (θ_{pwp}). Thus, at regional scale application, where mostly recommended values of these parameters are available, this error has to be considered when interpreting the model results.

Our results support the vital role of temperature in NH_3 exchange, showing a high correlation with the temperature parameters as well as strong sensitivity to them. Nevertheless, the GAG model provides only a modest overall temperature dependence in total NH_3 emission compared to what was reported in the literature earlier. A possible explanation for this is that, according to our results, the sensitivity to temperature is higher close to urine application than in the later stages and may depend also on interactions with other nitrogen cycling processes.

In addition, we found that wind speed and relative humidity are also significant influencing factors. In the case of RH we observed a dual effect through its effect on the modelled soil evaporation and the modelled deposition to leaf surfaces, with the latter being the dominant term for the present simulations.

In contrast to the NH_3 volatilization models published earlier for urea affected soils (Sherlock and Goh, 1985; Rachhpal and Nye, 1986), our model, incorporating a canopy compensation point model, accounts for the effect of the meteorological parameters on net canopy exchange of NH_3. Compared with the model constructed by Laubach et al. (2012), GAG is capable of simulating the influence of vegetation on NH_3 exchange. In addition, our model also simulates soil pH, the TAN and the water content of the soil, allowing it to predict net NH_3 emission, instead of operating only in "inverse" mode, calculating soil parameters based on flux measurements.

Rachhpal and Nye (1986) suggested a solution for dynamic modelling of soil pH with a set of continuity equations. However, in their approach the dissociation coefficients, as well as the urea hydrolysis rate, were independent of temperature. Even though the GAG model accounts for the same chemical reactions, it incorporates a different mathematical description and accounts for the missing temperature dependencies.

Dynamic simulation of soil pH is novel among the NH_3 exchange models on the ecosystem scale. In the PaSim ecosystem model (Riedo et al., 2002) pH is treated as a constant, and the same is true for the VOLT'AIR model (Génermont and Cellier, 1997) developed for simulating NH_3 emission related to fertilizer and manure application. Furthermore, the framework of GAG is simpler and requires less input data than the VOLT'AIR model. Therefore, for grazing situations, it is much easier to adapt GAG on both field and regional scale.

As our final goal is to apply the model to regional scale, simplicity was a key aspect of the model development, avoiding extra steps of model simplification in the later stages of our project. Therefore, the model operates with a single layer approach in the soil. Although this is a simpler approach compared to some of the above-mentioned models (Rachhpal and Nye, 1986; Génermont and Cellier, 1997; Riedo et al., 2002), the model code is easily amendable, which enables us to add new modules to GAG in the future.

Since all the input parameters can be obtained for larger scales, considering the possible errors, GAG is concluded to be suitable for larger-scale application, such as in regional atmospheric and ecosystem models. In addition, as it is dynamically driven by weather parameters, it can serve as a base for further studies of climate dependency of ammonia emission from grazed fields on both plot and regional scale.

8 Conclusions

We report the description of a process-based, weather-driven ammonia exchange model for a urine patch that is capable of simulating the TAN and the water content of the soil under a urine patch and also soil pH.

The model tests suggest that ammonia volatilization from a urine patch can be affected by the possible restart of urea hydrolysis after a rain event as well as CO_2 emission from the soil.

The vital role of temperature in NH_3 exchange is supported by our model results; however, the GAG model provides only a modest overall temperature dependence in total NH_3 emission compared with the literature. This, according to our findings, can be explained by the higher sensitivity to temperature close to urine application than in the later stages and may depend on interactions with other nitrogen cycling processes. In addition, we found that wind speed and relative humidity are also significant influencing factors. These relationships need to be further tested in relation to field measurements.

For simplicity, to allow subsequent regional upscaling, the model operates with a single soil layer approach, neglecting water movement and solution mixing in the soil. Although this is a limitation of the current model version, the model code is easily amendable, which facilitates to add new modules to GAG in the future.

Considering that all the input parameters can be obtained for larger scales, GAG is potentially suitable for field and regional scale application, serving as a tool for further investi-

gation of the effects of climate change on ammonia emissions and deposition.

The Supplement related to this article is available online at doi:10.5194/bg-13-1837-2016-supplement.

Acknowledgements. This work was carried out within the framework of the ÉCLAIRE project (Effects of Climate Change on Air Pollution and Response Strategies for European Ecosystems) funded by the EU's Seventh Framework Programme for Research and Technological Development (FP7).

Edited by: X. Wang

References

Allen, R. G., Pereira, L. S., Raes, D., and Smith, M.: Crop evapotranspiration-Guidelines for computing crop water requirements, FAO Irrigation and drainage paper 56, FAO, Rome, Italy, 1998.

Bates, R. G. and Pinching, G. D.: Acidic dissociation constant of ammonium ion at 0 °C to 50 °C, and the base strength of ammonia, J. Res. Nat. Bur. Stand., 42, 419–430, doi:10.6028/jres.042.037, 1949.

Betteridge, K., Andrewes, W. G. K., and Sedcole, J. R.: Intake and excretion of nitrogen, potassium and phosporus by grazing steers, J. Agr. Sci., 106, 393–404, 1986.

Burkhardt, J., Kaiser, H., Goldbach, H., and Kappen, L.: Measurements of electrical leaf surface conductance reveal re-condensation of transpired water vapour on leaf surfaces, Plant Cell Environ., 22, 189–196, doi:10.1046/j.1365-3040.1999.00387.x, 1999.

Burkhardt, J., Flechard, C. R., Gresens, F., Mattsson, M., Jongejan, P. A. C., Erisman, J. W., Weidinger, T., Meszaros, R., Nemitz, E., and Sutton, M. A.: Modelling the dynamic chemical interactions of atmospheric ammonia with leaf surface wetness in a managed grassland canopy, Biogeosciences, 6, 67–84, doi:10.5194/bg-6-67-2009, 2009.

Cooter, E. J., Bash, J. O., Walker, J. T., Jones, M. R., and Robarge, W.: Estimation of NH_3 bi-directional flux from managed agricultural soils, Atmos. Environ., 44, 2107–2115, doi:10.1016/j.atmosenv.2010.02.044, 2010.

Dasgupta, P. K. and Dong, S.: Solubility of ammonia in liquid water and generation of trace levels of standard gaseous ammonia, Atmos. Environ., 20, 565–570, doi:10.1016/0004-6981(86)90099-5, 1986.

Dijkstra, J., Oenema, O., van Groenigen, J. W., Spek, J. W., van Vuuren, A. M., and Bannink, A.: Diet effects on urine composition of cattle and N_2O emissions, Animal, 7, 292–302, doi:10.1017/S1751731113000578, 2013.

Doak, B. W.: Some chemical changes in the nitrogenous constituents of urine when voided on pasture, J. Agr. Sci., 42, 162–171, 1952.

EDGAR: Emissions Database for Global Atmospheric Research v4.2, available at: http://edgar.jrc.ec.europa.eu/ (last access: 20 May 2014), 2011.

Emberson, L., Simpson, D., Tuovinen, J.-P., Ashmore, M., and Cambridge, H.: Towards a model of ozone deposition and stomatal uptake over Europe, EMEP MSC-W Note 6/2000, The Norwegian Meteorological Institute, Oslo, Norway, 2000.

Farquhar, G. D., Firth, P. M., Wetselaar, R., and Weir, B.: On the Gaseous Exchange of Ammonia between Leaves and the Environment: Determination of the Ammonia Compensation Point, Plant. Physiol., 66, 710–714, doi:10.1104/pp.66.4.710, 1980.

Flechard, C. R., Fowler, D., Sutton, M. A., and Cape, J. N.: A dynamic chemical model of bi-directional ammonia exchange between semi-natural vegetation and the atmosphere, Q. J. Roy. Meteor. Soc., 125, 2611–2641, doi:10.1002/qj.49712555914, 1999.

Flechard, C. R., Massad, R.-S., Loubet, B., Personne, E., Simpson, D., Bash, J. O., Cooter, E. J., Nemitz, E., and Sutton, M. A.: Advances in understanding, models and parameterizations of biosphere-atmosphere ammonia exchange, Biogeosciences, 10, 5183–5225, doi:10.5194/bg-10-5183-2013, 2013.

Fowler, D., Coyle, M., Skiba, U., Sutton, M. A., Cape, J. N., Reis, S., Sheppard, L. J., Jenkins, A., Grizzetti, B., Galloway, J. N., Vitousek, P., Leach, A., Bouwman, A. F., Butterbach-Bahl, K., Dentener, F., Stevenson, D., Amann, M., and Voss, M.: The global nitrogen cycle in the twenty-first century, Philos. T. R. Soc. B, 368, 20130164, doi:10.1098/rstb.2013.0164, 2013.

Galloway, J. N., Townsend, A. R., Erisman, J. W., Bekunda, M., Cai, Z., Freney, J. R., Martinelli, L. A., Seitzinger, S. P., and Sutton, M. A.: Transformation of the Nitrogen Cycle: Recent Trends, Questions, and Potential Solutions, Science, 320, 889–892, doi:10.1126/science.1136674, 2008.

Génermont, S. and Cellier, P.: A mechanistic model for estimating ammonia volatilization from slurry applied to bare soil, Agr. Forest Meteorol., 88, 145–167, doi:10.1016/S0168-1923(97)00044-0, 1997.

Harned, H. S. and Davis, R.: The Ionization Constant of Carbonic Acid in Water and the Solubility of Carbon Dioxide in Water and Aqueous Salt Solutions from 0 to 50°, J. Am. Chem. Soc., 65, 2030–2037, doi:10.1021/ja01250a059, 1943.

Harned, H. S. and Scholes, S. R.: The Ionization Constant of HCO_3^- from 0 to 50°, J. Am. Chem. Soc., 63, 1706–1709, doi:10.1021/ja01851a058, 1941.

Hellsten, S., Dragosits, U., Place, C. J., Vieno, M., Dore, A. J., Misselbrook, T. H., Tang, Y. S., and Sutton, M. A.: Modelling the spatial distribution of ammonia emissions in the UK, Environ. Pollut., 154, 370–379, doi:10.1016/j.envpol.2008.02.017, 2008.

Hicks, B. B., Baldocchi, D. D., Meyers, T. P., Hosker Jr., R. P., and Matt, D. R.: A preliminary multiple resistance routine for deriving dry deposition velocities from measured quantities, Water Air Soil Pollut., 36, 311–330, doi:10.1007/BF00229675, 1987.

Hoogendoorn, C. J., Betteridge, K., Costall, D. A., and Ledgard, S. F.: Nitrogen concentration in the urine of cattle, sheep and deer grazing a common ryegrass/cocksfoot/white clover pasture, New Zealand, J. Agr. Res., 53, 235–243, doi:10.1080/00288233.2010.499899, 2010.

Horváth, L., Asztalos, M., Führer, E., Mészáros, R., and Weidinger, T.: Measurement of ammonia exchange over grassland in the

Hungarian Great Plain, Agr. Forest Meteorol., 130, 282–298, doi:10.1016/j.agrformet.2005.04.005, 2005.

Kielland, J.: Individual Activity Coefficients of Ions in Aqueous Solutions, J. Am. Chem. Soc., 59, 1675–1678, doi:10.1021/ja01288a032, 1937.

Laubach, J., Taghizadeh-Toosi, A., Sherlock, R. R., and Kelliher, F. M.: Measuring and modelling ammonia emissions from a regular pattern of cattle urine patches, Agr. Forest Meteorol., 156, 1–17, doi:10.1016/j.agrformet.2011.12.007, 2012.

Laubach, J., Taghizadeh-Toosi, A., Gibbs, S. J., Sherlock, R. R., Kelliher, F. M., and Grover, S. P. P.: Ammonia emissions from cattle urine and dung excreted on pasture, Biogeosciences, 10, 327–338, doi:10.5194/bg-10-327-2013, 2013.

Leuning, R., Freney, J. R., Denmead, O. T., and Simpson, J. R.: A sampler for measuring atmospheric ammonia flux, Atmos. Environ., 19, 1117–1124, doi:10.1016/0004-6981(85)90196-9, 1985.

Lin, X., Wang, S., Ma, X., Xu, G., Luo, C., Li, Y., Jiang, G., and Xie, Z.: Fluxes of CO_2, CH_4, and N_2O in an alpine meadow affected by yak excreta on the Qinghai-Tibetan plateau during summer grazing periods, Soil Biol. Biochem., 41, 718–725, doi:10.1016/j.soilbio.2009.01.007, 2009.

Ma, X., Wang, S., Wang, Y., Jiang, G., and Nyren, P.: Short-term effects of sheep excrement on carbon dioxide, nitrous oxide and methane fluxes in typical grassland of Inner Mongolia, New Zealand, J. Agr. Res., 49, 285–297, 2006.

Massad, R.-S., Tuzet, A., Loubet, B., Perrier, A., and Cellier, P.: Model of stomatal ammonia compensation point (STAMP) in relation to the plant nitrogen and carbon metabolisms and environmental conditions, Ecol. Model., 221, 479–494, doi:10.1016/j.ecolmodel.2009.10.029, 2010a.

Massad, R.-S., Nemitz, E., and Sutton, M. A.: Review and parameterisation of bi-directional ammonia exchange between vegetation and the atmosphere, Atmos. Chem. Phys., 10, 10359–10386, doi:10.5194/acp-10-10359-2010, 2010b.

Millington, R. J. and Quirk, J. P.: Permeability of porous solids, T. Faraday Soc., 57, 1200–1207, doi:10.1039/tf9615701200, 1961.

Misselbrook, T. H., Gilhespy, S. L., Cardenas, L. M., Chambers, B. J., Smith, K. A., Williams, J., and Dragosits, U.: Inventory of Ammonia Emissions from UK Agriculture, Inventory Submission Report, DEFRA, London, UK, 2012.

Nemitz, E., Sutton, M. A., Schjoerring, J. K., Husted, S., and Paul Wyers, G.: Resistance modelling of ammonia exchange over oilseed rape, Agr. Forest Meteorol., 105, 405–425, doi:10.1016/S0168-1923(00)00206-9, 2000.

Nemitz, E., Milford, C., and Sutton, M. A.: A two-layer canopy compensation point model for describing bi-directional biosphere-atmosphere exchange of ammonia, Q. J. Roy. Meteor. Soc., 127, 815–833, doi:10.1256/smsqj.57305, 2001.

NIWA: The National Climate Database, available at: http://cliflo.niwa.co.nz/ (last access: 2 December 2013), 2015.

Petersen, S. O., Sommer, S. G., Aaes, O., and Søegaard, K.: Ammonia losses from urine and dung of grazing cattle: effect of N intake, Atmos. Environ., 32, 295–300, doi:10.1016/S1352-2310(97)00043-5, 1998.

R Core Team: R: A language and environment for statistical computing. R Foundation for Statistical Computing, Vienna, Austria, 2012.

Rachhpal, S. and Nye, P. H.: A model of ammonia volatilization from applied urea. I. Development of the model, J. Soil Sci., 37, 9–20, doi:10.1111/j.1365-2389.1986.tb00002.x, 1986.

Riddick, S. N.: Global ammonia emissions from seabird colonies, Ph.D. thesis, Kings College, London, UK, 2012.

Riedo, M., Milford, C., Schmid, M., and Sutton, M. A.: Coupling soil–plant–atmosphere exchange of ammonia with ecosystem functioning in grasslands, Ecol. Model., 158, 83–110, doi:10.1016/S0304-3800(02)00169-2, 2002.

Sherlock, R. R. and Goh, K. M.: Dynamics of ammonia volatilization from simulated urine patches and aqueous urea applied to pasture I. Field experiments, Fert. Res., 5, 181–195, doi:10.1007/BF01052715, 1984.

Sherlock, R. R. and Goh, K. M.: Dynamics of ammonia volatilization from simulated urine patches and aqueous urea applied to pasture, II. Theoretical derivation of a simplified model, Fert. Res., 6, 3–22, doi:10.1007/BF01058161, 1985.

Shorten, P. R. and Pleasants, A. B.: A stochastic model of urinary nitrogen and water flow in grassland soil in New Zealand, Agric. Ecosyst. Environ., 120, 145–152, doi:10.1016/j.agee.2006.08.017, 2007.

Simpson, D., Benedictow, A., Berge, H., Bergström, R., Emberson, L. D., Fagerli, H., Flechard, C. R., Hayman, G. D., Gauss, M., Jonson, J. E., Jenkin, M. E., Nyíri, A., Richter, C., Semeena, V. S., Tsyro, S., Tuovinen, J.-P., Valdebenito, Á., and Wind, P.: The EMEP MSC-W chemical transport model – technical description, Atmos. Chem. Phys., 12, 7825–7865, doi:10.5194/acp-12-7825-2012, 2012.

Sutton, M. A. and Fowler, D.: A model for inferring bi-directional fluxes of ammonia over plant canopies, in: WMO Conference on the Measurement and Modeling of Atmospheric Composition Changes including Pollution Transport, WMO/GAW-91, Sofia, Bulgaria, 4–8 October 1993, WMO, Geneva, 179–182, 1993.

Sutton, M. A., Schjorring, J. K., and Wyers, G. P.: Plant-Atmosphere Exchange of Ammonia, Philos. T. R. Soc. A, 351, 261–276, doi:10.1098/rsta.1995.0033, 1995.

Sutton, M. A., Howard, C. M., Erisman, J. W., Bealey, W. J., Billen, G., Bleeker, A., Bouwman, A. F., Grennfelt, P., van Grinsven, H., and Grizzetti, B.: The challenge to integrate nitrogen science and policies: the European Nitrogen Assessment approach, in: The European Nitrogen Assessment: Sources, Effects and Policy Perspectives, edited by: Sutton, M. A., Howard, C. M., Erisman, J. W., Billen, G., Bleeker, A., Grennfelt, P., Van Grinsven, H., and Grizzetti, B., Cambridge University Press, Cambridge, UK, 82–96, 2011.

Sutton, M. A., Reis, S., Riddick, S. N., Dragosits, U., Nemitz, E., Theobald, M. R., Tang, Y. S., Braban, C. F., Vieno, M., Dore, A. J., Mitchell, R. F., Wanless, S., Daunt, F., Fowler, D., Blackall, T. D., Milford, C., Flechard, C. R., Loubet, B., Massad, R., Cellier, P., Personne, E., Coheur, P. F., Clarisse, L., Van Damme, M., Ngadi, Y., Clerbaux, C., Skjøth, C. A., Geels, C., Hertel, O., Wichink Kruit, R. J., Pinder, R. W., Bash, J. O., Walker, J. T., Simpson, D., Horváth, L., Misselbrook, T. H., Bleeker, A., Dentener, F., and de Vries, W.: Towards a climate-dependent paradigm of ammonia emission and deposition, Philos. T. R. Soc. B, 368, 20130166, doi:10.1098/rstb.2013.0166, 2013.

Vieno, M., Dore, A. J., Stevenson, D. S., Doherty, R., Heal, M. R., Reis, S., Hallsworth, S., Tarrason, L., Wind, P., Fowler, D., Simpson, D., and Sutton, M. A.: Modelling surface ozone during the

2003 heat-wave in the UK, Atmos. Chem. Phys., 10, 7963–7978, doi:10.5194/acp-10-7963-2010, 2010.

Vieno, M., Heal, M. R., Hallsworth, S., Famulari, D., Doherty, R. M., Dore, A. J., Tang, Y. S., Braban, C. F., Leaver, D., Sutton, M. A., and Reis, S.: The role of long-range transport and domestic emissions in determining atmospheric secondary inorganic particle concentrations across the UK, Atmos. Chem. Phys., 14, 8435–8447, doi:10.5194/acp-14-8435-2014, 2014.

Walter, I., Allen, R., Elliott, R., Jensen, M., Itenfisu, D., Mecham, B., Howell, T., Snyder, R., Brown, P., Echings, S., Spofford, T., Hattendorf, M., Cuenca, R., Wright, J., and Martin, D.: ASCE's Standardized Reference Evapotranspiration Equation, in: Watershed Management and Operations Management 2000, American Society of Civil Engineers, Fort Collins, Colorado, US, 20–24 June 2000, 1–11, 2001.

Wang, X., Huang, D., Zhang, Y., Chen, W., Wang, C., Yang, X., and Luo, W.: Dynamic changes of CH_4 and CO_2 emission from grazing sheep urine and dung patches in typical steppe, Atmos. Environ., 79, 576–581, doi:10.1016/j.atmosenv.2013.07.003, 2013.

Whitehead, D. C. and Raistrick, N.: The volatilization of ammonia from cattle urine applied to soils as influenced by soil properties, Plant Soil, 148, 43–51, doi:10.1007/BF02185383, 1993.

Whitehead, D. C., Lockyer, D. R., and Raistrick, N.: Volatilization of ammonia from urea applied to soil: Influence of hippuric acid and other constituents of livestock urine, Soil Biol. Biochem., 21, 803–808, doi:10.1016/0038-0717(89)90174-0, 1989.

Wilhelm, E., Battino, R., and Wilcock, R. J.: Low-pressure solubility of gases in liquid water, Chem. Rev., 77, 219–262, doi:10.1021/cr60306a003, 1977.

Wu, Y., Walker, J., Schwede, D., Peterslidard, C., Dennis, R., and Robarge, W.: A new model of bi-directional ammonia exchange between the atmosphere and biosphere: Ammonia stomatal compensation point, Agr. Forest Meteorol., 149, 263–280, doi:10.1016/j.agrformet.2008.08.012, 2009.